INFORMATION TO USERS

This manuscript has been reproduced from the microfilm master. UMI films the text directly from the original or copy submitted. Thus, some thesis and dissertation copies are in typewriter face, while others may be from any type of computer printer.

The quality of this reproduction is dependent upon the quality of the copy submitted. Broken or indistinct print, colored or poor quality illustrations and photographs, print bleedthrough, substandard margins, and improper alignment can adversely affect reproduction.

In the unlikely event that the author did not send UMI a complete manuscript and there are missing pages, these will be noted. Also, if unauthorized copyright material had to be removed, a note will indicate the deletion.

Oversize materials (e.g., maps, drawings, charts) are reproduced by sectioning the original, beginning at the upper left-hand corner and continuing from left to right in equal sections with small overlaps.

ProQuest Information and Learning
300 North Zeeb Road, Ann Arbor, MI 48106-1346 USA
800-521-0600

TiO_2-mediated Heterogeneous Photocatalysis of Saturated Aliphatic C1 to C5 Carboxylic Acids: Kinetics, Degradation Pathway, and Process Efficiency

Jean P. Martin

A Thesis
in
The Department
of
Chemistry and Biochemistry

Presented in Partial Fulfillment of the Requirements
for the Degree of Master of Science at
Concordia University
Montreal, Quebec, Canada

March 2003

Abstract

TiO_2-mediated Heterogeneous Photocatalysis of Saturated Aliphatic C1 to C5 Carboxylic Acids: Kinetics, Degradation Pathway, and Process Efficiency

Jean P. Martin

In this study, we first look at the relation between pH and extent of dark adsorption for aqueous suspensions of linear C1 to C5 saturated aliphatic carboxylic acids, their branched analogues, and their 2-hydroxy and 2-keto derivatives, over TiO_2 Degusa P25. We demonstrate that the observed trends between the extent of dark adsorption and pH can be rationalized by an electrostatic model. We also demonstrate the complete degradation and complete mineralization of these acids when irradiated over TiO_2 Degussa P25. We analyze the trends between the rate of degradations and the rates of mineralization and find that they are different. We demonstrate that this is attributed to the formation of carbon-containing intermediates that impact the overall observed rates of mineralization. An investigation of the rates of degradation of these acids is performed. The observed trends are explained on the basis of (1) extent of dark adsorption, (2) impact on dark adsorption by pH, (3) C-H bond strengths, and (4) stability of the radical intermediate products.

As a second step, we attempt without success to demonstrate that the primary degradation products of valeric acid are the alpha-hydroxy and the alpha-keto derivatives.

However, we confirm the identification of 15 degradation products. The nature of the degradation products allows us to determine that the first step in the degradation of valeric acid involves hydroxylation of the carbon backbone. Evidences for the formation of keto derivatives from hydroxylated degradation products is also presented.

Third, we investigate the possible changes in the nature of the surface of the photocatalyst upon light irradiation by determining the adsorption constant for a few selected acids from (1) adsorption isotherms and (2) Kinetically. A statistically significant difference between the constants obtained by the two methods is obtained.

Finally, the overall quantum yield of formic acid is determined from plots of the reciprocal of photonic efficiencies vs. the reciprocal of catalyst load. The photon flow from the light source needed for the determination of Photonic efficiencies (defined as the ratio of the initial reaction rate to the photon flow from the light source) is determined with the chemical actinometer Aberchrome 540. Using the concept of relative photonic efficiencies and the limiting photonic efficiency of formic acid, we propose quantum yields for acetic acid, propanoic acid, butanoic acid, valeric acid, and 2-methylbutanoic acid.

To Manon, Audrey Ann, Jade, and Zachary

Acknowledgements

Graduating as a Master of Science from Concordia University would not have been possible without the help and assistance of many persons. I would thus like to take a few moments to thank them.

I would first of all like to thank Dr. Nick Serpone, who gave me the opportunity to pursue my graduate studies at Concordia University and to do research in his laboratory. Everything began in Lyon (France) when, as an undergraduate student, he offered me a work term at Dr. Pierre Pichat's laboratory through an international student exchange program. I will always remember this tremendous experience.

I would like to thank Dr. John A. Capobianco and Dr. Marcus F. Lawrence, members of my advisory committee, for their time and advices over these years.

I would like to thank M. Dimitri Kolokotronis for his expertise and assistance with the GC-MS experiments that were required in my studies. Thanks also to Ms. Carole Coutts for her constant follow up and reminders about registration deadlines and the likes.

Thank you to M. Ephriam Kandelshein and Ms. Reesa Busgang, owners of Pharmetics inc., as well as M. Lee Carr, Director of Scientific Affairs at Pharmetics inc., for all the free time that was given to me for my studies.

Finally and above all, I sincerely want to thank my common law wife Manon, my two daughters Audrey Ann and Jade, and my son Zachary for their support, patience, and understanding.

Table of Contents

List of Figures

List of Tables

Preface

Dear Manon, Audrey Ann, Jade, and Zack. Did you know that each American household uses an average of 94,000 gallons of water per year? Because of its availability and accessibility to North Americans, this natural resource is often taken for granted. It is in everyone's best interest to be aware of this precious resource in order to conserve and protect it from many risks. Risks to drinking water come in many forms, such as municipal and industrial discharges, recreational activities or simply natural conditions and events. These can all put at risk the safety of our drinking water.

Many halogenated organic compounds end up in our drinking water, some of which are by-products of drinking water disinfection processes currently in use. Disinfectant by-products regulated by the Environmental Protection Agency include the trihalomethanes chloroform, bromodichloromethane, dibromochloromethane, and bromoform and the haloacetic acids monochloro, dichloro, trichloro, bromo, and dibromoacetic acid. They originate in drinking water following disinfection processes with chlorine (trihalomethanes) and chlorine dioxide (haloacetic acids). Trihalomethanes can cause liver, kidney or central nervous system problems and are an increased risk of cancer to the human, whereas haloacetic acids are associated to an increased risk of cancer. The maximum contaminant levels (MCL, defined as the highest level of a contaminant that is allowed in drinking water expressed in mg/L) associated to trihalomethanes and haloacetic acids are 0.08 mg/L (0.08 ppm) and 0.060 mg/L (0.06 ppm), respectively.

A suitable and safer method for drinking water treatment must be capable to remove contaminants below these levels and one such effective method to destroy low concentrated chlorinated and non-chlorinated organic pollutants is TiO_2-mediated heterogeneous photocatalysis. This method uses a semiconductor catalyst (TiO_2) and near-UV radiation (up to 380 nm) to decompose contaminants at room temperature. There are many advantages to this method. The destruction efficiencies at room temperature are high, and the complete oxidation of organics lead to carbon dioxide and water. There is no need for chemical additives such as chlorine and chlorine dioxide as only water, TiO_2, and a light source are required. It is also inexpensive due to the low cost of the semiconductor TiO_2 and required little energy to run.

In heterogeneous photo catalyzed oxidations of aromatic water pollutant such as phenols and related pesticides, some of the intermediates species formed subsequent to cleavage of the benzenic ring are saturated aliphatic carboxylic acids containing one or two carboxylic acid groups. Once the ring has cleaved, very little is known on the nature of the species formed and their subsequent fate. Our project therefore focuses on the photocatalyzed mineralization of aliphatic acids with one to five carbon atoms, employing irradiated titania suspensions. We look at the extent of destruction of these compounds, their rates of degradation and mineralization, and the efficiency of the photocatalytic process. Finally, we investigate the degradation products formed during the degradation of these compounds and attempt to propose a degradation pathway.

Chapter 1

Introduction and Fundamental Concepts

1.1 Heterogeneous photocatalysis

Heterogeneous photocatalysis involves photoreactions that occur at the surface of a catalyst, and on which the catalyst is in a state different from the reaction medium. Thus, in a typical slurry reactor, a semiconductor powder is suspended in an aqueous solution containing one or more contaminants, which may consist of organics, inorganics, or a combination of both. The initial photoexcitation takes place in the catalyst substrate, for example TiO_2, and the photoexcited catalyst then interacts with the ground state adsorbate molecule.

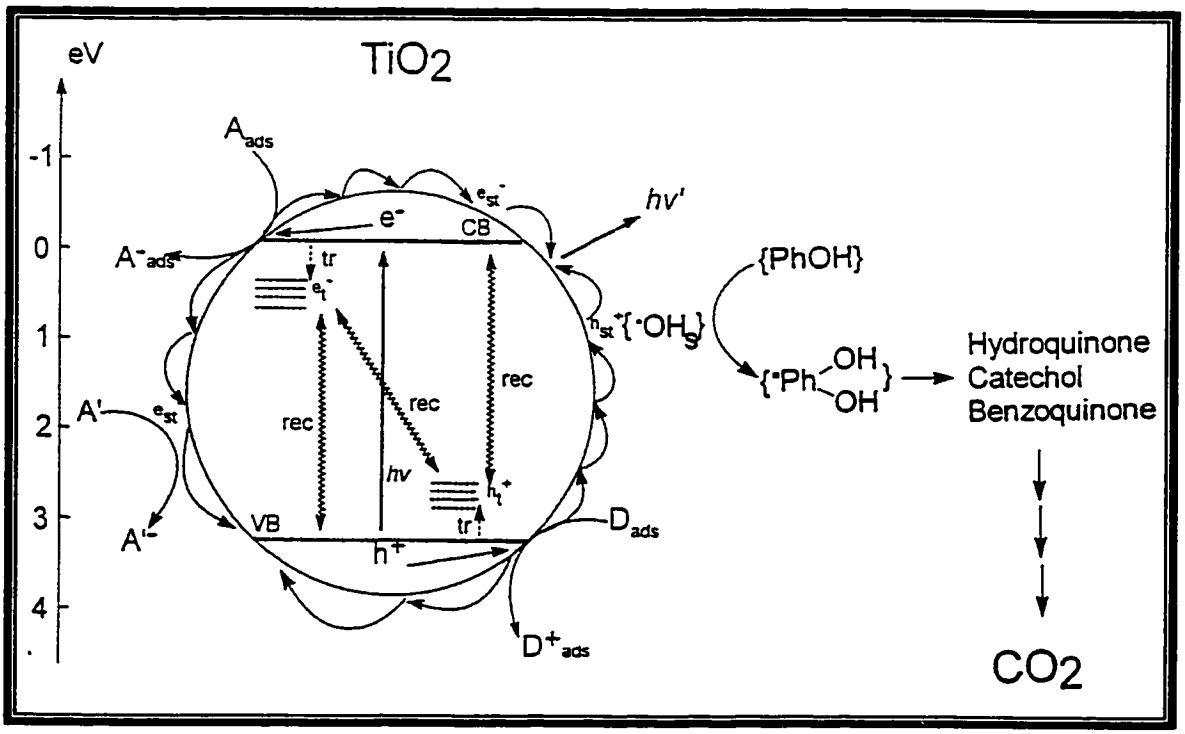

Figure 1.1: Graph showing the several events in and on the TiO_2 particle and subsequent events occurring on the surface towards the ultimate oxidation of an aromatic compound (reproduced from ref. 1)

Figure 1.1 illustrates the several events that may occurr in the bulk inside and on the surface of a TiO_2 particle, together with the subsequent chemical events occurring on the surface towards the ultimate oxidation of an aromatic compound.

In addition to water, the organic substrate may also adsorb on the catalyst surface. The extent of which depends on many factors: for example 1) the nature of the substrate, 2) the concentration of the substrate, 3) the nature of the catalyst, and 4) the pH of the solution, among others.

Upon irradiation of TiO_2 with light of wavelengths shorter than 410 nm for rutile or 385 nm for anatase (corresponding to a band gap energy E_g = 3.02 eV or 3.21 eV respectively), many events are triggered, the first of which is the absorption of photons of appropriate energy followed by electron transition from the valence band (2p of O^{2-})[1] to the conduction band (3d of Ti^{IV}) leaving behind a highly reactive valence band hole (h^+_v) [3, 4, 5] and electrons (e^-_c). These electrons and holes reach the surface rapidly and can be trapped before they recombine. Once on the surface, both charge carriers scan the surface visiting several sites to reduce adsorbed electron acceptors and to oxidize adsorbed electron donors in competition with surface recombination[6]. Serpone at al have estimated that ca. 93% of é /h^+ recombine in about 10 ns [1].

Those electrons and holes that escape recombination can reduce or oxidize species present in the external electrolyte solution. If reduction of a given species is to be carried out, its redox level must be positioned below the conduction band level of the semiconductor i.e.: at a potential more positive than the reduction potential of the conduction band (more precisely the Fermi level of the electron), a condition thermodynamically essential for the transfer of an electron from the conduction band of

the semiconductor to the species being reduced [1]. Thus, any species whose redox potential is more positive than the conduction band of TiO_2 can be reduced by the latter and the difference between the conduction band potential and that of the species being reduced is the thermodynamic force for reduction [8]. Therefore, the energy level at the bottom of the conduction band (LUMOs) reflects the reduction potential of the photo-electrons [6].

On the other hand, if oxidation of a donor species is desired, its redox potential should be located above the valence band level of the semiconductor, i.e.: at a potential less positive than the redox potential of the valence band, a condition thermodynamically required for the transfer of an electron from an adsorbate species (e.g.: an organic pollutant or a metal ion) to the valence band of the semiconductor (a photogenerated hole). The uppermost level of the valence band (HOMOs) is thus a measure of the oxidizing ability of the photo-holes [6].

Where the redox level of a species is located between the valence and conduction band of the semiconductors, both reduction and oxidation processes can occur [1]. This is all illustrated in Figure 1.2. Considering the latter and Figure 1.1, species A is reduced to species A^- by a photogenerated electron in the conduction band of the semiconductor and thus has a more positive redox potential than that of the conduction band of the semiconductor photocatalyst. Species D, which is being oxidized to species D^+ by electron transfer from the donor D to the valence, and of the semiconductor photocatalyst has a less positive redox potential than the latter. In terms of redox potential, both species are residing below the conduction band and above the valence band of the semiconductor photocatalyst, just as most species shown in Figure 1.2.

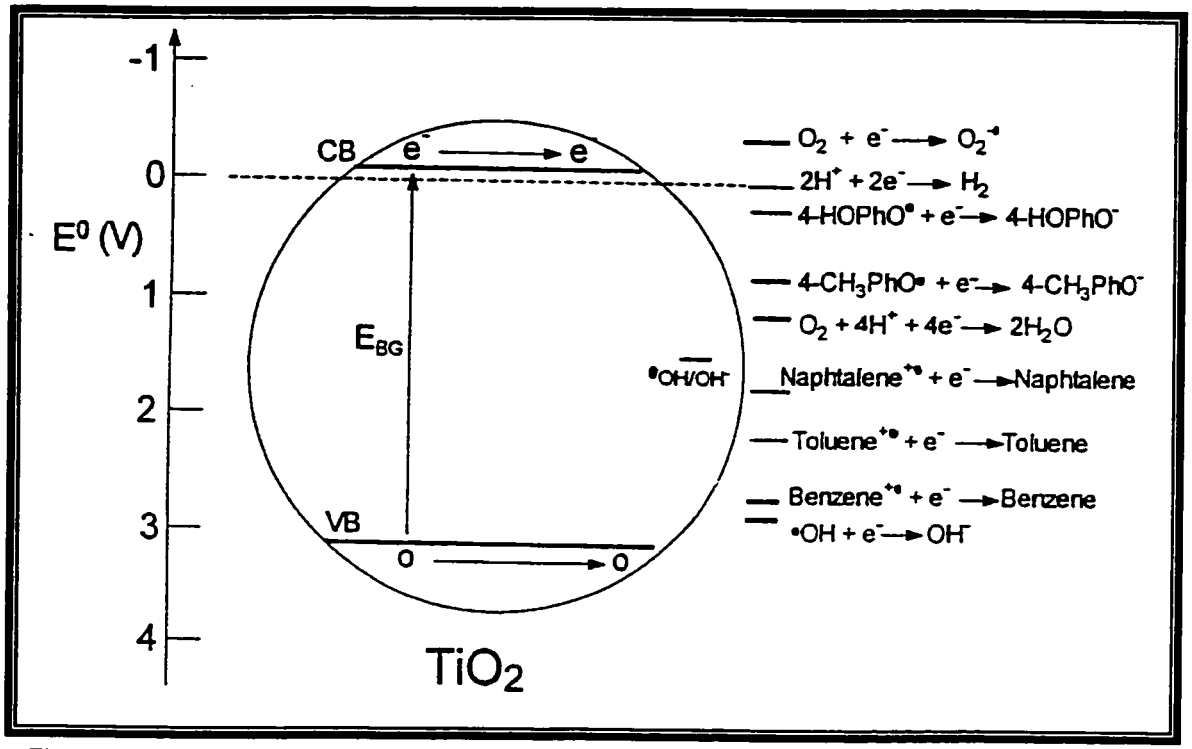

Figure 1.2: Redox potentials of the valence and conduction bands if TiO_2 particles and those of some organic compounds (reproduced from ref. 1).

The inhibition of electron-hole pair recombination is greatly enhanced by the presence of dissolved molecular oxygen. The formation of $O_2\bullet^-$ at the surface of bandgap irradiated semiconductor metal oxides is well documented. Accordingly, the essential role of O_2 is assigned to the e^- scavenging property of this molecule [9]. Oxygen plays an important role, just as water and hydrogen do. Generally, no photodegradation occurs in the absence of either O_2 or H_2O, or both [10]. Oxygen and water are essential species in the photomineralization process of organics using irradiated TiO_2. In the presence of air, oxygen acts of an oxidant [10] (an electron acceptor), enabling the separation of the photogenerated charge carriers. Experimental results indeed demonstrate that the presence of an electron acceptor (in this case, oxygen) in aqueous TiO_2 suspensions at

ambient temperature is necessary to separate the photogenerated charge carriers effectively and thereby enable the successive generation of hydroxyl radicals [11]. In fact, the overall efficiency of the photocatalytic process is associated with the rate of e^- trapping by O_2 [12].

As far as water is concerned, it is commonly accepted that a free hole will react with a water molecule upon arrival at the TiO_2 surface to create an adsorbed HO• radical, a process that will occur on a small particle within a few picoseconds [13]. Surface hydroxyl groups and/or water molecules thus act as reductants to give surface-bound hydroxyl radicals (≡M-$^{\bullet}$OH) [10].

Many mechanistic details are still debated and are yet to be clarified. Among them, there is the nature of the species that are responsible for the oxidization and for the reduction of the various species that have been treated by these processes. More specifically, the possibility of direct electron transfer from an adsorbed organic molecule to a valence band hole of the semiconductor photocatalyst is still raising many questions. Basically, two mechanisms are proposed in relation to the oxidative processes involved in heterogeneous photocalysis. The first mechanism postulates that the first photogenerated valence band hole reacts primarily with physisorbed H_2O and surface-bound HO^- on TiO_2 particles to give surface-bound •OH radicals (E^{o}_{redox} = + 1.5 ± 0.3 V vs. NHE)[1], which can then react with pre-adsorbed of photoadsorbed organic substrates. The potential for oxidation of H_2O or HO^- to free HO• lies above the valence flat band edge of TiO_2, so that a photogenerated hole at the edge would be sufficiently energetic to produce this species. If the hydroxyl radical formed is adsorbed at the TiO_2 surface, it would be stabilized and would require an even less positive potential for its reduction [14]. Under

both acidic and basic conditions, the oxidation of surface bound OH^- and H_2O by the TiO_2 valence band hole to form HO• is thermodynamically favorable and expected [2].

The second mechanism proposes a direct reaction between the valence band holes (E^o_{redox} = +3.0 V vs. NHE) and the organic substrates. Although conclusions were made where photooxidation was occurring mainly at the semiconductor surface via a trapped hole [13], it is usually assumed that the organic pollutant substrate does not undergo direct hole transfer but rather that oxidation takes place through a surface bound hydroxyl radical ($Ti^{IV}OH•+$) [15].

Unfortunately, these two mechanisms cannot be differentiated by product or kinetic analysis alone, since both pathways lead to the same primary radicals [1]. However, several pieces of evidence for •OH radical involvement in TiO_2/H_2O systems, in which complete mineralization occurs, exists[16]:

- TiO_2 in water is known to be covered with oxidizable hydroxyls groups;
- HO• radical was evidenced by ESR but could not be confirmed by others;
- HO• radical spin trap adducts have been characterized by ESR;
- Degradation products obtained with Fenton's reagent (generator of HO•) are similar to those obtained by heterogeneous photocatalysis using TiO_2;
- Kinetic Isotopic effect of solvent (H_2O vs. D_2O).

Direct electron transfer from adsorbate to TiO_2 have also been illustrated by considering the mechanism of the photocatalytic oxidation of diaryl and dibenzyl thioethers [16].

The other debate is related to the location where reactions occur. That is, do reactions occur exclusively on the catalyst surface or in solution? The requirement for adsorption of a molecular entity for a reaction to occur in heterogeneous catalysis in the gas phase is of no concerns. Obviously, the reactant must come in contact with the catalyst's surface for any reactions to take place. But in heterogeneous photocatalysis using a TiO_2 slurry reactor where the inter-TiO_2 particles' distance is not great, given that water is oxidized by the valence band holes of the photocatalyst to form HO• radicals, do the latter migrate away from the surface of the catalyst surface and create some kind of a HO• radical rich region between each particle and thus allow homogeneous oxidations to occur? Even though this seems possible, should there be any migration of HO• in the bulk? It would appear that their contribution is believed to be minimal [13]. The species to be oxidized is believed to be adsorbed on the surface of the particles. Photochemical reactions at the particle/solution interface are therefore controlled by both relative redox energies and adsorption characteristics [17]. It has been proposed that the HO• is surface bound and unlikely to desorb into solution [5]. Apparently, the HO• does not migrate far from the photogenerated active sites of TiO_2 so that the degradation must occur at the photocatalyst surface or within a few atomic distances from the surface [5]. To summarize then, the overall process involves:

1) Dissociative adsorption of water onto the TiO_2 catalyst surface gives rise to the formation of two distinctive hydroxyl groups (Figure 2.2 and equations 1 and 2) with a theoretical maximum surface coverage of 5 – 15 OH^-/nm^2 [2]. Organic reactant molecules may or may not adsorb onto the surface;

$$\equiv Ti\text{-}O\text{-}Ti\equiv + H_2O \Rightarrow \equiv Ti\text{-}O(H)\text{-}Ti\equiv + OH \quad (1)$$

$$\equiv O\text{-}Ti\text{-}O\equiv + OH \Rightarrow \equiv O\text{-}Ti(OH)\text{-}O\equiv \quad (2)$$

2) Charge separation in the TiO_2 particle following irradiation of the photocatalytic material with wavelength of proper energy (equation 3), basically with light of wavelengths shorter than 410 nm (corresponding to a band gap energy E_g = 3.02 eV for rutile), generating highly reactive valence band hole (h^+_v) [3, 4, 5] and a highly reactive photogenerated electrons (e^-_c), which may either recombine or get trapped on the surface of the photocatalyst. Charge separation requires the presence of dissolved molecular oxygen which traps conduction band electrons (equation-4);

$$TiO_2 + h\upsilon \Rightarrow TiO_2\{\acute{e}...h^+\} \Rightarrow \acute{e}_{cb} + h^+_{vb} \quad (3)$$

$$\acute{e}_{cb} + O_{2(surface)} \Rightarrow O_2\bullet^-_{(surface,\ in\ air\ equilibrated\ solutions)} \quad (4)$$

3) Oxidation of water adsorbed onto the catalyst surface yields highly oxidizing HO• radicals (equations 5 and 6);

$$\{Ti^{IV}\text{-}O^{2-}\text{-}Ti^{IV}\}\text{-}OH^- + h^+_{vb} \Rightarrow \{Ti^{IV}\text{-}O^{2-}\text{-}Ti^{IV}\}\text{-}OH\bullet \quad (5)$$

$$\{Ti^{IV}\text{-}O^{2-}\text{-}Ti^{IV}\}\text{-}OH_2 + h^+_{vb} \Rightarrow \{Ti^{IV}\text{-}O^{2-}\text{-}Ti^{IV}\}\text{-}OH\bullet + H^+ \quad (6)$$

4) Oxidation of an adsorbed organic reactant (OR) by the HO• radicals (equation-7). There might be a minimal contribution of HO• radicals in undergoing oxidation reactions in solution, but those should be minimal [13] since HO• radicals are not believed to migrate far from the photogenerated active sites onto TiO_2: the degradation process must occur at the photocatalyst surface or within a few atomic distances from the surface [5]. Oxidation reactions via direct charge transfer to the valance band of the photocatalyst may also occur [16] (equation-8) and in

such cases, the reduction potential of the organic entity must reside above that of the valence band (at less positive reduction potentials, thus behaving as an electron donor, denoted D);

$$\{Ti^{IV}\text{-}O^{2-}\text{-}Ti^{IV}\}\text{-}OH\bullet + OR_s \Rightarrow \{Ti^{IV}\text{-}O^{2-}\text{-}Ti^{IV}\}\text{-}OH^- + OR_s\bullet^+ \quad (7)$$

$$h^+_{vb} + D_s \Rightarrow D_s^+ \quad (8)$$

5) Concurrent reduction of adsorbed organic reactant molecules by the photogenerated conduction band electrons (equation-9). The reduction potential of the organic entity must reside below that of the conduction band (at more positive reduction potentials, thus behaving as an electron acceptor, denoted A).

$$\acute{e}_{cb} + A_s \Rightarrow A_s^- \quad (9)$$

Many other species are generated in these processes, some of which are being triggered by the formation of the superoxide radical anion $O_2\bullet^-$ (equation-4). In fact, the superoxide radical anion $O_2\bullet^-$ can be reduced further to the peroxide dianion O_2^{2-} [18]. Surface peroxo species can form either by hydroxyl radical (hole) pairing (equation-10), by sequential two-hole capture by the same OH group (equation-11) or by dismutation of $O2\bullet^-$ (equation-12) [18]:

$$2\{Ti^{IV}\text{-}O^{2-}\text{-}Ti^{IV}\}\text{-}OH\bullet \Rightarrow HO\bullet\bullet OH \quad (10)$$

$$\{Ti^{IV}\text{-}O^{2-}\text{-}Ti^{IV}\}\text{-}OH\bullet + h^+_{vb} \overset{-H^+}{\Rightarrow} (O)_{surface} \Rightarrow \tfrac{1}{2}O_{2ads} \quad (11)$$

$$2O_2\bullet^-_{ads} \Rightarrow O_{2ads} + O_2^{2-}{}_{ads} \quad (12)$$

Moreover, in acidic media (pH 3), in which most photo-oxidative decomposition of organics have historically been carried out, $O_2\bullet^-$ protonates to give $HO_2\bullet$ (pKa 4.88). Other reactions that may occur on the TiO_2 particle surface and that are solvent (water) related are summarized in equations 13 to 17:

$$2\ HO_2\bullet \Rightarrow H_2O_2 + O_2 \quad (13)$$

$$H_2O_2 + O_2\bullet^- \Rightarrow OH\bullet + OH^- + O_2 \quad (14)$$

$$H_2O_2 + \acute{e}_{cb} \Rightarrow OH\bullet + OH^- \quad (15)$$

$$H_2O_2 + 2\ h^+_{vb} \Rightarrow O_2 + 2H^+ \quad (16)$$

$$O_2\bullet^- + HO_2\bullet \Rightarrow O_2 + HO_2^- \Rightarrow H_2O_2 \quad (17)$$

All species appearing in the five equations above may also react with organic pollutants present in such systems. It thus becomes evident that under illumination, the electronic characteristics and the nature of the TiO_2 particle surface undergo dramatic changes and it is the extent of these changes that governs the events that take place along the photo-oxidative mineralization of organic substrates.

1.2 Limiting Photonic Efficiencies

The overall quantum yield $\Phi_{overall}$, is defined as the number of reactant molecules that react for each photon adsorbed [19].

$$\Phi_{overall} = \frac{rate\ of\ reaction}{rate\ of\ absorption\ \ of\ radiation} \qquad (18)$$

Because the semiconductor particles absorb, scatter and transmit light, the rate of adsorption of ultra-bandgap photons is very difficult to assess, which in turn makes the measurement the overall quantum yield difficult not to say rare [20]. The non-significant extent of light scattered or reflected by the particulate matter in the dispersion can reach 13% to 76% of the total incident photon flux, depending on the source of the titania sample [21]. This must be taken in consideration when performing measurements of photons absorbed by semiconductor metal oxide photocatalysts. Metal oxide materials such as TiO_2 particulates (anatase/rutile) cannot absorb all the incident photon flux from a given source. Much of this flux will be either reflected or scattered owing to significant differences in the index of refraction (n) of the materials making up the photocatalytic system under examination {for 365nm radiation, n = 1.0 for air, 1.33 for water, 1.5 - 1.7 for glass, 3.87 for rutile TiO_2, ca. 2.5 – 3 for anatase TiO_2}. The maximum quantity of photons that can be absorbed by TiO_2 would appear to be no more than ~ 65%.

In addition to the above constraints, the rate of reaction depends on many parameters, including the reactor geometry, the nature and concentration of the semiconductor, the oxygen and the substrate concentration, the light intensity, the temperature, the pH, the presence of interfering species and stirrer speed. As a result, in a study of the same system, the values of $\Phi_{overall}$ obtained by one research group may be

very different than those obtained by another. Because of the numerous factors that have an impact of the efficiency of these systems, there seem to be very little room for the probability to have alike inter-laboratory experimental conditions. Such differences are attributed to budgetary reasons, which govern the type and quality of equipment that can be afforded. The inherent differences between the equipments that are available form various suppliers of laboratory equipment is another one.

An ideal method used to determine process efficiency should require simple instrumentation. It should also be unaffected by the reactor design and the light source, among other factors that may affect the measurements. This is especially true for the determination of the overall quantum yield. Experiments carried out to show the dependence of initial rates of disappearance of organic substrates as a function of the amount of TiO_2 in solution (catalyst load) show a relationship that is similar to that of the Langmuir-Hinshelwood model:

$$R_{in} = \frac{A[TiO_2]}{1 + B[TiO_2]} \tag{19}$$

where A and B are constants. If the photon flow $R_{o,\lambda}$ remains constant, the functionality of the photonic efficiency ξ will follow a similar behavior [22]:

$$\xi = \frac{\xi_{\lim} C[TiO_2]}{\xi_{\lim} + C[TiO_2]} = \frac{R_{in}}{R_{o,\lambda}} \tag{20}$$

where ξ_{lim} represents the limiting photonic efficiency for large TiO_2 loadings and where C is a constant. This is illustrated in Figure 1.3.

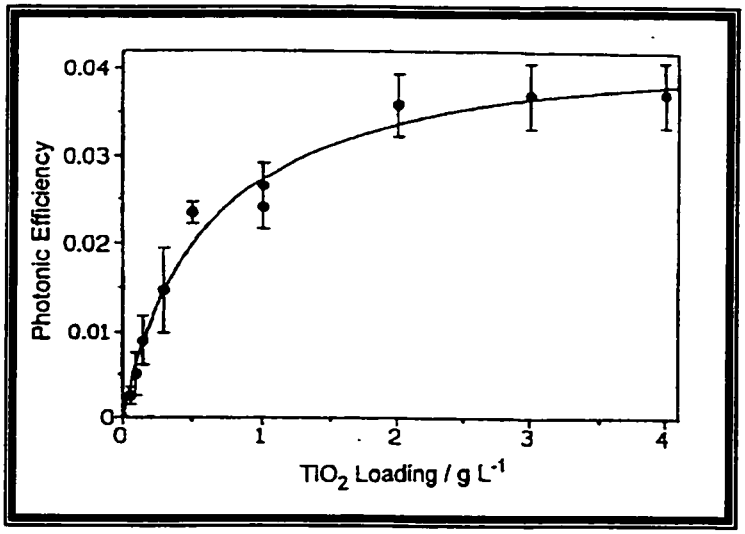

Figure 1.3: Dependence of the photonic efficiencies ξ for the intial photodegradation of phenol on the loading of Degussa P-25 titania [TiO_2] for irradiation at the wavelength of 365 nm ± 10 nm (adapted form 22).

The reciprocal of equation 20 shows that plotting the reciprocal of the photonic

$$\frac{1}{\xi} = \frac{1}{C[TiO_2]} + \frac{1}{\xi_{lim}} \qquad (21)$$

efficiency for a test molecule as a function of the reciprocal of the TiO_2 loading will give a straight line for which the y-intercept is equal to the reciprocal of the limiting photonic efficiency for the test compound (Figure 1.4). If the whole photon flow $R_{o,\lambda}$ impinging on the reactor system is totally absorbed by the photocatalyst at the loading used, it turns out that the above equation is by definition that of the quantum yield and thus:

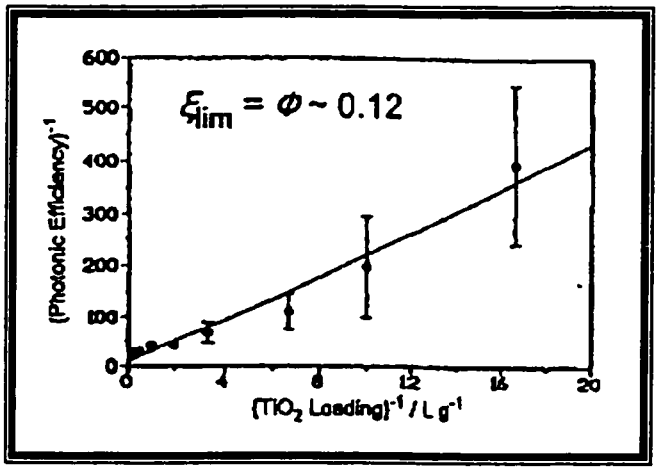

Figure 1.4 : The linear transform of the curve shown in figure 1.3 plotted as ξ^{-1} vs. $[TiO_2]^{-1}$. The intercept from the linear transform gives the limiting photonic efficiency ξ_{lim} (adapted from 22).

$$\xi_{\lambda} = \frac{R_{in}}{R_{o,\lambda}} = \Phi_{\lambda} \tag{22}$$

The quantum yield for a given process can thus be determined with very simple instrumentation i.e., a glass vessel (a reactor), a lamp, a monochromator, water, and an organic molecule to degrade. ξ [23, 24] being defined as

$$\xi = \frac{rate\ of\ reaction}{Photon\ flow} \tag{23}$$

or

$$\xi = \frac{R_{in}(substrate)}{R_{o,\lambda}} \tag{24}$$

photonic efficiencies can be determined from the ratio of the initial rate of reaction divided by the photon flow. The photon flow incident on the surface of the reactor can be determined by chemical actinometry, using compounds such as Aberchrome 540, which can be used for the 310 – 370 nm and the 436 – 546 nm ranges [25 - 27]. Its quantum yield is relatively insensitive to temperature changes, to changes in reactant concentration, photon flow, and the wavelength of absorbed light. Stirring needs to be maintained during irradiation to avoid some localized depletion of the chemical actinometer in solution, and the cell should be free of particulate matter that could reflect or scatter light since this could have a detrimental impact on the precision and accuracy of the quantum yield data. The concentration of the actinometer should also be such that the absorbance of the actinometer at the working wavelength be equal or greater than 2 during the entire range of irradiation period to ensure that more than 99% of the photons be absorbed by

the chemical actinometer. These methods are well established and chemical actinometers can be obtained commercially with a recommended general procedure.

Knowing the limiting photonic efficiency ξ_{lim} or overall quantum yielg $\Phi_{overall}$ for a reference compound allows for the determination of the overall quantum yield of any test compound. Indeed,

$$\Phi(substrate) = \frac{\xi(substrate)}{\xi(standard)}\Phi(standard) = \xi_r \Phi(standard) \qquad (25)$$

and since photonic efficiencies can be determined from the ratio of the initial rate of reaction divided by the photon flow (eq. 23 - 24), in turns out that

$$\xi_r = \frac{\xi(substrate)}{\xi(standard)} = \frac{\left[\frac{R_{in}(substrate)}{R_{o,\lambda}}\right]}{\left[\frac{R_{in}(standard)}{R_{o,\lambda}}\right]} = \frac{R_{in}(substrate)}{R_{in}(standard)} \qquad (26)$$

where ξ_r = relative photonic efficiency, ξ (substrate) = photonic efficiency for the substrate molecule, ξ (standard) = photonic efficiency for the standard molecule, R_{in} (substrate) = initial rate of degradation for the substrate molecule, R_{in} (standard) = initial rate of degradation for the standard molecule, $R_{o,\lambda}$ = rate of photons of monochromatic light incident inside the from window of the irradiation cell.

The relative photonic efficiencies are obtained from the ratio of the photonic efficiency for the photocatalytic process of a given substrate to the photonic efficiency for the photocatalytic process of a standard or reference compound under identical conditions. It is essential that the light source, the wavelength of irradiation, and the reactor all be the same for both the substrate of interest and the reference material.

Relative photonic efficiencies must be independant of light irradiance, reactor geometry, pH, temperature, but ore importantly, on catalyst loading and substrate concentration. These parameters must thus be controlled and the experimental conditions must be such that the working concentration of the substrate molecule as well as the catalyst loading must both be chosen such that the initial rate of disappearance of the substrate molecule is no more dependant on its own concentration nor on that of the catalyst. This is achieved by 1) deriving a plot of R_{in} vs $[TiO_2]$ and then 2) by deriving a plot of R_{in} versus [substrate] at constant catalyst load until the initial rates of disappearance of the substrate molecule reach a plateau using a catalyst load located in the plateau of the plot of R_{in} versus $[TiO_2]$ as derived in 1). Once this is done, both the standard test molecule and the substrate molecule under investigation may be degraded under the same conditions and the relative photonic efficiency thus obtained finally leads to the quantum yield of the substrate molecule, using equation 25.

The successful application of the concept of limiting photonic efficiencies was demonstrated with the determination of the quantum yield of phenol [28]. Using the protocol described above, a value of $\xi_{lim} = \Phi = 0.12$ [28] was obtained for phenol, which was in excellent agreement with the value of 0.14 ± 0.02 [22] found for the quantum yield of phenol by other means using the following relationship:

$$\Phi = \frac{R_{in,365}}{\left(R_{o,365}\right) \times \int_{365}} \tag{65}$$

where

$R_{in,365}$ was the initial rate of disappearance of phenol using monochromatic light at 365 nm ± 10 nm;

$R_{o,365}$ was the rate of photons of monochromatic light (365 nm ± 10 nm) incident inside the from window of the irradiation cell, as determined by chemical actinometry;

f_{365} was the fraction of the photons of monochromatic light (365 nm ± 10 nm) incident inside the from window of the irradiation cell actually absorbed by the photocatalyst, as determined from an integrating sphere method;

Finally, the robustness and usefulness of the method of relative photonic efficiency was clearly demonstrated by degrading some aromatic compounds under various conditions of light intensity (13% to 100% where 100% is 190 mW/cm^2), reactor geometry, pH (3 to 6), temperature (12 to 68°C), concentration of organic substrate (40 to 800 μm), and loading of titania (0.2 to 2 g/L). The results obtained for 2-methylphenol are shown in figure 1.5.

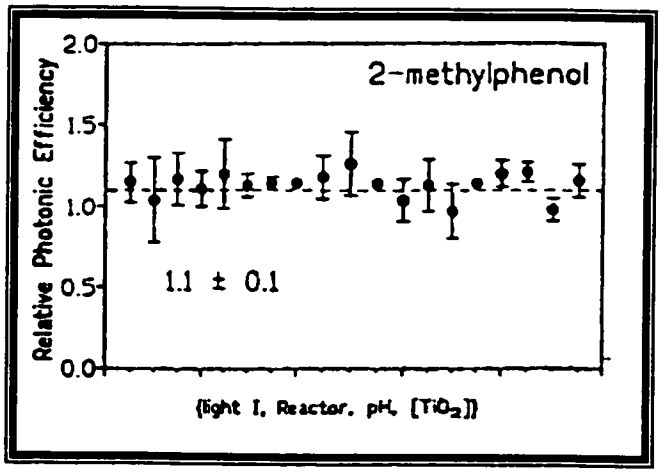

Figure 1.5 : Relative photonic efficiencies for 2-methylphenol for various conditions. Includes only the effect of light intensity, reactor geometry, pH and concentration of titania; [substrate] ≈ 20 mg L-1 (adapted from 28).

Despite these very interesting results that are clearly showing the robustness of the method and its potential as a to become standard procedure for the determination of process efficiencies, some claims that there is also a danger in quoting ξ_r values, since a ξ_r value of much greater than unity could be taken as an indication of a very efficient photochemical process, which may not

be [20]. For example, a ξ_r value of 2 for a process under test simply indicates that it is twice as fast as the degradation of phenol carried out under the same reaction conditions however, it provides no indication of how efficient the process is with respect to photons. Thus if the reaction was carried out in the presence of a high phosphate concentration, both the photoprocess under test and the photodegradation of phenol would be very slow and photochemically inefficient, and yet, a ξ_r value of two could easily be returned and misunderstood as implying an efficient photoreaction. As a result, the suggestion that the term photonic efficiency, together with ξ_r, should be used only when the number of incident photons impinging on the front window of the photolysis cell is known by actinometry (or by other means), represent a very sound and important safeguard when ξ_r values are used.

Chapter 2

Experimental Section

2.1 Reactors' specifications, irradiation set-ups, and Chemicals

2.1.1 Reactor – 1 specifications

Reactor 1 was a double wall pyrex reactor (capacity, ca. 60 ml; Figure 2.1) mounted with an outlet and an inlet port allowing for water circulation and temperature control. Its dimensions are indicated.

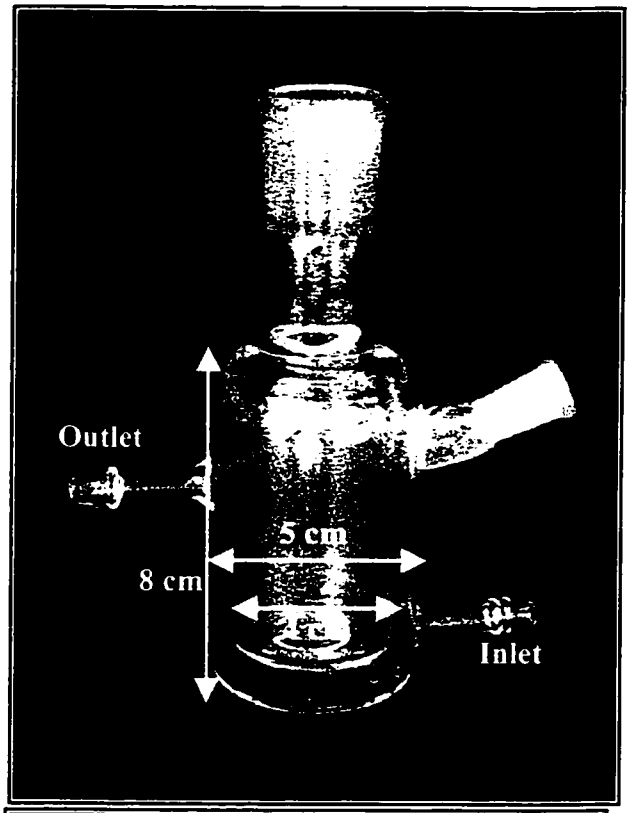

Figure 2.1 : Reactor-1 dimensions with identification of water circulation ports

2.1.2 Reactor – 2 specifications

This reactor was a single wall circular pyrex reactor (capacity, ca. 500 ml). It had two flat window diametrically opposite to each other. The dimensions of the reactor were approximately 9 cm high, outer diameter ca. 10 cm when measured on the axis of its two convex faces, and the distance between the two flat windows was ca. 8.5 cm.

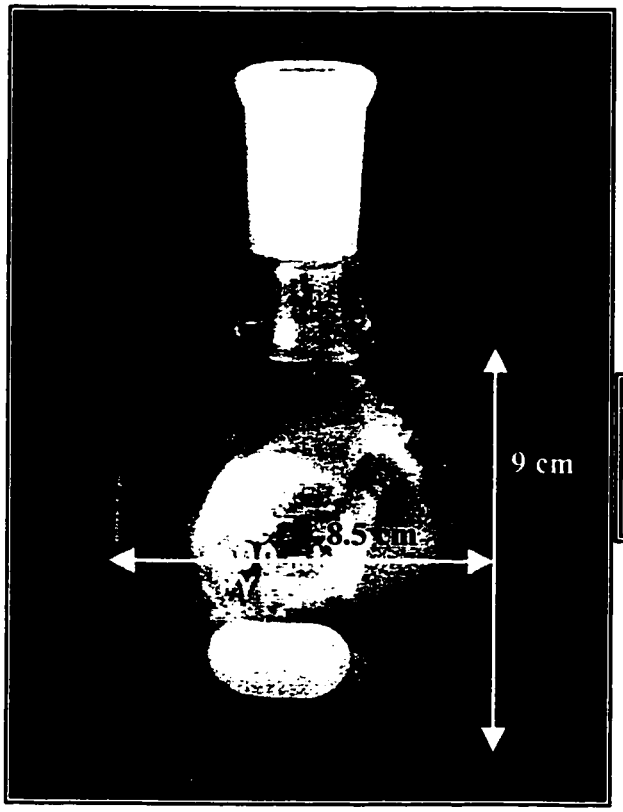

Figure 2.2 :

Reactor-2 with dimensions

2.1.3 Irradiation setup-1 (small scale experiments)

Reactor-1 was mounted on a stirring plate at 23 cm (center of the reactor to the exit of the light source) from an Oriel 1000 watts Hg/Xe arc lamp light source. A water circulating cooling/heating system (MGW – Lauda K4R Electronics) provided control on the temperature of the reactor during irradiation. A Pyrex water bath was positioned between the reactor and the light source just at the light source exit to filter infrared radiations. The reactor was left opened to the atmosphere at all times during irradiation except during dark adsorption equilibration.

2.1.4 Irradiation setup-2 (large scale experiments)

Reactor-2 was mounted onto a stirring plate at 23 cm (measured from the center of the reactor to the exit of the light source) from an Oriel 1000 watts Hg/Xe arc lamp light source. The reactor was air-cooled using and air blower. A Pyrex water filter was also used to filter out infrared radiations. Irradiation was performed under conditions that the dispersion was an air-equilibrated at all times.

2.1.5 Irradiation setup-3 (Limiting photonic efficiency)

In these experiments, reactor-1 was mounted 30 cm from the light source. A water circulating cooling/heating system (MGW – Lauda K4R Electronics) provided control on the temperature of the reactor during irradiation. A Baush & Lomb 0.25m monochromator (Grating, 1200 groves/mm, SN: 593AB) was positioned between the reactor and the light source and set to 365 nm. Air-equilibrated conditions were used at all times for the dispersions, except during dark adsorption equilibration

2.1.6 Chemicals

Formic acid 96% (Aldrich, 05102CN), Acetic acid glacial 99.8% (internal source), propanoic acid 99% (internal source), Butyric (butanoic) acid 99%+ (Aldrich, 10117KG), 2-methylbutanoic acid 98% (Aldrich, 04418EN), Valeric (pentanoic) acid 99+% (Aldrich, 03323LG & 10621BS), O-Phosphoric acid 85% (Fisher Scientific, 881549), Methanol (Fisher Scientific, HPLC grade, UV cutoff 205 nm), Buffer pH 1 (Fisher Scientific NIST traceable, SC8295332), Buffer pH 5 (Fisher Scientific, SC9018661),

Trimethylacetic acid 99% (Aldrich, 04627CN), TiO2 Degussa P25 (Titandioxid, 1118), Isovaleric (3-methylbutanoic) acid 99% (Aldrich, 06509K), Isobutyric (2-methylpropanoic) acid (Aldrich, 99+%, CG00113AF), Acetonitrile HPLC grade (Omnisolv), Potassium hydrogen phtalate acidimetric standard (Fisher Scientific, 746772), Compressed Air (Praxair, ultra zero gas), Acrylic acid (Aldrich, 99%, 06523 LQ), 2-hydroxypropanoic aicd (Aldrich, 85+% solution in water, 12817EQ), 2-ketopropanoic acid (Aldrich, 98%, 12202CN), 2-hydroxy-2-methylpropanoic acid (Aldrich, 99%, 00205EG), 2-hydroxybutanoic acid sodium salt (Aldrich, 97%, 03403AZ), 2-ketobutanoic acid (Aldrich, 99%, 01328HQ), 2-hydroxy-2-methylbutanoic acid (Aldrich, 98%, 09203CN), 2-ketovaleric acid sodium salt (Aldrich, 98%, 02629LN), 2-hydroxyvaleric acid sodium salt hydrate (Aldrich, 98%, 20825CR), Sodium hydroxide (A&C, Reagent, Low carbonate pellets, 200393/46200/930625), Perchloric acid, Hydrochloric acid (BDH, Assured ACS, 247122),), Diethyl ether ACS (BDH, Analytical reagent, 118483 – 61334), Dichloromethane, GC test solution (Hewlett Packard, Split Capillary Inlet Checkout sample, C_{16}/C_9 ratio 1.016, 1% w/w n-nonane (C_9) & n-hexadecane (C_{16}) in n-tetradecane (C_{14}), LA20897), Hydrogen (Prodair, High purity grade), Nitrogen (Praxair, Pre-purified), Magnesium sulfate anhydrous, BSTFA + TMCS 99:1 (Sylon BFT) (Supelco, LA73710), Aberchrome 540, Toluene (J.T. Baker, "Photrex" reagent for spectrophotometry, G50616).

2.2 Preliminary measurements

2.2.1 HPLC-UV linearity range of selected acids

Solutions of Formic acid, Acetic acid, Propanoic acid, Butanoic acid, 2-methylbutanoic acid, and Valeric acid that comprised the C_1 – C_5 linear series and a branched C_5 were prepared at various concentrations. They were analyzed by HPLC-UV to determine the instrumental settings that would give rise to a linear response as a function of concentration.

The HPLC system consisted of a Waters 501 isocratic pump mounted with a 20 μL injection loop, a Waters 441 UV absorbance detector with single wavelength capability @ 214 nm, a Hewlett Packard HP3396A integrator, and a Supelco Canada Spherisob reversed phase C_8 (5μm, 250mm x 4.6mm) HPLC column.

In a typical experiment, a carboxylic acid solution was prepared at a concentration of 9.79×10^{-3}M (~1000 ppm carbon for a C5 acid) by pipetting the required amount of the acid into a volumetric flask and completing to volume with pure water. Data pertaining to the preparation of the stock solution of the above acids follows:

Acid	Mol. Wgt. (g/mol)	Density (g/ml)	Vol. Acid (μL)	Final vol. (ml)
Formic	46.02	1.220	185	500
Acetic	60.05	1.0492	280	500
Propanoic	74.08	0.9930	365	500
Butanoic	88.11	0.9577	450	500
2-methyl butanoic	102.13	0.936	534	500
Valeric	102.13	0.9391	532	500

Table-2.1: preparation conditions in obtaining the above acid at a concentration of 9.79×10^{-3} M

All acids were then diluted to concentrations of 4.90 x 10-3M, 2.45 x 10-3M, 9.79 x 10^{-4} M, 4.90 x 10^{-4}M, and 2.45 x 10^{-4} M (equivalent to 500, 250, 100, 50, 25 ppm carbon, for a C5 acid) and analyzed by HPLC-UV, without any further treatment. Since we used an isocratic pump, different elution methods were developed and used throughout these experiments in order to minimize band broadening, achieve adequate peak integration (and thus repeatability), as well as to obtain practical elution times. Flow rate was 1.0 ml/min for all measurements, with the column being kept at ambient temperature, and pH was adjusted to 3.0 at all times with o-phosphoric acid as determined from the conductivity of the mobile phase (conductivity was converted into pH using a calibration curve (pH vs mv) derived daily prior to performing the measurements with standard buffer solutions), using a conductivity meter (in-house made device) mounted with an Accumet combination pH electrode with calomel reference. The mobile phases used for the various acids included in this experiment were as follows:

H2O (%v/v)	MeOH (%v/v)	Acids
99	1	Formic, Acetic
75	25	Propanoic
60	40	Butanoic, Pentanoic, 2-methylbutanoic

Table-2.2: mobile phase compositions for all C1 - C5 acids investigated. PH adjusted to 3 with o-phosphoric acid.

The UV detector FSD selector (full scale deflection) and the integrator attenuation factor were adjusted to obtain a peak of an acceptable intensity with minimal baseline noise. Peak areas were then plotted against concentration and the linearity of the

instrumental response with concentration was determined from the correlation coefficient obtained from these peak area vs. concentration curves.

2.2.2 Assessment of possible adsorption on reactor walls and/or filters

A 2.0 x 10^{-3} M solution of trimethylacetic acid (solution I) was prepared by pipetting an aliquot from a 9.79 x 10^{-3} M trimethylacetic acid stock solution into a volumetric flask and completing to volume with pure water. This acid was selected because it was the least water-soluble acid of the whole series under study and thus, the one for which the possibility of adsorbing significantly on the reactor's walls was the greatest. After placing 60 ml of the 2.0 x 10^{-3} M trimethylacetic acid solution quantitatively into the reactor, the reactor was capped and the solution stirred in the dark for ca. 60 minutes. A 2ml aliquot was taken from the reactor and set aside for future analysis (solution II). At the same time, another aliquot of 2 ml was taken from the reactor, filtered through a 0.2 μm filter (MSI #NO1SP01300) and saved also for future analysis (solution III). All three solutions were then repeatedly analyzed by the HPLC-UV method.

The results obtained for these three treatments were statistically analyzed to determine if they were significantly different. The mobile phase was MeOH:H_2O 40:60, pH adjusted to 3 with o-phosphoric acid (see section 2.2.1 for details), flow rate of 1.0 ml/min, and the column was kept at ambient temperature.

2.2.3 Determination of required dark adsorption time

In a first experiment, 72 mg of TiO_2 Degussa P25 was transferred to the reactor followed by the addition of 20 ml of 3.77×10^{-3} M butanoic acid. The reactor was then stoppered and kept in the dark during magnetic stirring. The reactor was sampled over a two hours period at 15 minutes intervals. Aliquots volume was roughly 300 – 400 μL. The procedure was repeated twice over two different days.

In a second experiment, about exactly 2g of TiO_2 Degussa P25 was transferred into a 1000 ml volumetric flask. The flask was filled to volume with purified water and sonicated for 5 minutes. The flask was then put into a water bath mounted with a thermometer and sitting on a magnetic stirrer. Following stirring of the suspension for 5 minutes, 220 μL of isovaleric acid was spiked into the flask by means of a micropipet. The flask was then stoppered, and its content was stirred in the dark over a three hours period over which 2 ml aliquot were sampled at various time intervals. The "time zero" sample was prepared exactly as described above, with the exception that no TiO_2 Degussa P25 was used. Temperature remained at 22°C throughout the entire experiment.

Each aliquot was filtered through 0.22 μm filters (MSI #NO1SP01300) and analyzed by HPLC using the Waters HPLC system described earlier. The mobile phase was MeOH:H_2O at a ratio of 35:65, pH adjusted to 3 with o-phosphoric acid (see section 2.2.1 for details), and the flow rate of 1.0 ml/min. The column was kept at ambient temperature.

2.3 Rates of disappearance of C1 – C5 carboxylic acids

50.0 ml of a 2.0 x 10^{-3} M solution of an acid {formic, acetic, propanoic, 2-methylpropanoic (isobutanoic), butanoic, 2-methylbutanoic, 3-methylbutanoic (isopentanoic), pentanoic, and trimethyacetic acid} was added to reactor-1 (see section 2.1.1 for reactor specifications) which was containing a pre-weighted amount of 0.1000g of TiO_2 Degussa P25. The mixture was magnetically stirred in the dark for 90 minutes, after which an aliquot of ca. 400 μL was taken from the reactor by means of a plastic syringe with a needle. Irradiation was then initiated using irradiation set-up 1 (see section 2.1.3 for details) and samples (same volume as just specified) were taken from the reactor at various time intervals. The sampling frequency was high at the beginning and then gradually reduced. Immediately following sampling, aliquots were filtered through 0.2 μm spartman-3 filters (Teflon membrane, Schleicher & Schuell, IGFZ162) into small glass vials, which were then capped and kept in the dark waiting to be analyzed with the HPLC system described earlier.

The lamp was operated at a power of about 910 watts. The lamp power was frequently monitored to ensure that is would not exceed the range 900 – 920 Watts, making the appropriate corrections when required. Special care was given to the lamp power at the beginning of each run; the stability of the system increased with operation time.

Infrared radiations were filtered by means of a glass water bath positioned between the light source and the reactor. The full lamp spectrum was used; however, wavelength shorter than 320 were excluded from the cell due to the reactor material type (silicate glass), thus avoiding the possible photolysis of the acids taken here as potential

pollutants. The reactor (double jacketed) temperature was kept at 20 ± 1°C using a circulating water heating-cooling system.

In monitoring the temporal changes in the concentration of organic pollutants by isocratic HPLC, different elution methods were developed and used throughout these experiments to minimize band broadening, to achieve adequate peak integration (and thus repeatability), and to obtain respectable elution times. The flow rate was 0.8 ml/min for all measurements; the column was kept at ambient temperature, and pH was adjusted to 3.0 at all times with o-phosphoric acid (see section 2.2.1 for details). The mobile phases used in studies of the various acids are summarized in table 2.3:

H2O (%v/v)	CH3CN (%v/v)	Acids
100	0	Formic, Acetic, Propanoic
90	10	Butanoic, isobutanoic
80	20	Pentanoic, Isopentanoic, 2-methylbutanoic, Trimethylacetic

Table-2.3: mobile phase compositions for all C1 – C5 acids investigated. PH adjusted to 3 with o-phosphoric acid.

The residual amount of acid in each sample was determined from the HPLC peak area of the acid in each sample relative to that of the standard solution prepared for the experiment. The percent concentration of acid found in each sample was then plotted against time. A least-squares fit was derived for the linear portion of the curve, to obtain the rate of disappearance of the acid from the slope of the latter.

2.4 Disappearance rates of Total Organic Carbon for C1 – C5 carboxylic acids

Total Organic Carbon (TOC) analyses were performed concurrently with the HPLC measurement of the rates of disappearance of the pollutants using the experimental conditions described above in section 2.3. Sampling of the reactor contents was performed once. The 400 μL aliquot was of a sufficient volume to satisfy both the needs of the chromatographic method and those of the total organic carbon analytical method.

The Shimadzu TOC-500 Total Organic Carbon analyzer range and flow rate were set to 10 and 150 ml/min respectively. Injections of 40 μL were used. Because the instrument was not mounted with an auto sampler, a minimum of two injections per sample was performed. A two points calibration curve was prepared daily prior to analysis using potassium hydrogen phtalate working standards (as recommended by the manufacturer). These standards were prepared by appropriate dilutions of a mother solution of about 1000.0 ppm of carbon. Working standards were prepared at concentrations bracketing the samples' carbon content. The stock solution was stored at 4°C and prepared fresh monthly by crushing the standard with a mortar and pestle, followed by drying at about 120 °C for 90 minutes in an oven, and diluting the required amount of standard with purified water in a volumetric flask.

The residual amount of total organic carbon in each sample was measured as described above and was plotted against time (moles of Carbon vs., irradiation time). A least-squares fit was derived for the linear portion of the curve, and the rate of disappearance of total organic carbon was calculated from the slope of the latter.

2.5 Investigation of selected carboxylic acids for the presence of oxidized intermediates by HPLC-UV co-elution experiments

2.5.1 Determination of required irradiation time

Propanoic, butanoic, and valeric acid (linear C3 – C5 aliphatic carboxylic acids) as well as isobutanoic acid (or 2-methylpropanoic acid, branching on the carbon located at the alpha position) and 2-methylbutanoic acid (again, branching on the carbon at the alpha position) were degraded in an aqueous suspension of TiO_2 Degussa P25 and their degradation profiles were followed by HPLC techniques.

In a typical experiment, 60.0 ml of a solution of 1000 ppm of an acid was added to the glass reactor-1 containing about exactly 0.1200 g of the semiconductor TiO_2 powder. The suspension was stirred over a magnetic stirrer for a few seconds and then placed in a sonicator bath for 5 minutes, following which it was stirred again for about 60 minutes in the dark. The solution was then irradiated at wavelength greater than 320 nm using the Hg/Xe lamp operated at a ca. 910 watts. Other procedural details were the same as above (see section 2.3). The reactor-1 (double jacketed) temperature was kept at 20 ± 1°C using a recirculating water heating-cooling system.

One milliliter aliquots collected from the reactor at various time intervals were filtered through 0.2 μm filters into glass vials, which were capped and kept in the dark until the specimens were analyzed. The disappearance of the organic pollutants and the concurrent formation of intermediates were monitored by the HPLC method already described above.

Analytical conditions were adapted as required for each acid. The overall irradiation and analytical conditions are given in table 2.4.

	$PrCO_2H$	$IsoBuCO_2H$	$ValCO_2H$	$IsoValCO_2H$	$2\text{-}MeBuCO_2H$	$BuCO_2H$
Irradiation conditions						
Lamp Power (W)	910 ± 10	905 ± 5	910 ± 10	910 ± 10	910 ± 10	900
Distance cell from source (cm)	23 ± 0.5	23 ± 0.5	23 ± 0.5	23 ± 0.5	23 ± 0.5	23 ± 0.5
Analytical conditions						
T (°C)	20	20	20	20	20	
[Acid]\ppm	1000	1000	1000	1000	1000	1097
Vol. (ml)	60.0	60.0	60.0	60.0	60.0	60.0
Wt. TiO_2 (g)	0.1223	0.1190	0.1220	0.1220	0.1200	0.1200
Sampling. Vol (ml)	1.0	1.0	1.0	1.0	1.0	n.r.
Mobile phase	H_3PO_4 aq. PH 3.0	H_3PO_4 aq. PH 3.0	25:75 MeOH:H_2O pH 3.0	25:75 MeOH:H_2O pH 3.0	25:75 MeOH:H_2O pH 3.0	H_3PO_4 aq. PH 3.0
Flow rate (ml/min)	0.9	0.8	0.8	0.8	0.8	0.8
Inj. Vol. (μL)	20	20	20	20	20	20
Detector FSD (Au)	0.05	0.05	0.05	0.05	0.05	0.05
Detection λ (nm)	214	214	214	214	214	214
Attenuation	1	1	1	1	1	1
Chart speed (cm/min)	0.5	.03	0.5	0.5	0.5	0.3
Threshold	0	3	0	0	0	2

Table-2.4: irradiation and analytical conditions for all acids investigated for their degradation profile.

Analytical conditions						
Peak width	0.2	2	0.2	0.2	0.2	0.2
Run time (min)	12	40	25	20	25	40

Table-2.4 (Cont.): irradiation and analytical conditions for all acids investigated for their degradation profile.

For each acid, the peak areas of the major intermediates detected by HPLC-UV were plotted against time and the irradiation time where most intermediates reached their highest concentration was determined. All subsequent irradiations were performed for the same irradiation times.

2.5.2 HPLC-UV co-elution experiments

Following the degradation of an acid under the conditions described in section 2.5.1, the entire solution was filtered through 0.2μm 25mm o.d. filters (mounted onto a syringe) into a glass bottle. The bottle was then capped and kept in the dark until used for the co-elution experiments.

In the co-elution experiments, a small volume of an aqueous solution of a potential degradation intermediate or product was added to an aliquot of the irradiated solution of the acid under investigation, and the mixture was analyzed by the HPLC-UV detection technique. The resulting chromatogram was then compared with the one obtained for the irradiated solution and with the one obtained for the potential degradation product alone.

Solutions of the possible degradation products, or intermediates, were prepared by weighing an amount of the substance (liquid or solid) into a small glass vial followed by addition of a volume of water such that the resulting solution was of concentration

yielding an acceptable signal when added in small quantities to an aliquot of the irradiated solution; in all cases we made certain that the signal for the mixture of compounds present in the irradiated solution was not greatly diminished. The adequate concentration of the possible intermediate solution, as well as its proportion relative to the solution of the irradiated sample, was determined by injecting solutions of the suspected intermediate after mixing with water at various proportions (e.g.: 50:50, 40:60, 30:70, and others). For the co-elution experiment, water was replaced with the irradiated solution of the acid under investigation. The potential intermediates investigated for the acids enumerated in section 2.5.1 and table 2.4 are given in table 2.5 with information regarding their concentration and proportion relative to the degraded solution of the acid.

Valeric Acid ($ValCO_2H$), $[\ ]_o$ = 1000 ppm		
Intermediate	**[Intermediate] \ ppm**	**Intermediate : $ValCO_2H$**
$BuCO_2H$	200	10 : 90
$PrCO_2H$	1000	5 : 95
$AcCO_2H$	200	10 : 90
2-$HOPrCO_2H$	1000	10 : 90
2-$OprCO_2H$	1227	5 : 95
2-$HOBuCO_2H$	1026	10 : 90
Valeric Acid ($ValCO_2H$), $[\ ]_o$ = 1000 ppm (Cont.)		
Intermediate	**[Intermediate] \ ppm**	**Intermediate : $ValCO_2H$**
$AcrCO_2H$	50	10 : 90
2-$OvalCO_2H$	101	10 : 90
2-$HOValCO_2H$	1006	10 : 90
2-$OBuCO_2H$	119	10 : 90

Table 2.5: details concerning the preparation of mixtures of a potential intermediate spiked into a filtered aliquot of an irradiated solution of an acid. Initial concentration of the irradiated acid, concentration of the potential intermediate solution, and the ratio of the latter with respect to the former are given.

Propanoic Acid ($PrCO_2H$) – [ ]$_o$ = 1000 ppm		
Intermediate	**[Intermediate] \ ppm**	**Intermediate : $ValCO_2H$**
$2\text{-}HOPrCO_2H$	1000	20 : 80
$2\text{-}OprCO_2H$	100	10 : 90
$AcCO_2H$	1000	20 : 80
Butanoic Acid ($BuCO_2H$) – [ ]$_o$ = 1097 ppm		
Intermediate	**[Intermediate] \ ppm**	**Intermediate : $ValCO_2H$**
$2\text{-}HOBuCO_2H$	1000	10 : 90
Isobutanoic Acid ($IsoBuCO_2H$) – [ ]$_o$ = 1000 ppm		
Intermediate	**[Intermediate] \ ppm**	**Intermediate : $ValCO_2H$**
$2\text{-}HO\text{-}2\text{-}MePrCO_2H$	1000	10 : 90
2-Methylbutanoic Acid ($2\text{-}MeBuCO_2H$) – [ ]$_o$ = 1000 ppm		
Intermediate	**[Intermediate] \ ppm**	**Intermediate : $ValCO_2H$**
$2\text{-}HO\text{-}2\text{-}MeBuCO_2H$	1026	20 : 80

Table 2.5 (Cont.): details concerning the preparation of mixtures of a potential intermediate spiked into a filtered aliquot of an irradiated solution of an acid. Initial concentration of the irradiated acid, concentration of the potential intermediate solution, and the ratio of the latter with respect to the former are given.

2.6 Rates of disappearance of selected alpha-hydroxy and alpha-keto acids

Fifty milliliters (50.0 ml) of a solution 2.0 x 10^{-3} M solution in acid (2-hydroxybutanoic acid, 2-hydroxyvaleric acid, 2-ketovaleric acid, 2-methyl-2-hydroxybutanoic acid) was added to the reactor-1 containing a pre-weighed amount of 0.1000g of TiO_2. The mixture was magnetically stirred in the dark for 90 min, after which an aliquot of ca. 500 μL was collected from the reactor by means of a plastic syringe mounted with a stainless steel needle. Irradiation was then initiated and samples

(same volume as just specified) were taken from the reactor at 5-min intervals. Immediately following this sampling, aliquots were filtered through 0.2 μm spartman-3 filters (Teflon membrane, Schleicher & Schuell, IGFZ162) into small glass vials, which were capped and kept in the dark waiting for the samples to be analyzed with the HPLC system described earlier.

The specifications of the lamp and details of the experimental setup used in these experiments are given in Section 2.1.3. Details of the irradiation methods have also been described above. The reactor-1 (double jacketed) temperature was kept at 20°C ± 1°C using a circulating water heating-cooling system.

The disappearance of the organic pollutants was monitored by HPLC using the Waters 501 isocratic apparatus described earlier. The mobile phase for 2-hydroxyvaleric acid, 2-ketovaleric acid, and 2-methyl-2-hydroxybutanoic acid was MeOH:H_2O 25:75, whereas a 10:90 MeOH:H_2O mobile phase was used for 2- hydroxybutanoic acid. In all cases, the pH of the mobile phase was adjusted to 3.0 with o-phosphoric acid (see section 2.2.1 for details); the flow rate was set at 1.0 ml/min, and the column was kept at ambient temperature.

The residual amount of acid in each sample was determined from the HPLC peak area of the acid in each sample relative to that of the standard solution prepared for the experiment. The percent acid (100% corresponding to 2.0×10^{-3} M) found in each sample was then plotted against time. A least-squares fit was derived for the linear portion of the curve, and the rate of disappearance of the acid was calculated from the appropriate slope.

2.7 Dark adsorption measurements

Fifty milliliters (50.0 ml) of a 2 x 10^{-3} M aliphatic carboxylic acid solution (formic, acetic, propanoic, butanoic, trimethylacetic, 2-methylbutanoic, isobutanoic, valeric, 3-methylbutanoic, 2-hydroxyvaleric, 2-ketovaleric, 2-hydroxy-2-methylbutanoic) was introduced into a glass container containing 0.1000 g of TiO_2 Degussa P25 and a stirring bar. The glass container was stoppered, sonicated for 5 minutes, and the suspension was then stirred over a magnetic stirrer in the dark for a period of 90 min, after which the conductivity of the solution was measured using a conductivity meter (home-made device) mounted with an Accumet combination pH electrode with calomel reference. The conductivity of the solution was converted into pH using a calibration curve (pH vs. mV) derived daily prior to performing the measurements with standard buffer solutions. The container was sampled with a plastic syringe mounted with a stainless steel needle. The aliquot was filtered through 0.2 μm spartman-3 filters (Teflon membrane, Schleicher & Schuell, IGFZ162) into small glass vials. Vials were capped and stored in the dark for later analyses. All the manipulations just described were performed in a dark room lit with a red light. Samples were analyzed by HPLC using the apparatus described earlier. The mobile phases were as described in Table 2.6.

H2O (%v/v)	MeOH (%v/v)	Acids
99	1	Formic, Acetic, Propanoic
75	25	2-ketovaleric, 2-hydroxyvaleric
65	35	Butanoic, isobutanoic Pentanoic, Isopentanoic, 2-methylbutanoic, 2-hydroxy-2-methylbutanoic, Trimethylacetic

Table-2.6: pH adjusted to 3 with o-phosphoric acid. Flow rate 1.0 ml/min, ambient temperature.

Dark adsorption measurements were determined by dividing the peak area obtained for the filtered aliquot sampled from the glass container by the peak area obtained for an aliquot of the remaining same solution of the acid. This avoided additional variation that could be introduced by the preparation of an additional solution. Multiple injections of both the standard (not in contact with TiO_2) and the sample were performed, the number of which varied for each acid depending on the stability of the HPLC system at the time of measurement. Multiple runs were also performed for each acid, as needed, based on the reproducibility of the results obtained.

2.8 Dark adsorption measurements at high catalyst load

2.8.1 Determination of required dark adsorption time

Twenty five milliliters (25 ml) of a 2 x 10^{-3}M valeric acid solution whose pH was adjusted to 3.7 with perchloric acid or sodium hydroxide was introduced into a flask containing about exactly 0.5000 g of TiO_2 Degussa P25 (catalyst load of 20g/L) and a stirring bar. The pH of the solution was determined from its conductivity as described above.

The glass container was stoppered, sonicated for 10 min, and the suspension was then stirred magnetically in the dark for 60 min. The suspension was sampled at the beginning of the stirring period and then every 20 minutes thereafter with a plastic syringe mounted with a stainless steel needle. Samples were filtered through 0.2 μm spartman-3 filters (Teflon membrane, Schleicher & Schuell, IGFZ162) into small glass vials, which were then capped and kept in the dark for later analyses. All the

manipulations just described were performed at night, in a dim red light lit room (dark room). Samples were analyzed by the HPLC method using the Waters 501 isocratic chromatograph described earlier. The mobile phase was 35:65 MeOH:H_2O adjusted to pH 3.0 with o-phosphoric acid (see section 2.2.1 for details). The flow rate was 1.0 ml/min and the column was kept at ambient conditions.

2.8.2 Dark adsorption measurements

Formic acid, acetic acid, propanoic acid, butanoic acid, and 2-methylbutanoic were treated as described in section 2.8.1 with the exception that only one sample was collected from the suspension at the end of a 60 min dark adsorption equilibration. Liquid chromatographic conditions are given in Table 2.7.

H2O (%v/v)	MeOH (%v/v)	Acids
99	1	Formic, Acetic, Propanoic
65	35	Butanoic, 2-methylbutanoic

Table-2.7: pH adjusted to 3 with o-phosphoric acid. Flow rate 1.0 ml/min, ambient temperature.

Dark adsorption measurements were carried out by dividing the peak area obtained for the filtered aliquot sampled from the glass container by the peak area obtained for an aliquot of the remaining same solution of the acid as above. Multiple injections of both the standard (not in contact with TiO_2) and the sample were performed and the number of injections performed for each acid varied depending on the stability of the HPLC system at the time of measurement.

2.9 Kinetic determination of the rate constant k and of the adsorption equilibrium constant K for selected aliphatic carboxylic acids

Fifty milliliters (50.0 ml) of a solution of an aliphatic carboxylic acid (formic, acetic, propanoic, butanoic, 2-methylbutanoic, and valeric) at various concentrations (4.90×10^{-4} M, 7.34×10^{-4} M, 9.79×10^{-4} M, 1.47×10^{-3} M, 1.96×10^{-3} M, 3.92×10^{-3} M, and 5.87×10^{-3} M, corresponding to 50, 75, 100, 150, 200, 400, and 600 ppm of carbon based on a C_5 aliphatic carboxylic acid, e.g.: valeric acid) was adjusted to pH 3.7 with perchloric acid and/or sodium hydroxide by the procedure described earlier.

One of the above solution was then added to the reactor-1 containing a pre-weighted amount of 0.1000g of TiO_2 Degussa P25 (giving a catalyst load of 2.0 g/L). The resulting heterogeneous system was magnetically stirred in the dark for 60 minutes, after which an aliquot of about 500 μL was taken from the reactor by means of a plastic syringe with a needle. Irradiation was then initiated and samples (same volume as just specified) were taken from the reactor at various time intervals. Immediately following sampling, aliquots were filtered through 0.2 μm spartman-3 filters (Teflon membrane, Schleicher & Schuell, IGFZ162) into small glass vials that were then capped and kept in the dark for later analyses. All HPLC analyses were performed within 3 hours of sampling. The specifications of the lamp and experimental setup used in these experiments are given in section 2.1.3. The lamp was operated at 910 watts.

Infrared radiation wavelengths were filtered by means of a glass water filter positioned between the light source and the reactor. Wavelength shorter than 320 were excluded from the cell due to the reactor material type (silicate glass), thus avoiding the possible photolysis of the acids. The reactor (double jacketed) temperature was kept at

20 ± 1°C using a circulating water heating/cooling system. The reactor was thermostated at the very beginning, i.e., at the commencement of the dark equilibration period.

The disappearance of the aliphatic carboxylic acids was monitored by high-performance liquid chromatography using a HPLC system already described above. The flow rate was 1.0 ml/min for all measurements, with the column being kept at ambient temperature. The pH of the acid solutions was adjusted to 3.0 at all times with o-phosphoric acid (see section 2.2.1 for details). The mobile phases used for the various acids studied are summarized in table 2.8.

H_2O (%v/v)	MeOH (%v/v)	Acids
99	1	Formic, Acetic
75	25	Propanoic,
60	40	Butanoic, Valeric, 2-methylbutanoic

Table-2.8: mobile phase compositions for all C1 – C5 acids investigated. pH adjusted to 3 with o-phosphoric acid.

For each acid, and at each concentration, the amount of acid quantified in each sample was plotted against irradiation time. The rate of disappearance of the acid was derived from the slope of the curve located in the linear region of the degradation profile of the acid. All rate data were then plotted against concentration (initial rate vs concentration) and the apparent constants k (rate constant) and K (the adsorption equilibrium constant) were determined from the double reciprocal plot of the latter, that is a plot of k^{-1} vs. $[acid]^{-1}$.

2.10 GC-FID investigation of Valeric acid intermediates

2.10.1 Development of the extraction procedure – Selection of the extracting solvent

Two solutions containing valeric acid, butanoic acid, 2-hydroxyvaleric acid, and 2-ketovaleric acid, at a concentration of ca. 1000 ppm in each acid were prepared by weighing 0.1000 g of the acids into a 100-ml volumetric flask and completing to volume with water. 60-ml sample of each solution was transferred into a separatory funnel and acidified with 5 drops of concentrated hydrochloric acid. One of the two solutions thus prepared was extracted with three portions of 25 ml of ether (method EP-1); the other solution was extracted with dichloromethane (method EP-2). After each extraction, the aqueous phase was sampled using a plastic syringe mounted with a stainless steel needle, and then filtered through 0.2 μm filters. The samples were analyzed by the HPLC-UV technique using the chromatograph already described above. The mobile phase was 25:75 MeOH:H_2O acidified to pH 3.0 with o-phosphoric acid (see section 2.2.1 for details). The flow rate was 1.0 ml/min for all measurements and the column was kept at ambient temperature.

The percent recovery of these organic acids from the aqueous phase was evaluated by comparing the peak area of the appropriate acid in the non-treated solution (i.e.: the standard) to those obtained from the samples collected in the aqueous phase following each extraction.

2.10.2 Optimization of the extraction procedure with a real sample

Valeric acid was degraded under the conditions described in section 2.5.1. A 500 μL sample was taken from the reactor, filtered through a 0.2 μm filter into a glass

vial that was stoppered and stored in the dark until analyzed by HPLC-UV. The entire solution was then filtered through 0.2μm (25mm o.d.) filters into a glass bottle, it was transferred to a separatory funnel, acidified with 5 drops of concentrated hydrochloric acid and then extracted first with three portions of 25 ml of ether and later with three portions of 120 ml of ether. Once the extraction procedure completed, the aqueous phase was sampled by means of a plastic syringe mounted with a stainless steel needle, filtered through 0.2 μm filters. The filtrates were then analyzed by HPLC-UV using the system described earlier (see Section 2.10.1). The mobile phase was 25:75 MeOH:H_2O acidified to pH 3.0 with o-phosphoric acid (see Section 2.2.1 for details). The flow rate was 1.0 ml/min for all measurements and the column was kept at ambient temperature.

The efficiency of the extraction procedure was evaluated by comparing the peak area for the sample taken from the irradiated solution prior to performing the extraction to those obtained for the water phase that was sampled following the execution of the extraction procedure.

2.10.3 Verification of the GC-FID performance

The performance of the GC-FID Hewlett Packard 5890 series II system was verified using a Hewlett Packard Split Capillary Inlet Checkout sample (C_{16}/C_9 ratio 1.016, 1% w/w n-nonane (C_9) & n-hexadecane (C_{16}) in n-tetradecane (C_{14})), as recommended by the manufacturer. The adequacy of the system was thus established by comparing the chromatogram obtained from the GC-FID and that from the manufacturer for the same solution under like conditions. Both chromatograms were found to be the same.

2.10.4 Development of the derivatization procedure

In a typical experiment, and for those acids commercially available as a liquid, 1 drop of a pure acid (approximately 13 mg for valeric acid or 1.27×10^{-4} mole) was transferred into a glass vial and weighed by difference. 400 μL of BSTFA +1%TMCS 99:1, equivalent to 1.5×10^{-3} mole (the minimum recommended BSTFA to labile proton ratio was 2:1), was added to the vial which was capped and placed on a hot plate (low heat, to avoid violent boiling). It was heated for half an hour and vortexed every 5 minutes. 2 μL of the resulting solution was injected into the GC-FID Hewlett Packard 5890 series II system.

For those acids commercially available as solids (sodium salt), the acid was weighed into a glass vial followed by the addition of 400 μL of methanol and 100 μL of 0.5N HCl. The solution was then evaporated to dryness under a stream of Argon and then 400 μL of BSTFA was added to the vial. The rest of the procedure was as described above. The same applies to the injection volume and the instrumental settings. Representative experimental data are given in Table 2.9.

Acid	State	Weight (mg) or Volume (μL)	Volume BSTFA (μL)	Molar ratio
$ValCO_2H$	Liquid	12.81	400	12
$BuCO_2H$	Liquid	13.52	400	10
$ProCO_2H$	Liquid	15.52	400	7
$AcCO_2H$	Liquid	14.18	400	6
$2\text{-}OHPrCO_2H$	Liquid	17.54	400	4

Table-2.9: Representative experimental data for the derivatization of the acids listed. Molar ratio is the ratio of derivatizating agent (BSTFA + TMCS 99:1) to labile protons.

Acid	State	Weight (mg) or Volume (μL)	Volume BSTFA (μL)	Molar ratio
2-OprCO_2H	Liquid	16.76	400	8
AcrCO_2H	Liquid	14.28	400	8
2-OBuCO_2H	Liquid	17.37	400	9
OHAcCO_2H	Solid	8.44	400	7
2-OHBuCO_2Na	Solid	3.71	400	26
2-OHValCO_2 Na	Solid	3.18	400	33
2-OValCO_2Na	Solid	6.34	400	33

Table-2.9 (Cont.): Representative experimental data for the derivatization of the acids listed. Molar ratio is the ratio of derivatizating agent (BSTFA + TMCS 99:1) to labile protons.

The completeness of the above procedure was evaluated by injecting the above samples over time and ensuring that the peak areas thus obtained remained constant (within experimental error). GC eluting conditions were also optimized and were primarily retention times driven, i.e. long enough not to appear in the solvent front and not too long to avoid ending with a significant time-consuming procedure. These conditions were:

- Initial temperature: 50°C;
- Holding time: 2 minutes;
- Ramp-1: 10°C/min up to 80°C;
- Ramp-2: 25°C/min up to 270°C;
- Holding time: 10 minutes;

2.10.5 Confirmation of the efficiency of the derivatization procedure with a simulated sample

60 ml of an aqueous solution containing about exactly 1000 ppm of valeric acid, butanoic acid, 2-hydroxyvaleric acid, and 2-ketovaleric acid was transferred into a separatory funnel, acidified with 5 drops of concentrated hydrochloric acid and extracted with 3 portions of 120 ml of ether. The ethereal extract was dried over magnesium sulfate anhydrous, filtered under water vacuum through a Buckner funnel mounted with a 0.2 µm fritted disk (Pyrex USA no. 36060, 60 ml, ASTM 10 – 15 M), and then, the ether was evaporated using a Buchï Rotavapor-R rotary evaporator immersed into a water bath set at 50°C. The round bottom flask containing the residue was transferred under a stream of argon followed by the addition of 3 ml of derivatizing agent (BSTFA / 1% TMS). The flask was stoppered and heated over a water bath at 80°C for 30 minutes with magnetic stirring.

Following the above, GC analyses were performed using a Hewlett Packard 5890 series II GC-FID on (1) the pure derivatizing agent, (2) the derivatized extract (two first portions of 120 ml of ether), and (3) the last ethereal extract of the extraction procedure, which was treated like the latter (dried, filtered, evaporated, derivatized, and finally heated). The GC conditions were the same as those determined under section 2.10.4. The chromatograms thus obtained were compared to evaluate the entire procedure, i.e.: from the extraction phase down to derivatization and analysis.

2.10.6 Relative retention times' determination

The acids commercially available as a liquid and those commercially available as a solid where treated as described in Section 2.10.4 with the exception that 1 drop of valeric acid (approximately 13 mg or 1.27×10^{-4} mole) was also added to the glass vial. 1 μL of the resulting solution was injected into the GC-FID system. The temperature programming was as follows:

- Initial temperature: 50°C;
- Holding time: 2 minutes;
- Ramp-1: 70°C/min up to 270°C;
- Holding time: 10 minutes;

The relative retention times of all acids versus valeric acid were calculated and the standard deviation on these values was estimated from the variance on the retention time obtained for the peak of valeric acid, who was present in all solutions. These relative retention times were compared to those obtained for the peaks of a chromatogram for an irradiated valeric acid solution analyzed under the same conditions in trying to identify some of these unknown intermediates. The latter chromatogram was also compared to that of a blank. Sample preparation was as follows:

400 ml of a 1000 ppm valeric acid solution was transferred into reactor-2 (see section 2.1.2 for details) containing about exactly 0.8000 g of TiO_2 Degussa P25, providing a catalyst load of 2 g/L. The resulting heterogeneous system was sonicated for 5 minutes. Irradiation was initiated immediately. The specifications of the lamp used in these experiments are given in Section 2.1.4. The lamp was operated at 910 watts as described previously.

Infrared radiations were filtered by means of a glass water filter positioned between the light source and the reactor. Wavelength shorter than 320 were excluded from the cell due to the reactor material type (silicate glass). The reactor could not be thermostated by means of a water-cooling system since it was not double jacketed. Instead, an air blower was used (blowing air onto the reactor) and the temperature was monitored during the run at random intervals using a partial immersion glass thermometer. Temperature remained in the range 20 – 24 °C throughout the degradation, which was performed for 8 hours.

Following the degradation, the entire suspension was filtered under water vacuum through a Buckner funnel mounted with a fritted disk (Pyrex USA no. 36060, 60 ml, ASTM 4 – 4.5 F). 60 ml of the filtrate was subsequently treated as described earlier in section 2.10.5. The blank was prepared as per the exact procedure above with the exception that no valeric acid was present in the solution that was irradiated.

2.11 Optimized overall procedure for method transfer to GC-MS

The irradiation procedure was as described in section 2.10.6. Once the degradation was completed, the entire suspension was filtered under water vacuum through a Buckner funnel mounted with a fritted disk (Pyrex USA no. 36060, 60 ml, ASTM 4 – 4.5 F). 120 ml of the filtrate was treated as described earlier in Section 2.10.5 but the amount of all the chemicals used in this treatment was increased by two fold. These steps were repeated until all of the 400 ml filtrate was extracted.

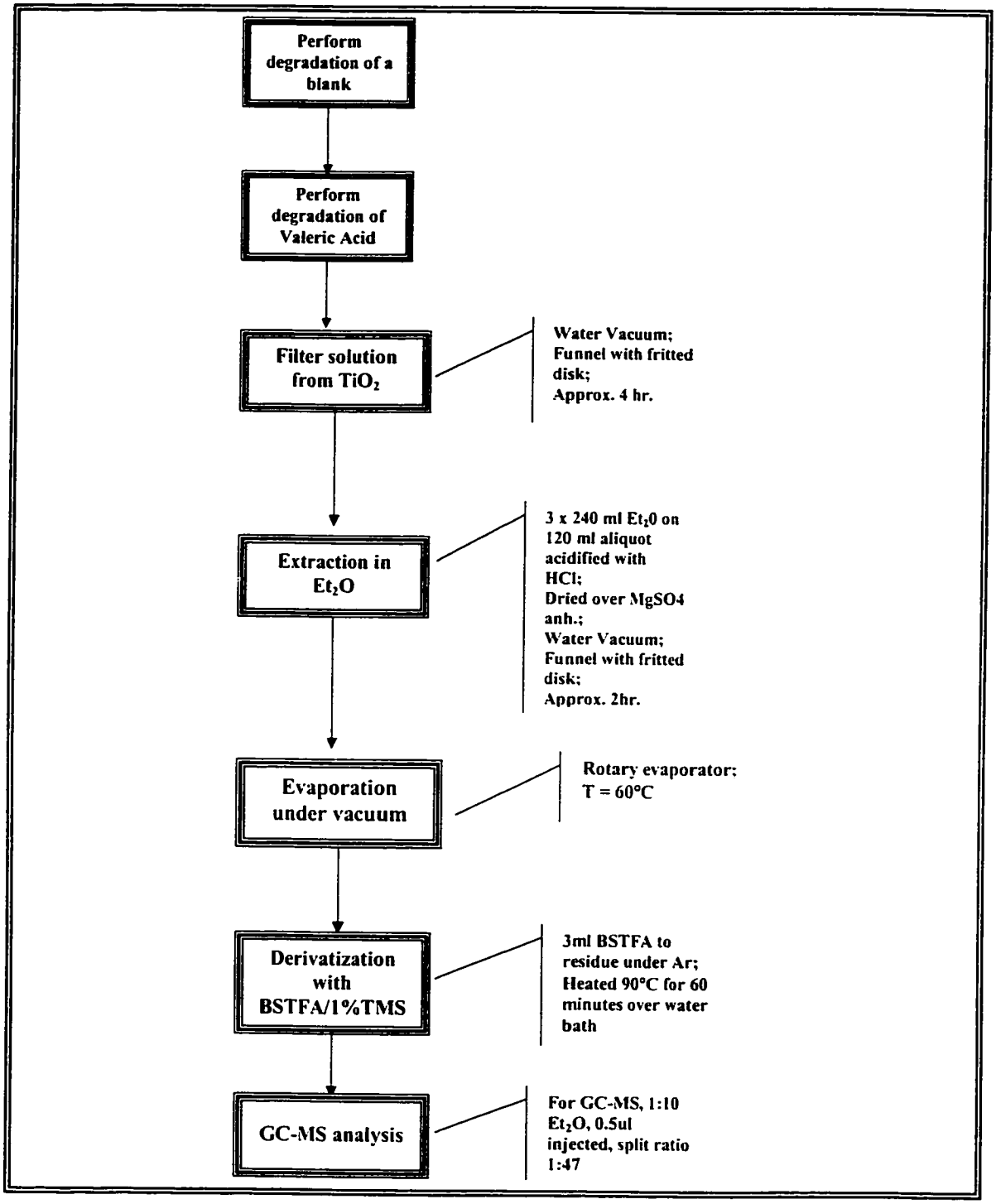

Figure 2.2: Global representation of the procedure starting from the irradiation process down to analysis.

The round bottom flask containing the residue was also treated as described earlier in Section 2.10.5. A blank was also ran by performing the entire above procedure, excluding valeric acid from the reactor. A schematic of the entire procedure is given in Figure 2.2.

2.12 GC-MS investigation of the intermediates of Valeric acid

400 ml of a 1000 ppm valeric acid solution was treated as described in section 2.11. 400 ml of a blank solution (i.e. purified water) was also treated the same way. After completion of the derivatization procedure, the derivatized residue as well as the blank was diluted by a factor of 10 with anhydrous ether and 0.5μL of each sample was analyzed by GC-MS. Chromatographic conditions were:

- Solvent delay: 5.5 min;
- Flow rate: 0.7 ml/min;
- Split ratio: 1:47
- Initial temperature: 30°C;
- Holding time: 5 minutes;
- Ramp-1: 70°C/min up to 120°C;
- Holding time: 1 minutes;
- Ramp-2: 40°C/min up to 240°C;
- Ramp-3: 70°C/min up to 270°C;
- Holding time: 3 minutes;

The total ion chromatogram obtained for the blank was compared to that of the irradiated sample. The peaks found in the latter that did not appear in the chromatogram of the blank were located and used for identification purposes which was performed using a mass spectra library. The validity of the proposed identification of the intermediates of irradiated valeric acid by the library was analyzed based on their retention times and molecular weights, using the information that was gained with the chromatographic behavior of these compounds (as per section 2.10.4).

2.13 Limiting Photonic efficiency of Formic acid

50.0 ml of a 3.92 x 10^{-3} M solution of formic acid was added to a reactor containing various pre-weighted amount of TiO_2 Degussa P25 (about exactly 0.3000g, 0.6000g, 0.9000g, 1.2000g, 1.5000g, 1.8000g, and 2.1000g) and the pH of the resulting suspension was adjusted to 3.70 with sodium hydroxide and/or perchloric acid as described earlier.

Following pH adjustment, the solution was sonicated for 5 minutes and then magnetically stirred for 60 minutes, time after which an aliquot of about 400 μL was taken from the reactor by means of a plastic syringe with a needle. All these operations were performed in the dark. Irradiation was then initiated and samples (same volume as just specified) were taken from the reactor over time. Immediately following sampling, aliquots were filtered through 0.2 μm spartman-3 filters (Teflon membrane, Schleicher & Schuell, IGFZ162) into small glass vials. HPLC analyses were performed immediately.

The specifications of the lamp and of the experimental setup are given in section 2.1.5. The lamp was operated at 910 watts in the same manner as described earlier. The reactor (double jacketed) temperature was kept at 20 ± 1°C using a circulating water heating/cooling system. Single wavelength irradiation was used using a monochromator positioned between the light source and the reactor. A wavelength of 365 nm was used for all runs.

The disappearance of formic acid was monitored by high-performance liquid chromatography using the HPLC system consisting of a Waters 501 isocratic pump mounted with a 20μL injection loop, a Waters 441 UV absorbance detector with single wavelength capability @ 214 nm, a Hewlett Packard HP3396A integrator, and a Supelco

Canada Spherisob octyl 5μm, 250mm x 4.6mm HPLC column. The mobile phase was 1:99 MeOH:H_2O with pH adjusted to 3.0 with o-phosphoric acid (same way as for pH of the solutions). The flow rate was 0.8 ml/min for all measurements, with the column being kept at ambient temperature. The residual amount of acid in each sample was determined from the HPLC peak area of the acid in each sample relative to that of the standard solution prepared for the experiment. The quantity in μg of formic acid found in each sample was plotted against time.

A least-squares fit was derived for the linear portion of the curve, and the rate of disappearance of the acid was calculated from the slope of the latter. These initial rate data were converted into photonic efficiencies by dividing them by the photon flow from the light source reaching the interior of the reactor, value that was determined by chemical actinometry using Amberchrome 540 (see below). A plot of the reciprocal of photonic efficiencies versus the reciprocal of catalyst concentrations (g / L) was derived, from which the limiting photonic efficiency of formic acid, which is in fact its quantum yield, was obtained from the y-intercept. This value was finally used to determine the quantum yields of acetic, propanoic, butanoic, 2-methylbutanoic, and valeric which were degraded under the exact same conditions as formic acid (see section entitled "Kinetic determination of the rate constant k and of the adsorption equilibrium constant K for selected aliphatic carboxylic acids").

For the determination of the photon flow from the light source reaching the interior of the reactor, 33.49 mg of Amberchrome 540 was weighed into a 25 ml volumetric flask and completed to volume with toluene (recommended concentration is 25 mg per 20 ml). An aliquot of the solution was transferred into a 1cm quartz cuvette

containing a micro-magnetic stirring bar. The cuvette was mounted onto a magnetic stirring plate at the exact same distance where the front of the reactor used for the above experiment stood from the light source and the Amberchrome solution was irradiated under the same conditions as those used for formic acid. The absorbance of the solution was measured at 494 nm at various time intervals and the absorbance of the solution was plotted against time. The photon flow was determined from the slope of the curve (change in absorbance at 494 nm per unit time).

Chapter 3

Results & Discussion

3.1 General considerations

3.1.1 HPLC-UV linearity range of selected acids

3.1.1.1 Introduction

Prior to performing any kinetics measurement, it was essential to ensure that under specific experimental conditions, the HPLC peak areas (instrumental response) obtained for a series of samples taken from the reactor at various time intervals would be directly proportional to concentration and free from instrumental bias. Without this condition being met, kinetic data thus derived would not reflect the true process output and could lead to draw erroneous conclusions. Another key information is the limit of quantification of the methods in question. Prior to degrading any acids, it was important to ensure that the chosen working concentration could be handled by the instruments available in the laboratory.

3.1.1.2 Results

The linearity range of the methods used throughout this study was determined for the whole linear series of C1 to C5 carboxylic acids (formic acid, acetic acid, propanoic acid, butanoic acid, and pentanoic or valeric acid) as well as for a branched C5 acid, 2-methylbutanoic acid. The series C1 to C5 carboxylic acids was selected to include all of the chromatographic eluting conditions that were developed for these acids. Using the HPLC-UV isocratic method, different eluting conditions were developed and used

throughout. This was essential in minimizing retention time and in contributing to minimize band broadening, allowing to achieve adequate peak integration which impacts on the repeatability of a method. Even though eluted under the same chromatographic conditions as valeric acid (both are C5 acids), 2-methylbutanoic acid was chosen as a representative "member" of the branched acids included in this study.

A good example that clearly demonstrates the importance of doing such preliminary investigation is illustrated in figure 3.1.1.2-1. Over the concentration range 9.79 x 10^{-4} M to 9.79 x 10^{-3} M (45 - 450 ppm), with the detector's full scale deflection set to 0.02 a.u. (absorbance units) and the integrator's attenuation factor set to 3, the instrumental response was not linear, as evident in figure 3.1.1.2-1; the determination coefficient r^2 for this plot was 0.9289 (correlation factor r = 0.9638) . However, when the same solutions were used with different instrumental settings (detector's full scale deflection set to 0.05 a.u., the integrator's attenuation factor same as above), a much better

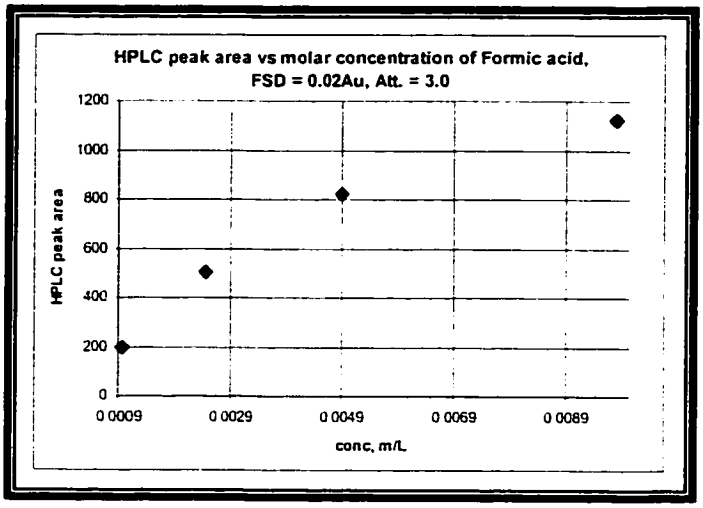

Figure 3.1.1.2-1 : HPLC peak area vs formic acid concentrations of (a) 9.79 x 10-4 M; (b) 2.45 x 10-3 M; (c) 4.90 x 10-3 M; (d) 9.79 x 10-3 M. Waters 441 UV absorbance detector with single wavelength capability @ 214 nm, FSD = 0.02. Hewlett Packard HP3396A integrator, attenuation of 3

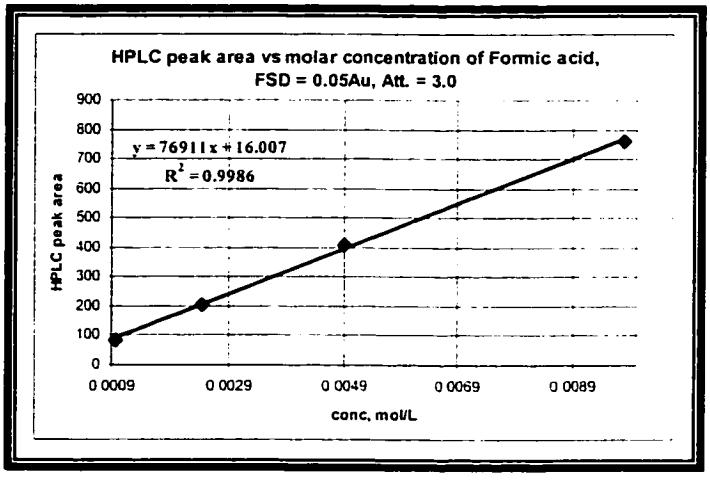

Figure 3.1.1.2-2 : same conditions as in figure 3.1.1.2-1, but with the detector's FSD set to 0.05

linearity was obtained (see figure 3.1.1.2-2), with r = 0.9993. In the above example, having proceeded with the degradation of formic acid at a concentration of 9.79 x 10^{-3} M (450 ppm) with the conditions giving rise to the HPLC peak area vs concentration profile illustrated in figure 3.1.1.2-1, a higher decrease in formic acid concentration would have been obtained at any time point than what would have been uniquely caused by the degradation of the acid exposed to the photocatalytic process, because the decrease in acid concentration measured at any time interval would have been influenced in part by the fact that the instrumental response was not linear in this concentration range. The overall results for this investigation are given in table 3.1.1.2-1 below:

Valeric Acid								
[mol/L] range		**Mobile phase**				**Detector**	**Integrator**	**Linearity**
From	**to**	**MeOH**	**H2O**	**pH**	**Flow (ml/min)**	**FSD\Au**	**Attenuation**	**r**
0.000245	0.000979	40	60	3.0	1.0	0.01	2	0.9955
0.000979	0.00979	40	60	3.0	1.0	0.02	3	0.9972
2-methylbutanoic acid								
[mol/L] range		**Mobile phase**				**Detector**	**Integrator**	**Linearity**
From	**to**	**MeOH**	**H2O**	**pH**	**Flow (ml/min)**	**FSD\Au**	**Attenuation**	**r**
0.000245	0.000979	40	60	3.0	1.0	0.01	3	0.9968
0.000979	0.00979	40	60	3.0	1.0	0.05	3	0.9998

Table 3.1.1.2-1 : Global results from the linearity range study for a few selected acids. The HPLC system consisted in a Waters 501 isocratic pump mounted with a 20µL injection loop, a Waters 441 UV absorbance detector with single wavelength capability @ 214 nm, a Hewlett Packard HP3396A integrator, a Supelco Canada Spherisob octyl 5µm, 250mm x 4.6mm HPLC column. Concentration range investigated spanned from 2.45 x 10^{-4} M to 9.79 x 10^{-3} M.

Butanoic acid								
[mol/L] range		Mobile phase				Detector	Integrator	Linearity
From	to	MeOH	H2O	pH	Flow (ml/min)	FSD\Au	Attenuation	r
0.000245	0.000979	40	60	3.0	1.0	0.01	2	0.9965
0.00245	0.00979	40	60	3.0	1.0	0.05	3	1.0000
Propanoic acid								
[mol/L] range		Mobile phase				Detector	Integrator	Linearity
From	to	MeOH	H2O	pH	Flow (ml/min)	FSD\Au	Attenuation	r
0.000245	0.000979	25	75	3.0	1.0	0.01	2	0.9986
0.000979	0.00979	25	75	3.0	1.0	0.05	3	0.9994
Acetic acid								
[mol/L] range		Mobile phase				Detector	Integrator	Linearity
From	to	MeOH	H2O	pH	Flow (ml/min)	FSD\Au	Attenuation	r
0.000245	0.000979	1	99	3.0	1.0	0.01	2	0.9979
0.000979	0.00979	1	99	3.0	1.0	0.05	3	1.0000
Formic acid								
[mol/L] range		Mobile phase				Detector	Integrator	Linearity
From	to	MeOH	H2O	pH	Flow (ml/min)	FSD\Au	Attenuation	r
0.000245	0.000979	1	99	3.0	1.0	0.01	2	0.9988
0.000979	0.00979	1	99	3.0	1.0	0.05	3	0.9993

Table 3.1.1.2-1: same as above.

In the range of 9.79 x 10^{-4} M to 9.79 x 10^{-3} M, an acceptable linearity was achieved for all acids with the detector's full scale deflection set to 0.05 a.u. and the integrator's attenuation factor set to 3, with the exception of valeric acid for which the detector's full scale deflection was set to 0.02 a.u. The correlation coefficients ranged from 0.9972 for valeric acid up to 1.000 for butanoic acid and acetic acid, an example of

which is illustrated in figure 3.1.1.2-3. At concentrations lower than 9.79 x 10^{-4} M, the integrator's full-scale deflection had to be reduced from 0.05 to 0.01 a.u. because the signal (or HPLC peak area) was not intense enough, causing integration problems and a lack or repeatability. However, linearity was not affected. The integrator's attenuation factor also had to be reduced from 3 to 2. With these settings, the correlation coefficients ranged from 0.9955 for valeric acid up to 0.9988 for formic acid. For most acids, the lowest workable concentration was found to be 2.45 x 10^{-4} M corresponding to approximately 11 ppm of formic acid and 25 ppm of valeric acid. At concentrations lower than 2.45 x 10^{-4} M, and with the previously mentioned instrumental settings, the signal to noise ratio began to be important. The detector's full-scale deflection and the integrator's attenuation factor could not be reduced further without significantly affecting the methods' repeatability.

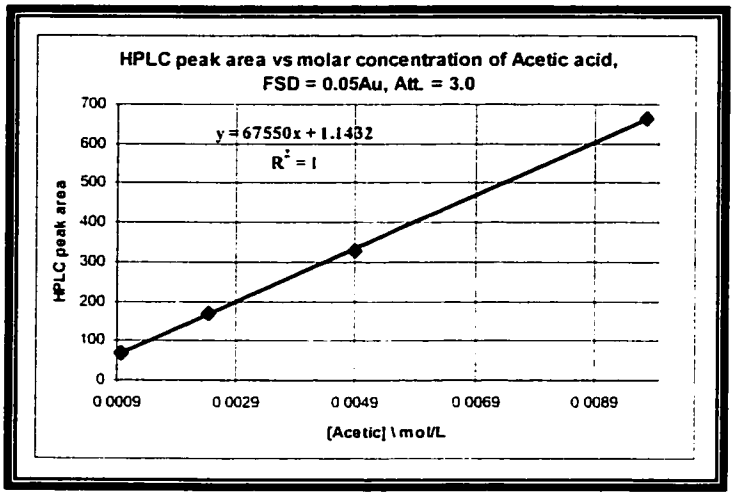

Figure 3.1.1.2-3 : HPLC peak area vs acetic acid concentrations of (a) 9.79 x 10-4 M; (b) 2.45 x 10-3 M; (c) 4.90 x 10-3 M; (d) 9.79 x 10-3 M. Waters 441 UV absorbance detector with single wavelength capability @ 214 nm, FSD = 0.05. Hewlett Packard HP3396A integrator, attenuation of 3

All kinetics experiments were carried out by using the instrumental settings given in table 3.1.1.2-1. A large proportion of the kinetics run that were carried out in this study were performed at an acid concentration of 2.0 x 10^{-3} M which corresponds to the concentration range for which the settings of 0.05 a.u. and 3 for the detector's FSD and integrator's attenuation factor were used and which yielded meaningful results. Note that

a valeric acid concentration of 2.0 x 10^{-3} M corresponds to ca. 204 ppm. As stated previously, the lowest workable concentration was 2.45 x 10^{-4} M or approximately 25 ppm. Since our kinetics experiments dealt with initial rates of disappearance, this lower concentration of 25 ppm, which corresponds to roughly 12% of the initial acid concentration, was of no concern, since the degradation data that were used to determine rate data were at much higher concentrations than 12% of initial. No experiments were performed at concentration lying outside the range 2.45 x 10^{-4} M to 9.79 x 10^{-3} M.

3.1.2 Assessment of possible adsorption on reactor walls and/or filters

3.1.2.1 Introduction

Dark adsorption measurements were performed on numerous occasions in this study, because we were in part interested to determine if there was a clear trend between the initial rates of degradation of the acids under investigation and their associated dark adsorption values (this will be covered in a later section). All of the samples that were collected from a reactor were filtered before they were injected into the HPLC system. This brings up the possibility that some of the acids under investigation could adsorb onto the filter's membrane, thus leading to higher dark adsorption values than those that are exclusively attributed to the catalyst and the solute alone. This is explained by the fact that dark adsorption values were determined from the peak area obtained for the sample of an acid solution exposed to the photocatalyst for a given time period in the dark and compared to the peak area for a sample of the same solution which had not been exposed to the catalyst, as described by equation 3.1.2.1-1 below:

$$DA = 100 - \left[\frac{PA_{CES}}{PA_{CFS}} \times 100 \right] \qquad (3.1.2.1\text{-}1)$$

where DA stands for dark adsorption, PA_{CES} stands for peak area, catalyst-exposed solution, and PA_{CFS} stands for peak area, catalyst-free solution. The adsorption of an acid onto a filter will cause PA_{CES} to be lower, and thus the calculated dark adsorption value will be higher than if adsorption onto the filter had not occurred. Since adsorption phenomena are solute/substrate specific, if adsorption occurs on the filters during the filtration step, it can be anticipated that different solutes will adsorb to the filter's membrane to different degrees, thus yielding an overall erroneous trend. This assumes of course that adsorption is relatively significant for some acids while being insignificant for others.

3.1.2.2 Results

The HPLC results that were obtained for (1) a 2.0 x 10^{-3} M trimethylacetic acid standard solution, (2) the same solution as in (1) but exposed to the reactor, and (3) the same solution as in (2) followed by filtration, are shown in table 3.2 and illustrated in figure 3.1.2.2-1. A visual inspection of the graph shown in figure 3.1.2.2-1 clearly indicates that solute adsorption on reactor walls, as well as on the filter membrane does not occur, if any it is negligibly small. This was further confirmed by performing a single-factor analysis of variance (α = 0.05,) for which the null hypotheses H_o was that all three sets of data were the same, or that $\mu_{std} = \mu_{reactor} = \mu_{reactor + filter}$. The calculated f value ($f_{calc.}$) was 0.40 and was smaller than its critical value (f_{crit} = 4.74.). We are thus 95% confident that

	HPLC peak area		
	STD (1)	Reactor (2)	Reactor & filter (3)
	831	831	853
	848	828	849
	836	840	823
		839	
Mean	838	835	842
std	8.74	5.92	16.29
RSD	1.04	0.71	1.94

Table 3.1.2.2-1: HPLC individual peak areas, mean, standard deviation and relative standard deviation obtained for (1) a 2x 10^{-3} M standard solution of trimethylacetic acid (STD), (2) same solution as in (1) but that have been exposed to the reactor prior to analysis, and (3) same solution as in (2) but that was filtered prior to analysis.

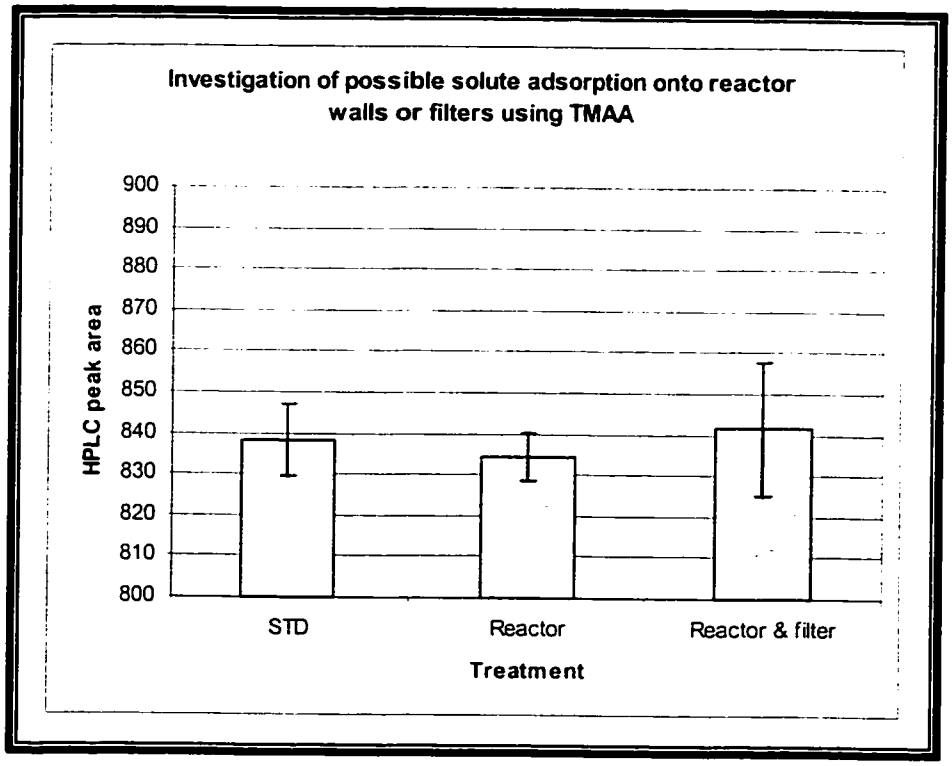

Figure 3.1.2.2-1 : same explanation as in table 3.1.2.2-1. Bars represent the mean HPLC peak area for each data set while error bars are equal to ± 1S from the mean

this hypothesis is valid and that the difference between the three treatments is not significant.

This experiment was performed only with trimethylacetic acid because it was the least soluble of the series. This compound thus offered the highest challenge with respect to possible adsorption onto the filter's membrane and or onto the reactor's walls. In water, it solubility is 0.025g/ml, as opposed, for example, to valeric acid (pentanoic acid) or 3-methylbutanoic acid (isobutanoic acid) for which the solubility in water is 0.033g/ml and 0.050 g/ml respectively. All C_4 and lower than C_4 acids were more soluble in water. Thus, the above results are appropriate for all of the acids examined in this study.

3.1.3 Determination of required dark adsorption time

3.1.3.1 Introduction

Dark adsorption time profiles were performed with butanoic acid and isovaleric acid to determine the time required to reach not net change in dark adsorption values over time and thus ensure that meaningful dark adsorption data were obtained. Butanoic acid was selected to represent the linear series of the carboxylic acids included in this study, whereas isovaleric acid (3-methylbutanoic acid) was selected to represent the branched acids.

3.1.3.2 Results

Results obtained for the two experiments performed with butanoic acid over two different days are shown below:

Time	HPLC Area		Mean	stdev	RSD
15	36.8	38.1	37.5	0.92	2.45
30	37.1	36.4	36.8	0.49	1.35
45	36.4	36.7	36.6	0.21	0.58
60	36.9	37.4	37.2	0.35	0.95
75	37.5	36.9	37.2	0.42	1.14
90	36.2	36.7	36.5	0.35	0.97
105	36.3	37	36.7	0.49	1.35
120	36.1	36	36.1	0.07	0.20

Table-3.1.3.2-1: HPLC individual peak areas, means, standard deviations and relative standard deviations for butanoic acid samples taken over time in a reactor that was kept in the dark. $[BuCOOH]_o$ was 3.77 x 10^{-3} M, $[TiO_2$ P25] was 3.6 g/L. Initial volume of 20 ml.

Time	HPLC Area		Mean	stdev	RSD
15	35.7	36.6	36.2	0.64	1.76
30	36.7	36.2	36.5	0.35	0.97
45	36.5	36.4	36.5	0.07	0.19
60	36.2	36.4	36.3	0.14	0.39
75	36.4	36.7	36.6	0.21	0.58
90	36.5	36.6	36.6	0.07	0.19
105	36.7	36.6	36.7	0.07	0.19
120	36.9	36.8	36.9	0.07	0.19

Table-3.1.3.2-2: Same as for table 3.1.3.2-1. Experiment performed on a second day.

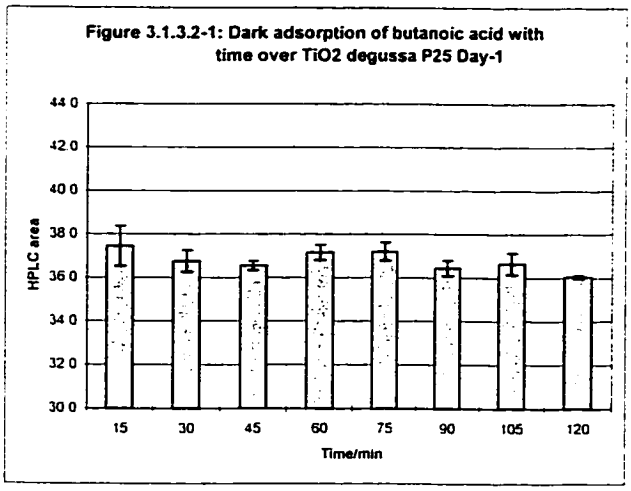

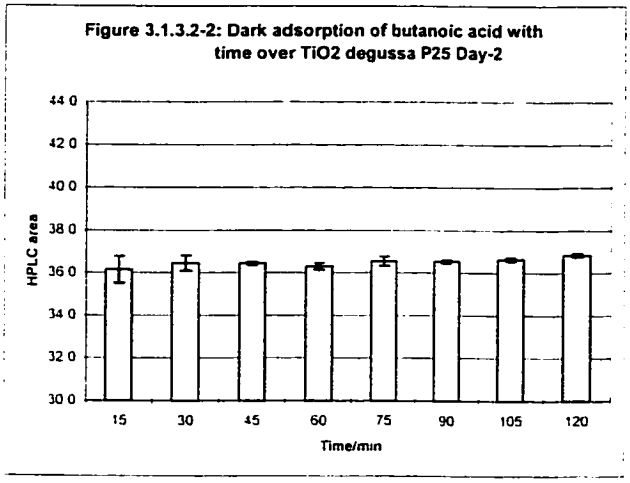

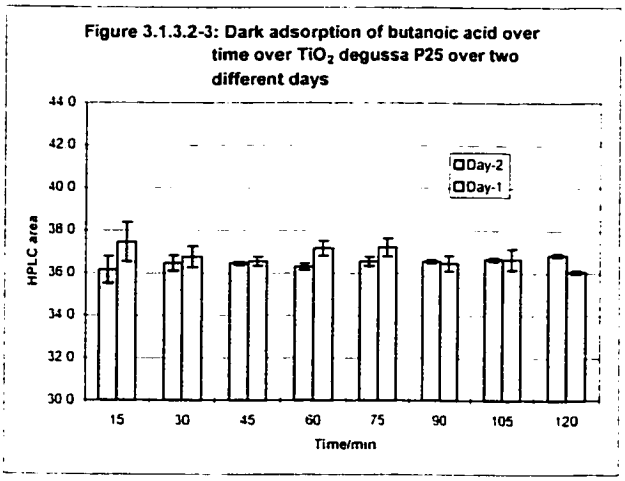

A one-factor analysis of variance ($\alpha = 0.05$) was performed on the data set obtained for day-1. The calculated f value (f_{calc}) was 1.86 and was lower than its associated critical f value (f_{crit}) which is 3.50. The difference between the HPLC peak areas at all time points is thus not statistically different at a confidence level of 95%. The same applies to the data set obtained on the second day (f_{calc} = 1.18 < f_{crit} = 3.50). A visual inspection of the dark adsorption time profiles, shown in figure 3.1.3.2-1 and 3.1.2.3-2 for the experiments performed on day 1 and on day 2 respectively, clearly illustrates that these hypotheses are indeed valid. There are no clear trends indicating a decrease in HPLC area over the time period investigated.

A two-factor analysis of variance with replication (i.e. time and day, using the individual values at each time points rather than the means) was also performed on the two data sets. The calculated f value associated to the inter-day variation was 4.35, whereas its related critical value was 4.49. Thus, it cannot be claimed that the inter-day difference in the HPLC peak areas is significant. Once again, a visual inspection of the two profiles (figure 3.1.3.2-3) helps to understand this conclusion, since for most time points there is an overlap between the dispersion (graphically illustrated by the error bars representing 1 standard deviation) of the data between the data sets obtained on the two different days. It can thus be concluded that no significant change in adsorption of butanoic acid on TiO_2 Degussa P25 occurred over the time period 15 – 120 minutes, under the applied experimental conditions. An applied dark adsorption time of 15 minutes would thus be sufficient for dark adsorption measurements or for kinetic runs.

The results obtained for the experiment involving isovaleric acid follows (table 3.1.3.2-3):

Time	HPLC Area				Mean	stdev	RSD
0	573	585	590	572	580	8.9	1.54
15	559	545	542	539	546	8.8	1.62
30	558	565	550	542	554	9.9	1.80
60	566	552	548	542	552	10.2	1.85
120	554	549	550	547	550	2.9	0.54
180	545	534	542	554	544	8.3	1.52

Table-3.1.3.2-3: HPLC individual peak areas, means, standard deviations and relative standard deviations for isovaleric acid samples taken over time in a reactor that was kept in the dark. $[I\text{-}ValCOOH]_0$ was 2.0 x 10^{-3} M, $[TiO_2$ P25] was 2.0 g/L. Initial volume of 25 ml.

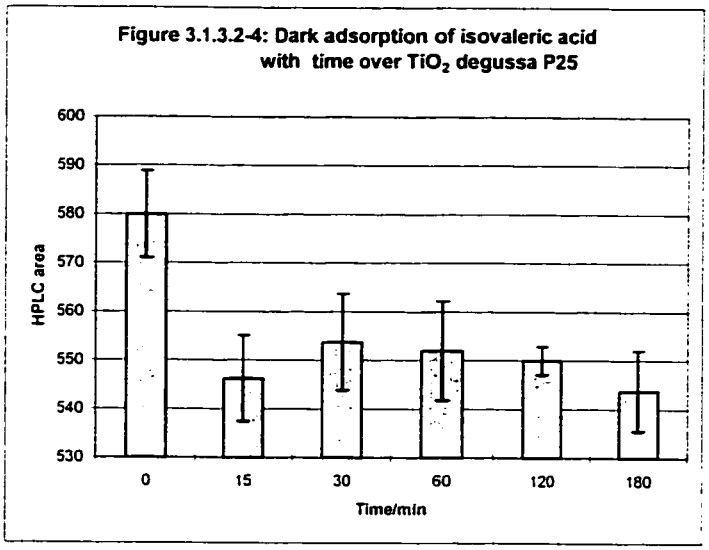

This time, with a time zero sample included, it seems rather obvious when looking at figure 3.1.3.2-4 that adsorption of the carboxylic acid occurred over the first 15 minutes of the experiment and remained practically unchanged thereafter. This was confirmed by a single factor analysis of variance that was performed on the data sets obtained over the time period spanning from 15 to 180 minutes, and for which the result indicates no statistical significant difference between the HPLC peak area over these time points ($\alpha = 0.05$, $f_{calc} = 0.94 < f_{crit} = 3.06$). The significant difference between the time points 0 and 15 minutes was demonstrated by conducting a two sample t-test assuming equal variance at a confidence level of 95% and for which the calculated t value (t_{calc}) of 5.38 was higher than its associated critical value (tcrit = 2.45, when $t_{calc} > t_{crit}$, reject the null hypothesis H_o: $\mu_1 = \mu_2$). Once again, and just like for butanoic acid, no significant change in adsorption of isovaleric acid on TiO_2 degussa P25 occurred beyond a dark adsorption time of 15 minutes under the applied experimental conditions. An applied dark adsorption time of 15 minutes would thus be sufficient for dark adsorption measurements or for kinetic runs.

3.1.4 Determination of required dark adsorption time at high catalyst load

3.1.4.1 Introduction

A dark adsorption time profile at high catalyst load (20 g/L as opposed to 2.0 g/L) was performed with valeric acid (pentanoic) to determine the time required to reach not net change in dark adsorption values over time at high catalyst load and thus ensure that meaningful dark adsorption data would be obtained. This was judged necessary as it might have been risky to use the previously obtained data at catalyst load of 2 g/L and assume no impact of catalyst load on the time required to reach dark adsorption equilibrium. Valeric acid was selected to represent the linear series of the carboxylic acids included in this work. No branched acids were included in this study as there was no difference obtained in the dark adsorption time profile obtained for valeric acid and isovaleric acid (2-methylbutanoic acid) at constant TiO_2 loads of 2.0 g/L.

3.1.4.2 Results

Results obtained for valeric acid are shown below (table and figure 3.1.4.2-1):

time	HPLC peak area			mean	std	RSD
0	540	538		539	1.4	0.3
20	452	439	448	446	6.7	1.5
40	460	417	432	436	21.8	5.0
60	448	435	437	440	7.0	1.6

Table-3.1.4.2-1: HPLC individual peak areas, means, standard deviations and relative standard deviations for valeric acid samples taken over time in a reactor that was kept in the dark. $[ValCOOH]_0$ was 2.0×10^{-3} M, [TiO_2 P25] was 20.0 g/L. Initial volume of 50 ml.

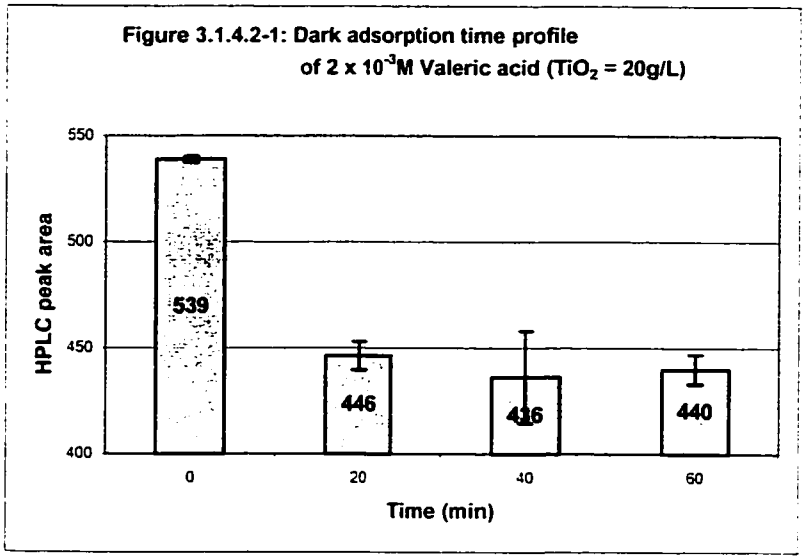

Just as obtained from the previously described dark adsorption time profiles at catalyst loads of 2.0 g/L, most if not all of the dark adsorption occurred during the first 20 minutes of the experiment. The percentage of valeric acid adsorbed onto TiO_2 remained relatively constant over the last 40 minutes of the experiment. An analysis of variance (single factor, $\alpha = 0.05$) was performed on the data set obtained from time 20 minutes to time 60 minutes (time zero was excluded because of its obvious difference with the other time points) and for which the result of this analysis is shown in figure 3.1.4.2-2 below:

Anova: Single Factor

SUMMARY

Groups	*Count*	*Sum*	*Average*	*Variance*
20	3	1339	446.333	44.3333
40	3	1309	436.333	476.333
60	3	1320	440	49

ANOVA

Source of Variation	*SS*	*df*	*MS*	***F***	*P-value*	***F crit***
Between Groups	153.556	2	76.7778	**0.40433**	0.68434	**5.14325**
Within Groups	1139.33	6	189.889			
Total	1292.89	8				

Figure 3.1.4.2-2: Results of a single factor analysis of variance at a confidence level of 95% ($\alpha = 0.05$) performed on the data set obtained from time 20 minutes to time 60 minutes (time zero was excluded because of its obvious difference with the other time points).

The calculated F value (0.40) was lower than the critical F value (5.14) indicating that the differences observed between the data obtained between 20 and 60 minutes are statistically insignificant. The differences observed between these three time intervals are thus no more important than the experimental error associated with these measurements.

3.2 Degradation of $C_1 - C_5$ carboxylic acids

3.2.1 Introduction

Many known water pollutants consist of aromatic compounds. Benzene, for instance, is produced in Canada for use mainly in the manufacture of other chemicals. It is present in gasoline at concentrations of approximately 1 to 2%, and vehicular emissions constitute the main source of benzene in the environment. Benzene is introduced into water from industrial effluents and atmospheric pollution [29]. Carboxylic acids are known to form from the degradation of aromatic compounds via the hydroxylation of the aromatic moiety that leads to ring opening [30, 31]. For this technology to be used for water purification purposes at the industrial scale, and more specifically to produce water of a good enough quality such that standards for drinking water quality that are applicable in any given countries can be met, determining the extent at which any specific contaminant is degraded, if at all, is of primary importance.

Linear carboxylic acids having 1 to 5 carbon atoms and the corresponding branched isomers (e.g.: butanoic acid and 2-methylpropanoic acid) were exposed to UV radiation in aqueous TiO_2 suspensions to determine the extent that these compounds are degraded by this heterogeneous TiO_2-mediated photocatalysis. The rates of disappearance of these acids, relative to each other, can also prove useful in understanding how they are degraded to CO_2 and water. The correlation between the rates of disappearance of such compounds and their C-H bond energies has been demonstrated and was interpreted as evidence for the participation of •OH radicals in these systems [32].

3.2.2 Linear C1 – C5 series: Relation between pH and Dark Adsorption

Many parameters have an influence on the rate of degradation of organic compounds onto titanium dioxide and a complete analysis of the observed rate obtained for a compound, as opposed to another, can only be performed if most (if not all) of them are accounted for. Such parameters include but are not limited to: Catalyst load, solute concentration, oxygen concentration, extent of adsorption, pH, photon flux, temperature, the presence of inorganic ions, the presence of added oxidants, and the reactor design. Some of the above parameters where controlled so that the trends observed could be rationalized. Thus, catalyst load, solute concentration, photon flux, medium temperature and reactor design were kept constant through all the experiments. Inorganic ions were absent from dispersions since ultra-pure water was used. No oxidants other than O_2 (air) were added; experiments were carried out under air-equilibrated conditions at which the concentration of oxygen is ~ 2.4×10^{-4} M [33]. Note that rates of reaction may be limited by the rate of electron transfer to oxygen if solute concentration is greater than 10^{-3} $mol{\cdot}dm^{-3}$ and P_{O2} small (e.g. 0.05 atm or less) [34]. However, this was not the case here since P_{O2} was 1 atm and solute concentration was around 10^{-3} M range. Thus, the only parameters left variable were (1) the pH of the solution and (2) extent of adsorption of the organic solute onto the catalyst's surface. The latter parameter is not an experimental condition that is prone to any control since it is an intrinsic consequence of the system that may be influenced by the pH of the solution. For example, the extent of dark adsorption of organic acids on TiO_2 decreases as pH increases because of a repulsion between ionized acid and negatively charged TiO_2 surface [35]. The pH of the solution was not controlled as it was governed by the carboxylic acid being degraded. Observed

trends will be rationalized on the basis of the pH of the solutions, and the extent of dark adsorption.

Figure 3.2.2-1 illustrates the adsorption and pH results that were obtained for the linear C1 – C5 carboxylic acids series:

Fig 3.2.2-1: pH and adsorption for C1 to C5 linear carboxylic acids after 90 minutes in darkness onto TiO_2 Degussa P25

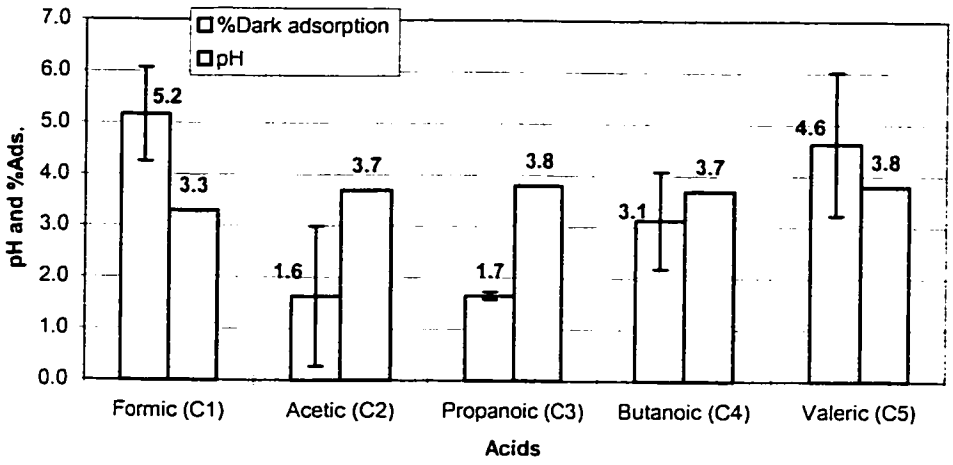

Each bar represents the mean value obtained for a minimum of 2 and up to a maximum of 6 runs per acid, the error bars represent the standard deviation of the data sets (1s). No error bars are shown for the pH data, as they were quite similar between runs, and thus, the variance around the mean was negligible.

The pH of the suspensions containing acetic acid, propanoic acid, butanoic acid, and valeric acid (i.e. pentanoic acid) was similar, whereas that obtained when formic acid was present was lower. This was expected as the pKa of formic acid is less than that of the other 4 acids. Indeed, the pKa of formic acid is 3.75 whereas the pKa's of acetic acid, propanoic acid, butanoic acid, and valeric acids are 4.75, 4.87, 4.81, and 4.82

respectively. Of all 5 acids, dark adsorption was the highest for formic acid (5.2% after 90 min exposure to the catalyst). Adsorption of formic acid onto the reactor's walls was negligible, as evidenced by trimethylacetic acid, a model compound, which was the least water soluble compound of all of acids examined in this study (see previous section). All manipulations were done at night over a red light, so that any possibility of degradation of formic acid in the filtrate occurring during sample manipulation and storage (between filtration and HPLC analysis) is of no consequence. Moreover, all samples were analyzed immediately after they where filtered, thus avoiding a possible decay upon storage.

The highest degree of adsorption was obtained for the acid for which the pKa is the lowest and where the pH of the solution was the lowest as well. TiO_2 is material having an isolectric point around pH 5.5 – 6 [36]. At pH's below this point, the surface of TiO_2 is positively charged, at pH's above this point, the surface of TiO_2 is negatively charged whereas it is neutral at pH's lying at its zero-point-of-charge. Solutes that are, because of their nature, also charged at the prevaling pH conditions in a given system, will show a detrimental effect on rates if the solute and the semiconductor surface are of like charge while the contrary arises when the solute and the semiconductor are of opposite charge. At pH 3.3, 26% of formic acid exists in the deprotonated form, thereby favoring adsorption through electrostatic attraction. For the other acids, the pH was higher than that of the formic acid solution so that the extent of adsorption was less since the degree of deprotonation of these acids was also smaller than for formic acid.

When looking at acetic acid, propanoic acid, butanoic acid, and valeric, there seems to be a trend by which the extent of dark adsorption increases as the chain length

of the acid increases. However, this must be interpreted with care since the coefficient of variation for the above results range between 4.3% and 83.3% for propanoic acid and acetic acid respectively. Obviously, the 5 acids thus far discussed adsorb poorly on TiO_2. This caused some analytical problems because the degree of adsorption of these acids lies near the method's repeatability. That is the differential between the peak areas obtained from the analysis of the acid solution not exposed to the catalyst and that exposed to the catalyst is roughly equal to the method's repeatability. This made the determination of the extent of dark adsorption difficult and prone to errors.

To overcome this problem and possibly better determine if the above trend was not rather attributable to the significant experimental error that was inherent to these measurements, dark adsorption runs were performed at high catalyst load (20 g/L rather than 2 g/L). The concentration of the organic acid was however kept the same as above (2.0×10^{-3} M) such that more of the latter would adsorb onto the catalyst, giving rise to a higher degree of adsorption, which in turn would make the method's repeatability less of a problem. The results for this series of experiments are illustrated in figure 3.2.2-2:

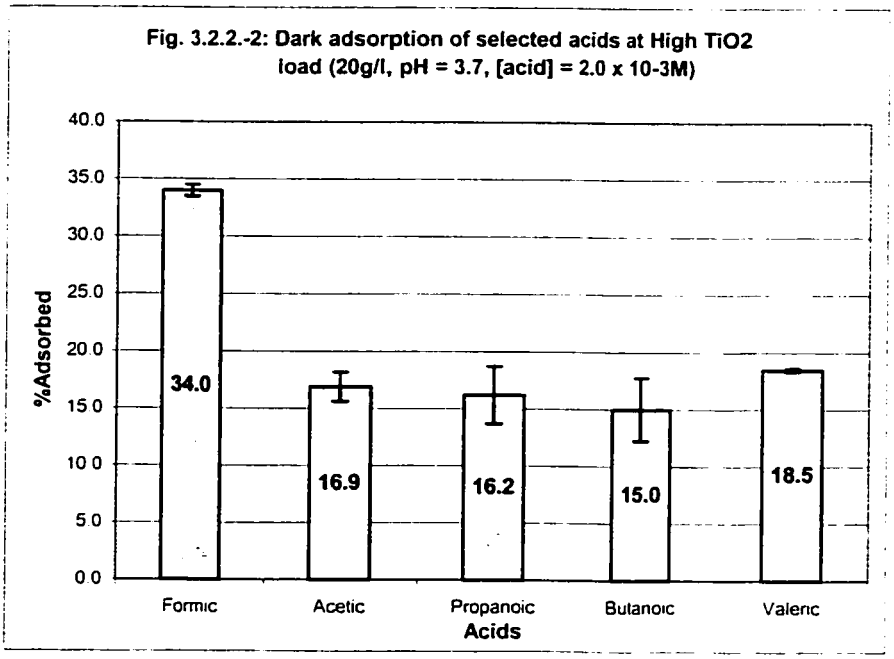

Each bar represents the mean value obtained for 2 runs per acid; the error bars represent the standard deviation of the data sets (1s). No more than two runs were performed because the results were reproducible. Note that unlike the previous set of experiments, the suspensions were buffered at pH 3.7 with perchloric acid and sodium hydroxide. At constant pH, the lower the pKa of an acid the higher its degree of deprononation. Designing the experimental protocol this way thus allowed to establish if there is a phenomenon other than electrostatic attaction by which these acids adsorb on the surface of the photocatalyst. Since the pKa's of acetic acid (4.75), propanoic acid (4.87), butanoic acid (4.81), and valeric acid (4.82) are relatively similar, the extent of adsorption of these acids on the surface of the photocatalyst should also be similar.

Qualitatively, figure 3.2.2-2 reveals that formic acid, the acid having the lowest pKa of the five acids examined, exhibited a near two fold greater adsorption on TiO_2, whereas dark adsorption of acetic acid, propanoic acid, butanoic acid, and valeric acid (pentanoic) were similar, with no clear trend among them. An analysis of variance (single factor, $\alpha = 0.05$) performed on the data set associated with acetic acid, propanoic acid, butanoic acid, and valeric acid (formic acid excluded) is shown in figure 3.2.2-3 below (raw data are given in table 3.2.2-1). The calculated F value (1.12) was lower than the critical F value (6.56) indicating that the differences observed between the data obtained for these 4 acids are statistically insignificant. These differences are no more important than the experimental error associated with these measurements. The major factor impacting dark adsorption values of linear carboxylic acids seems to be exclusively the pH of the medium. An electrostatic model can account for this behavior.

	% Adsorbed	
Acid	**Trial-1**	**Trial-2**
Formic	34	34
Acetic	16	18
Propanoic	18	15
Butanoic	13	17
Valeric	18	19

Table 3.2.2-1: Raw dark adsorption data obtained at high catalyst load (20 g/ml). % dark adsorption calculated from the ratio of the peak area of a filtered sample taken from the suspension to that of the same acid solution that was not exposed to the semiconductor.

Anova: Single Factor

SUMMARY

Groups	*Count*	*Sum*	*Average*	*Variance*
Acetic	2	33.7	16.85	1.805
Propanoic	2	32.5	16.25	6.125
Butanoic	2	29.9	14.95	7.605
Valeric	2	37	18.5	0.02

ANOVA

Source of Variation	*SS*	*df*	*MS*	***F***	*P-value*	***F crit***
Between Groups	13.02375	3	4.34125	**1.11636**	0.4412	**6.59139**
Within Groups	15.555	4	3.88875			
Total	28.57875	7				

Figure 3.2.2-3: Results of a single factor analysis of variance at a confidence level of 95% ($\alpha = 0.05$) performed on the data set of acetic acid, propanoic acid, butanoic acid, and valeric acid.

At constant pH, a condition under which the degree of protonation of TiO_2 is controlled and thus constant, the degree of dark adsorption of these acids is inversely proportional to their pKa. This can be explained by the fact that the extent of deprotonation of these acids is higher the lower their pKa is and thus the number of molecules bearing a negative charge is higher under these conditions. Formic acid, the acid for which the pKa

was the lowest of the five, gave rise to the highest dark adsorption value, whereas the other four acids having similar pKa's gave rise to a similar dark adsorption values.

3.2.3 Linear C1 – C5 series: Completeness of destruction

To be successful as a water purification process applied to drinking water, it is essential that this TiO_2-mediated heterogeneous photocatalytic degradation process leads to the almost, if not complete destruction of water contaminants, or at least that the residual products remaining in water at the end of the purification process be harmless. The disappearance of the C1 to C5 linear series of carboxylic acids was thus monitored over time by high performance chromatography to determine the degree of mineralization by this advanced oxidation method when applied to this class of compounds. The absence of a peak on the chromatogram of an acid at its predetermined retention time indicates a successful degradation but not necessarily mineralization as there still might be some residual amount present in solution for which the concentration lies below the

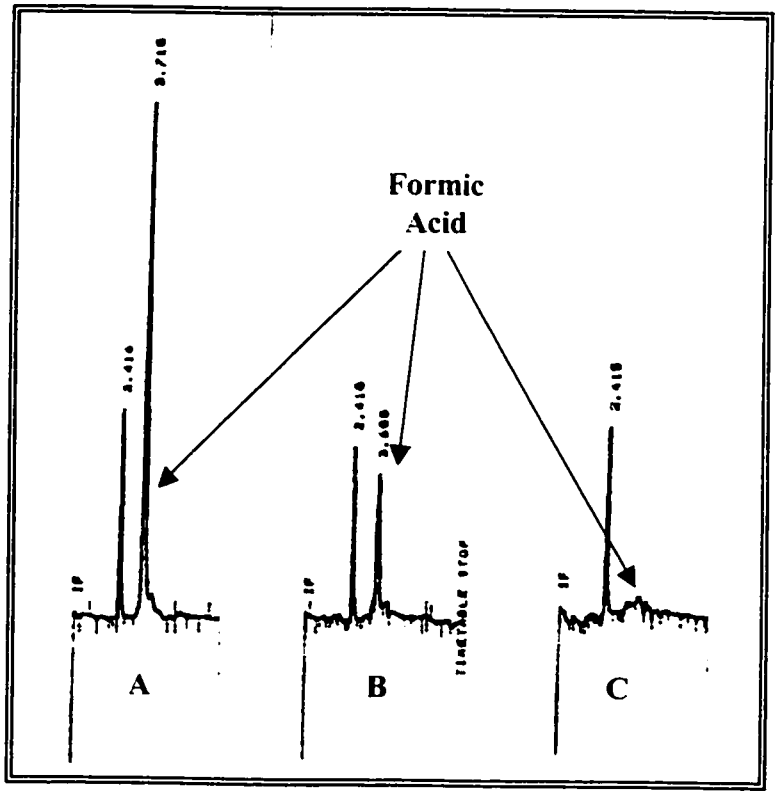

Figure 3.2.3-1: A) time 10 minutes, B) time 20 minutes, C) time 30 minutes

detection limit of the analytical method selected to monitor the progress of the process over time. Figures 3.2.3-1 to 3.2.3-5 show three chromatograms per acid: the first one taken prior to or at the very beginning of the irradiation process, the second one taken approximately half-way through the irradiation process and finally, the third one taken at the end of the run.

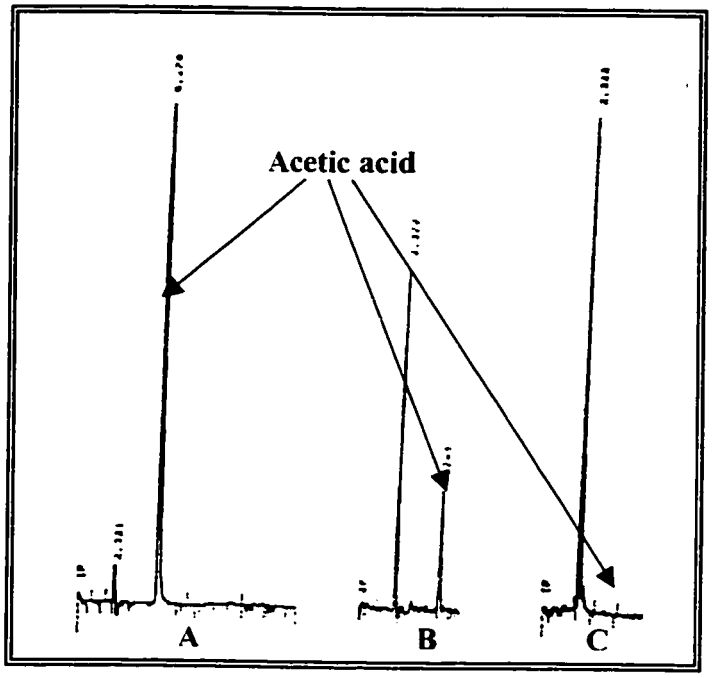

Figure 3.2.3-2: A) time 0 minutes, B) time 75 minutes, C) time 150 minutes

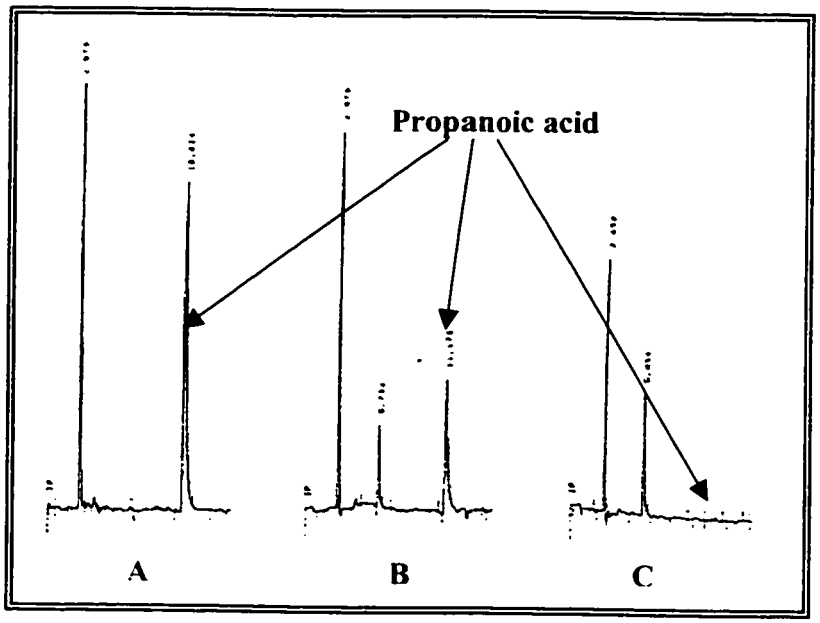

Figure 3.2.3-3: A) time 0 minutes, B) time 30 minutes, C) time 76 minutes

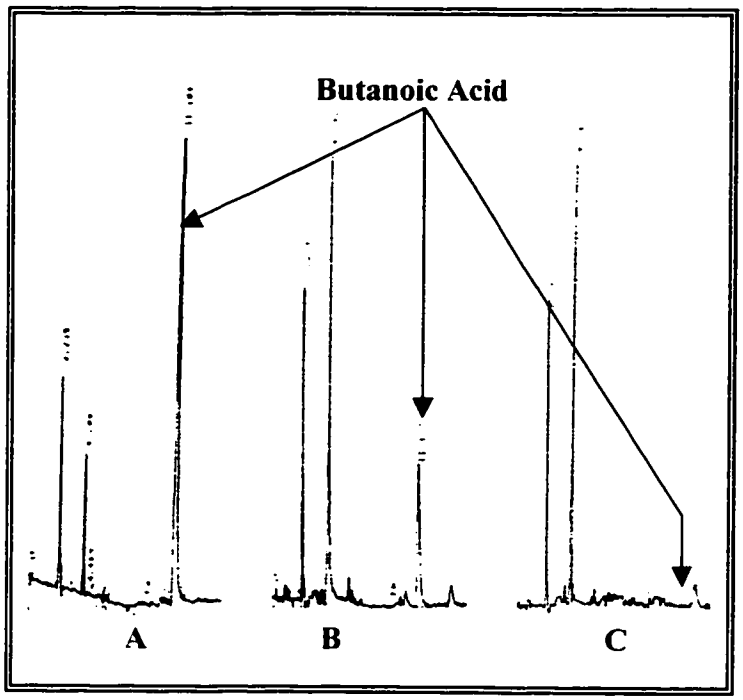

Figure 3.2.3-4: A) time 0 minutes, B) time 60 minutes, C) time 120 minutes

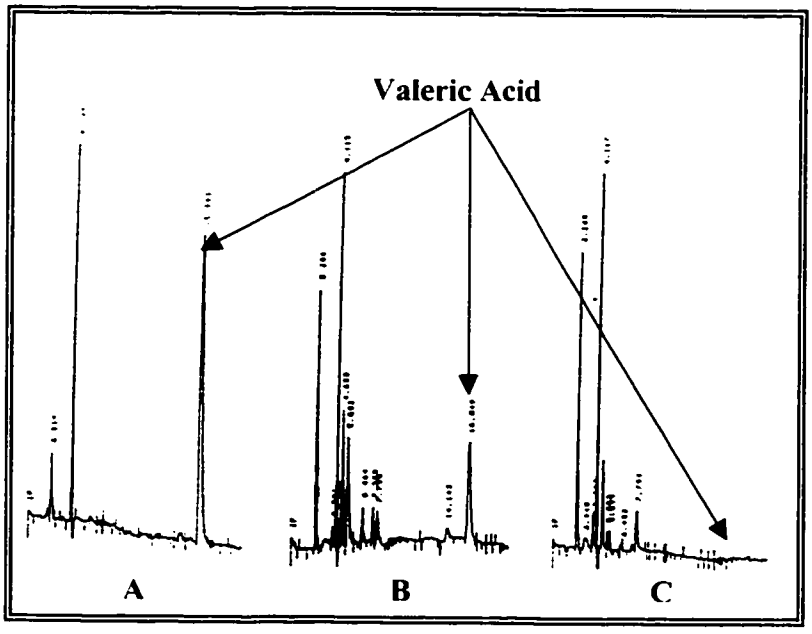

Figure 3.2.3-5: A) time 0 minutes, B) time 60 minutes, C) time 120 minutes

Referring to chromatogram C of figure 3.2.3-1, no peak for formic acid can be found on this chromatogram as opposed to chomatograms A and B that were obtained from

samples taken at time 10 and 20 minutes respectively. Thus, 30 minutes were sufficient to completely degrade this acid to a level below the detection limit of the analytical method. The same applies to all other acids, i.e. they were also completely degraded with the only difference residing in the time required to reach complete destruction. For acetic acid, 150 minutes of irradiation were required to observe no peak on the chromatograms (figure 3.2.3-2, chromatogram C), whereas 76 minutes were required for propanoic acid (figure 3.2.3-3, chromatogram C) and 120 minutes for both butanoic acid and valeric acid (figures 3.2.3-4 and 3.2.3-5 respectively). TiO_2-mediated heterogeneous photocatalysis is thus a proper method to employ to remove linear organic carboxylic acids from water.

Just considering the disappearance of a compound of interest is not good enough when dealing with water treatment methods, especially when the goal is to produce water of such a quality that it meets existing governmental standards for drinking water, as there might be intermediates that are formed during the degradation process of theses acids and which might be more refractory to this method then their parent compounds or even worst, more harmful to human health. Figures 3.2.3-1 and 3.2.3-2 (chromatograms C) for formic acid and acetic acid respectively do not reveal the presence of any residual intermediates at the end of the degradation process as no other peak than the solvent front is observed on the chromatograms obtained for the samples collected at the end of the process. This assumes however that no such intermediates eluted in the solvent front. This is, however, not the case for propanoic acid, butanoic acid and valeric acid. For propanoic acid, the intermediate that appears on chomatogram B of figure 3.2.3-3 (between that of the solvent front and that of propanoic acid) was still present in solution even though propanoic acid was completely degraded. Given that a reverse-phase

column was used, this unidentified compound might be a lower than a C3 linear organic carboxylic acid (for instance, acetic acid), an oxidized derivative of propanoic acid (for example, a hydroxylated derivative of propanoic acid like 2-hydroxypropanoic acid ($CH_3CH\mathbf{OH}CO_2H$) or perhaps a keto derivative of propanoic acid like 2-ketopropanoic acid ($CH3C\mathbf{O}CO_2H$)) or any other compound of lower molecular weight or of higher water solubility than propanoic acid, since the only way by which this intermediate could have a lower retention time than propanoic acid would be by having less affinity to the column stationary phase (a revese-phase C8) for which the conditions just described are mandatory. This is not impossible as the formation of lower molecular weight carboxylic acid from higher molecular weight like compounds (for example, butanoic acid from pentanoic acid, propanoic acid from butanoic acid, or hydroxylated derivatives of any such acids) have been previously reported. For instance, it has been shown that HO• abstract ∝-H on such compounds and indeed, glycolate ($\mathbf{HO}CH_2COO^-$) and glyoxylate ($\mathbf{O}CHCOO^-$) have been identified as acetic acid intermediates [37]. As part of the aliphatic intermediates of 1-2 dimethylbenzene, hexanedioc acid is known to form as well as its dimethyl esters [38]. The GC-MS analysis of dodecane intermediates showed the presence of several dodecanone isomers while formaldehyde and traces of formic acid were also detected [39]. Finally, the degradation of 4-ketopentanoic acid was shown to lead to 2-oxobutane, propanoic acid, acetic acid, ethanol, acetaldehyde, dimethylketone, ethylacetate, ethane, methane, and methanol [40].

The situation just described above for propanoic acid is also true for butanoic acid as well as for pentanoic acid (i.e.: intermediates still present in solution beyond the complete destruction of their parent compound) with the exception that for butanoic acid,

a peak appearing at higher retention time than that of butanoic acid was noted on the chromatograms (refer to figure 4.2.3-4, chromatograms B & C). This can only be possible if this unidentified compound is better retained by the column's packing, a condition requiring that this compound be more hydrophobic than butanoic acid, which could happen if this intermediate had a higher carbon load than its parent compound. The presence of alkyl radicals in such systems and their role in leading to the formation of products having more carbon atoms than the starting materials has been proposed earlier [41]. Indeed, formation of C5 compounds (valeric acid and 2-methylbutanoic acid) from propanoic acid have already been evidenced [41].

The above chromatographic patterns can thus all be rationalized on the basis of existing data. However, the key issue here is not to specifically deal with the nature of these intermediates and the mechanism explaining their formation, but to point out the fact that even though the five acids thus far considered have all been shown to undergo complete destruction when exposed to this advanced oxidation method, there are still some contaminants left behind that we need to be concerned with. The disappearence of total organic carbon from solution over time has been declared to be a better indicator of photoreaction efficiency since the goal of the heterogeneous photocatalysis of organic compound is to mineralize pollutants. In this regard, monitoring pollutants disappearance may be misleading if they degrade fast but intermediates formed are resistant to oxidation [42]. Accordingly, the percent total organic carbon left in solution over time was also measured during the degradation of these acids. The results are shown in the following figures:

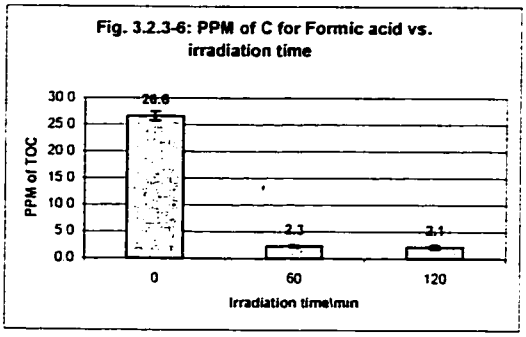

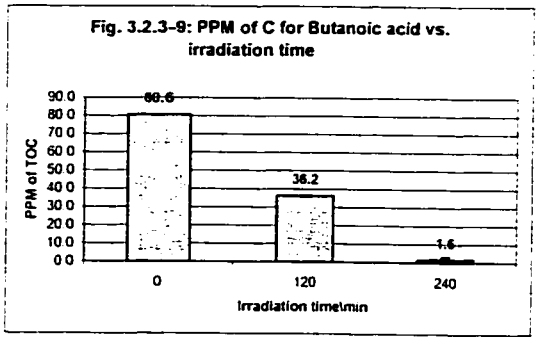

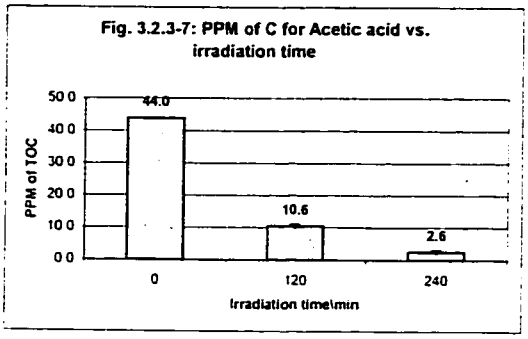

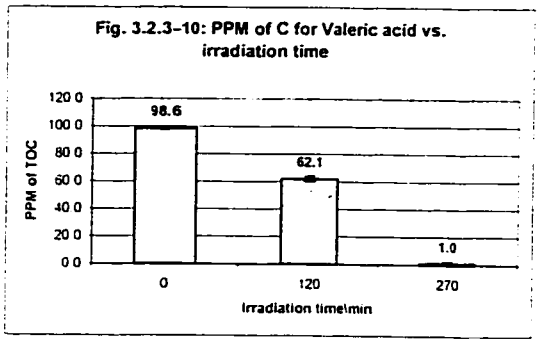

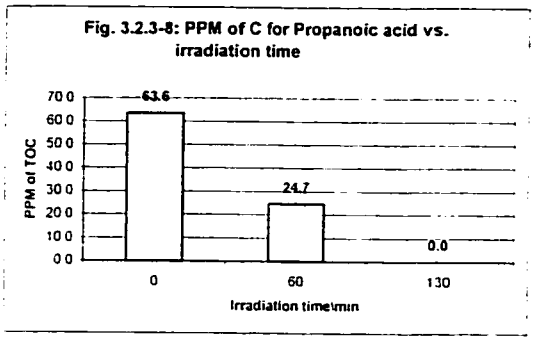

As indicated by the above figures, the total organic carbon content decreased over time throughout the irradiation process, indicating that these five acids were not simply converted into another chemical entity, which would have been the case if the total organic carbon level had remained constant over time. It shows that a non-quantitative conversion of these acids into water and carbon dioxide occurred. Except for propanoic acid where no organic carbon was detected after 2 hours of irradiation, residual amounts were still present after 120 minutes of irradiation for formic acid, 240 minutes of

irradiation for both acetic acid and butanoic acid, and 270 minutes of irradiation for valeric acid. The 99% confidence interval on these residual amounts was calculated and the lower and upper limits of these intervals are shown in table 3.2.3-1:

Acid	Irradiation time	Lower 99% C.I.	Upper 99% C.I.
Formic	120	0.1	4.1
Acetic	240	1.27	3.93
Butanoic	240	-2.5	5.7
Valeric	270	-4.3	6.4

Table 3.2.3-1: Lower and upper 99% confidence interval on the measured amount of total organic carbon expressed in PPM at the final stage of irradiation.

The lower 99% confidence interval on the total organic carbon level expressed in PPM for butanoic acid and valeric acid is negative. Even though this is a purely statistical value and that in practice it is impossible to have a less than zero PPM content of total organic carbon in solution, these intervals give the range over which there is a probability of 99% to find the true mean. Thus, for these two acids, we cannot be 99% certain that the true mean lies above zero PPM; these residual measured amounts are thus insignificant. The same rationale does not hold for formic acid and for acetic acid since their respective lower 99% confidence interval limit lies above zero. There is thus a certainty of 99% that there was some total organic carbon left in solution when the irradiation process was stopped. There is however no expectation to see any such difference between all five acids as they are of the same "species", the only difference among them residing in the length of their carbon chain. It is important to note that the primary reason for a TOC analysis was to obtain data on the rate of disappearance of total organic carbon from solution for these acids, and to compare these rates to rates of disappearance of these acids from HPLC methods.

3.2.4 Linear C1 – C5 series: Rates of disappearance

The temporal disappearance of the entire C1 to C5 linear carboxylic acid series is illustrated in figure 3.2.4-1 to 3.2.4-5 below:

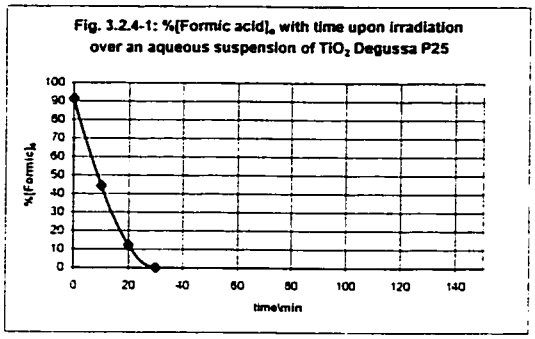

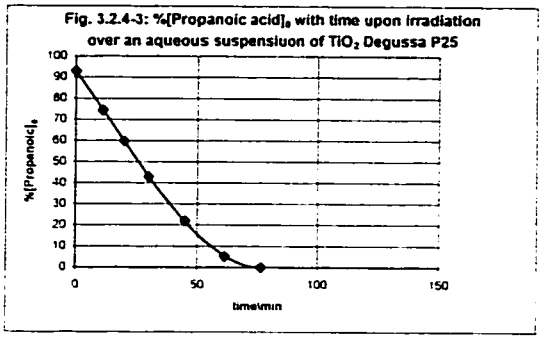

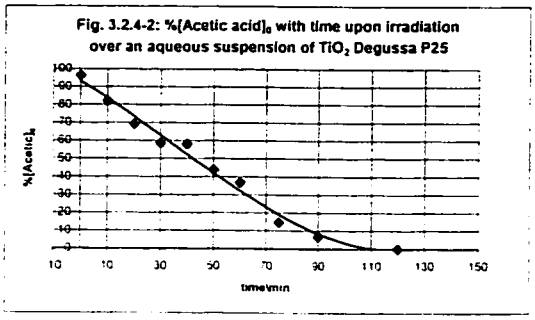

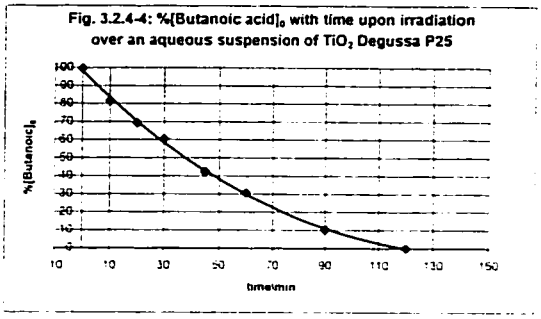

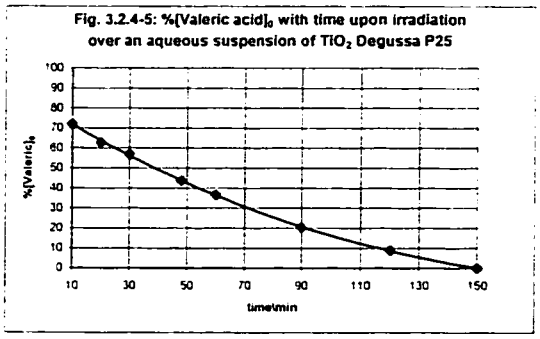

Each graph uses the same scale for an easier comparison. In all cases, $[Acid]_o$ was 2.0 x x10^{-3} M. For all five acids, a linear decrease in acid concentration was observed in the initial stage of the irradiation process to then deviate from linearity at longer irradiation time. Whereas the decrease in concentration over time for formic acid remained

relatively linear during the first 20 minutes of irradiation, time at which 10% of the initial acid concentration remained in solution, this linear decay lasted approximately 75 minutes for acetic acid, 30 minutes for propanoic acid, 45 minutes for butanoic acid, and 60 minutes for valeric acid, time at which the percentage of the initial acid concentration left in solution was 14.6%, 42.9%, 42.5%, and 36.6% for acetic acid, propanoic acid, butanoic acid, and valeric acid respectively. Zero order kinetics was thus observed in the initial stages of the degradation process to then drift at longer irradiation time, a trend that is consistent with the Langmuir-Hinshelwood model that has been reported many times by others [43 - 53] and which is indicative of a surface reaction.

The zero-order rates of disappearance of these acids were derived from the slope of the linear regression curve that was plotted through the linear section of the above graphs (see figures 3.2.4-1 to 3.2.4-5 above). These linear regression curves are shown in figures 3.2.4-6 to 3.2.4-10 and the rate data are summarized in table 3.2.4-1 below:

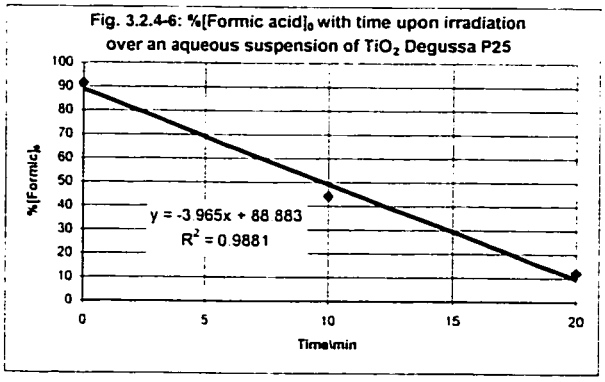

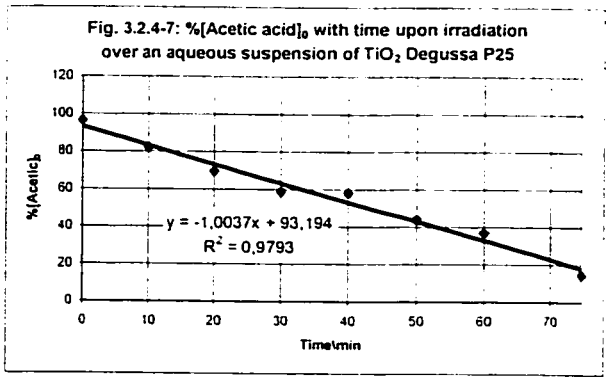

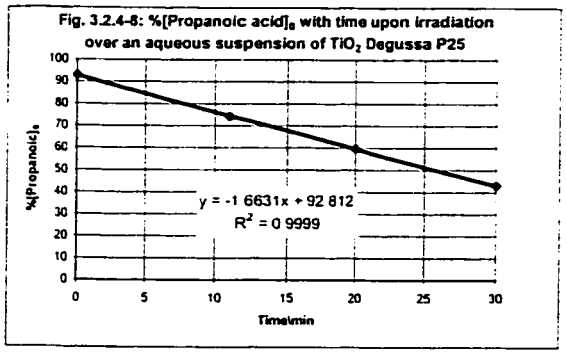

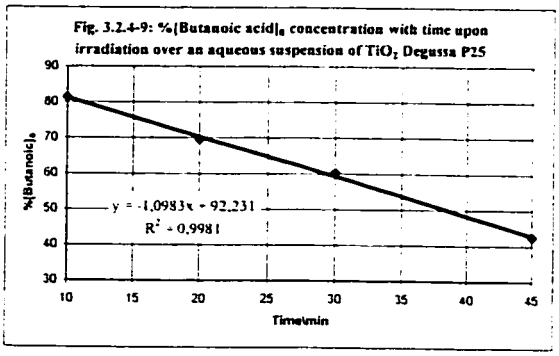

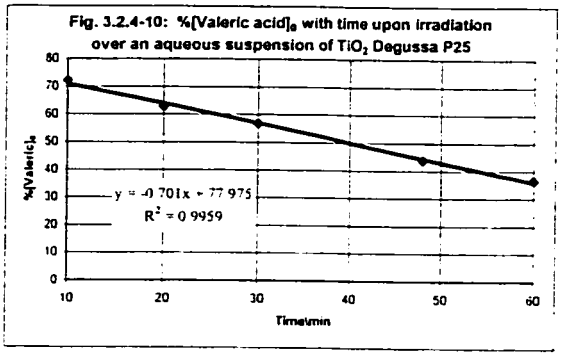

Acid	Rate (umol/hr)	Correlation factor r
Formic	238 ± 26	0.9940
Formic[1]	224 ± 25	
Acetic	60 ± 4	0.9896
Propanoic	100 ± 0.5	0.9999
Butanoic	55 ± 2	0.9990
Valeric	42 ± 2	0.9979
Valeric[1]	45 ± 4	

Table 3.2.4-1: Rate data for the C1 – C5 linear carboxylic acid series. (1) Performed on two different months.

Globally, there is a trend showing a decrease in rate with increasing chain length with the exception of acetic acid, which was more resistant to oxidation than propanoic acid. Because of the various parameters that have an impact on the rates of disappearance of organic compounds onto TiO_2, any conclusion made from these results

without taking some of these parameters into consideration may be tenuous. However, as discussed earlier (section 3.2.2), most of the parameters that can impact on the performance of such systems were controlled with the exception of the pH that was governed by the acid being degraded. Since the pH of a solution and the degree of adsorption of an acid onto TiO_2 are intrinsically related, it might be relevant to compare these rates to the degree of adsorption that these acids showed in the dark. This is illustrated in the histogram of figure 3.2.4-11:

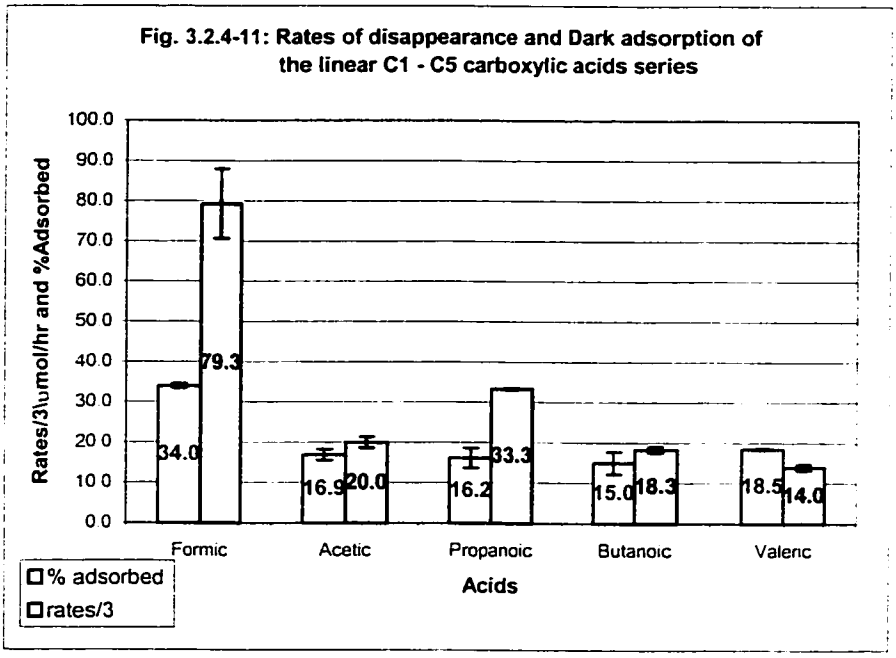

The dark adsorption data shown in figure 3.2.4-11 are those that were obtained at high catalysts load (20g/L) and we have previously demonstrated statistically that the difference observed between the dark adsorption values of acetic acid, propanoic acid, butanoic acid, and valeric acid was not significant. However, the same condition does not apply to the difference observed between the rates of disappearance of these acids and the correlation factor between the rates of disappearance and their dark adsorption value

is 0.3925 (formic acid excluded from the analysis). For acetic acid, propanoic acid, butanoic acid and valeric acid, there is no clear correlation between dark adsorption values and rates of disappearance, indicating that there are other factors than dark adsorption to account for these observed rates. Nevertheless, adsorption of the substrate onto the catalyst cannot be excluded entirely since the latter four acids all had a much smaller degree of adsorption on TiO_2 than formic acid, which has the highest rate of disappearance.

Many explanations can be proposed to explain this trend. First, it appears that rates of disappearance correlate with bond strengths where the former are higher the weaker the bonds [54, 55]. The C-H bond strength follows the trend primary C > secondary C > tertiary C, for which the dissociation energies (ΔH^{o}_{diss}) are 104 kcal/mol, 95 kcal/mol and 92 kcal/mol respectively. This was presented as a rationale to explain the role of HO• radicals in these reactions. The proposed mechanism involved electron transfer from the substrate to the semiconductor, with formation of a radical cation as a primary intermediate during the semiconductor-catalyzed photooxidation of unsaturated hydrocarbons [56]. Since alkyl radical stability follows the trend tertiary > secondary > primary > methyl, it seemed logical to expect higher rates of disappearance for substrates containing tertiary C-H bonds which, following hydrogen abstraction via an oxidative process, would lead to a more stabilized radical intermediate because of a lower activation energy needed for this process. Formic acid has only primary C-H bonds, whereas all of the other four acids contain secondary C-H bonds. Should C-H bond strength and alkyl radical stability be the dominant factors involved, one would expect

formic acid to have the lowest rate of disappearance of all five acids under discussion, which is not the case here.

The change in oxidation power of TiO_2 with pH is well-documented [57]. Indeed, the position of the bands shift at more reducing potentials as pH increases. However, the band gap remains the same thus permitting to manipulate the redox chemistry by using the pH while still using photons of the same energy. Among all of these unbranched acids, formic acid had the lowest pKa and thus caused the reaction medium's pH to be the lowest of all. This forcibly caused the reduction potential of TiO_2 to be at higher value (more positive) than with any of the remaining four acid that had a fairly similar pKa, thus causing TiO_2 to behave more like an oxidant with formic acid than with any other four acids. In addition to that, formic acid is a well-known strong reducing agent. Even though determining the process or route by which formic acid was destroyed was not the scope of this study, the fact that 1) it was more adsorbed to TiO_2 than any of the other four acids 2) it is a strong reducing agent, 3) in its presence, the pH of the solution was the lowest causing TiO_2 to be a better oxidant than with the other four acid, certainly contributed to create condition by which the destruction of this acid was more thermodynamically favorable than for the other four acids. Redox energies and adsorption characteristics therefore seem to be dominant factors that affect the rates of disappearance of these acids, in good agreement with the literature [58 - 61].

As previously discussed, following the disappearance of any given pollutant in assessing the adequacy of a water treatment method that is to be used ultimately to generate water of drinking quality is not sufficient since intermediates products may be more harmful than the primary pollutants. TOC evolution is a better indicator of photoreaction efficiency since the goal of these methods is to mineralize pollutants [62]. The temporal decrease of TOC for the five acids under consideration is shown in figures 3.2.4-12 to 3.2.4-16 below:

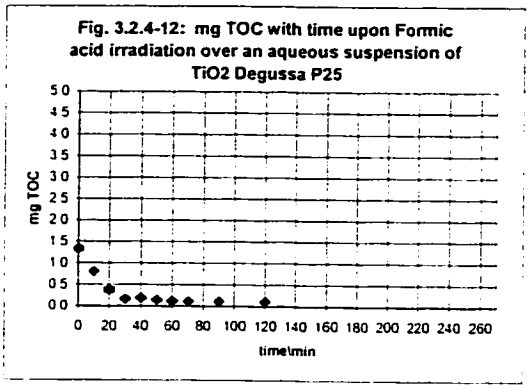

Fig. 3.2.4-12: mg TOC with time upon Formic acid irradiation over an aqueous suspension of TiO2 Degussa P25

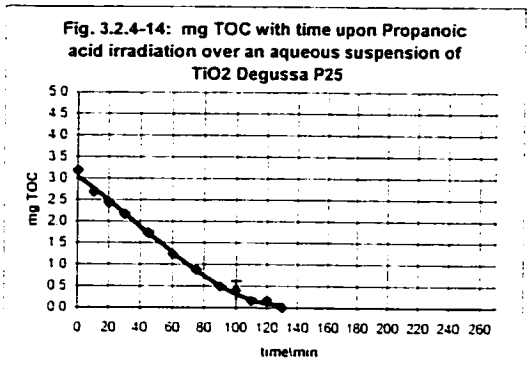

Fig. 3.2.4-14: mg TOC with time upon Propanoic acid irradiation over an aqueous suspension of TiO2 Degussa P25

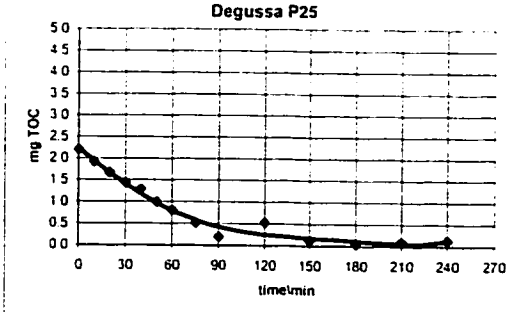

Fig. 3.2.4-13: mg TOC with time upon Acetic acid irradiation over an aqueous suspension of TiO2 Degussa P25

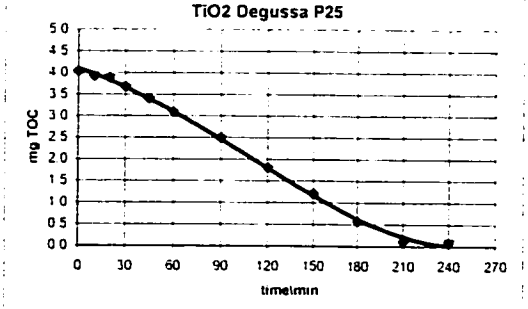

Fig. 3.2.4-15: mg TOC with time upon Butanoic acid irradiation over an aqueous suspension of TiO2 Degussa P25

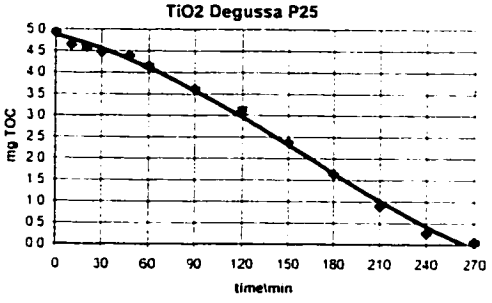

Fig. 3.2.4-16: mg TOC with time upon Valeric acid irradiation over an aqueous suspension of TiO2 Degussa P25

The graphs above were plotted dusing using the same scale for easier comparison. Once again nearly zero-order kinetics was observed for all acids and this observation is in agreement with the work of others [63, 64]. A slight difference is however observed in the decay pattern of butanoic acid and valeric acid where there seems to be an induction period at the beginning of the degradation process and where the rates of disappearance are slower. In fact, for these two acids, the decay pattern of TOC over time has a sigmoidal shape. Such a pattern was not observed for the rates of disappearance of these acids when followed by HPLC. Such a phenomenon has been previously reported [65, 66] and has been attributed to the production of kinetically important intermediate species formed during the reaction and where a substantial fraction of the total mineralization time would be taken by the further oxidation of these intermediates. Indeed, in these studies, the incubation period was found to increase with increasing solute concentration. It was suggested that this was attributable to the fact that the intermediate decomposition products competed with the original solute for the photo-generated radical oxidizing species. However, this pattern was not observed for formic acid, and this was rationalized in terms of a consequence of a more direct conversion to CO_2 than for other solutes. This all makes sense as the chromatograms that were obtained during the degradation of these acids, some of which were shown in figures 3.2.3-1 to 3.2.3-5, did not show the presence of intermediate products for formic acid and for acetic acid, while an incremental number of intermediates were observed when going from propanoic acid to valeric acid.

As done for the determination of the initial rates of disappeareance of these acids by HPLC, the zero-order rates of disappearance of TOC were derived from the slope of the linear regression curve that was plotted through the linear section of the above graphs (see figures 3.2.4-12 to 3.2.4-16 above). These linear regression curves are shown in figures 3.2.4-17 to 3.2.4-21 and the rate data are summarized in table 3.2.4-2 below:

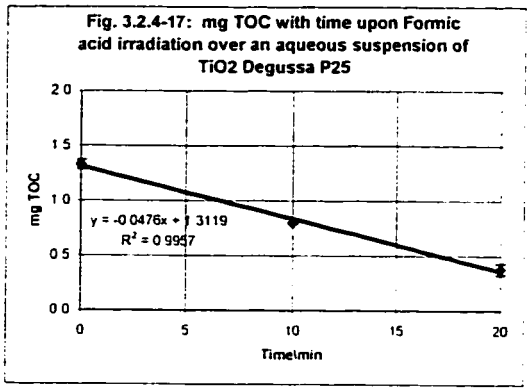

Fig. 3.2.4-17: mg TOC with time upon Formic acid irradiation over an aqueous suspension of TiO2 Degussa P25

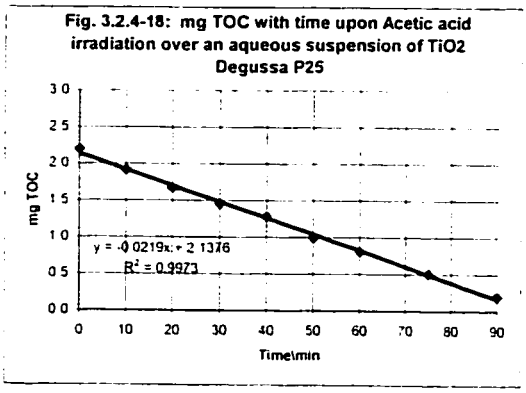

Fig. 3.2.4-18: mg TOC with time upon Acetic acid irradiation over an aqueous suspension of TiO2 Degussa P25

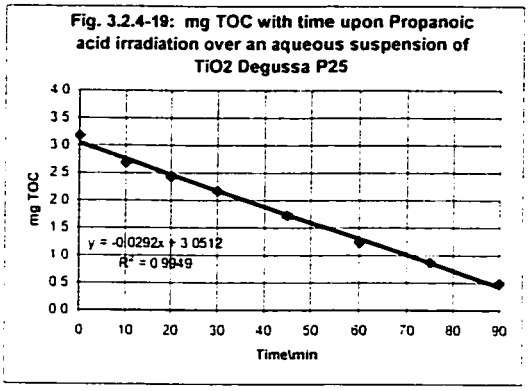

Fig. 3.2.4-19: mg TOC with time upon Propanoic acid irradiation over an aqueous suspension of TiO2 Degussa P25

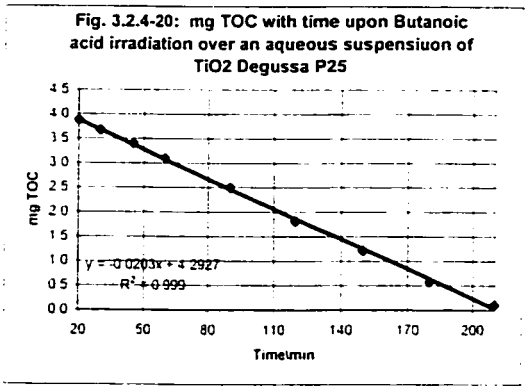

Fig. 3.2.4-20: mg TOC with time upon Butanoic acid irradiation over an aqueous suspensiuon of TiO2 Degussa P25

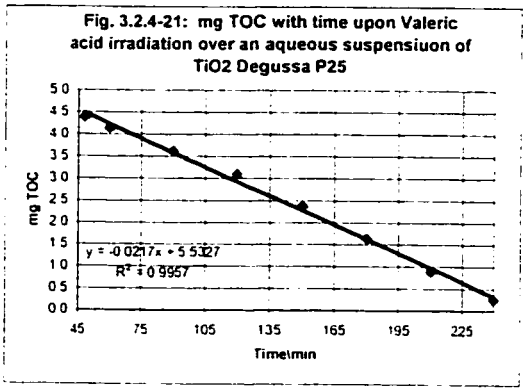

Fig. 3.2.4-21: mg TOC with time upon Valeric acid irradiation over an aqueous suspensiuon of TiO2 Degussa P25

Acid	Rate (mg TOC/hr)	Correlation factor r
Formic	2.9 ± 0.2	0.9978
Acetic	1.3 ± 0.03	0.9986
Propanoic	1.8 ± 0.1	0.9974
Butanoic	1.22 ± 0.01	0.9995
Valeric	1.3 ± 0.03	0.9978

Table 3.2.4-2: TOC rate data for the C1 – C5 linear carboxylic acid series

The global trend in the above rates of TOC disappearance is not exactly the same as the one that was obtained for the rates of acid disappearance obtained from HPLC data. Formic acid displayed the highest rate of TOC as also shown earlier by the rates of degradation. However, unlike the rates of acid disappearance where a decrease was observed with increasing chain length, the situation is different with the rates of TOC disappearance. There is little difference between butanoic acid and valeric acid, whereas the rate of disappearance of acetic acid was greater than that of butanoic acid. The initial rates of TOC disappearance of these three acids are very similar. One explanation for this difference resides in the fact that intermediate products formed in the course of the degradation of the original substrate contribute to the TOC content of the solution and the decay in TOC over time must forcibly be affected by their presence. This difference must also be more pronounced for substrates, which upon degradation, lead to intermediate products that are more refractory to oxidation than the former. The rates of acid disappearance and the rates of TOC disappearance are graphically illustrated in figure 3.2.4-22 below for comparative purposes:

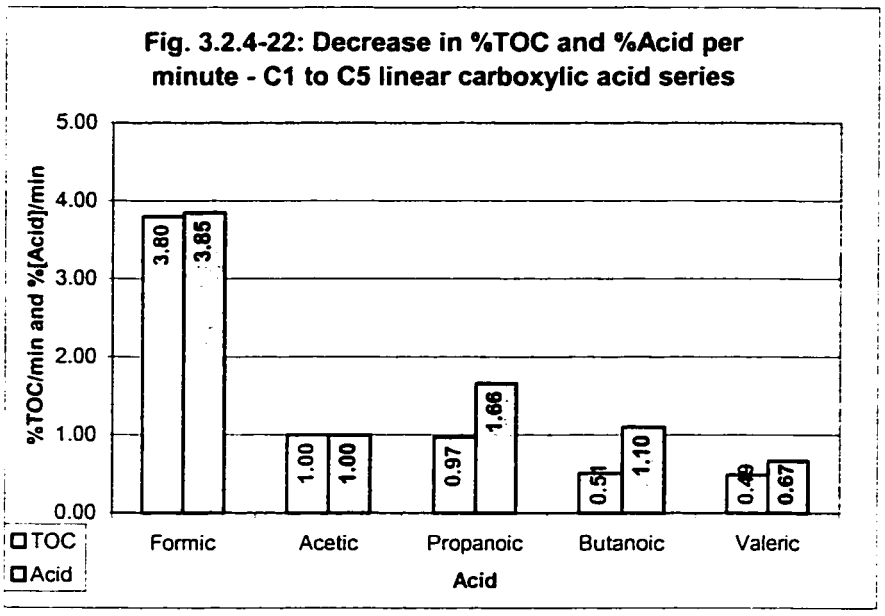

Note that the rates of TOC disappearance and the rates of acid disappearance are reported as percentage to facilitate comparison between the two. This was essential because even though all acids were initially present at the same molar concentration, there is no correlation between molarity and carbon load for these acids that differ in the number of carbons, thus making very difficult comparison of rates expressed in μmol of acid per unit time to rates expressed in mg TOC per unit time.

Figure 3.2.4-22 shows that there was no significant difference between the rates of TOC disappearance and the rates of acid disappearance both for formic acid and acetic acid whereas the rates of TOC disappearance were lower than the rates of acid disappearance for propanoic acid, butanoic acid, and valeric acid. This difference is attributable to the presence of intermediate products in solution for the three latter acids, as opposed to the two former acids for which no intermediates were seen on their respective chromatograms (see figures 3.2.3-1 to 3.2.3-5). In this regard, figures 3.2.4-23 and 24 are quite revealing:

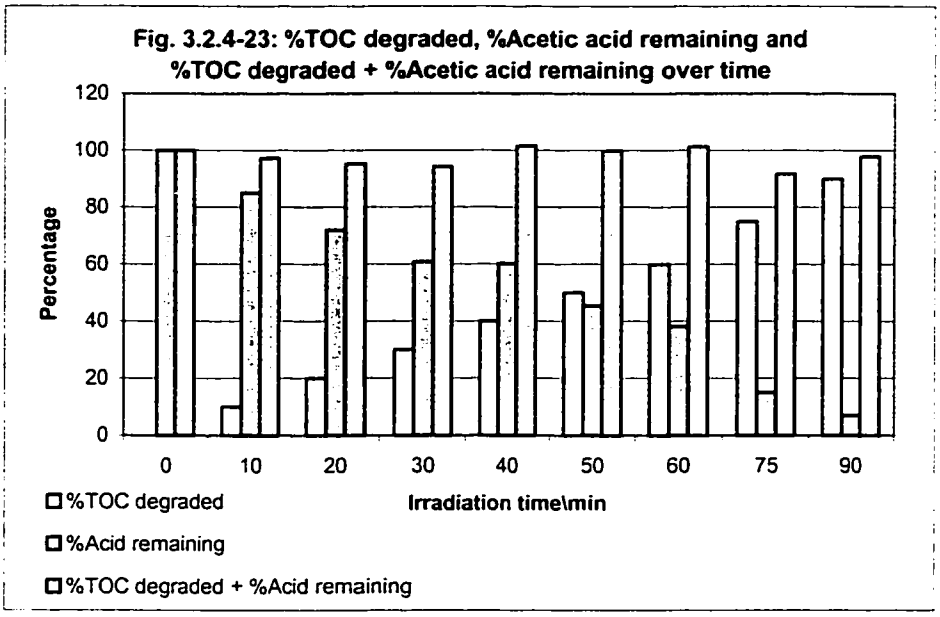

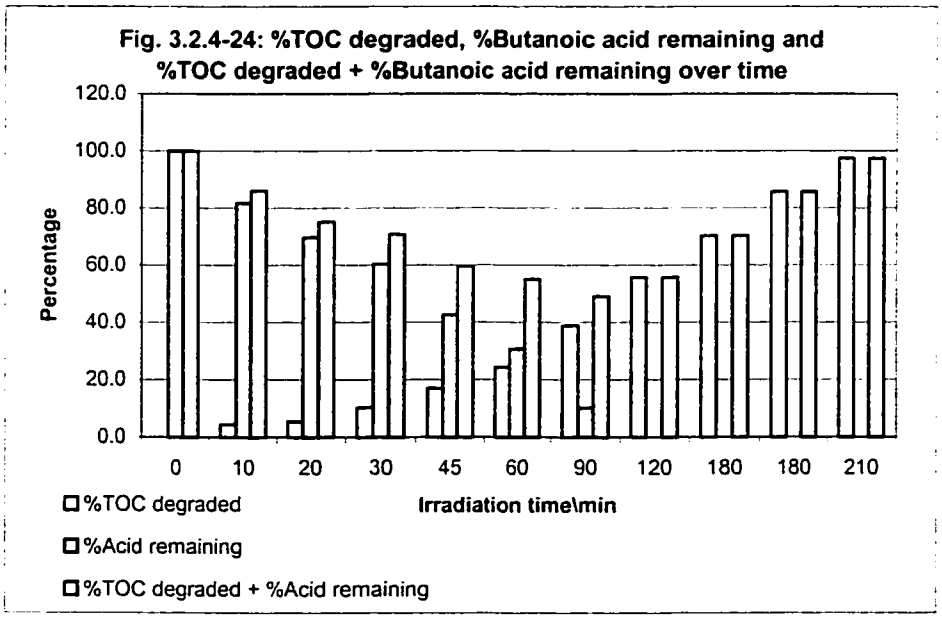

These graphs show, both for acetic acid (rate of TOC disappearance and rate of acid disappearance were identical) and butanoic acid (rate of TOC disappearance different from rate of acid disappearance) (1) the %TOC removed from solution over time, (2) the %acid left in solution over time, and (3) the sum of the two previous one.

Given that there is no significant amount of intermediate products formed in the course of the degradation of the original substrate, the summation of the %TOC removed from solution over time and of the %acid left in solution over time should equal 100% at all sampling points. This is the case for acetic acid for which the sum is nearly constant and equal to 100% all sampling points. The deviation of butanoic acid from this pattern is obvious. As the irradiation progresses, the concentration of butanoic acid in solution decreasese while the %TOC removed from solution increases. This indicates that there is a certain proportion of the acid which has undergone complete mineralization. However, the sum of the two (%acid remaining + %TOC removed), even though equal to 100% at the beginning of the irradiation process, is deviating negatively from 100% until a minimal value corresponding to the complete disappearance of butanoic acid itself is attained. There is thus an accumulation of carbon-containing intermediates in solution that accompanies the disappearance of the original substrate. Following the complete destruction of butanoic acid, the intermediates present in solution are themselves mineralized as shown by the continuous increase in %TOC removed from solution. The intermediate products that form as the original substrate degrades thus have a significant impact on the observed rate of TOC disappearance.

It was reported that the TOC decay is a sum of exponentials to which only the slower step contributes [67]. Given the data that were just presented, this is now easy to understand. It turns out that even though TOC analysis is a very good indicative method to evaluate the effectiveness of TiO_2-mediated heterogeneous photocatalysis as a water treatment technology, and because it focuses on the complete mineralization of organic contaminants present in solution, including the intermediate products, it is not the method

of choice to perform the kind of analysis that was performed above with the HPLC-determined rates of disappearance of these acids. TOC is a non-specific method and does not allow to relate any substrate-specific physical characteristics to the observed rates, because the latter are not associated with a "unique" entity. This is why in a later section of this chapter, only the difference between the rates of TOC disappearance and rates of acid disappearance are explained. The view taken in this work is that relating dark adsorption, pH, redox potential, and any other such characteristics to the rates of TOC disappearance of a given substrate would be tenuous or at the very least, misleading.

3.2.5 Branched C1 – C5 series: Relation between pH and Dark Adsorption

The discussion that started section 3.2.2 (Linear C1 – C5 series, Relation between pH and Dark Adsorption) also applies to this section and will therefore not be repeated. Globally, the experimental conditions under which these branched acids were studied were the same as those used for the C1 – C5 linear series. Therefore, the only parameter not controlled in these experiments was the pH of the solution, which was governed by the nature of the carboxylic acid. Figure 3.2.5-1 illustrates the adsorption and pH results that were obtained for the branched C4 – C5 carboxylic acids series:

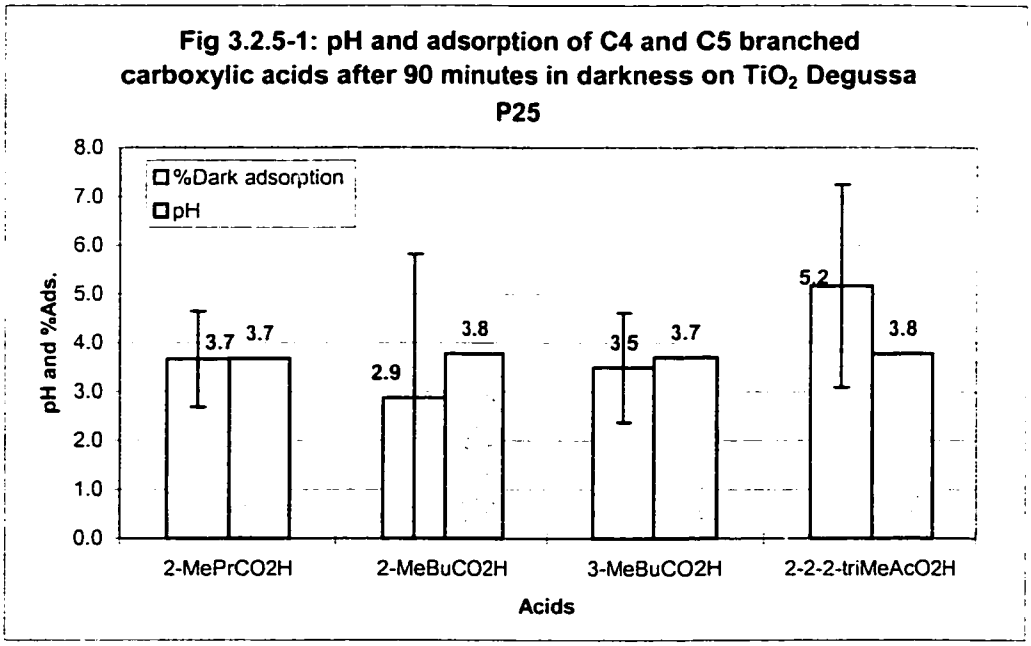

Fig.3.2.5-1: 2-MePrCO$_2$H = 2-methylpropanoic acid or isobutanoic acid, 2-MeBuCO$_2$H = 2-methylbutanoic acid, 3-MeBuCO$_2$H = 3-methylbutanoic acid or isovaleric acid, and 2-2-2-triMeAcO$_2$H = trimethylacetic acid.

For the dark adsorption values, each bar represents the mean value calculated from the results of 4 runs per acid and the error bars represent the standard deviation of the data sets (1s). No error bars are shown for the pH data, as they were similar between

runs and thus, the variance around the mean was negligible. The important data spread (standard deviation of each data set) on the dark adsorption values will be noted; it is attributed to the fact that these dark adsorption measurements were obtained at normal catalyst load of 2.0 g/L prior to the initiation of the irradiation process. Because these acids are obviously poor adsorbers, the difference in the peak area obtained from the HPLC analysis of the samples taken from the acid solution collected prior to and after being exposed to the catalyst was small and of the same magnitude as the method's intermediate precision (% adsorbed is roughly 3 – 5% whereas the method's system precision was of the order of 2%).

The pH of the suspensions containing all of these four branched acids were similar, as expected from the pKa of these acids (4.84, 4.77, and 5.05 for 2-MePrCO_2H, 3-MeBuCO_2H, and 2-2-2-triMeAcO_2H respectively). Accordingly, the dark adsorption value for all four acids were also similar. A one-factor analysis of variance performed on these data sets confirmed that the observed difference between the dark adsorption values of these acids is not statistically significant ($f_{calc.}$ (0.46) ≤ $f_{crit.}$ (3.49)). The details of this analysis are given in figure 3.2.5-2.

As discussed in section 3.2.2, this less than 100% recovery cannot be attributed to (1) the adsorption of these acid onto the reactor's walls, (2) adsorption of these acid onto the filters used to filtrate these samples prior to their HPLC analysis, nor to (3) their degradation in the filtrate during sample manipulation and storage.

SUMMARY

Groups	*Count*	*Sum*	*Average*	*Variance*
2-MePrCO$_2$H	4	14.7	3.675	0.6425
2-MeBuCO$_2$H	4	11.5	2.875	8.649167
3-MeBuCO$_2$H	4	14	3.5	1.253333
2-2-2-triMeAcO$_2$H	4	17.7	4.425	3.4825

ANOVA

Source of Variation	*SS*	*df*	*MS*	***F***	*P-value*	***F crit***
Between Groups	4.88187	3	1.62729	**0.464029**	0.71267	**3.4903**
Within Groups	42.0825	12	3.50688			
Total	46.9644	15				

Figure 3.2.5-2: Results of a single factor analysis of variance at a confidence level of 95% (α = 0.05) performed on the dark adsorption data sets of all four branched acids.

The situation here is similar pH's and similar dark adsorptions for four compounds belonging to the same class (branched carboxylic acids). This trend is in good agreement with the earlier statement (section 3.2.2) that the extent of dark adsorption of aliphatic carboxylic acids on TiO_2 can be rationalized by an electrostatic model. The same situation applies to the comparison of each branched acid with its unbranched isomer, namely (1) 2-methylpropanoic acid (isovaleric acid) vs. butanoic acid (two C4's), and (2) 2-methylbutanoic acid, 3-methylbutanoic acid, 2-2-2-trimethylacetic acid vs. valeric acid (four C5's), as shown in the following figures 3.2.5-3 and 3.2.5-4:

Fig 3.2.5-3: pH and adsorption for the C4 carboxylic acids after 90 minutes in darkness onto TiO_2 Degussa P25

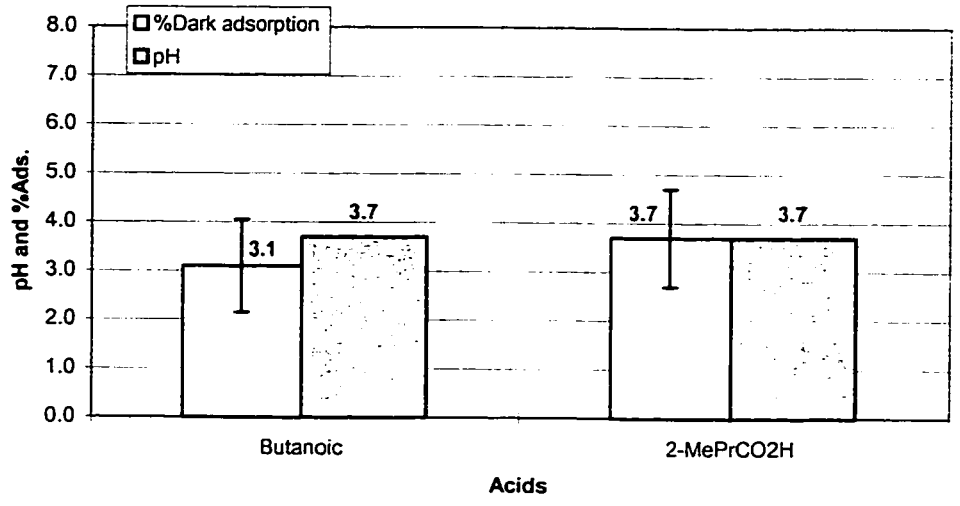

Fig 3.2.5-4: pH and adsorption for the C5 carboxylic acids after 90 minutes in darkness onto TiO_2 Degussa P25

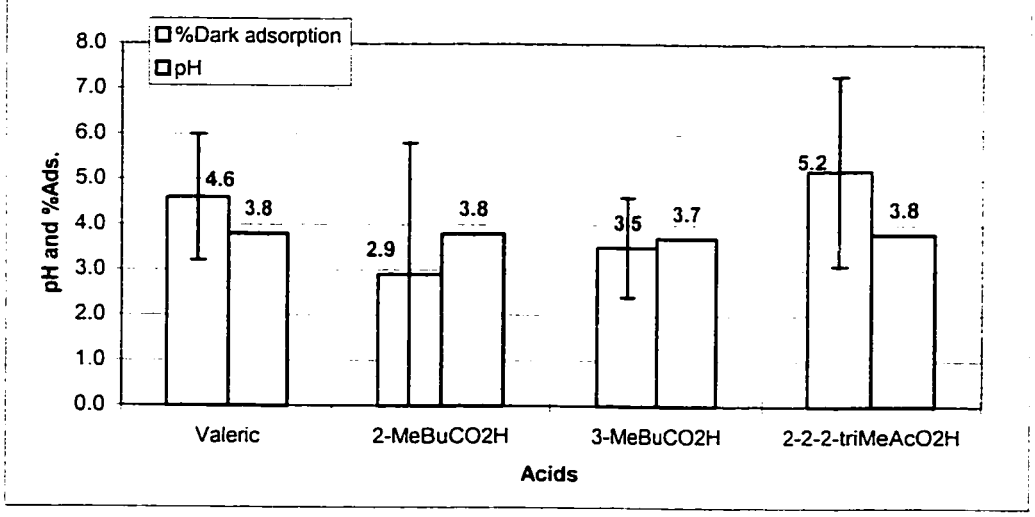

Without formally performing an analysis of variance on these two data sets and consideration of the error associated to each dark adsorption value, it is evident that there is no difference between dark adsorption values of the branched acids, and there is no more difference between the C4 isomers nor between the C5 isomers. Again, the pH of all of these solutions was about the same. Thus branching has no impact what ever on the

dark adsorption of C4 to C5 aliphatic carboxylic acids, and thus is can be deduced that branching has a little (if any) to play in the adsorption process.

3.2.6 Branched C1 – C5 series: Completeness of destruction

As done for the C1 to C5 linear series of carboxylic acids, the disappearance of C4 to C5 branched carboxylic acids was monitored by high performance chromatography to determine the degree of degradation of this class of compounds. Figures 3.2.6-1 to 3.2.6-4 show three chromatograms per acid: at time 0, 60 and 120 min of irradiation.

All the C4 to C5 branched carboxylic acids included in this study were completely degraded as noted by the absence of the HPLC peak corresponding to each of these four acids. Thus, 90 minutes were sufficient to completely destroy 2-methylpropanoic acid, while 120 minutes were needed for the three others. Branched acids are thus completely destroyed, just like the linear acid series was. TiO_2 mediated heterogeneous photocatalysis is thus a proper method to remove branched organic carboxylic acids from water.

Upon degradation, all of these four acids gave rise to formation of intermediates. These can be seen on chromatograms B and C of figures 3.2.6-1 to 3.2.6-4. Except for trimethylacetic acid, where once completely destroyed, no evidence of intermediates in solution could be found (figure 3.2.6-4, chromatogram C), some intermediates were still present in solution at the time where the acid being destroyed was completely removed

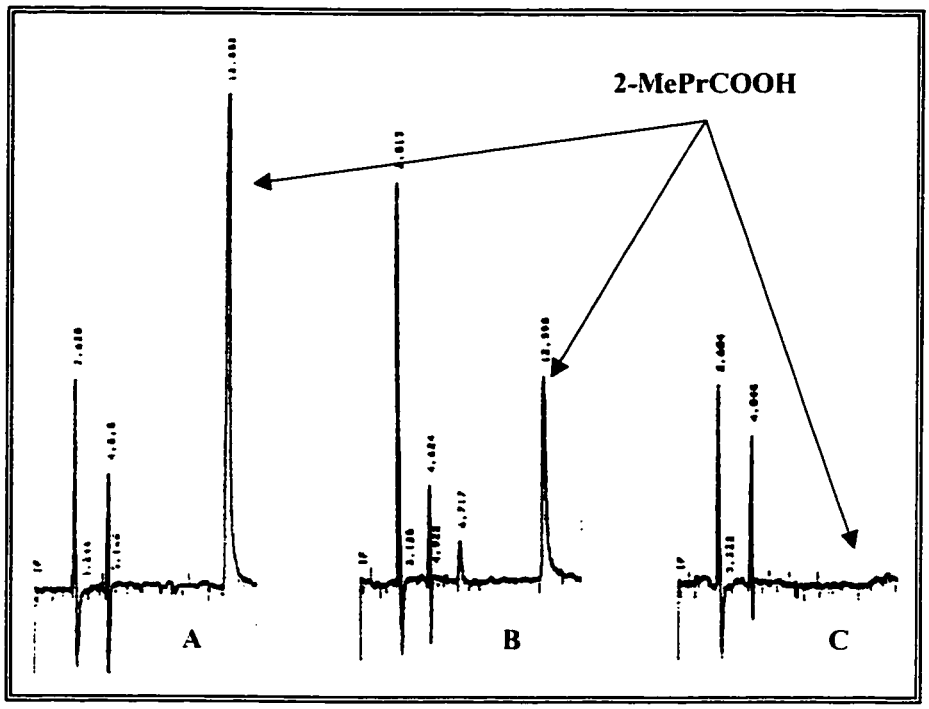

Figure 3.2.6-1: A) time 0 minutes, B) time 40 minutes, C) time 90 minutes

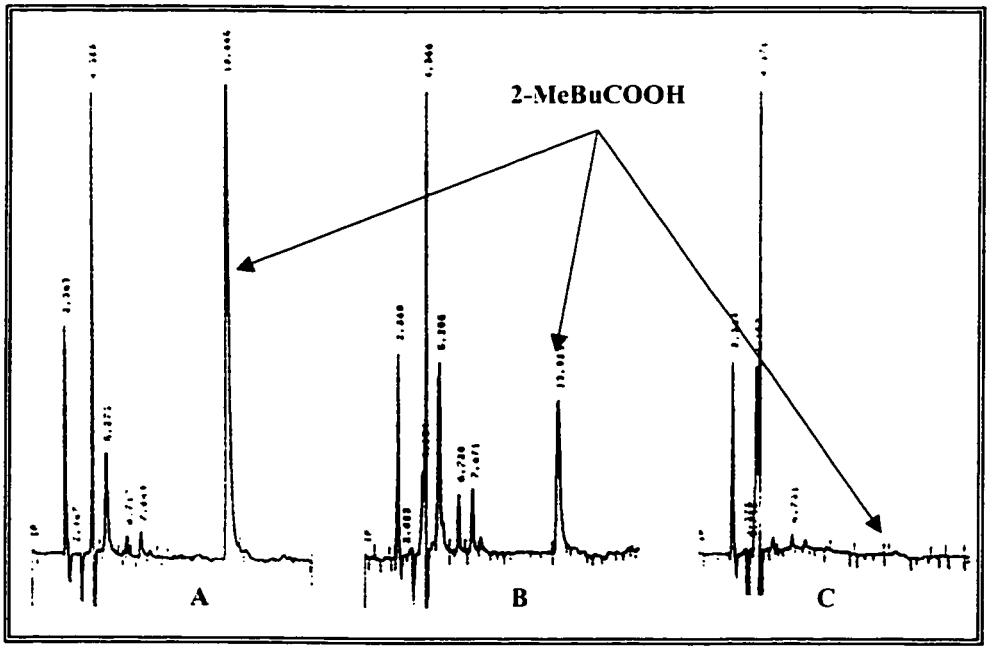

Figure 3.2.6-2: A) Time 0 minutes, B) Time 60 minutes, C) Time 120 minutes

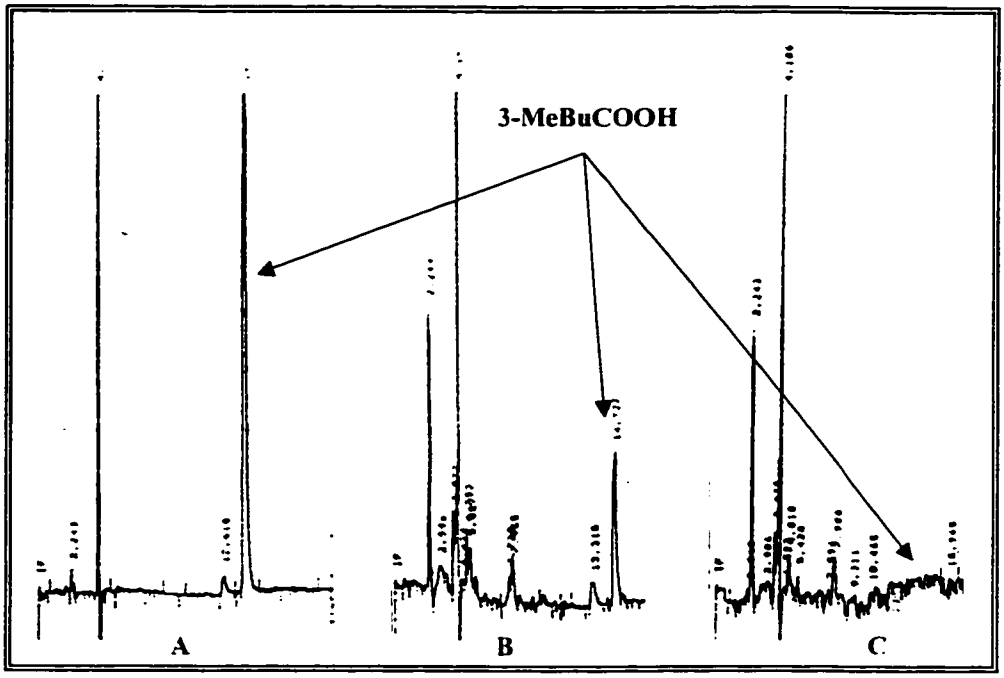

Figure 3.2.6-3: A) Time 0 minutes, B) Time 60 minutes, C) Time 120 minutes

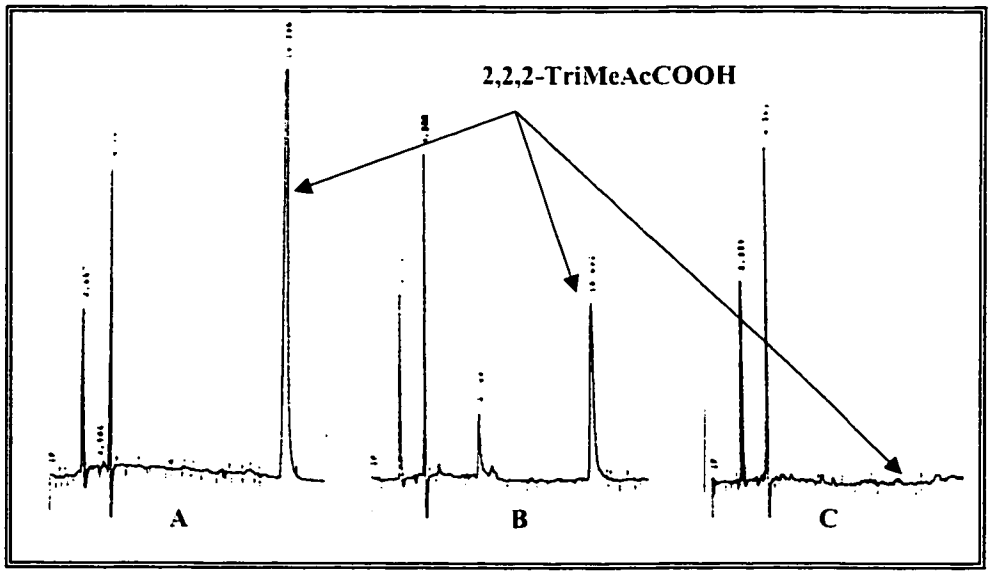

Figure 3.2.6-4: A) Time 0 minutes, B) Time 60 minutes, C) Time 120 minutes

from solution (figure 3.2.6-1 to 3.2.6-3, chromatograms C). All of these intermediates have a lower retention time than their "parent" compound, indicating that (1) they contain less carbon atom than their "parent" compound, (2) they are in a more oxidized form than their parent compound, namely through the addition of oxygen atoms on their structure, or (3) a combination of 1) and 2). These hypotheses are made on the basis that a reverse-phase column was used for the HPLC analyses and with which retention times decrease with an increase in the hydrophilicity of the compounds being analyzed. Taking as an example 2-methlypropanoic acid, it can be envisaged that the preferential site of hydrogen abstraction by a hydroxyl radical would be the alpha-hydrogen ($CH_3C\mathbf{H}_{\alpha}(CH_3)COOH$). Not only does this compound bear an alpha hydrogen atom, but the latter is bounded to a tertiary carbon atom, making the C-H bond weak. The "stable" tertiary alky radical thus created ($CH_3C\bullet(CH_3)COOH$), being even further stabilized by the presence of the carboxyl group nearby (stabilized by resonance), could lead to an alpha-hydroxycarboxylic acid through the addition of an additional hydroxyl radical ($CH_3C(\mathbf{OH})(CH_3)COOH$). Such an intermediate would likely have a lower retention time than its parent compound because the addition of a hydroxyl group to the structure of the latter will increase its solubility in water, thus reducing its affinity for the stationary phase of the column. It is also of interest to note that the HPLC system was mounted with a UV detector (detection wavelength of 214 nm) and that all of the intermediates that appear on the above chromatograms must bear a double bond of such an energy level that photons of 214 nm can be adsorbed for a signal to be seen. It would thus be very unlikely that the carboxylic group was removed at this stage. The same

rationale applies to 2 and 3-methylbutanoic acid and other acids as well. This view is consistent with a mechanism proposed in the literature (refer to section 3.2.3).

Keeping in mind that the goal of the heterogeneous photocatalysis of organic compound is to mineralize pollutants, including the intermediates products, the temporal decrease in total organic carbon left in solution was also measured for the branched series. The results are shown in the following figures:

Fig. 3.2.6-5: PPM of TOC for 2-methylpropanoic acid vs. irradiation time

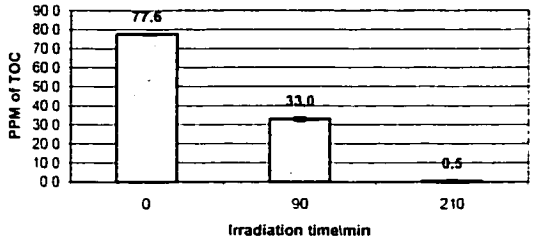

Fig. 3.2.6-7: PPM of TOC for 3-methylbutanoic acid vs. irradiation time

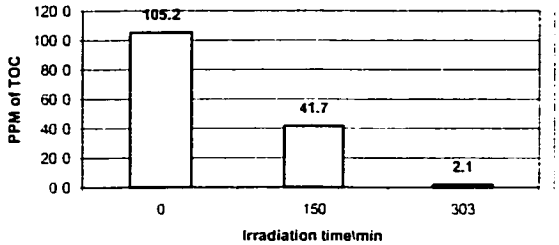

Fig. 3.2.6-6: PPM of TOC for 2-methylbutanoic acid vs. irradiation time

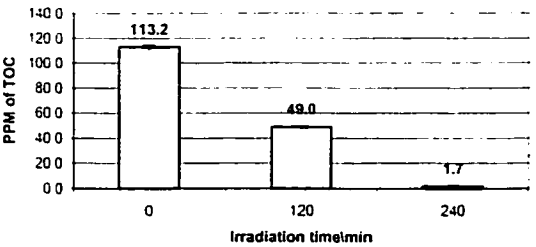

Fig. 3.2.6-8: PPM of TOC for trimethylacetic acid vs. irradiation time

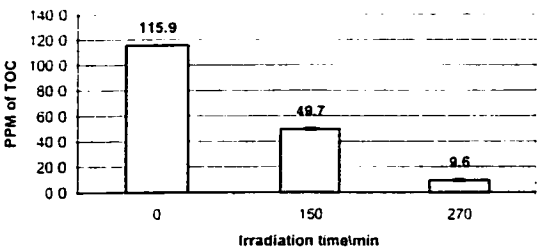

The total organic carbon content decreased over time throughout the irradiation process, indicating that these four branched acids were mineralized. This shows that complete conversion of these acids into water and carbon dioxide occurred. Low residual amounts of carbon were still present in solution after 210 minutes, 240 minutes, 303 minutes, and 270 minutes of irradiation for 2-methylpropanoic acid, 2-methylbutanoic acid, 3-methylbutanoic acid and 2,2,2-trimethylacetic acid respectively. The 99%

confidence interval on these residual amounts was calculated and the lower and upper limits of these intervals are shown in the following table:

Acid	Irradiation time	Lower 99% C.I.	Upper 99% C.I.
2-methylpropanoic	210	-2.0	3.0
2-methylbutanoic	240	-0.65	4.12
3-methylbutanoic	303	-1.13	5.23
2,2,2-trimethyl acetic	270	6.3	13.0

Table 3.2.6-1: Lower and upper 99% confidence interval on the measured amount of total organic carbon expressed in PPM at the final stage of irradiation.

The lower 99% confidence intervals on the total organic carbon level expressed in ppm for 2-methylpropanoic acid, 2-methylbutanoic acid, and 3-methylbutanoic acid are negative indicating that we cannot be 99% confident that the true mean is greater than zero and thus these residual measured amounts can thus be declared to be insignificant. The same rationale does not hold for trimethylacetic acid since its lower 99% confidence interval limit resides above zero. Further irradiation would have made TOC levels lower. Figure 3.2.6-9 shows the decrease in TOC over time. Thus a complete destruction of these branched acids and of their intermediate products from water is demonstrated. Complete mineralization was achieved.

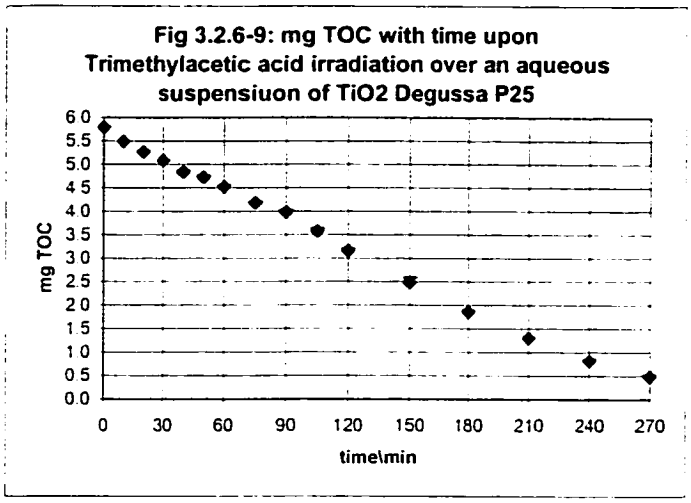

3.2.7 Branched series: Rates of disappearance

The temporal disappearance of the entire branched carboxylic acid series is illustrated in figures 3.2.7-1 to 3.2.7-4 below:

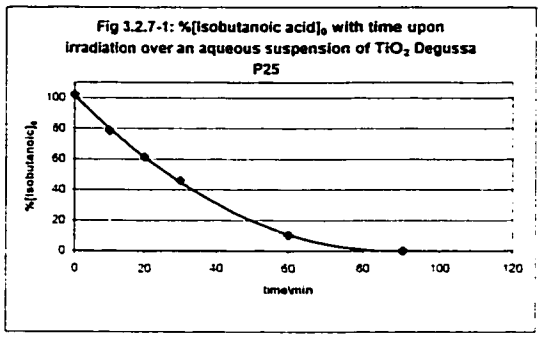

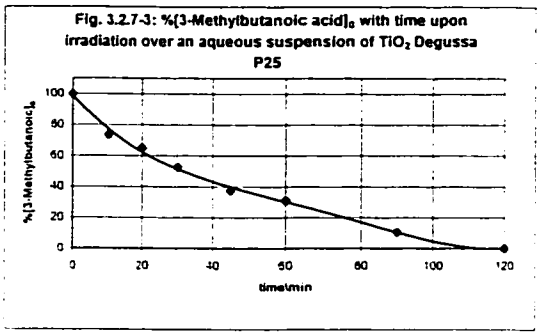

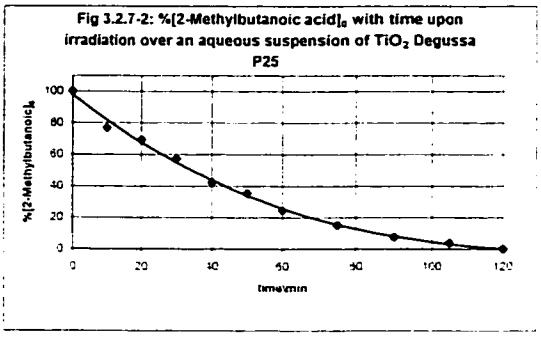

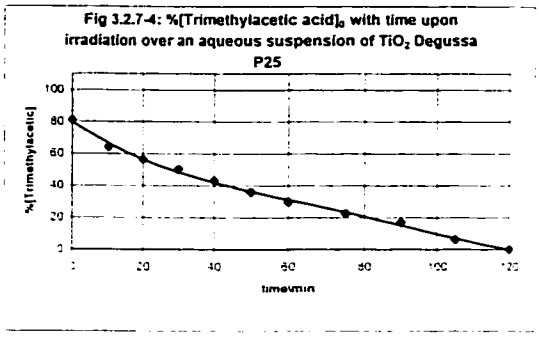

For all four branched acids, a trend similar to that observed for the linear series was obtained and where the concentration of acid decreased linearly with irradiation time to ultimately depart from linearity at low concentration. With the exception of 3-methylbutanoic acid, for which the temporal decrease in concentration remained constant for 45 minutes, time at which 37.5% of the acid was still left in solution, linearity was maintained over 60 minutes for all of the three other acids, time at which 10.4%, 24.5%, and 29.8% of the initial acid concentration was still present in solution for 2-methylpropanoic acid (isobutanoic acid), 2-methylbutanoic acid, and trimethylacetic acid respectively.

The zero-order rate of disappearance of these acids was derived from the slope of the linear regression curve plotted through the linear section of the above graphs (see figures 3.2.7-1 to 3.2.7-4 above). These linear regression curves are shown in figures 3.2.7-5 to 3.2.7-8 and the rate data are summarized in table 3.2.7-1 below:

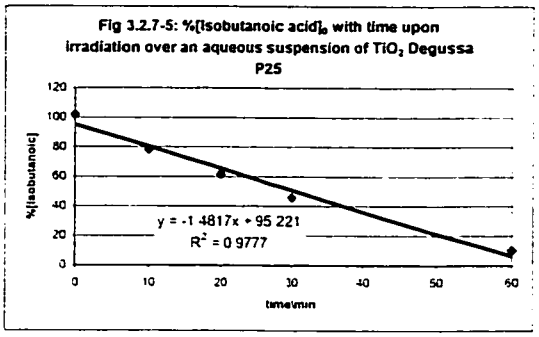

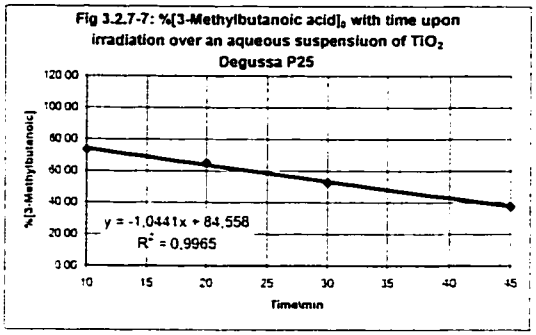

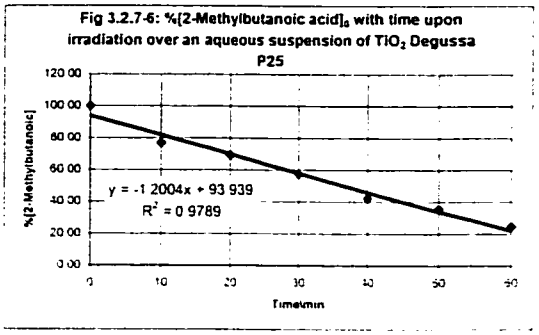

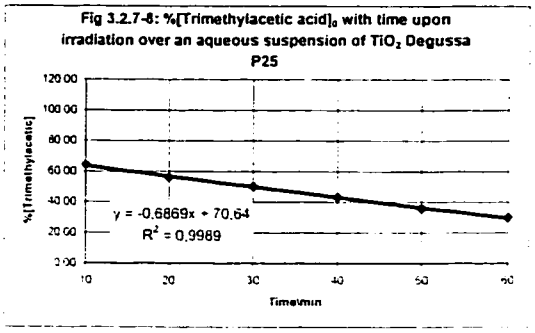

Acid	Rate (umol/hr)	Correlation factor r
2-methylpropanoic	86 ± 5	0.9918
2-methylpropanoic[(1)]	89 ± 8	0.9888
2-methylbutanoic	72 ± 5	0.9889
3-methylbutanoic	63 ± 2	0.9982
Trimethylacetic	41 ± 2	0.9994

Table 3.2.7-1: Rate data for the branched carboxylic acid series. (1) Performed on two different weeks.

Globally, the above rates of disappearance reveal the following trend: 2-methylpropanoic acid > 2-methylbutanoic acid > 3-methylbutanoic acid >

trimethylacetic acid. As done for the linear C1 – C5 linear carboxylic acid series, most of the parameters that can have an impact on the rates of disappearance of these acids were controlled (see section 3.2.2 for a discussion) with the exception of the pH of the solutions that was governed by the acid being degraded. The pH of a solution and the degree of adsorption of an acid onto TiO_2 are intrinsically related and are known to play a role in the heterogeneous photocatalytic disappearance of organic compounds. Figure 3.2.7-9 below compares dark adsorption data for these acids with their rates of disappearance:

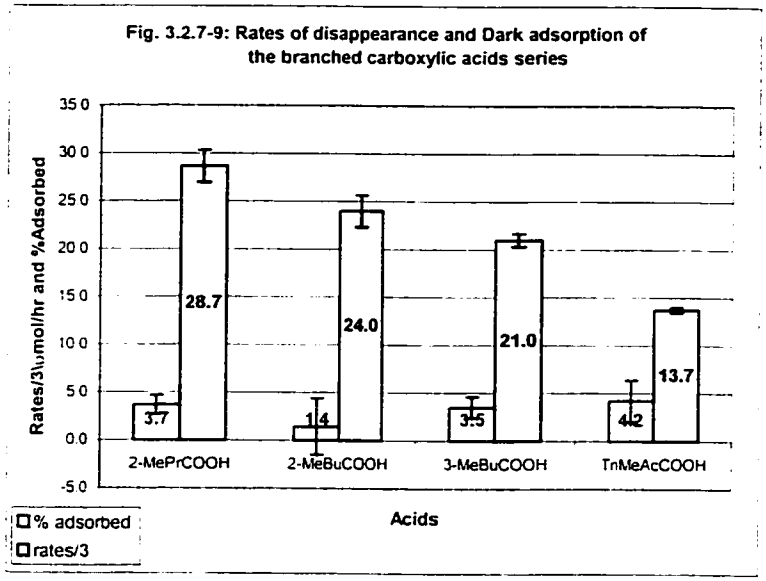

First, just like for their linear parents, these branched acids are all poor adsorbers, the highest extent of dark adsorption having been obtained for trimethylacetic acid (4.2% ± 2.2%). These dark adsorption data were compared statistically and were not found to be significantly different (α = 0.05, Fcal.(2.123) ≤ Fcrit(4.07), refer to figure 3.2.7-10 below), meaning that the observed dark adsorption data can be considered to be similar when taking into account their associated experimental error.

Anova: Single Factor

SUMMARY

Acids	*Count*	*Sum*	*Average*	*Variance*
2-MePrCOOH	3	11	3.66667	0.96333
2-MeBuCOOH	3	4.3	1.43333	0.50333
3-MeBuCOOH	3	10.2	3.4	1.81
TriMeAcCOOH	3	12.5	4.16667	4.82333

ANOVA

Source of Variation	*SS*	*df*	*MS*	*F*	*P-value*	*F crit*
Between Acids	12.9266667	3	4.30889	**2.12785**	0.1749	**4.06618**
Within Groups	16.2	8	2.025			
Total	29.1266667	11				

Fig. 3.2.7-10: Single factor anova with $\alpha = 0.05$ performed on the dark adsorption data set.

Nevertheless, the same cannot be said about the rate data where the observed difference between each acid is more pronounced and for which the errors associated with the measurements are much smaller. Since the dark adsorption values for these acids are all comparable and the same cannot be said about their rates of disappearance, there are obviously other factors than dark adsorption that play a role in this observed trend. Such factors might be, as discussed in section 3.2.4 (1) C-H bond strength, (2) alkyl radical stability, and (3) the pH-dependent oxidation power of the semiconductor. Considering C-H bond strength and alkyl radical stability, among all four branched acids under consideration, trimethylacetic acid is the only acid that do not bear secondary or tertiary C-H bonds, which are of lower dissociation energy than primary C-H bonds. By contrast, 2-methylpropanoic acid, 2-methylbutanoic acid, and 3-methylbutanoic acid all bear tertiary C-H bonds, which should contribute positively on their rates of

disappearance. Upon losing a primary C-H bond following hydroxyl radical attack, trimethylacetic acid would lead to a primary alkyl radical intermediate, which would in turn be less stabilized than the tertialy alkyl radical that would be produced for the other three acids upon losing a tertiary C-H bond. On this basis, it can be expected that trimethylacetic acid will show the slowest rate of disappearance of all 4 acids which indeed is the case. The lower rate of disappearance of trimethylacietic acid as opposed to the other three acids can thus be in part attributed to C-H bond strengths (no tertiary C-H bonds present on its structure) and the poor stability of the primary alkyl radical that would be produced following loss of a hydrogen on one of its carbon. Even though greater than trimethyacetic acid, there are significant differences between the rates of disappearance of 2-methylpropanoic acid, 2-methylbutanoic acid and 3-methylbutanoic. All three acids bear a tertiary C-H bond (at the branching site) and 2 of these acids (2-methylpropanoic acid and 2-methylbutanoic acid) have their tertiary C-H bond at the alpha carbon where the hydrogen is known to be labile. Should hydrogen abstraction by an hydroxyl radical be a significant step in the degradation pathway of these acids, one would expect to observe higher rates of disappearance for 2-methylpropanoic acid and 2-methylbutanoic acid since the favored site for hydroxyl radical attack would be directed toward the hydrogen located on the alpha carbon of these two acids. This is exactly what is observed as 2-methylpropanoic acid and 2-methylbutanoic acid, which have a tertiary C-H bonds located on an alpha-carbon, gave higher degradation rates than 3-methylbutanoic acid for which the tertiary C-H bond does not reside on the alpha-carbon of that acid. Considering this analysis, it seems rather obvious that there is a relation between the lability of the hydrogens located on the carbon skeleton of these acids, the

stability of the alkyl radical that would be produced following hydrogen abstraction, and their rates of disappearance.

As far as the pH-dependent oxidation power is TiO_2 is concerned, and where the position of the bands shift at more reducing potential with an increase of pH (hence becoming a poorer oxidant), it is interesting to note that the pH of the solutions of 2-methylpropanoic acid, 2-methylbutanoic acid, 3-methylbutanoic acid, and trimethylacetic acid was 3.8, 3.7, 3.7 and 3.9 respectively. The pH was thus the highest for the acid that showed the lowest degradation rate of all four acids, which is consistent with this model (TiO_2 not as good an oxidant against this acid). This could in turn explain the difference that is observed between the rate of disappearance of 2-methylpropanoic acid and that of 2-methylbutanoic acid since both acids have a very similar molecular structure, the only difference between them residing in the length of their respective carbon chain. The trend that is observed between the rates of disappearance of these acids is thus attributed to, without being limited to, (1) C-H bond strength, (2) alkyl radical intermediate stability and (3) the redox potential of these systems. This last point was clearly evidenced with the heterogeneous photocatalytic treatment of metal-containing waters. It was reported that in most cases, the rate of metal deposition relative to another could be predicted from their E°. The general trend is that the rates are proportional to the E° of metal and this phenomenon can be used for selective deposition of a mixture [68].

The rate of TOC disappearance of these acids was also measured and the temporal evolution of TOC for these four acids under consideration is shown in figures 3.2.7-11 to 3.2.7-14 below:

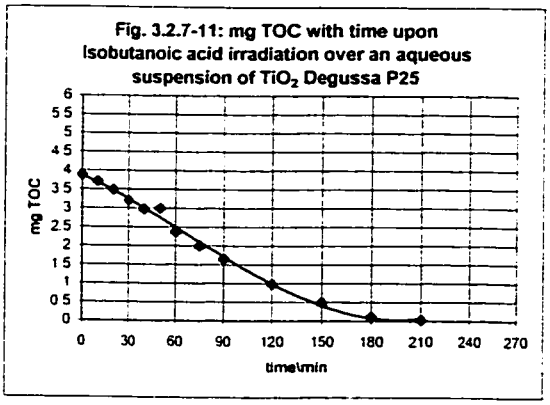

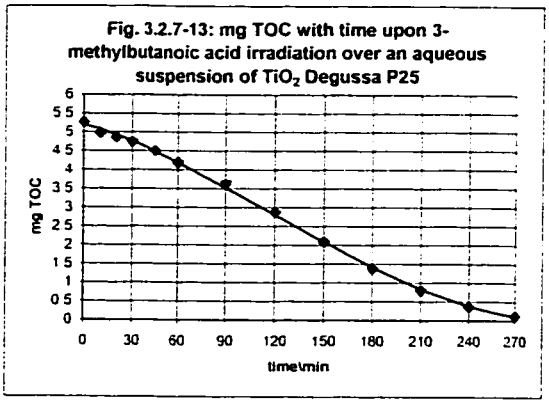

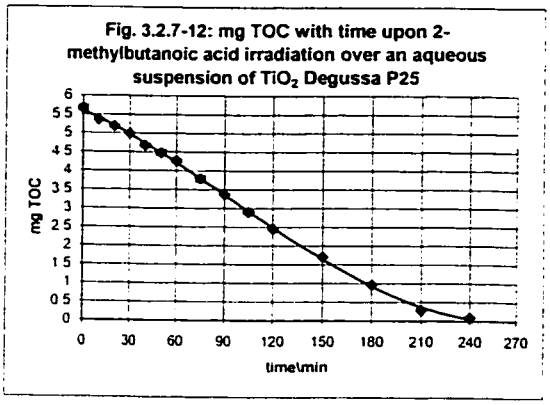

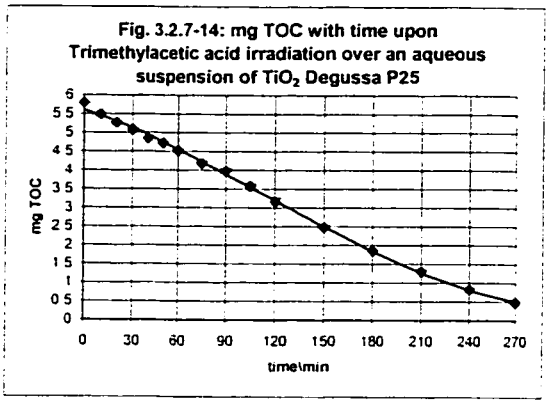

Like it was observed for the linear series, zero-order kinetics was observed for all four branched acids. An induction period at the beginning of the degradation process is observed for all four branched acids. This sigmoidal shaped decay pattern of TOC over time was noted for some acids of the linear series (refer to section 3.2.4) and was not observed for the rates of disappearance of these acids when followed by HPLC. The explanation for such an observation was given in section 3.2.4 and has been attributed to the production of kinetically important intermediate species formed during the reaction and where a substantial fraction of the total mineralization time is taken by the further oxidation of these intermediates. In this regard, one will perhaps note that this induction period seems to be more pronounced for 2 and 3-methylbutanoic acid. A review of figures 3.2.6-1 to 3.2.6-4 of section 3.2.6 shows that among these four acids, more

intermediates were observed on the chromatograms of 2 and 3-methylbutanoic acid. The correlation between the amount of intermediate products in solution and the relative importance of the induction period is thus once again in good agreement.

The initial rates of disappearance of TOC were derived from the slope of the linear regression curve that was plotted through the linear section of the above graphs (figures 3.2.7-11 to 3.2.7-14). These linear regression curves are shown in figures 3.2.7-15 to 3.2.7-18 and the rate data are summarized in table 3.2.7-2 below:

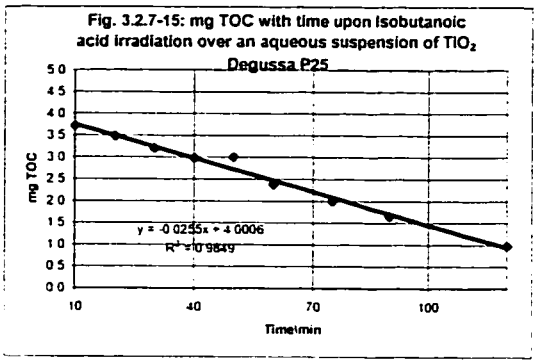

Fig. 3.2.7-15: mg TOC with time upon Isobutanoic acid irradiation over an aqueous suspension of TiO_2 Degussa P25

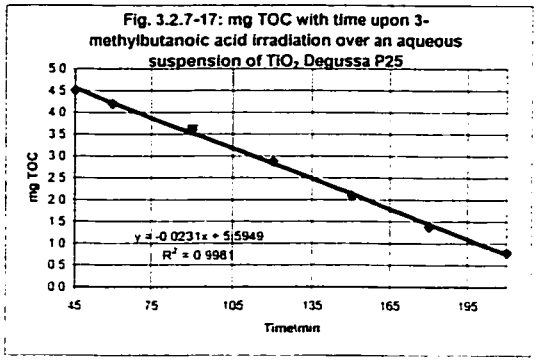

Fig. 3.2.7-17: mg TOC with time upon 3-methylbutanoic acid irradiation over an aqueous suspension of TiO_2 Degussa P25

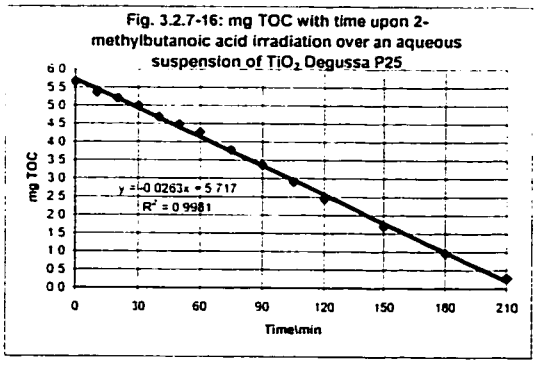

Fig. 3.2.7-16: mg TOC with time upon 2-methylbutanoic acid irradiation over an aqueous suspension of TiO_2 Degussa P25

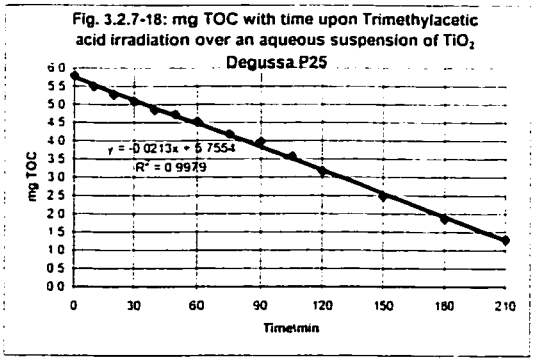

Fig. 3.2.7-18: mg TOC with time upon Trimethylacetic acid irradiation over an aqueous suspension of TiO_2 Degussa P25

Acid	Rate (mg TOC/hr)	Correlation factor r
2-methylpropanoic	1.53 ± 0.07	0.9924
2-methylpropanoic [1]	1.66 ± 0.04	0.9990
2-methylbutanoic	1.58 ± 0.02	0.9990
3-methylbutanoic	1.39 ± 0.03	0.9990
Trimethylacetic acid	1.6 ± 0.2	0.9989

Table 3.2.7-2: TOC rate data for the branched carboxylic acid series. (1) Performed on two different weeks.

The global trend in the above rates of TOC disappearance is different from the one that was obtained for the rates of acid disappearance that were followed by HPLC. This observation is consistent with the one that was made for the linear carboxylic acid series earlier (section 3.2.4). Whereas the observed trend for the HPLC monitored rates of disappearance if these acids was 2-methylpropanoic acid > 2-methylbutanoic acid > 3-methylbutanoic acid > trimethylacetic acid and where the differences between these rates were statistically significant, the above rates of TOC disappearance are all equivalent. The explanation (section 3.2.4) resides in the fact that intermediate products formed in the course of the degradation of the original substrate contribute to the TOC content of the solution and the decay in TOC over time must forcibly be affected by their presence. This difference must also be more pronounced for substrates, which upon degradation, lead to intermediate products that are more refractory to oxidation than the former. In the present case, even though 2-methlylpropanoic acid, 2-methylbutanoic acid, and 3-methylbutanoic acid all showed higher rates of disappearance than trimethylacetic acid for reasons involving C-H bond strength, alkyl radical intermediate stability, and the redox potential of these systems, the presence of intermediates and their behavior that are inherent to their physico-chemical properties "mask" the decay pattern of the pollutant

being degraded by significantly contributing to the overall rates of TOC disappearance. The rates of acid disappearance and the rates of TOC disappearance are graphically illustrated in figure 3.2.7-19 below for comparative purposes.

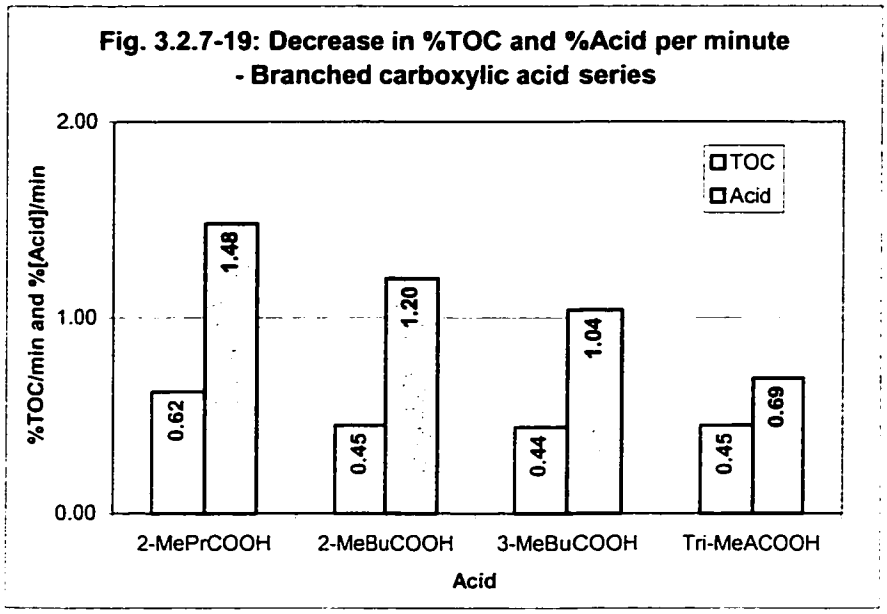

For all four acids under consideration, the rates of TOC disappearance are lower than the rates of disappearance of these acids. The only possible explanation, as given above and which is reinforced by the chromatograms shown in figures 3.2.6-1 to 3.2.6-4 of section 3.2.6, is that in the course of the degradation of these acids, there was an accumulation of carbon-containing intermediates that contributed to the global observed TOC decay, some of which might be more resistant to oxidation than their parent compound or in other cases, that are competing with their parent compound for the same active site. Figure 3.2.7-20 further validates this hypothesis:

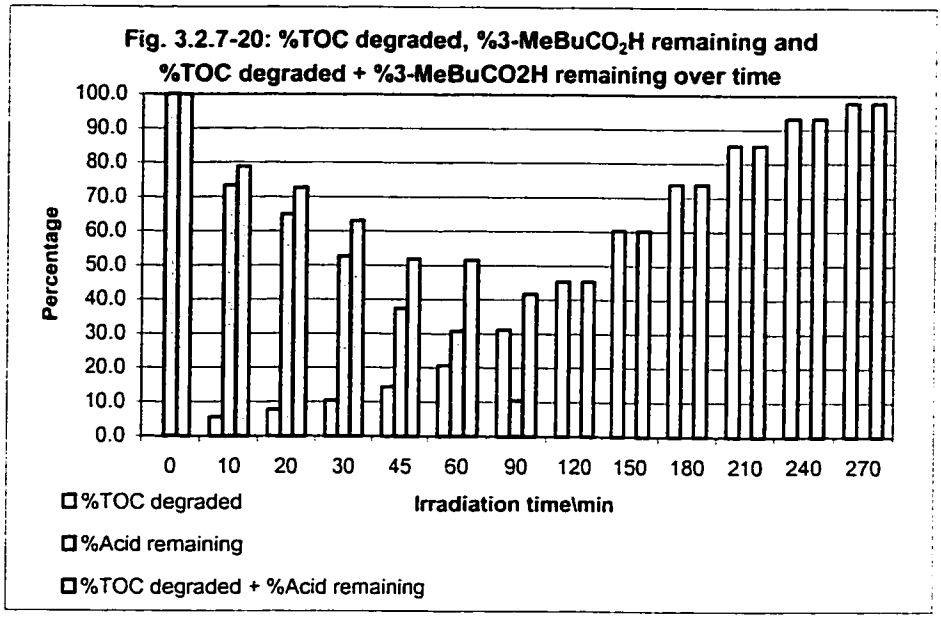

Between time 0 and 90 minutes, the gap between the %3-MeBuCOOH remaining in solution and the summation of the latter and the %TOC degraded increases while at the same time, this summation negatively deviates from 100%. There is thus an accumulation of carbon-containing intermediate products in solution and in this regard, the rate of disappearance of TOC in solution can only be less than the rate of disappearance of the acid itself. Just as claimed previously (section 3.2.4), TOC analysis might be a good method to evaluate the degree of removal of total contaminant is solution but a specific method of analysis such as HPLC is by far the best choice to use in trying to interpret general trends among different pollutants.

Coming back on the impact of branching on the rate of disappearance of this class of compounds, we recall that when the rates of disappearance of these acids were compared among themselves, the explanations that were provided to explain the observed trend were principally based on C-H bond strength and the stability of the alkyl radical

intermediates that would be produced following the abstraction of a hydrogen atom by a hydroxyl radical. We have for instance explained the rates of disappearance of trimethylacetic acid, the lowest of all four, by the fact that it does not bear any tertiary C-H bonds and that following the loss of a hydrogen atom on its carbon skeleton, it could only lead to an unstable primary alkyl radical intermediate. We have also attributed the higher rates of degradation of the 2-methyl acids versus the 3-methyl acid to the fact that branching at the alpha-carbon would make the alpha-hydrogen even more labile, thus contributing to increase the rate of disappearance of the 2-methyl acids. If this is to hold as a general trend rather than to be attributed to a coincidence, the rates of disappearance of all of the branched acids included in this study must be higher than the rates of disappearance of their linear constitutional isomer. Such a comparison is shown in figures 3.2.7-21 and 3.2.7-22 below:

Fig. 3.2.7-21: Rates of disappearance of the C4 isomers

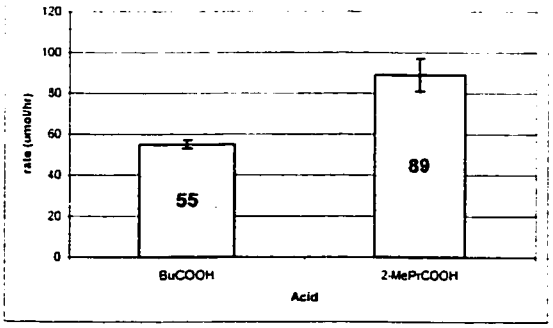

Fig. 3.2.7-22: Rates of disappearance of the C5 isomers

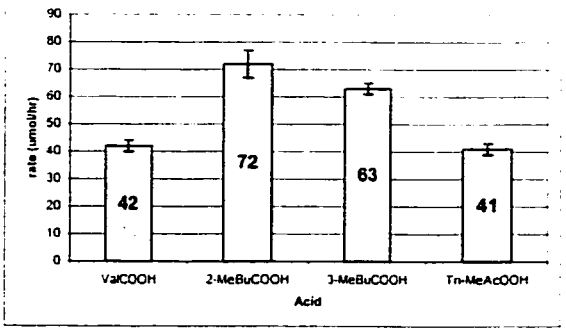

With the exception of trimethlyacetic acid for which the rate of disappearance is comparable to its linear constitutional isomer, all branched acids were degraded at a higher rate than their linear "parent". There is thus no doubt that branching makes these compounds less resistant to oxidation for the reasons that were given earlier. It is not believed that the fact that trimethlyacetic acid was not degraded faster than valeric acid is an exception to the rationale that has thus far been presented. In fact, should the

explanation that have thus far been given be valid, the expectation is that valeric acid should be degraded faster than trimethyacetic acid, since unlike the latter, which bears only primary C-H bond, valeric acid 1) contains many secondary C-H bonds which have lower dissociation energy than primary C-H bonds, 2) can lead to the formation of more stable secondary alky radical intermediates and 3) bears 2 alpha hydrogens on its carbon skeleton, three conditions that are not present for trimethylacetic acid.

3.2.8 Alpha-hydroxy and alpha-keto C4 and C5 aliphatic carboxylic acids: Relation between pH and Dark Adsorption

Alpha-hydroxy and alpha keto acids were investigated at a later time during this study as potential inytermediates among the many degradation products that are formed during the degradation of the linear series using HPLC co-elution experiments. The results from these will be presented in a later section. However, the explanations of our findings are linked to this section since they are intrinsically related. Only selected alpha-hydroxy and alpha-keto acids were examined, namely 2-hydroxy-2-methylbutanoic acid (2-OH-2-MeBuCO$_2$H), 2-hydroxyvaleric acid (2-OHValCO$_2$H), and 2-ketovaleric acid (2-OValCO$_2$H). The experimental conditions used for these acids were the same as those used for the linear series and for the branched series. The only parameter not controlled in these experiments was the pH of the solution, which was governed by the carboxylic acid examined. Figure 3.2.8-1 illustrates the adsorption and pH results that were obtained for the three alpha-hydroxy and alpha-keto acids noted above:

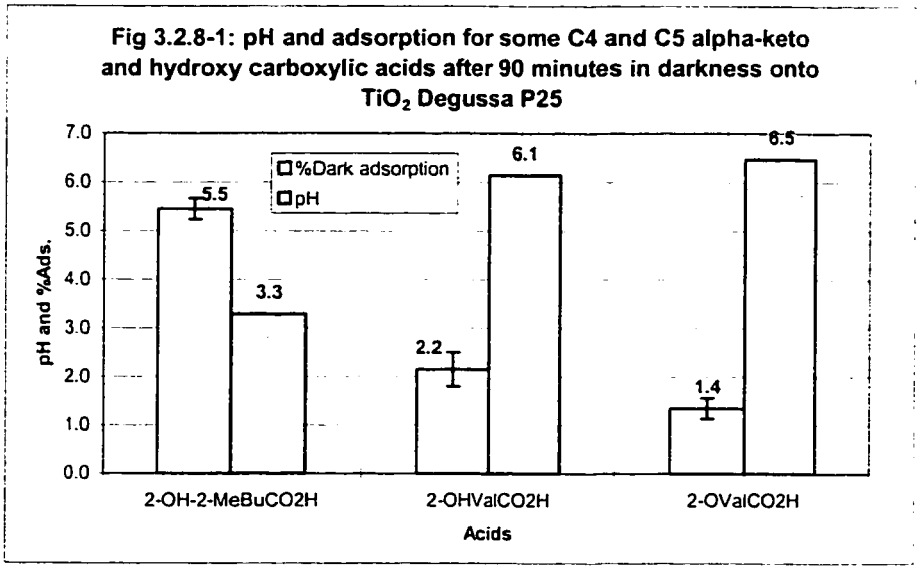

Fig.3.2.8-1: 2-OH-2-MeBuCO$_2$H = 2-hydroxy-2-methylbutanoic acid, 2-OHValCO$_2$H = 2-hydroxyvaleric acid, and 2-OValCO$_2$H = 2-ketovaleric acid.

The pH's of the suspensions containing 2-OHValCO$_2$H and 2-OValCO$_2$H (6.1 and 6.5 respectively) are higher than that of the corresponding suspension that contained the non-oxidized parent (valeric acid 3.8, section 3.2.2). As any factor that stabilizes the carboxylate anion product (following the dissociation of the acid) should drive the equilibrium toward increased dissociation resulting in increased acidity. This is in fact the case for 2-OH-2-MeBuCO$_2$H versus 2-methylbutanoic acid for which the pH's of their suspensions are 3.3 and 3.8 respectively. As noted in section 2.1.6, the 2-OHValCO$_2$H and 2-OValCO$_2$H were obtained as sodium salts (i.e., as bases), whereas 2-OH-2-MeBuCO$_2$H was obtained as an acid.

The trend between pH and dark adsoption is clear: there is an inverse relation between the pH of the suspensions and the dark adsorption of these acids. As discussed in section 3.2.2, this less than 100% recovery cannot be attributed to 1) the adsorption of these acid onto the reactor's walls, 2) the adsorption of these acid onto the filters used to filtrate these samples prior to their HPLC analysis, nor to 3) their degradation in the filtrate upon sample manipulation and storage.

Similar to the linear and the branched series, this trend is in good agreement with the statement made earlier (section 3.2.2) in that the extent of dark adsorption of aliphatic carboxylic acids onto TiO_2 can be rationalized in terms of an electrostatic model. The same situation applies globally when comparing for a given acid, the pH's and the dark adsorption data that were obtained for the non-oxidized acid, the alpha-hydroxy acid and the alpha-keto acid, as shown in figures 3.2.8-2 and 3.2.8-3:

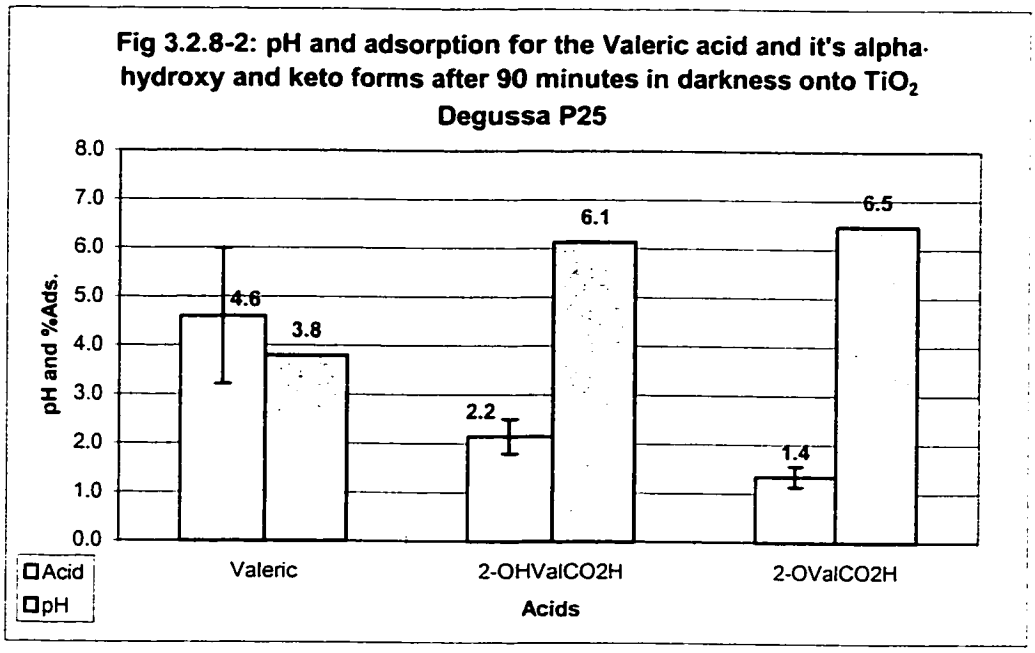

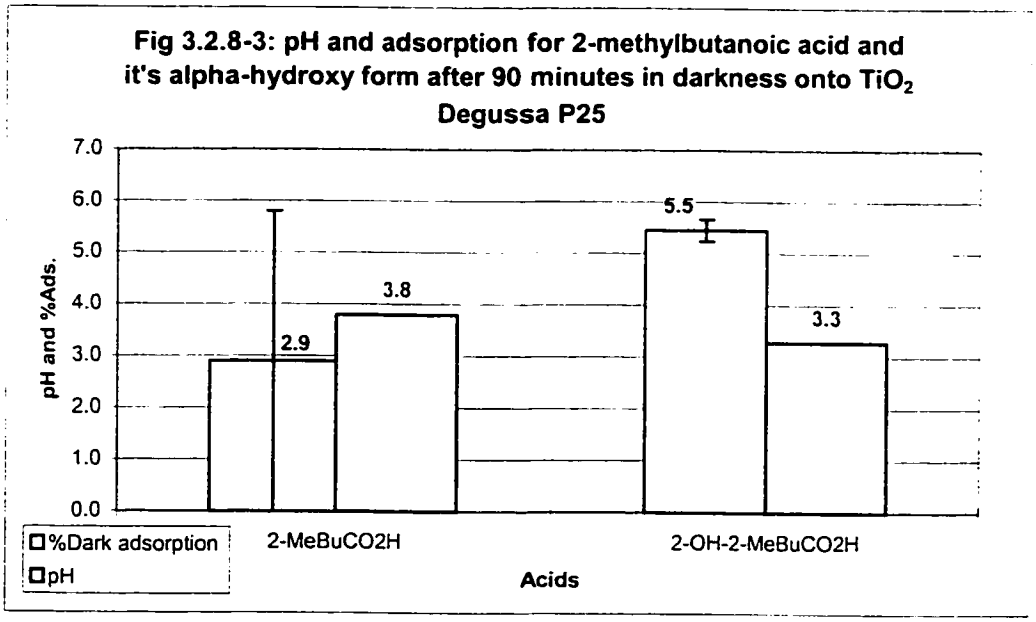

While the pH's of the suspensions containing valeric acid, 2-hydroxyvaleric acid, and 2-ketovaleric acids were 3.8, 6.1 and 6.5 respectively, the dark adsorption values for these acids were 4.6% ± 1.4% , 2.2% ± 0.4%, and 1.4% ± 0.2% respectively. The inverse relationship between pH and dark adsorption still holds. The same applies for 2-methylbutanoic acid and 2-hydroxy-2-methylbutanoic acid where the pH's of their

suspensions were 3.8 and 3.3, respectively whereas their related dark adsorption values were 2.9% ± 2.9% and 5.5% ± 0.2%, respectively. The dominant factor that influences the dark adsorption of these acids seems to be the pH of their suspensions.

3.2.9 Alpha-hydroxy and alpha-keto C4 and C5 aliphatic carboxylic acids: Completeness of destruction

Hydroxy and keto acids were also degraded in this study to gather information on their rates of degradation. Such acids were thought as possible intermediates in the degradation of C1 to C5 linear acid series. Only a few of the possible alpha and keto-hydroxy carboxylic acids that exist for the C3, C4, and C5 linear acids were selected. Among these, they were not degraded completely because the primary interest in their degradation was to obtain their rates of disappearance. This was done for two acids, namely 2-hydroxyvaleric acid and 2-methyl-2-hydroxybutanoic acid. Figures 3.2.9-1 and 3.2.9-2 show three chromatograms per acid at three different irradiation times. These two acids, one an alpha-hydroxy acid and the other an alpha-keto acid, were completely or near by completely destroyed as indicated in the respective chromatograms 3.2.9-1 and 3.2.9-2. No peak could be found for 2-ketovaleric acid after 44 minutes of irradiation (figure 3.2.9-1, chromatogram C) whereas a very small peak was still present after 20 minutes of irradiation for 2-hydroxy-2-methylbutanoic acid (figure 3.2.9-2,

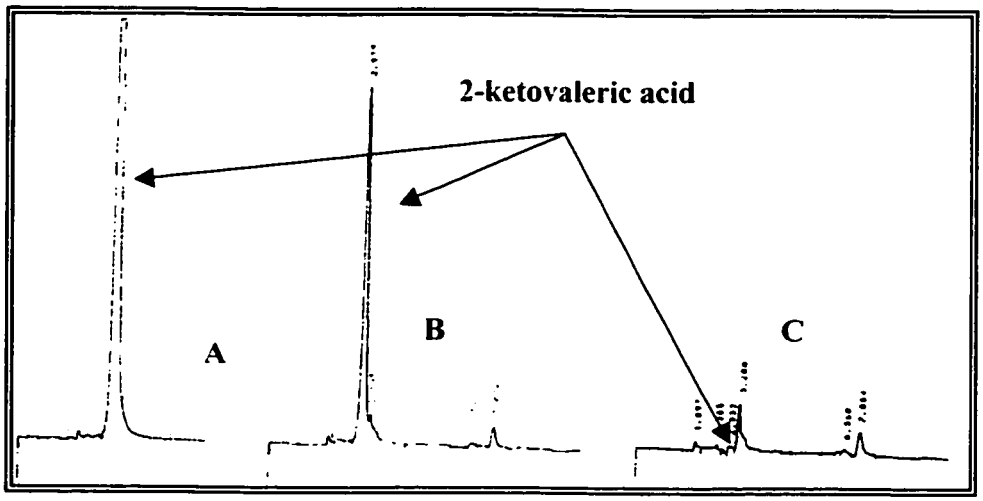

Figure 3.2.9-1: A) Time 5 minutes, B) Time 22 minutes, C) Time 44 minutes.

chromatogram C) thought, in principle, it is possible that intermediates eluted very close to it and made distinction tenuous.

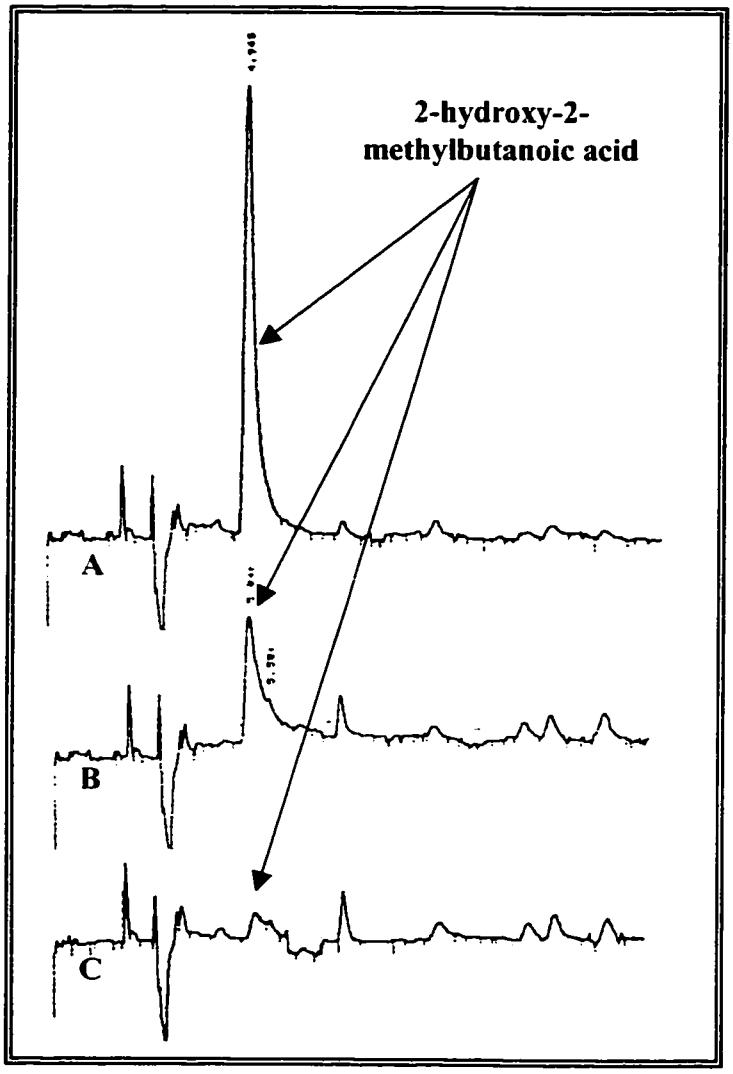

Figure 3.2.9-2: A) Time 5 minutes, B) Time 15 minutes, C) Time 20 minutes.

Futher irradiation beyond 20 minutes would have led to further degradation. Note that the goal of these experiments, at least for these alpha-hydroxy and keto acids, was to obtain information on their rates of disappearance. These acids degrade much faster than their non-oxidized straight chain analogues. Since the latter were clearly demonstrated to fully mineralize when exposed to such a water treatment process, it is deduced that these acids are fully mineralized when treated by the same oxidation method. Alpha-hydroxy and alpha-keto acids are thus completely destroyed, just like the linear acid series and the branched acid series. TiO_2 mediated heterogeneous photocatalysis is thus a proper method to employ to remove such aliphatic carboxylic acids from water.

Figures 3.2.9-1 and 3.2.9-2 also show that most, if not all, of the intermediates that were detected on the chromatograms obtained from samples taken during the degradation of 2-ketovaleric acid and 2-hydroxy-2-methylbutanoic acid eluted at longer elution times than the acids. However, for 2-hydroxyvaleric acid and 2-hydroxybutanoic acid some intermediate products were observed at shorter retention times than these acids during the degradation of the latter (figure 3.2.9-3):

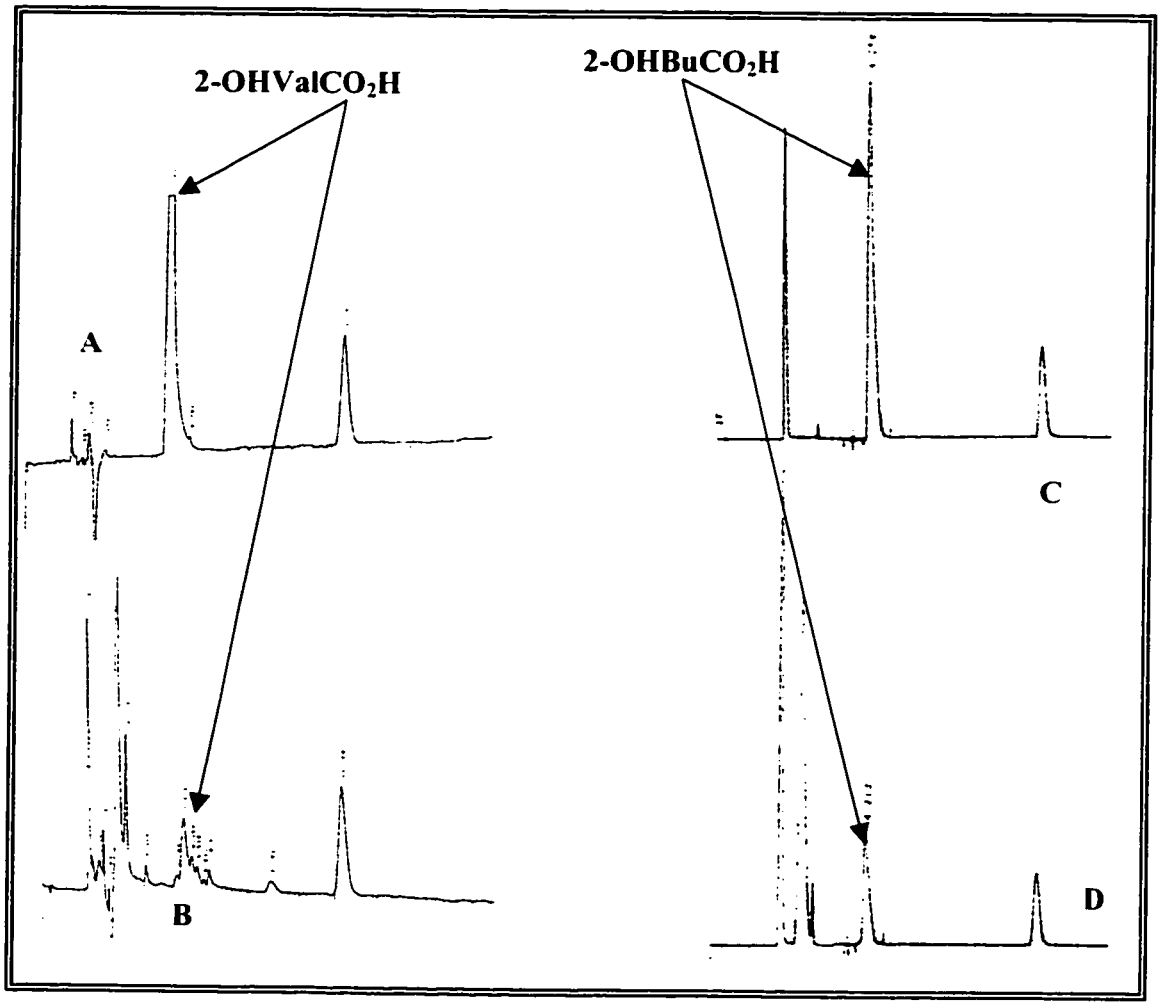

Figure 3.2.9-3: A) Time 0 minutes, B) Time 30 minutes, C) Time 0 minutes, D) Time 20 minutes

It is noteworthy that for both hydroxy acids a peak appears at the end of the chromatograms at time 0 minutes of irradiation. No attempt was made to identify these compounds. They are attributed to adventitious impurities in the starting material. They may be a dehydrated form of the starting material (e.g., 2-butenoic acid from 2-hydroxybutanoic acid). The absence of the hydroxyl group would thus explain the long retention time, since 2-butenoic acid is less water soluble than 2-hydroxybutanoic acid The maximum molar extinction coefficient for the ethylenic system is 10,000 ($\pi \rightarrow \pi^*$ transition, 193 nm) as opposed to 60 for the carboxyl system ($n \rightarrow \pi^*$ transition, 204 nm). Peak intensity than has thus nothing to do with concentration and the intensity of the peaks should not be taken as an impure starting material.

That most (if not all) of the intermediates of 2-ketovaleric acid and 2-hydroxy-2-methylbutanoic acid eluted at longer retention times than these two acids indicates that these intermediates have more affinity for the stationary phase (reverse-phase C8), thus are likely less water soluble then the starting materials. Many species could meet this simple requirement, e.g., aldehydes of approximately the same chain length, lower molecular weight non-oxidized carboxylic acids, unsaturated carboxylic acids, alkenes, alcohols, and others. For instance, butanal ($CH_3CH_2CH_2CHO$) and butanoic acid ($CH_3CH_2CH_2CO_2H$) could form from the decarboxylation of 2-ketovaleric acid. Although these species have one carbon atom less than 2-ketovaleric acid should not cause them to elute at shorter retention times since the 2-keto and 2-hydroxy compounds eluted at shorter retention times than non-oxidized acids of lower molecular weight, with the keto-compounds eluting first. For example, the retention time of butanoic acid was found to be longer than that of 2-hydroxy and 2-keto C5 acids when eluted under the

same chromatographic conditions. The same rationale applies to the intermediates of 2-hydroxyvaleric acid and 2-hydroxybutanoic acid except that intermediates eluted at shorter retention times. These had less affinity for the stationary phase and were likely more water soluble than the 2-hydroxy acids. They might have been lower molecular weight compounds, oxidized or not. Both acids might lead to their keto form (e.g., 2-ketovaleric acid from 2-hydroxyvaleric acid). In fact, the retention time of 2-ketovaleric acid was the same as one of the intermediates of 2-hydroxyvaleric acid that eluted at shorter retention times than the latter.

No TOC degradation was performed on these acids, although on the basis of the evidence that has thus far been presented for the linear and branched carboxylic acid series, the degradation of which can lead to hydroxy and keto acids as intermediate products, they could be mineralized.

3.2.10 Alpha-hydroxy and alpha-keto C4 and C5 aliphatic carboxylic acids: Rates of disappearance

The temporal disappearance of a few selected 2-hydroxy and 2-keto carboxylic acids is illustrated in figure 3.2.10-1 to 3.2.10-4 below:

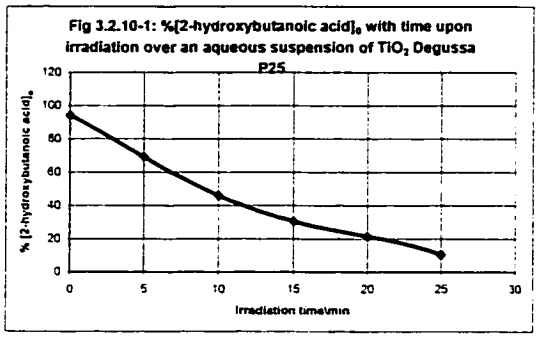

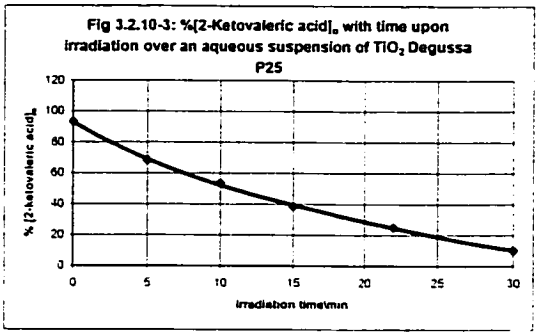

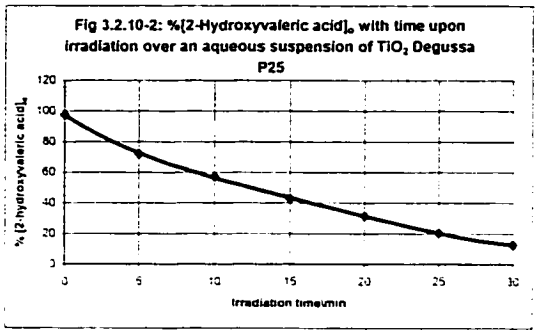

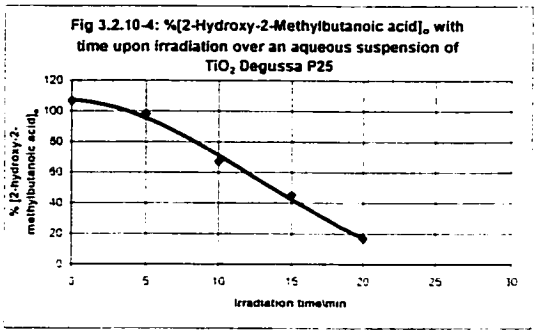

For the four alpha-keto and alpha-hydroxy acids, a trend similar to that observed for the linear series and for the branched series was obtained. The concentration of acid ($[]_o$, 2.0 x 10^{-3} M) decreased linearly with irradiation time to ultimately depart from linearity at lower concentrations. However, unlike the other two series, linearity was maintained over a much shorter period, being maintained approximately over 10 minutes for 2-hydroxybutanoic acid, 15 minutes for 2-hydroxyvaleric acid and 2-ketovaleric acid, and finally over approximately 20 minutes for 2-hydroxy-2-methylbutanoic acid, times at which the remaining amount of acid in solution in the order just listed was 45.9%, 42.9%, 38.6%, and 16.8% of initial concentration. The fact that the time over which linearity

was maintained over a much shorter period for these acids as opposed to the acids of the linear series as well as those of the branched series is solely attributable to the early observation that they degrade much faster than the former acids. However, the difference is negligible when looking at the concentration range over which linearity was maintained. In the present case, linearity was maintained between 16.8% and 45.9% of initial concentration (all four acids included), a situation comparable to what was observed for the acids of the linear series (10% - 42.9%) as well as those of the branched series (10.4% - 37.5%).

The zero-order rate of disappearance of these acids was derived from the slope of the linear regression curve that was plotted through the linear section of the above graphs (see figures 3.2.10-1 to 3.2.10-4 above). These linear regression curves are shown in figures 3.2.10-5 to 3.2.10-8 and the rate data are summarized in table 3.2.10-1 below:

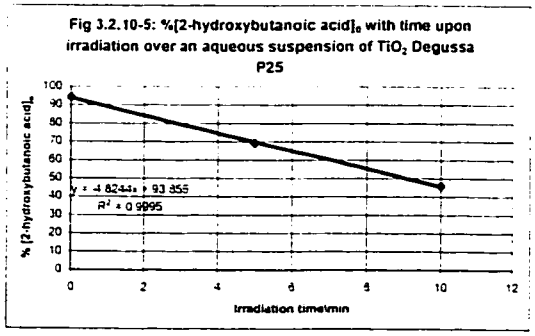

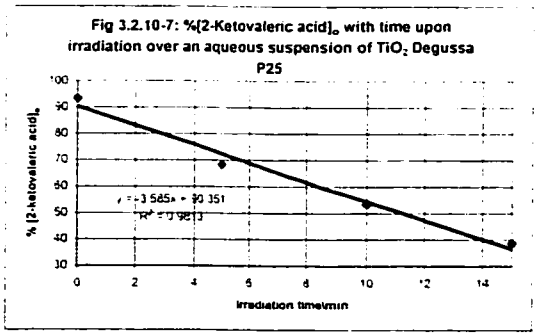

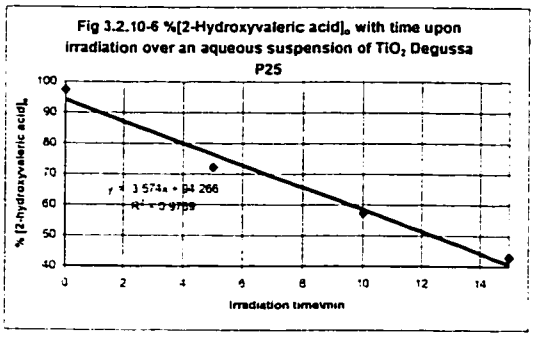

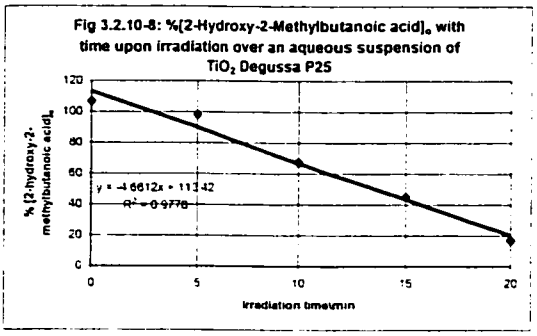

Acid	Rate (umol/hr)	Correlation factor r
2-hydroxybutanoic acid	289 ± 7	0.9997
2-hydroxyvaleric acid	214 ± 22	0.9894
2-ketovaleric acid	215 ± 21	0.9906
2-hydroxy-2-methylbutanoic acid	280 ± 24	0.9888

Table 3.2.10-1: Rate data for some apha-hydroxy and alpha-keto carboxylic acid.

The rates of disappearance were the highest for 2-hydroxybutanoic acid (289 ± 7 μmol/hr) and 2-hydroxy-2-methybutanoic acid (280 ± 24 μmol/hr), whereas the alpha-hydroxy and alpha-keto forms of valeric acid exhibited the slowest rates of the series (214 ± 22 μmol/hr and 215 ± 21 μmol/hr respectively). As done for the linear C1 – C5 linear carboxylic acid series and for the branched C1 – C5 linear carboxylic acid series, the parameters that impact on the rates of disappearance of these acids were controlled (refer to section 3.2.2 for a discussion) with the exception of the pH of the solutions that was governed by the acid being degraded. The pH of a solution and the degree of adsorption of an acid onto TiO_2 are intrinsically related and are known to play a role in the heterogeneous photocatalytic disappearance of organic compounds. Figure 3.2.10-9 below compares dark adsorption data for these acids with their rates of disappearance.

Consistent with the linear series and the branched series, these alpha-hydroxy and alpha-keto acids are all poor adsorbers, the highest extent of dark adsorption obtained for 2-hydroxy-2-methylbutanoic acid (5.5% ± 0.2%). These dark adsorption data were not compared statistically, but they are significantly different when considering their associated errors. The two acids that showed the highest degree of dark adsorption (2-hydroxybutanoic acid and 2-hydroxy-2-methylbutanoic acid) gave rise to the highest

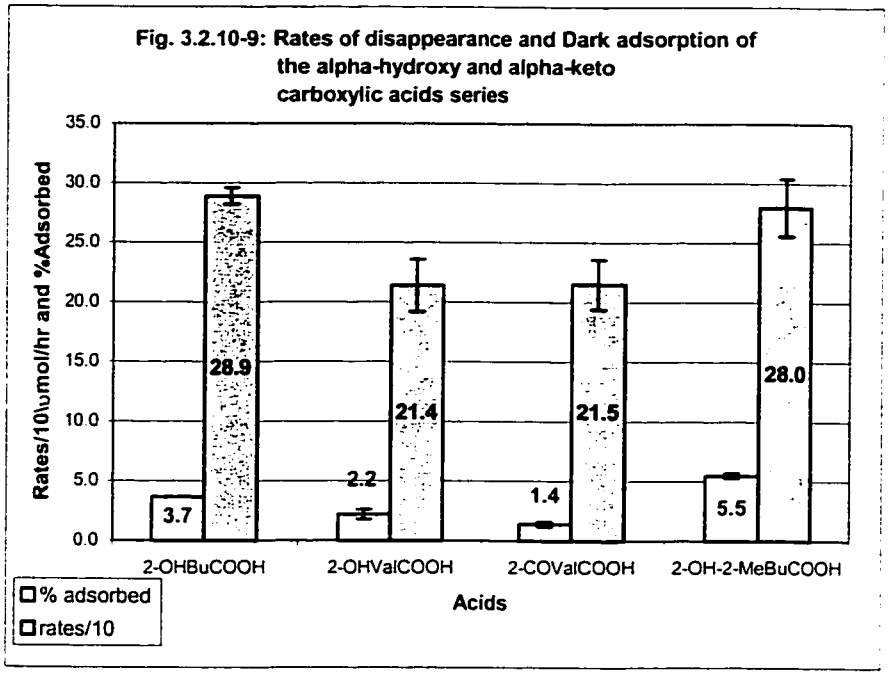

rates of disappearance, an observation that is to be expected if these reactions occur at the surface of the photocatalyst rather than in the bulk of the reaction medium. It is also interesting to note that the pH of the reaction medium for the two acids that gave rise to the lowest rates of disappearance was the highest. Note that the pH's of the 2-hydroxyvaleric acid and 2-ketovaleric acid solutions were 6.1 and 6.5 (sodium salts used), respectively, as opposed to a pH of 3.3 for 2-hydroxy-2-methylbutanoic acid. The oxidation power of TiO_2 is pH dependent and becomes more reducing as pH increases. Thus, the lower rates of disappearance obtained for 2-hydroxyvaleric acid and 2-ketovaleric acid, as opposed to the other two acids, can be rationalized in terms of the pH of their suspension since the latter impacts the adsorptivity of these acids on the catalyst surface (electrostatic attractions) and the oxidative power of the catalyst.

At pH 6.1 and 6.5, pH's slighlty above the isoelectric point of TiO_2 (5.5 – 6.0)[69], the surface of the photocatalyst is slightly negatively charged and thus of the same charge

as the carboxylate salts, a situation that does not favor adsorption of these acids on the photocatalyst surface because of electrostatic repulsion. Indeed, the extent of the dark adsorption of 2-hydroxyvaleric acid was higher than that of 2-ketovaleric acid and its pH was lower. At the same time, the oxidative power of TiO_2 under such conditions was smaller. These two factors forcibly contribute to the fact that these two acids had low rates of disappearance as opposed to the other two.

For all of the acids thus far covered, the experimental observations have been accounted for by considering (1) the extent of dark adsorption of these acids onto the surface of the photocatalyst, (2) the pH of the suspensions which impacts on the former factor as well as on the oxidative power of the photocatalyst, (3) C-H bond strengths and (4) the stability of the radical intermediate products that form following the abstraction of a hydrogen atom from the carbon skeleton of these acids. Should all of the explanations provided thus far be valid, they should hold true if an attempt was to explain the differences observed across all three series of carboxylic acids. Such an analysis begins with valeric acid, 2-hydroxyvaleric acid and 2-ketovaleric acid (linear vs. oxidized).

Fig. 3.2.10-10: Rates of disappearance, Dark adsorption, and pH of Valeric acid and its oxidized forms

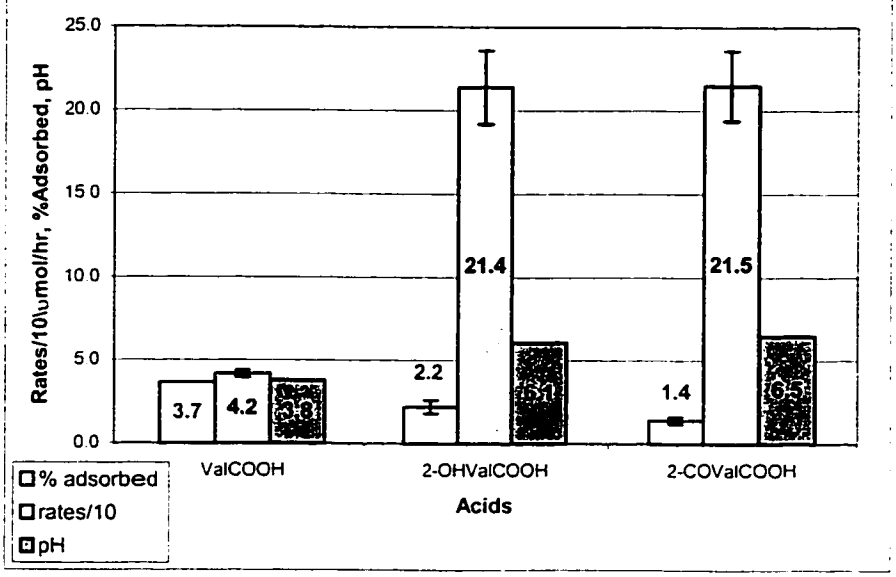

Figure 3.2.10-10 shows the pH, the dark adsorption and the rate of disappearance obtained for these three acids. The pH of the suspensions of these acids and their dark adsorption value are inversely proportional as expected. The pH of the suspension suspension containing valeric acid was lower than the isoelectric point of TiO_2. Hence TiO_2 was positively charged, a situation that contributed to the attraction of the negatively charged deprotonated valeric acid molecules toward its surface. At the other extreme, 2-ketovaleric acid gave rise to the lowest degree of dark adsorption on TiO_2 and its pH was the highest of all three acids. Despite its highest dark adsorption and the low pH of its suspension, two factors that should contribute to a high rate of disappearance, valeric acid gave rise to the lowest rate of these three acids. One could claim that 2-hydroxyvaleric acid bears a probable labile hydrogen atom on its alpha carbon, because of the presence of the hydroxyl group on the same carbon. However, this does not hold true for 2-ketovaleric acid, which bears a hydrogen-free alpha carbon atom. Proton abstraction is not a mandatory and unique pathway toward mineralization of these compounds.

Carboxylic acids can undergo decarboxylation reactions yielding CO_2 and an alkyl radical. The stability of the alkyl radical thus generated impacts on the ease at which these reactions proceed to completion. In this regard, one expects that the better stabilized the generated radical intermediate, the higher the rates. On decarboxylation, valeric acid should yield a butyl radical intermediate. Such primary alkyl radicals are poorly stabilized. On the other hand, both alpha-hydroxy and alpha-ketovaleric acid would, on decarboxylation, lead respectively to a hydroxy and keto-alkyl radical which

can be resonance stabilized (with the hydroxyl group or the keto group). This enhances the degradation rates of these two compounds as opposed to valeric acid. The stability of the radical intermediate products thus accounts for the observed rates. The same analysis is made between 2-methylbutanoic acid and its alpha-hydroxylated form, for which figure 3.2.10-11 shows the pH, the dark adsorption and the rate of disappearance. Once again, an inverse relationship between dark adsorption values and pH of these suspensions was obtained. However, as anticipated and contrary to the data shown above, the trend observed on the rates of disappearance shows a higher rate of disappearance for the acid having the highest degree of dark adsorption on the catalyst surface, and for which the suspension pH was lowest. Nevertheless, considering the fact that (1) both acids' suspensions are of a very similar pH, (2) that their extent of dark adsorption onto the catalyst surface differs by a factor of roughly two, and (3) that 2-hydroxy-2-methylbutanoic acid does not bear any hydrogen atom on its alpha carbon skeleton but yet shows a rate of disappearance that is roughly four fold higher than that of 2-methylbutanoic acid indicates (once again) that other factors account for these rates than pH, extent of dark adsorption and presence of labile protons. Following decarboxylation, 2-methylbutanoic acid leads to a secondary alkyl radical whereas 2-hydroxy-2-methylbutanoic acid leads to a hydroxy-alkyl radical that

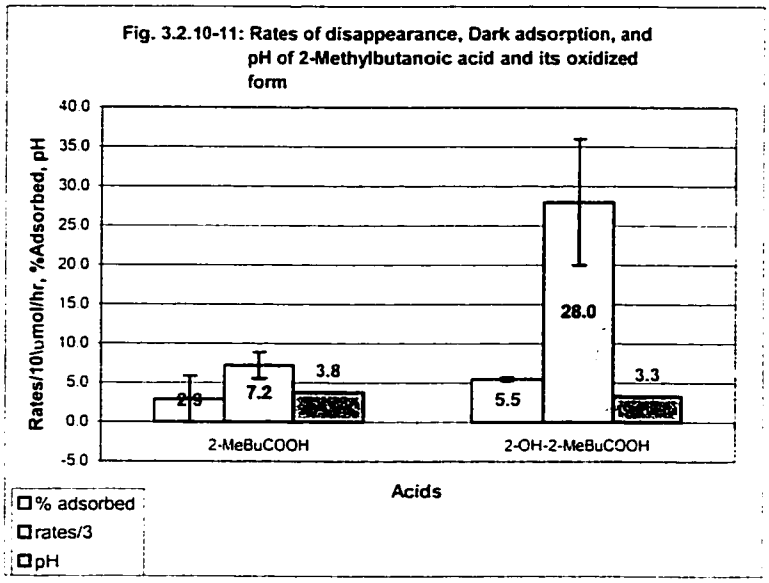

can be resonance stabilized due to the presence of the hydroxyl group attached to the carbon bearing the "lone" electron. There is thus a correlation between stability of the radical intermediates that can form during these reactions and the observed rates of disappearance of these acids.

In accord with the above, similar observations were made in experiments where metals-containing waters were treated by this advanced oxidation method [70]. Most metals can be extracted from water by photoelectrodeposition onto a semi-conductor suspended in water under various conditions. In most cases, the rate of a metal deposition relative to another can be predicted from its reduction potential E°. As a general rule, the higher the reduction potentials the higher the rates. This can be used for selective deposition of a mixture. There are no reasons why this cannot also hold true for organic compounds. Thus, the magnitude of the potential of the redox couple might be the ultimate factor governing the observed rates of disappearance of these acids.

3.3 Investigation of selected carboxylic acids for the presence of oxidized intermediates by HPLC-UV co-elution experiments

3.3.1 Introduction

In explaining the trends that were observed on the rates of disappearance of the linear and branched series of C1 to C5 carboxylic acids, it was noted that the branched acids had, as a general rule, higher degradation rates than their linear counterpart. These observed trends were, explained among other things, on the basis of the strength of the C-H bonds residing on the carbon skeleton of these acids. Indeed, the presence of an alkyl group on an alpha carbon atom (say CH_3-CH**R**-COOH) lowers the dissociation energy of the C-H bonds residing on that carbon because the dissociation energy of C-H bonds follows the trend primary > secondary > tertiary. At the same time, the stability of alkyl radicals follow the trend tertiary > secondary > primary. Since the branched acids degraded faster than their linear parent, and given the effect that branching has on C-H bond strength and on the stability of alkyl radicals, it was hypothesized that the branched acids were "attacked" by hydroxyl radicals on the alpha-carbon, thus losing their alpha hygrogen and leading to a stabilized tertiary alkyl radical. Because of the presence of hydroxyl radical molecules nearby, it seemed very probable that hydroxylation occurred on the alpha carbon, thus generating an alpha-hydroxy acid. The investigation of selected acids for the presence of oxidized intermediates was thus decided on that basis. We have, at the same time investigated these selected acids for other acids than only alpha-hydroxy and alpha keto compounds in attempting to gain some knowledge on the intermediates that are formed during the photocatalytic degradation of these acids.

3.3.2 Determination of required irradiation time

The temporal evolution of the degradation of the acids that were investigated for some potential intermediates was followed by HPLC to determine the best time where to stop the degradation. The primary condition in identifying a degradation product intermediate is of course that the latter be present in solution at a high enough concentration to be detected. The best time at which to stop a degradation was thus selected as the time where most of the intermediates detected (seen on the chromatograms) reached their maximal concentration. Some compromises had to be done. For instance, in some cases, intermediates with high peak areas were allowed to decline (degradation allowed to proceed beyond their point of maximum concentration) in favor of intermediates of low peak area that were still in the process of rising in concentration.

A typical example is shown in figures 3.3.2-1 and 3.3.2-2 for isobutanoic acid. Whereas intermediate I-3 reached a maximum after 4 hours of irradiation, intermediate I-1 is seen only after 5 hours of irradiation. In addition, intermediate I-2 kept trending upward after 8 hours of irradiation, while I-1 and I-3 had already reached their maximum concentration and were declining. The optimal irradiation time for isobutanoic acid, under the applied experimental conditions, was thus selected at 5 hours since this is the time where intermediate I-1 was at its highest concentration, whereas even though intermediate I-3 was declining, it was still present in significant quantity when compared to its maximum at time 4 hours. The same applies to

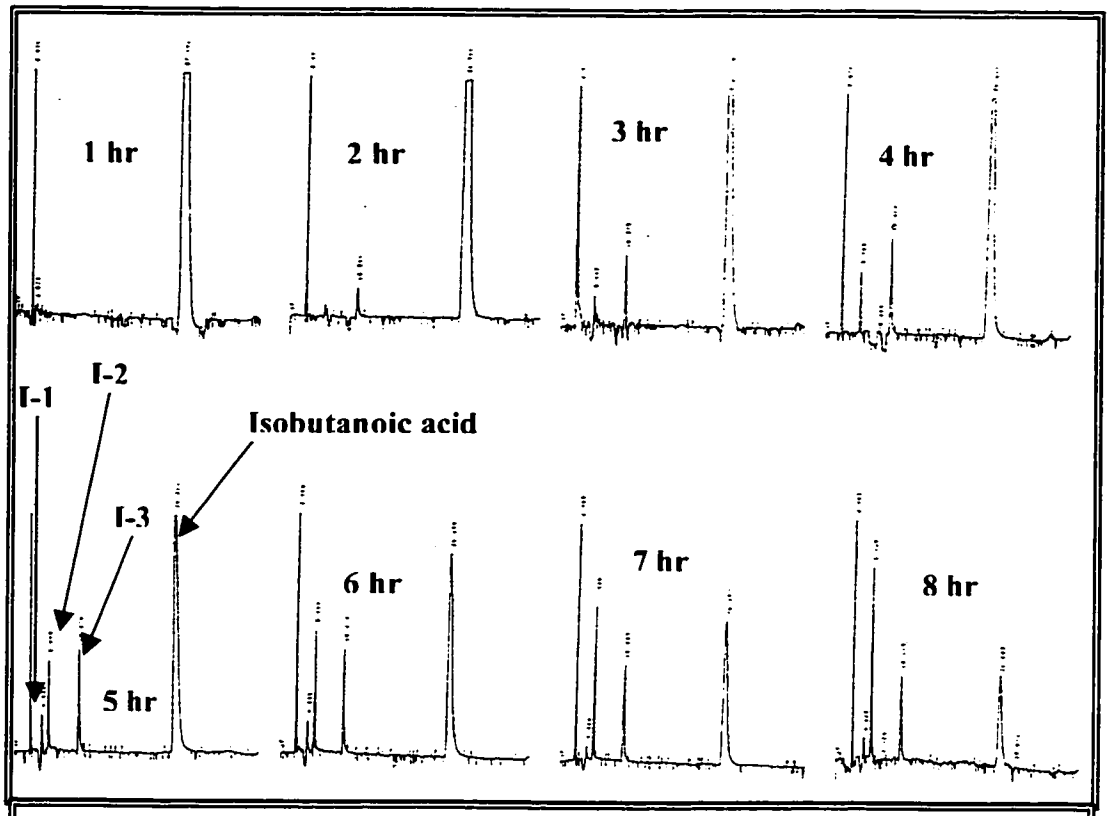

Figure 3.3.2-1 Chromatograms obtained from the analysis of samples taken hourly in a reactor during the degradation of a 1000 ppm of isobutanoic acid in an aqueous TiO_2 suspension. I-1, I-2, and I-3 refer to intermediate-1, 2, and 3 respectively.

Figure 3.3.2-2: Peak areas of the intermediates of isobutanoic acid against irradiation time

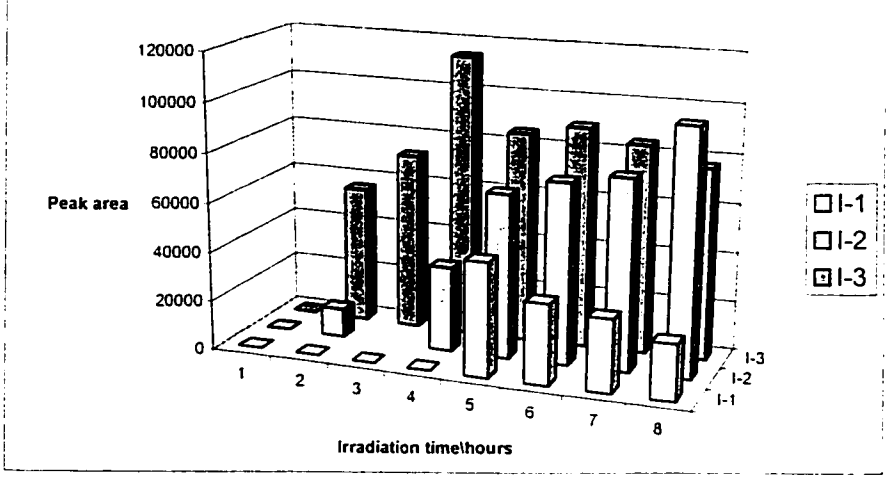

intermediate I-2 for which the concentration was still rising but not drastically lower than what was found after 8 hours of irradiation. Hence, 5 hours was an appropriate irradiation time for most of these intermediates as they all displayed acceptable peak height to perform co-elution runs. The same procedure was used for all other four acids. The results are shown in table 3.3.2-1:

Acid	Optimal irradiation time
Propanoic	8.5 hours
Butanoic	5.5 hours
Isobutanoic	5 hours
Valeric	6 hours
2-methylbutanoic	8 hours

Table 3.3.2-1: Optimal irradiation time of selected aliphatic carboxylic acids for co-elution experiments.

3.3.3 HPLC-UV co-elution experiments

Even though limited as a method, co-elution experiments were performed in attempting to identify the intermediate products that were detected by HPLC methods during the degradation of selected aliphatic carboxylic acids. This method was chosen as a first step for its convenience and simplicity, and also because we expected hydroxylated and keto compounds formed as primary intermediates following the abstraction of a hydrogen atom on the alpha carbon of these acids, followed by the addition of hydroxyl radicals on their carbon skeleton. Under such circumstances, co-elution experiments provided a quick screening method.

The method consisted of the following steps: 1) obtain a chromatogram of the irradiated solution of a given acid, 2) spike an aliquot of the irradiated solution of that acid with the pure acid that is believed to be a potential intermediate and determine if there is a peak overlap between the pure spiked acid and a peak of the irradiated acid. An peak overlap (a peak of the irradiated sample increases in height due to the spiked acid whereas all other peaks decrease in height because of the dilution caused by the spike) provides a positive identification whereas a lack of overlap (an additional peak appears on the chromatogram of the irradiated acid which belongs to the spiked acid) indicates a negative identification. A simple example is shown in figure 3.3.3-1 for propanoic acid (simple because of the very small number of intermediates that were detected in the irradiated solution of that acid). Figure 3.3.3-1-B shows the chromatogram obtained from the irradiated solution of propanoic acid. This chromatogram and that of figure 3.3.3-1-C are identical with the only difference that the middle peak found in figure 3.3.3-1-C has a higher peak area than that of figure 3.3.3-1-B while the two other peaks of figure 3.3.3-1-C are lower than that of figure 3.3.3-1-B. Chromatogram C was obtained from a sample prepared by spiking an aliquot of an irradiated solution of propanoic acid (for the amount of time specified in table 3.3.2-1) with acetic acid. There is clearly an overlap between acetic acid and the middle peak which is an intermediate of propanoic acid. This is an example of a positive identification. At the other extreme, figure 3.3.3-1-A shows a chromatogram that was obtained from a sample prepared by

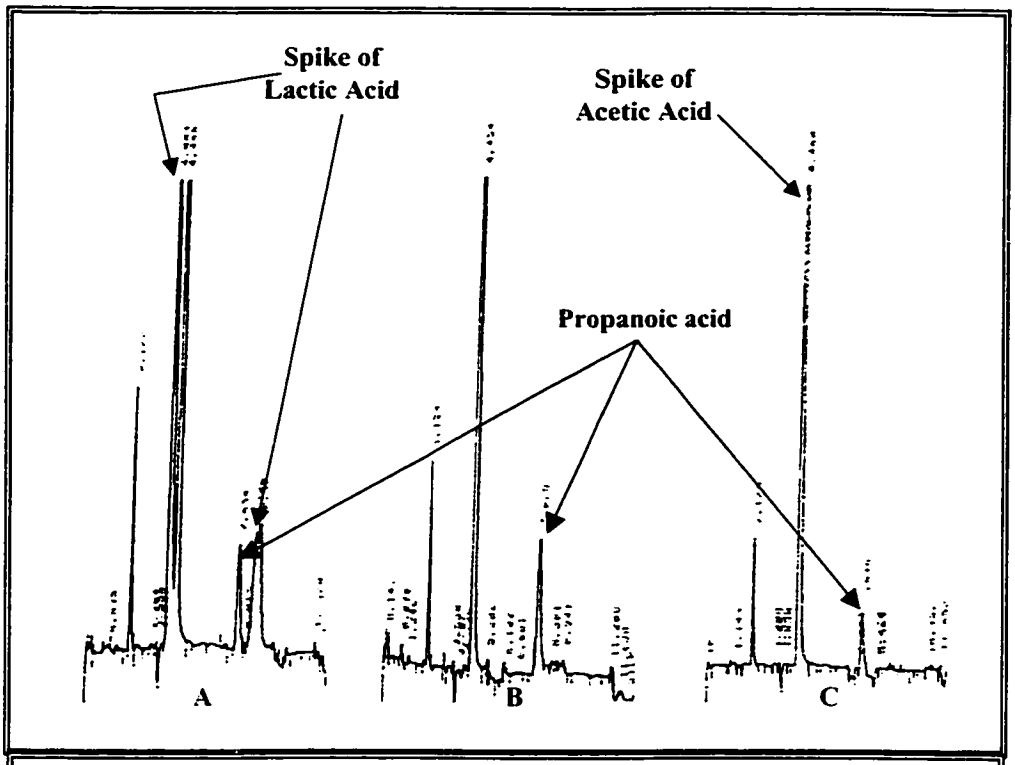

Figure 3.3.3-1 A = Irradiated solution of propanoic acid spiked with lactic acid, B = Irradiated solution of propanoic acid, C = Irradiated solution of propanoic acid spiked with acetic acid.

spiking an aliquot of an irradiated solution of propanoic acid with lactic acid. Comparison of chromatograms A and B shows that lactic acid is not an intermediate in the degradation of propanoic acid. The overall results of this procedure are shown in table 3.3.3-1:

Propanoic acid intermediates investigation		
Acid investigated	**Co-elution**	
	Yes	**No**
2-hydroxypropanoic		X
2-ketopropanoic		X
Acetic	X	

Table 3.3.3-1: Results of the co-elution experiments in trying to identify the intermediates of selected aliphatic carboxylic acids

Butanoic acid intermediates investigation		
Acid investigated	**Co-elution**	
	Yes	**No**
2-hydroxybutanoic		X
Isobutanoic acid intermediates investigation		
Acid investigated	**Co-elution**	
	Yes	**No**
2-hydroxy-2-methylpropanoic		X
Valeric acid intermediates investigation		
Acid investigated	**Co-elution**	
	Yes	**No**
Acetic	X	
Propanoic	X	
Butanoic	X	
2-hydroxypropanoic		X
2-ketopropanoic		X
2-hydroxybutanoic	X	
2-ketobutanoic		X
Valeric acid intermediates investigation (cont.)		
Acid investigated	**Co-elution**	
	Yes	**No**
Acrylic	X	
2-ketovaleric		X
2-hydroxyvaleric		X

Table 3.3.3-1 (Cont.): Results of the co-elution experiments in trying to identify the intermediates of selected aliphatic carboxylic acids.

2-methylbutanoic acid intermediates investigation		
Acid investigated	**Co-elution**	
	Yes	**No**
2-hydroxy-2-methylbutanoic		X

Table 3.3.3-I (Cont.): Results of the co-elution experiments in trying to identify the intermediates of selected aliphatic carboxylic acids.

The initial goal of these experiments was to provide an explanation to the trends observed in the degradation rates of the linear acids. Recall that in most cases (if not all), degradation of branched acids was much faster than unbranched acids. Some of the explanations offered to account for these trends were based on: 1) C-H bond strength which follows the trend primary > secondary > tertiary, 2) the stability of the alkyl radical intermediates that can be formed following the abstraction of a hydrogen atom by an hydroxyl radical attack on the carbon skeleton of these acids which follows the trend 3°>2°>1°, and 3) the lability of the hydrogen atoms located on the alpha carbon of these acids. The alpha carbon was the preferred site for hydrogen abstraction by the hydroxyl radicals, and would in turn lead to formation of an alpha-hydroxylated acid derivative that could be further oxidized to an alpha-keto compound. The above results are, however, deceiving except for 2-hydroxybutanoic acid which was identified as a possible intermediate of valeric acid. In no other cases were alpha-hydroxy acids and alpha-keto acids formally identified as possible intermediates of the selected acids investigated.

It has been clearly demonstrated earlier (section 3.2.10) that the rates of disappearance of alpha-hydroxycarboxylic acids and alpha-ketocarboxylic acids are five fold faster to those of their parent substrate. Hence this would explain why such intermediates were not identified by this HPLC-UV co-elution method.

This is consistent with previous studies of others [71]. For instance, it was reported that some dodecyl derivatives, e.g. dodecan-1-ol and dodecanoic acid are degraded rapidly, at rates about 100 times faster than dodecane, and that CO_2 is evolved almost at the same rate at which dodecane disappears. These observations suggested that the steady-state concentration of oxygenated intermediates is very low [71]. Other sources reported that the first step in the degradation of acetic acid on suspended TiO_2 particles involves the formation of surface-bound hydroxyl radicals (HO•) through hole trapping, that HO• abstracted ∝-H on the acid molecule yielding glycolate ($HOCH_2COO^-$) and glyoxylate ($OCHCOO^-$) species [72]. By contrast, heterogeneous photocatalytic studies involving organic acids in aqueous media and more specifically, acetic acid, propanoic acid and butanoic acid, showed no formation of alpha-hydroxy acids or alpha-keto compounds. In fact, aldehydes, ketones, and alcohols were identified as well as other carboxylic acids having more or less carbon atoms (different chain length) [73]. Differences with this study reside in the applied experimental conditions and in the selected analytical tools and techniques used for the identification of the intermediates formed in the process.

Identification of aliphatic carboxylic acids having a shorter chain length than the parent compound (the acid being degraded) was expected as reported earlier. The mechanism proposed is shown in scheme 3.3.3-1 [73]:

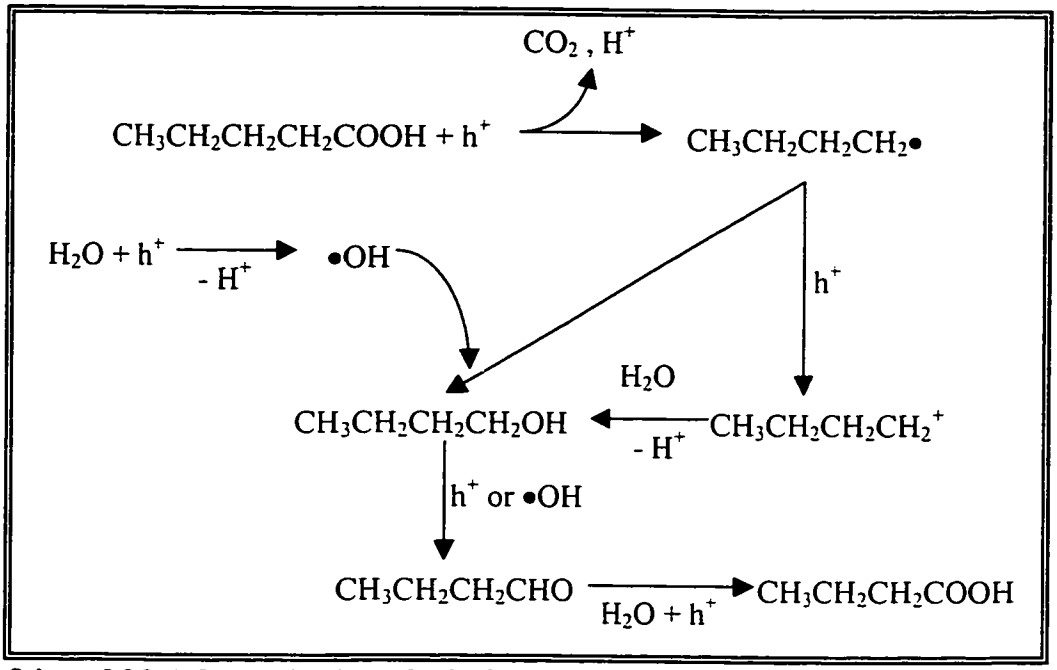

Scheme 3.3.3.-1: Proposed pathway for the formation of a C4 acid from a C5 acid

3.4 GC-FID Investigation of Valeric Acid Intermediates

3.4.1 Introduction

Even though investigated by HPLC-UV, the intermediates of Valeric acid were investigated further by GC-FID as a confirmatory procedure. Although the HPLC-UV co-elution experiments performed on valeric acid gave a positive identification of acetic acid, propanoic acid, butanoic acid, acrylic acid and 2-hydroxybutanoic acid as intermediate degradation products, this procedure does have some limitations. For example, it is not uncommon for two different chemical entities to have the same retention time when eluted under specific column/solvent systems. Thus it is always better to perform such experiments with at least two different columns, or better, by two different methods. The latter option was chosen whereby a gas chromatographic method was used as a complementary method to the HPLC method. In addition, there is always the possibility that not all intermediates from valeric acid present in solution were detected.

Two requirements had to be met for any intermediate to be detected (beside being present at a high enough concentration to be detected): (i) they had to be retained to some extent by the column, (ii) they had to be capable of absorbing 214-nm photons. The study focused solely on valeric acid because 1) it was the one of the series with the longest chain length, 2) shorter chain linear aliphatic carboxylic acids form from longer chain linear aliphatic carboxylic acid and 3) all linear aliphatic carboxylic acids are expected to degrade via the same route.

3.4.2 GC-FID Investigation

Unlike the HPLC-UV co-elution experiment where aliquots of the degraded solution were simply filtered and injected in the liquid chromatograph, the GC-FID method presented a higher challenge in that the chemical entities contained in the degraded solution had to be extracted from water, derivatized (carboxylic acids do not elute well on a GC column as they interact with the packing through hydrogen bonding giving rise to significant tailing), and then injected into the gas chromatograph. Appropriate experimental conditions had to be found for this procedure to be successful. Such conditions included but were not limited to: (1) extraction solvent, (2) volume of extraction solvent per extraction, (3) number of extraction, (4) volume of derivatizing agent relative to the product mix being degraded, (5) reaction time of the derivatization process, (6) temperature of the reaction. Accordingly, we carried out some preliminary experiments systematically to ensure that each step was optimized. This was essential as some intermediates are present in very small concentrations, so that care must be taken to ensure that in the final sample they will be present in high enough concentration so as not to go undetected. The following steps were followed in achieving the GC-FID analysis of a real sample: (1) Solvent selection with a simulated sample, (2) optimization of the extraction procedure with a real sample, (3) Confirmation of the efficiency of the derivatization procedure with a simulated sample, (4) Analysis of real samples.

Two commonly used solvent used for extraction procedures were tested with a simulated sample containing valeric acid (the acid being degraded), butanoic acid (a shorter chain acid that was identified as an intermediate product of the degradation of valeric acid), 2-ketovaleric acid, and two hydroxyvaleric acid. The last two acids were

included in the simulated sample since we were still trying to find alpha-hydroxy and alpha-keto compounds as primary intermediate products forming from the degradation of aliphatic linear carboxylic acids. It was thus important to ensure that they would be extracted from the aqueous solution, especially since they were more water-soluble than their parent compound valeric acid.

Figure 3.4.2-1.1 shows the HPLC chromatograms of the simulated sample when analyzed at different stages of the extraction procedure when ether was used as the solvent:

Figure 3.4.2-1: %acid extracted from a 60ml aqueous solution in 25ml ether extracts

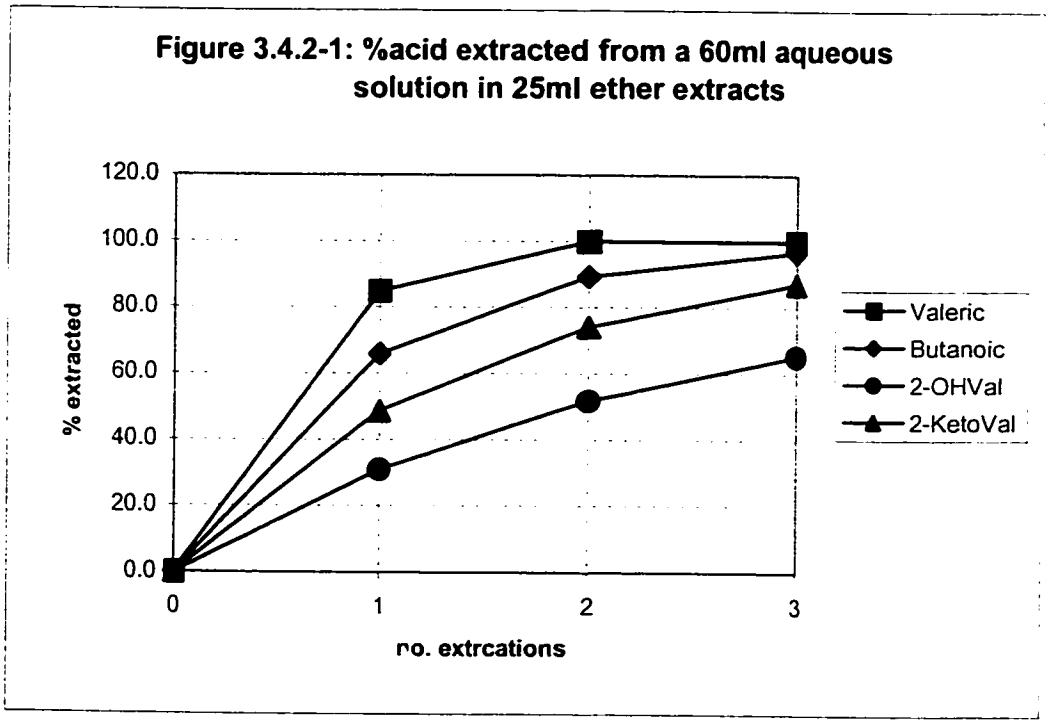

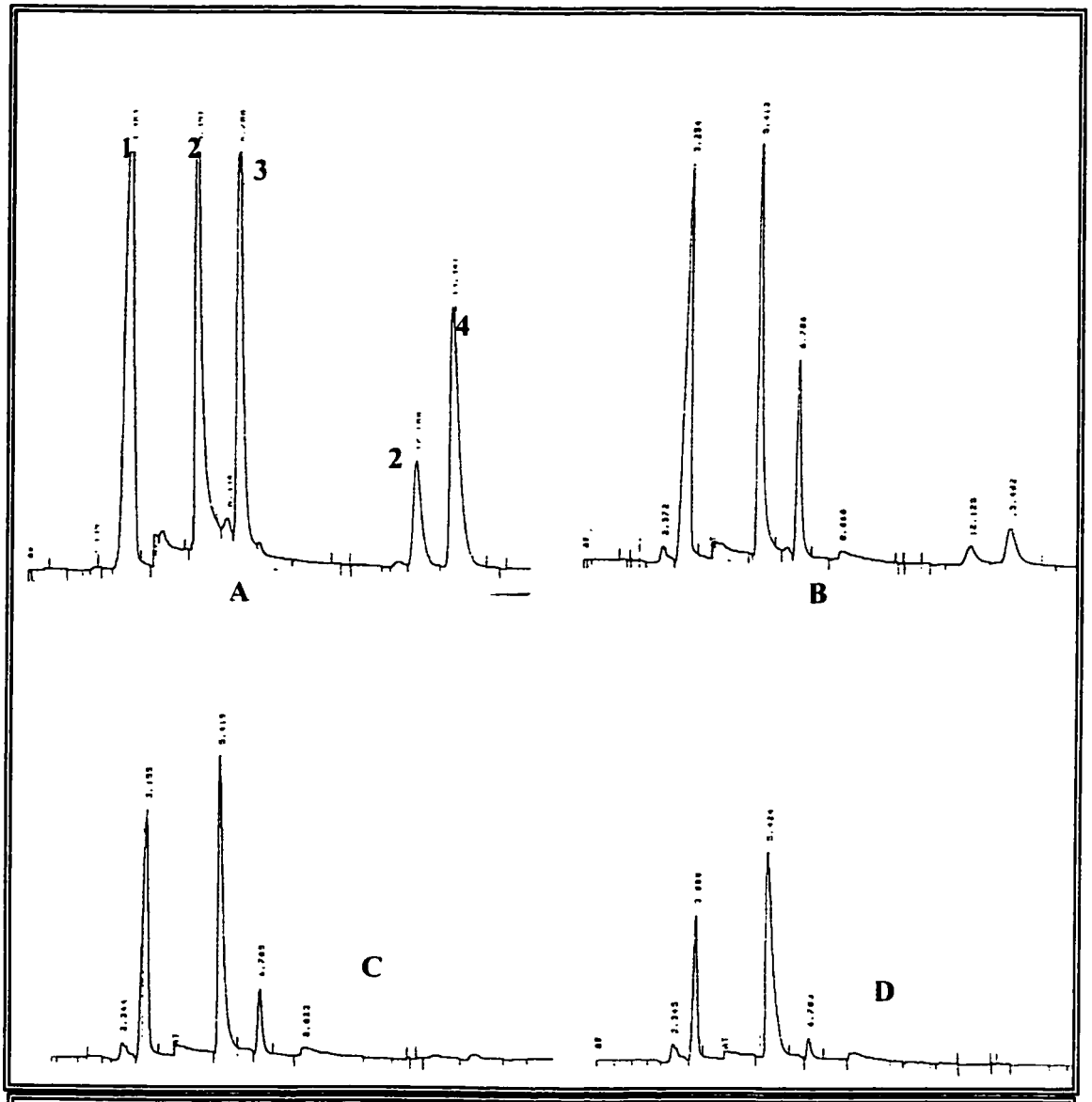

Figure **3.4.2-1.1** : A = simulated sample, B = aqueous phase of simulated sample after extraction-1, C = Aqueous phase of simulated sample after extraction-2, D = Aqueous phase of simulated sample after extraction – 3. 1 = 2-ketovaleric acid, 2 = 2-hydroxyvaleric acid, 3 = butanoic acid, 4 = valeric acid.

Valeric acid and butanoic acid were completely removed from the aqueous simulated sample after three extractions with ether, whereas 2-ketovaleric acid and 2-hydroxyvaleric acid were still present in solution at the end of the procedure. This was not surprising as they are less hydrophobic than the two other acids. Figure 3.4.2-1

shows the extraction profile of each of these acids. With ether as the extraction solvent, a 100% recovery was achieved for valeric acid and butanoic acid, while 2-ketovaleric acid and 2-hydroxyvaleric acid were recovered at 87.2% and 62.4% respectively. Figures 3.4.2-2 to 3.4.2-5 shows the difference in the %recovery that was achieved for each of these four acids using an extraction method with dichloromethane for comparison to that using ether:

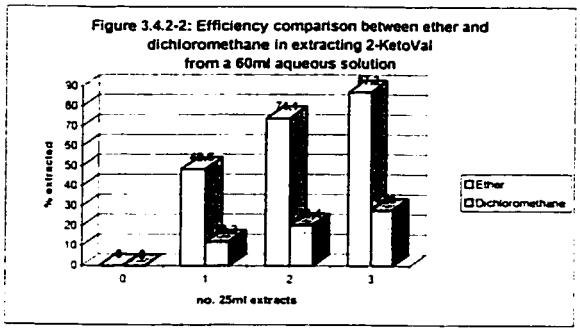

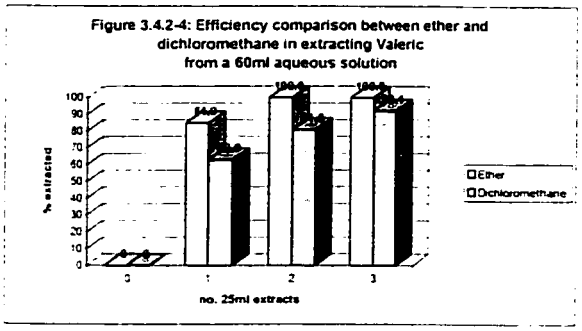

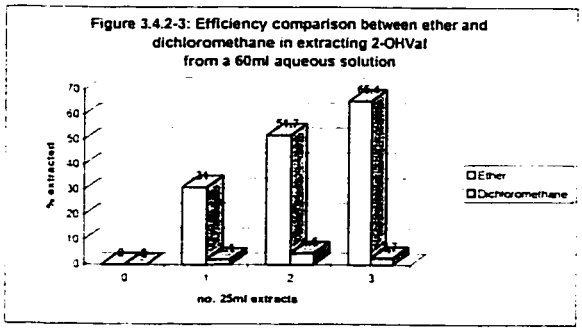

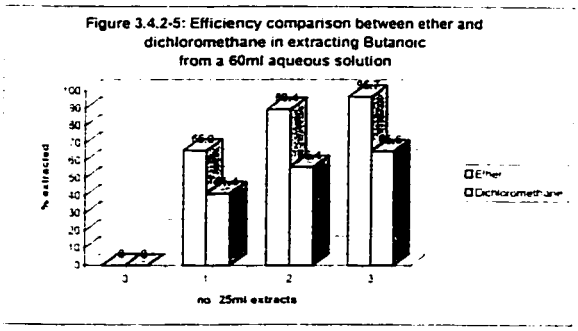

Obviously, ether was more effective in recovering all acids from solution, especially for the 2-keto acid and for the 2-hydroxy acid. Because the %recovery decreases with decreasing chain length for the linear series and because the %recovery is less for the oxygenated acids as opposed to the non-oxidized series, as further evidenced by the data in figure 3.4.2-6, ether was chosen as the preferred extraction solvent. This increases the chances of extracting a sufficient amount of all intermediates present in the

degraded valeric acid solution. Such methodology must precede any investigation to ascertain

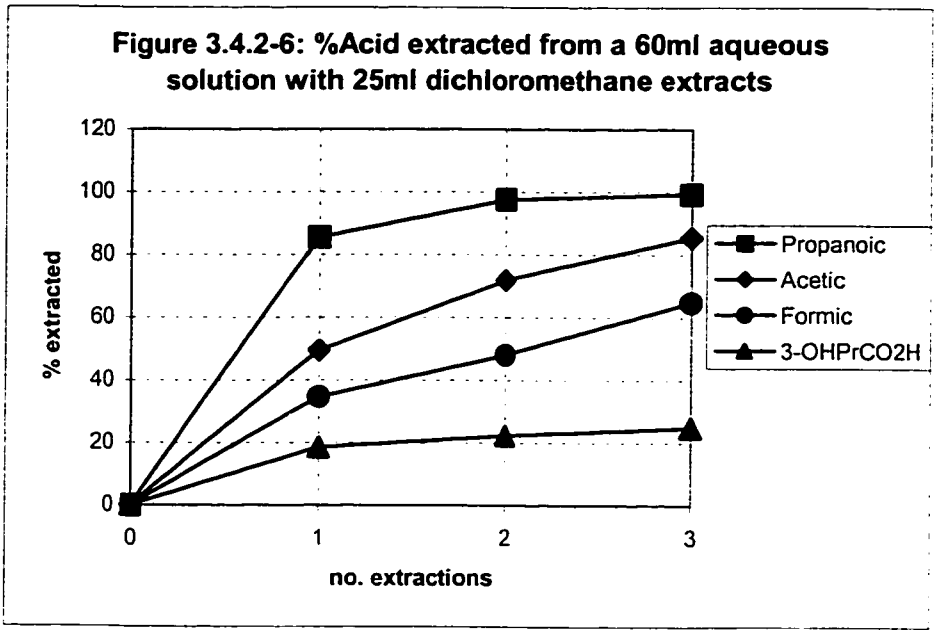

the presence of and identify intermediate products, since an improper methodology will leave some intermediates undetected.

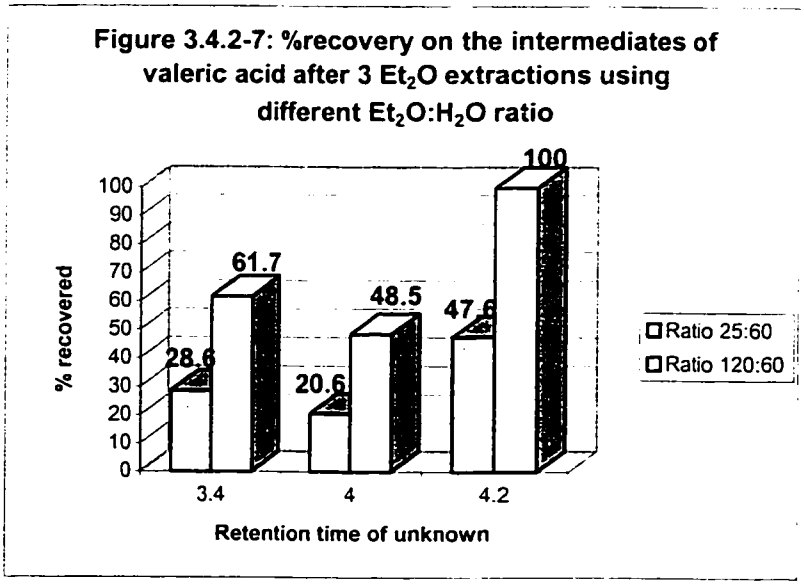

Next the extraction procedure was optimized to achieve the highest recovery possible for all the detected intermediates on the HPLC chromatograms of the degraded solution of valeric acid. Figure 3.4.2-8 (below) illustrates the improvement that was

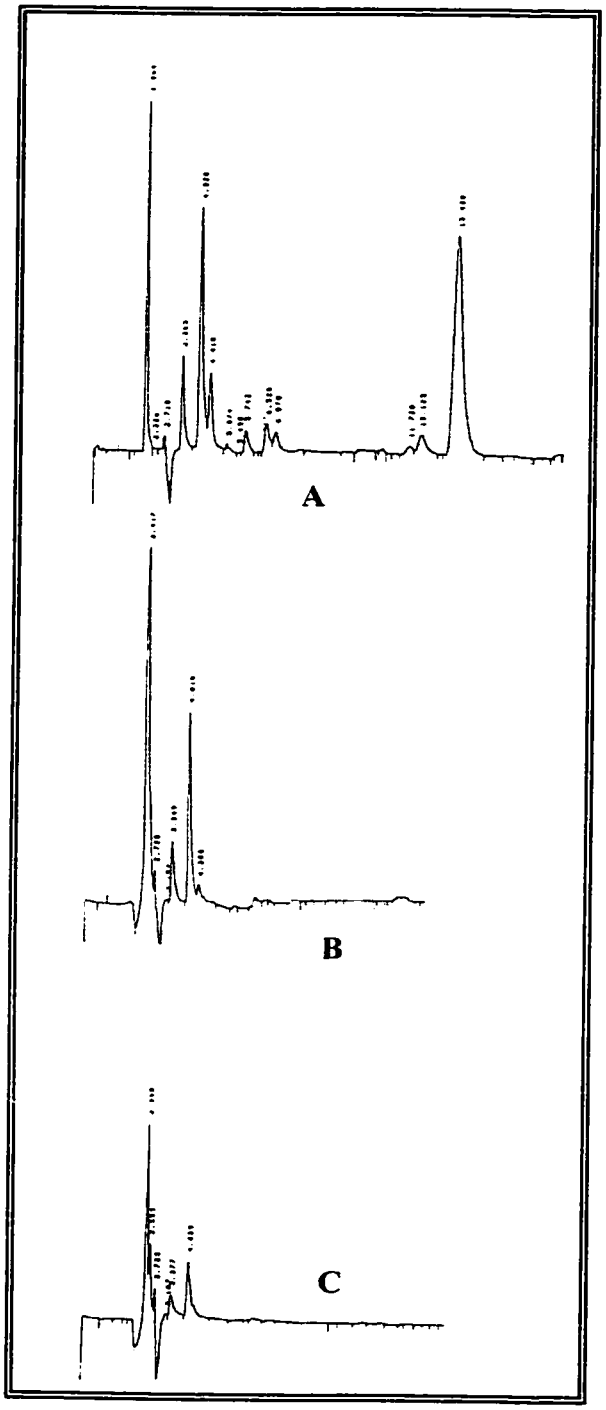

Figure 3.4.2-8: A = irradiated solution of valeric acid, no extractions, B = after 3 extractions with 60 ml of ether, C = after 3 extractions with 120 ml of ether.

achieved with a real sample by optimizing the amount of ether per extraction step. The data are graphically shown in figure 3.4.2-7 (above), where peak areas are compared for specific intermediates. The compounds belonging to the peaks appearing at the shortest retention times were the most difficult to extract. These compounds were likely short chain compounds or oxidized compounds, since the HPLC column was a reverse-phased C8 having more affinity for compounds with a high carbon load.

While the intermediates that eluted at ca. 3.4 minutes, 4.0 minutes and 4.2 minutes were recovered at 28.6%, 20.6%, and 47.6%, respectively, with three 25ml extractions, they were recovered at 61.7%, 48.5%, and 100% respectively when 120 ml of ether was used for each extraction. This is important since most (if not all) intermediates present in the degraded solution of valeric

acid were extracted to an acceptable level. These three unknowns eluted early. They are likely low molecular weight compounds or oxygenated compounds of slightly higher molecular weight, e.g., hydroxy and keto acids.

The next step was to validate the derivatization procedure. After testing it with a few pure acids by injecting them at various time interval (heating time) to ensure that the reaction had reach completion, as indicated by a reproducible peak area for the derivatized acid from injection to injection, the method was tested on a simulated sample

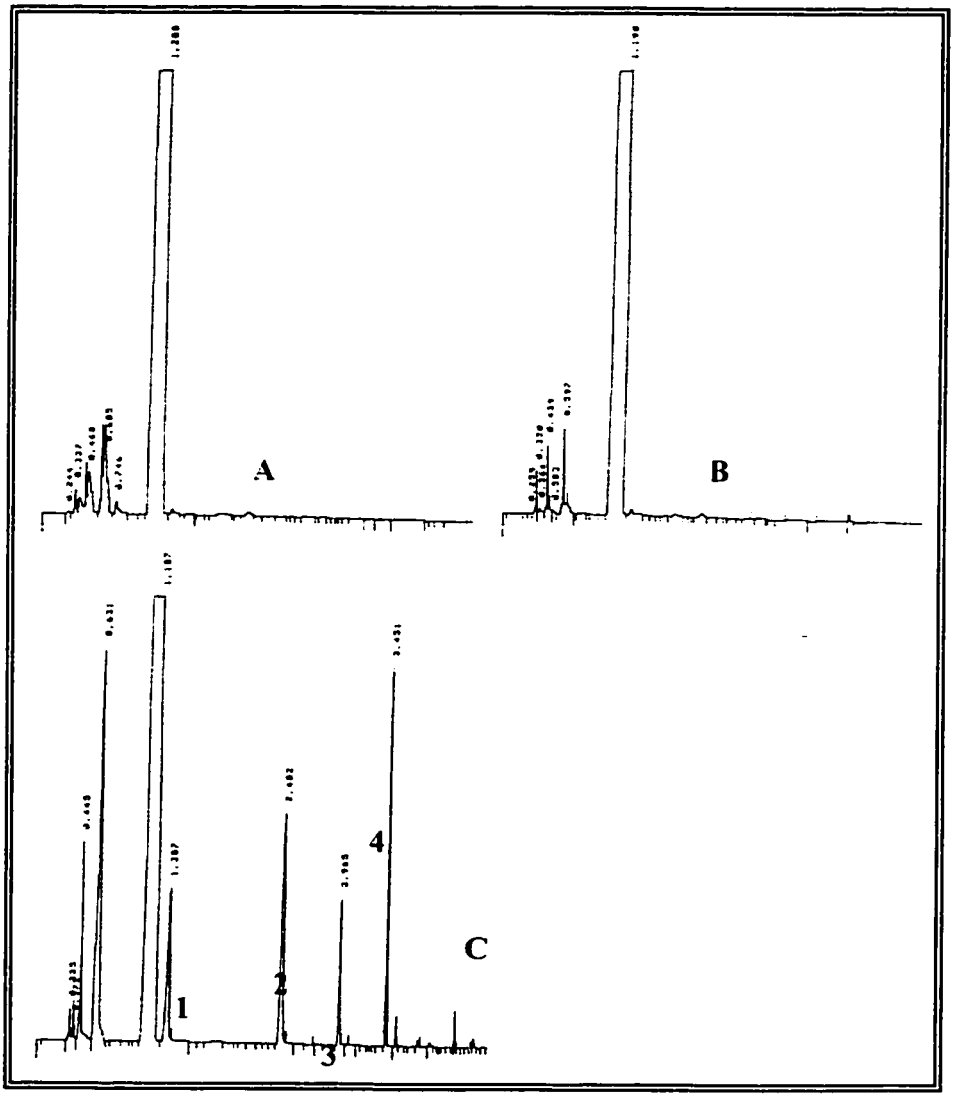

Figure 3.4.2-9: A = derivatizing agent, B = derivatized 3rd ether extract, C = derivatized extract of the simulated sample where 1 = butanoic acid, 2 = valeric acid, 3 = 2-ketovaleric acid, 4 = 2hydroxyvaleric acid. [Acid], 1000 ppm.

composed of valeric acid, butanoic acid, 2-ketovaleric acid, and 2-hydroxyvaleric acid. The same principles used for the pure acids were used for the simulated sample. The derivatized sample was injected a few times to ensure that a constant peak area was obtained. A few typical GC chromatograms are shown in figure 3.4.2-9 (above). The fact that the derivatizing agent (BSTFA with 1% TMS) and the derivatized third extract (figure 3.4.2-9-A and figure 3.4.2-9-B, respectively) gave rise to identical chromatographic patterns indicates that no organic compound was extracted from the aqueous phase during the third extraction (see figures 3.4.2-1 and 3.4.2-6). Note that previous results for which the aqueous phase was sampled and analyzed by HPLC under the exact same conditions showed some residual amounts of intermediate compounds present in the aqueous phase. The intermediate for which the recovery was the lowest was approximately 50% (see figure 3.4.2-7, ratio 120:60). Chromatogram C of figure 3.4.2-9 is that of the derivatized ethereal extract of the simulated sample that contained valeric acid, butanoic acid, 2-ketovaleric acid, and 2-hydroxyvaleric acid. All four acids (derivatized) were detected and displayed appreciable signal intensities.

The above results demonstrate that: 1) the extraction solvent was appropriate, 2) the extraction procedure was optimized to a level where recoveries achieved are acceptable, and 3) the derivatizing procedure allows for the nearly complete conversion of these acids into their trimethylsilylester derivatives. When applied to an irradiated solution of valeric acid, this procedure lead to the following chromatogram:

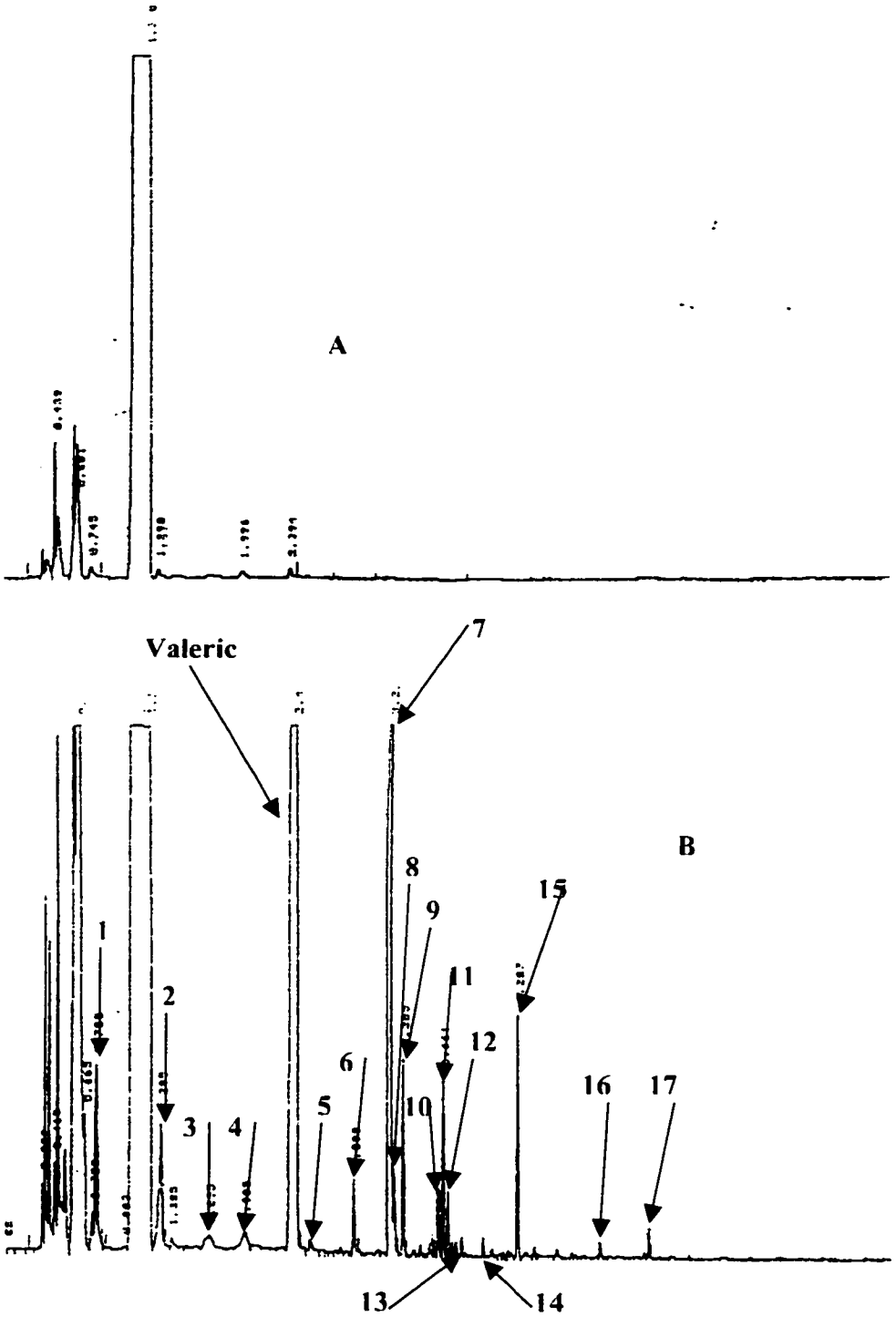

Figure 3.4.2-10 : A) Blank, B) Derivatized irradiated valeric acid, [ ] = 1000 ppm, irradiation time as in table 4.3.2-1.

A comparison between the blank (chromatogram 3.4.2-10-A) and the derivatized irradiated solution of valeric acid (chromatogram 3.4.2-10-B) shows that four peaks appear at shorter retention times than valeric acid, whereas 13 peaks were detected at retention times longer than that of valeric acid. On the type of column that was mounted in the gas chromatograph (polysiloxane DB-5, 5% phenyl: 95% methyl), the elution order was directly proportional to the molecular weight of the compounds being analysed for a given class of compounds. Table 3.4.2-1 shows the retention time results that were obtained for all derivatized acids.

Acid	Mol. wt. ($g \cdot mol^{-1}$)	Retention time (min.)
$AcCO_2Si(CH_3)_3$	132.23	Overlap with blank
$AcrCO_2Si(CH_3)_3$	144.25	3.59
$ProCO_2Si(CH_3)_3$	146.26	0.82
$BuCO_2Si(CH_3)_3$	160.29	1.41
$2\text{-}OprCO_2Si(CH_3)_3$	162.26	1.49
$2\text{-}OBuCO_2Si(CH_3)_3$	174.27	2.59
$ValCO_2Si(CH_3)_3$	174.31	2.43
$2\text{-}OValCO_2Si(CH_3)_3$	188.30	2.97
$(CH_3)_3SiOAcCO_2Si(CH_3)_3$	220.42	3.03
$2\text{-}[(CH_3)_3Si\ O]PrCO_2Si(CH_3)_3$	232.43	3.00
$2\text{-}[(CH_3)_3Si\ O]BuCO_2Si(CH_3)_3$	248.47	3.22
$2\text{-}[(CH_3)_3Si\ O]ValCO_2Si(CH_3)_3$	262.50	3.45

Table-3.4.2-1: retention times and molecular weights for all derivatized acids. General formulas include the trimethylsilyl group replacing the proton of the carboxylic acid group and the alcoholic proton of the hydroxyl group located on the alpha carbon.

Except for acrylic acid, which bears a double bound, it is evident that for the linear aliphatic carboxylic acid series, the retention times followed the order acetic < propanoic < butanoic < valeric acid. Interestingly, the molecular weights for the

derivatized forms of these acids in the enumerated order are 133.23 g/mol, 146.26 g/mol, 160.29 g/mol, and 174.31 g/mol. For oxidized acids vs. non-oxidized acids, the elution order was linear form < 2-keto form < 2-hydroxy form. As an example, for the C3 acids, the order of elution was propanoic acid < 2-keto propanoic acid < 2-hydroxypranoic acid (molecular weights of derivatized form are 146.26 g/mol, 162.26 g/mol, and 232.43 g/mol, respectively). Note that the retention time of the derivatized form of acetic acid was too short to be detected; as it came out with the peaks from the blank. Therefore, all non-oxidized acids having less than 3 carbon atoms and no double bonds could not be separated with the analytical procedure used in this investigation. This means that formic acid and acetic acid could not be identified by this method. The same applied to formic acid when investigated by HPLC-UV. However, acetic acid was positively identified with the latter method, but could not be confirmed by GC-FID.

Therefore, the peaks that eluted at retention times shorter than valeric acid but yet, that did not co-eluted with the peaks found in the blank were probably compounds with post-derivatization molecular weights between that of acetic acid (132.23 g/mol) and valeric acid (174.21 g/mol). In principle, these would be species such as less than C5 non-oxidized acids (butanoic acid and propanoic acid) or alcohols (e.g. derivatized form of butanol, $C_7H_{18}SiO$, molecular weight of 146.30 g/mol), whereas the peaks that eluted at longer retention times than valeric acid might be species such as more than C_5 linear or branched acids, hydroxylated C_2 and more than C_2 acids, unsaturated C_2 and more than C_2 non-oxidized acids, to mention of few. Compounds such as butanol, and alcohols in general, are difficult to detect HPLC-UV because of their hydrophilicity and more importantly, because of the absence of a chomophore (no or little absorption of photons

at 214 nm). Therefore, any alcohols formed during the degradation of valeric acid, were more easily detected by GC-FID than by HPLC-UV. Consequently, more peaks would be obtained in a gas chromatogram for the derivatized sample of the degraded valeric acid solution than in an HPLC chromatogram for the same sample.

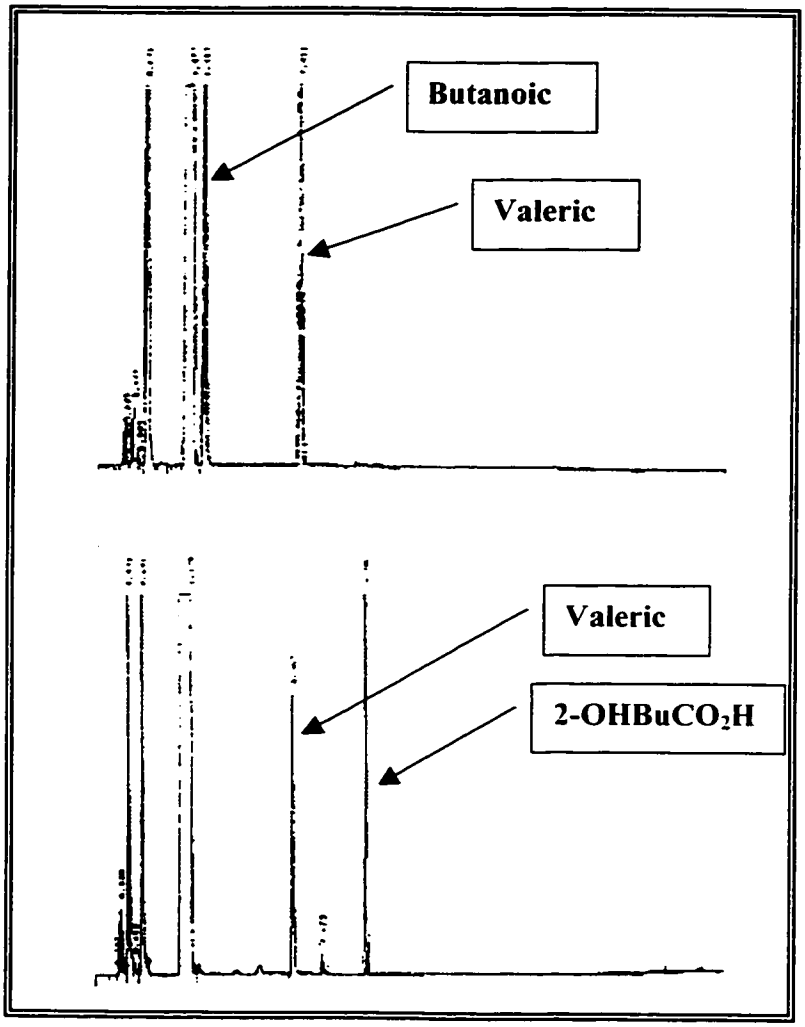

Figure 3.4.2-11 : GC chromatograms obtained for the Valeric/Butanoic couple and for the Valeric/2-hydroxybutanoic acid couple.

Figure 3.4.2-11 shows typical GC-FID chromatograms obtained when screening valeric acid for specific intermediates. In order to obtain relative retention times, mixtures of valeric acid (a standard, not the derivatized acid) and of an acid of interest were derivatized and then injected into the gas chromatograms. The use of relative retention times instead of absolute retention times was made because the GC used was not equipped with an auto-sampler nor did it have a feature that starts the run automatically once the sample is injected. The run was started manually after sample injection, which may contribute to increase the

variance on retention times. Relative retention times avoid this problem. The repeatability of relative retention times for replicate runs were of the order of ± 0.003. Any difference in relative retention time between the standards and the peaks found on the chromatogram of the irradiated solution of valeric acid of 0.012 (3 std) or less was thus considered as being a positive identification. The relative retention time data for the acids that were included in this investigation are given in table 3.4.2-2. Table 3.4.2-3 gives the relative retention times of all the intermediates that were detected by GC-FID (figure 3.4.2-10) and indicates the acid with which a match was obtained on the basis of relative retention times. Finally, table 3.4.2-4 provides the combined results of the HPLC-UV experiment and the GC-FID experiments for confirmation purposes. Basically, when investigated by HPLC-UV, five valeric acid intermediates were positively identified (acetic, propanoic, butanoic, 2-hydroxybutanoic, and acrylic acid), whereas with the GC - FID method, four valeric acid intermediates gave positive identification (propanoic, butanoic, 2-hydroxybutanoic, and 2-ketovaleric acid). Only three intermediates were positively identified by the two methods. They were propanoic acid, butanoic acid, and 2-hydroxybutanoic acid. The fact that a positive identification has been obtained by two different methods for these three acids is

Acid	Rel. RT
Propanoic	0.32
Butanoic	0.54
2-ketopropanoic	0.57
Valeric	1
2-ketobutanoic	1.06
2-hydroxypropanoic	1.23
2-ketovaleric	1.25
2-hydroxyacetic	1.27
2-hydroxybutanoic	1.35
2-hydroxyvaleric	1.45
Acetic	N/A
Formic	N/A
oxalacetic	1.85

Table 3.4.2-2: Relative retention times for selected carboxylic acids.

Unknown no.	rel. RT	Matches with
1 (Major)	0.31	Propanoic
2 (Major)	0.54	Butanoic
3 (Minor)	0.70	No match
4 (Minor)	0.82	No match
5 (Minor)	1.05	2-ketobutanoic
6 (Major)	1.20	No match
7 (Major)	1.34	2-hydroxybutanoic
8 (Major)	No RT assigned	No match
9 (Major)	1.37	No match
10 (Major)	1.50	No match
11 (Major)	1.52	No match
12 (Major)	1.54	No match
13 (Minor)	1.55	No match
14 (Minor)	1.56	No match
15 (Major)	1.78	No match
16 (Minor)	2.04	No match
17 (Minor)	2.22	No match

Table 3.4.2-3: Relative retention times of the intermediates of valeric acid as determined by GC-FID and the corresponding acids that they are believed to be.

Acid investigated	Positive id by HPLC-UV	Positive id by GC-FID
Formic	No [1]	No [1]
Acetic	Yes	No [1]
Propanoic	Yes	Yes
Butanoic	Yes	Yes
2-hydroxypropanoic	No	No

Table 3.4.2-4: Combined HPLC-UV and GC-FID identification results for the investigation on the intermediates of valeric acid. [1] Eluted in the solvent front.

Acid investigated	Positive id by HPLC-UV	Positive id by GC-FID
2-ketopropanoic	No	No
2-hydroxybutanoic	Yes	Yes
2-ketobutanoic	No	Yes
Acrylic	Yes	No
2-ketovaleric	No	No
2-hydroxyvaleric	No	No
2-hydroxyacetic	No	No
Oxalacetic	No	No

Table 3.4.2-4 (Cont.): Combined HPLC-UV and GC-FID identification results for the investigation on the intermediates of valeric acid.

evidence of their presence. As far as acetic acid is concerned, no such confirmation could be obtained because of the low volatility of the derivatized form of this acid that lead to its elution in the solvent front. Despite the limited identification made by this entire methodology, the good news is that an alpha-hydroxyacid (2-hydroxybutanoic acid) could be identified formally, which shows that hydroxylation on the alpha-carbon does take place. However, it would have been desirable to ascertain whether alpha-hydroxy and alpha-ketoacids were the primary intermediates in the degradation process of a carboxylic acid. For this, the presence of 2-hydroxyvaleric and of 2-ketovaleric acid would have had to be demonstrated.

It is clear that the GC-FID method also has its limitations, and thus cannot provide an accurate picture of events occurring when a compound is degraded by this advance oxidation method. Both methods (HPLC-UV and GC-FID) are limited in doing so because of the vast spectrum of compounds that likely form during the degradation process (17 peaks obtained by the GC-FID method), each compound being present in a

wide range of concentration (from very low to fairly high), and each compound having a wide range of degradation rates (from low to high), which can possibly cause key intermediates to go unnoticed. The fact that different classes of compounds are formed (e.g.: alcohols, aldehydes, alkanes, shorter or longer chain acids, etc.) makes the detection of all species a challenging taste.

3.5 GC-MS Investigation of Valeric Acid Intermediates

3.5.1 Introduction

In this section we employ the GC-MS methodology to identify intermediates formed from the heterogeneous photocatalyzed degradation of valeric acid, and more specifically, to show that 2-hydroxyvaleric acid and 2-ketovaleric acid are present in solution as primary intermediates that form following hydroxyl radical attack at the alpha-carbon of the acid backbone. The main driving factor that leads to the use of GC-MS to identify intermediate products for this acid is to overcome some of the limitations of the two previous method, HPLC-UV co-elution methods and GC-FID methodology with relative retention time determination. These two methods rely almost exclusively on commercially available reference standards to identify intermediates, thus the limitation. GC-MS is a more powerful method since mass spectra can more reliably identify spectra as opposed to relying exclusively on retention times. Moreover, since spectral libraries are commonly available as an additional tool to assist identifying unknown compounds provides greater capability for this type of investigations.

3.5.2 GC-MS Investigation

The same sample preparation methodology used for GC-FID experiments was employed for the GC-MS investigation. The adequacy of the extraction procedure and of the derivatization procedures were clearly demonstrated. Thus, no changes were made to them except that in the present case, a scale-up was performed whereby the extraction procedure was applied to the entire 400 ml of filtrate (recovered following the irradiation

of the acid) instead of on an aliquot of 60 ml of the latter. A much larger amount of intermediate compounds was recuperated. The derivatized filtrate was also analyzed by GC-FID prior to perform GC-MS runs in order to fully optimize the separation method. This was required because of the possible larger numbers of compounds being detected that could have been improperly separated by the prior method. The resulting pre-GC-MS GC-FID chromatograms for the blank and the derivatized sample are shown in figure 3.5.2-1. The difference between this chromatogram (scaled-up extraction procedure) and that shown in figure 3.4.2-4 (section 3.4.2-10, original optimized extraction method) resides in the number of peaks. More than forthy peaks were detected with the up scaled extraction procedure as opposed to seventeen with the former method. This shows the enormous challenge that the identification of the intermediates formed from the heterogeneous photocatatalytic degradation of an organic compound is, even when as simple as a linear aliphatic carboxylic acid. It also puts emphasis on the previously claimed limitations of the HPLC-UV method and the GC-FID method.

The GC-MS chromatograms obtained for the derivatized sample of the irradiated solution of valeric acid following the application of the scaled up extraction procedure are shown in figures 3.5.2-2 to 3.5.2-4. The chromatograms have been magnified and separated into three sections for clarity. The peaks that are numbered have been formally identified by using a computerized mass spectral library. All other peaks that have not been numbered were either (1) not found in the blank or could not be matched to any reference mass spectra in the library, no identification could be made from their mass spectral data, or (2) they were also found in the blank at the same retention time. The overall results of this investigation are given in table 4.5.2-1.

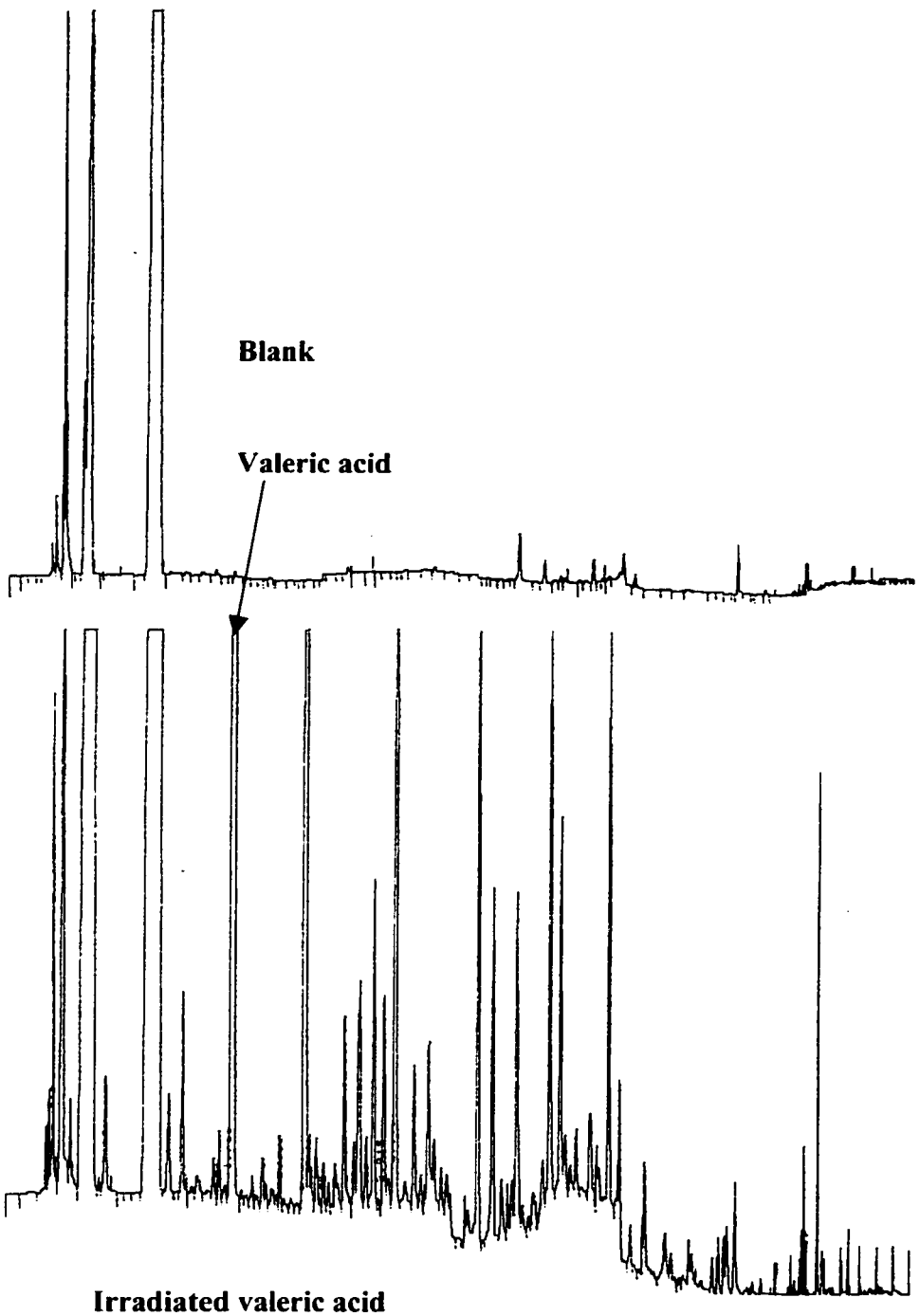

Figure 3.5.2-1 : Chromatogram obtained for the derivatized sample of the irradiated aqueous TiO_2 suspension of valeric acid extracted with the scaled up procedure and that obtained for a blank treated under the exact same conditions.

In this table, "Peak no." refers to the peak numbers on the total ion chromatogram shown in figures 3.5.2-2 to 3.5.2-4. "Compound" refers to the derivatized compounds that have been identified by using the mass spectral library following the GC-MS analysis of the derivatized extract. "Correlates to" refers to the underivatized form of these compounds. "Molecular weight" refers to the molecular weight of the derivatized compounds that have been identified by using the mass spectral library following the GC-MS analysis of the derivatized extract. As shown in this table, peak no.-3 (see figure 3.5.2-2) is that of valeric acid. Its presence is attributed to the fact that its degradation was not driven to completion. The spectral library assigned an 80% match to this peak, even though this peak is definitely that of valeric acid as confirmed with a derivatized standard of that acid. The explanation for the lower than expected match for this acid rest on the fact that valeric acid co-eluted with some compounds that were present in the total ion chromatogram of the blank (peaks appearing at time 6.57 minutes and 6.64 minutes in figure 3.5.2-2-A). This shows some pitfalls of the procedure used for the preparation of the sample. The scale-up of the extraction procedure whereby the entire 400 ml of the irradiation solution of valeric acid was extracted with ether consumed a large amount of the extraction solvent. Three aliquots of 120 ml of the irradiated solution were extracted with three portions each of 240 ml of ether (thus 720 ml of ether were required per aliquot of irradiated solution), accounting for 360 ml of the irradiated solution. The residual 40 ml of irradiated solution were also extracted with three portions of 80 ml of ether, for a total of 240 ml. Thus, the total amount of ether required for the complete extraction procedure was approximately 2.4 L. The evaporation of the entire amount

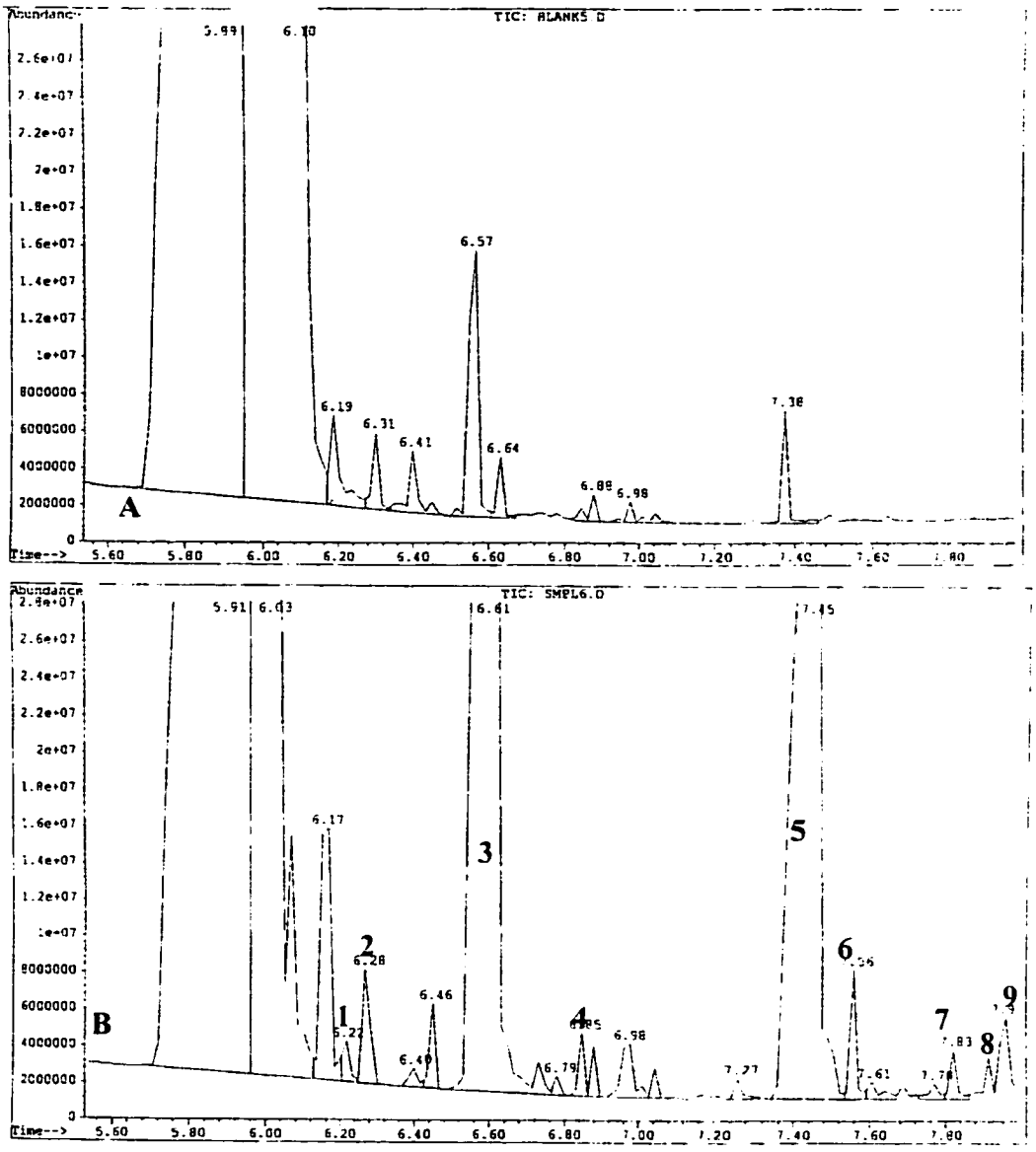

Figure 3.5.2-2: Total ion chromatogram following the solvent delay ranging from 5.5 to 8.0 minutes of A) a blank that was treated in the exact same manner as the sample and B) the irradiated solution of valeric acid. The peaks that are numbered have been formally identified by using a computerized mass spectral library.

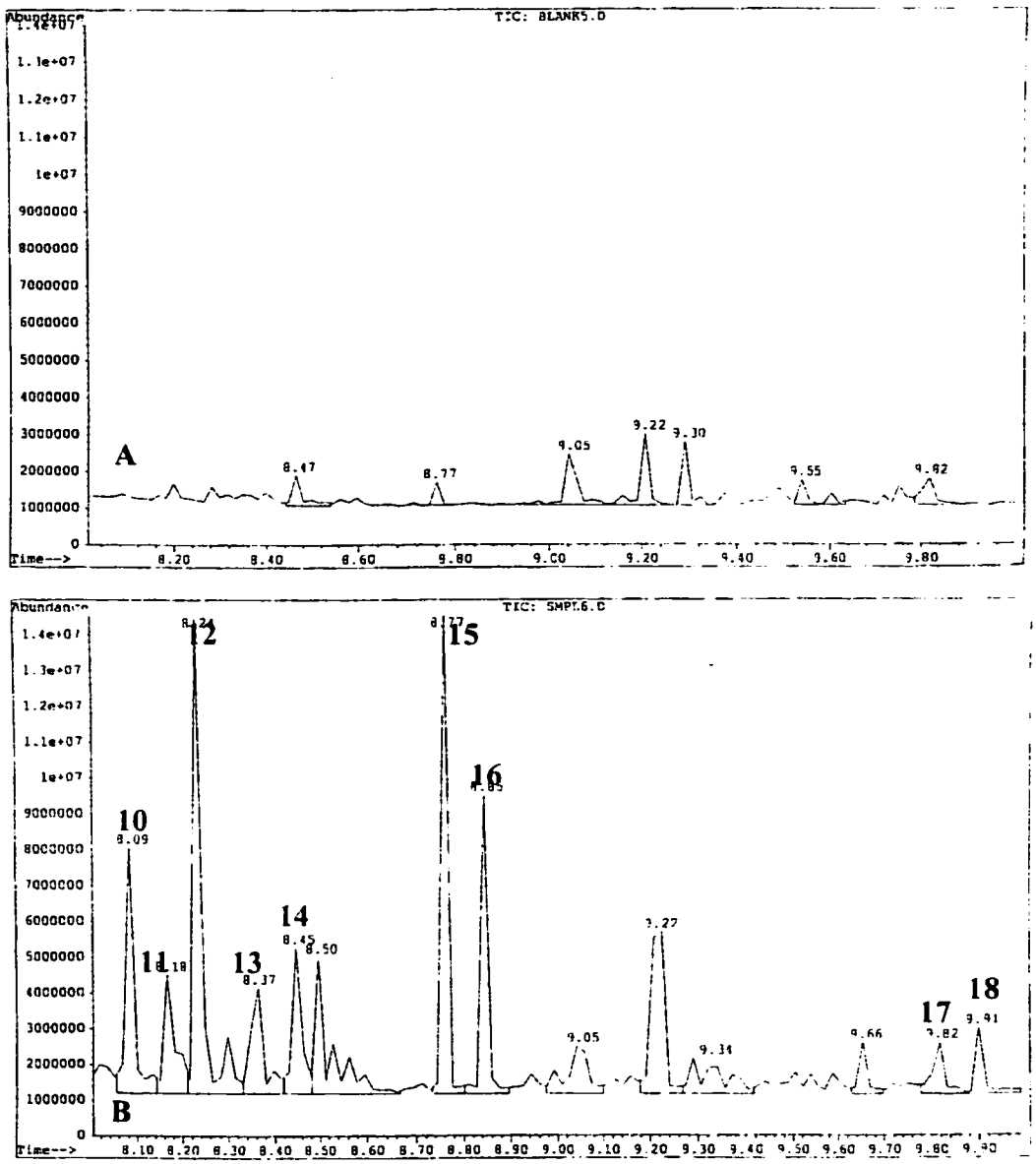

Figure 3.5.2-3: Total ion chromatogram following the solvent delay ranging from 8.0 to 10.0 minutes of A) a blank that was treated in the exact same manner as the sample and B) the irradiated solution of valeric acid. The peaks that are numbered have been formally identified by using a computerized mass spectral library.

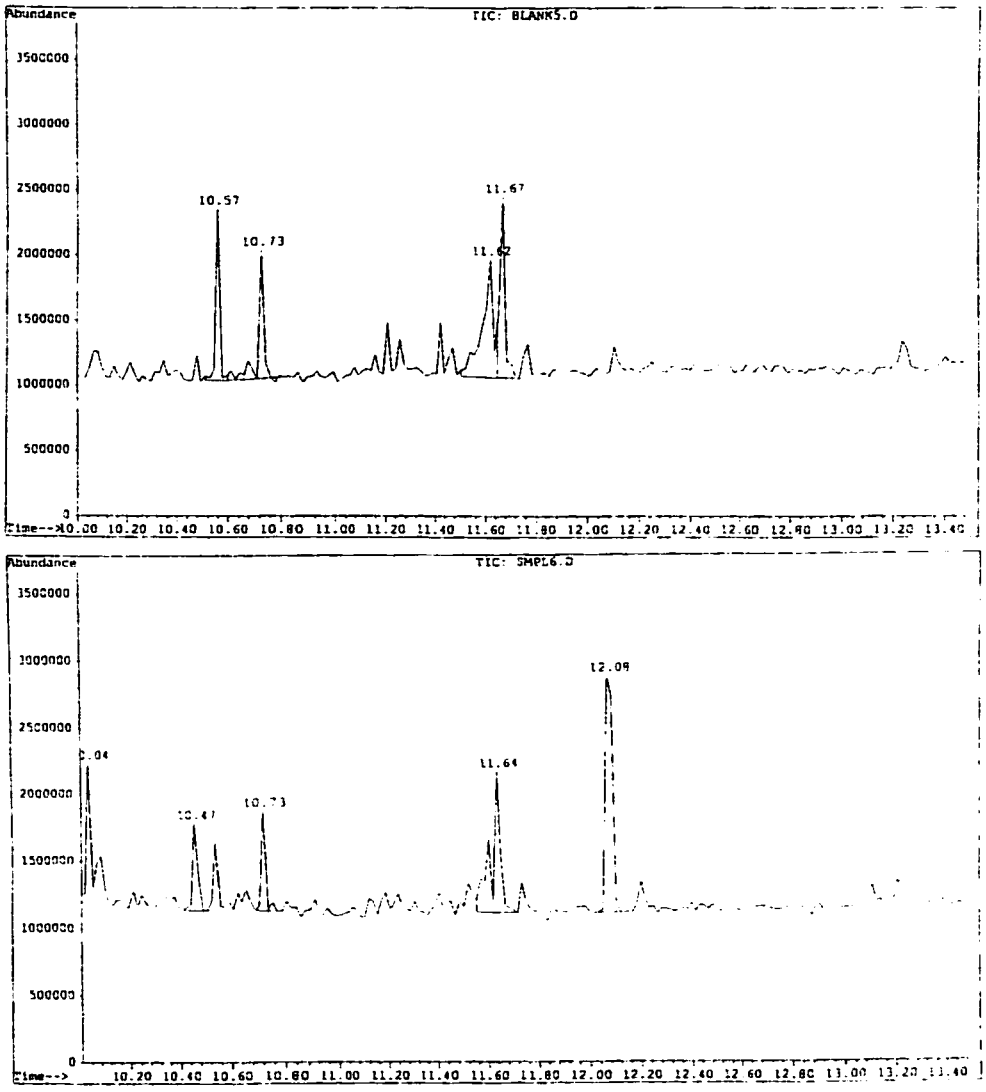

Figure 3.5.2-4: Total ion chromatogram following the solvent delay ranging from 10.0 to 13.5 minutes of A) a blank that was treated in the exact same manner as the sample and B) the irradiated solution of valeric acid. No peaks have been formally identified by using a computerized mass spectral library.

Peak no.	Compound	General formula	Correlates to	Molecular weight	Retention time	% match
1	Butanoic acid, trimethylester	$C_7H_{16}SiO_2$	Butanoic acid	160.29	6.22 (minor)	40
2	Butanoic acid, 2-methyl-, trimethylester	$C_8H_{18}SiO_2$	2-methylbutanoic acid	174.31	6.28 (minor)	72
3	**Pentanoic, trimethylsilylester**	**$C_8H_{18}SiO_2$**	**Valeric acid**	**174.31**	**6.6 (major)**	**80**
4	Butanoic acid, 2-[(trimethylsilyl)oxy]-, trimethylsilylester	$C_{10}H_{24}Si_2O_3$	2-hydroxybutanoic acid	248.47	6.85 (minor)	47
4	Ethanedioic acid, bis(trimethylsilyl) ester	$C_8H_{18}Si_2O_4$	Ethanedioic acid	234.40	6.85 (minor)	47
5	Pentanoic acid, 4-oxo-, trimethylsilyl ester	$C_8H_{16}SiO_3$	4-ketovaleric acid	188.30	7.45 (major)	93
6	Propanoic acid, 2-methyl-2-[(trimethylsilyl)oxy]-, trimethylsilyl ester	$C_{10}H_{24}Si_2O_3$	2-hydroxy-2-methylpropanoic acid	248.47	7.56 (minor)	14
7	Silane, (2-methoxyethoxy)trimethyl-	$C_6H_{16}SiO_2$	2-methoxyethanol	148.28	7.83 (minor)	56
8	2-pentenoic acid, 2-[(trimethylsilyl)oxy]-, trimethylsilyl ester	$C_{11}H_{24}Si_2O_3$	2-hydroxy-2-pentenoic acid	260.48	7.91 (minor)	64
9	Butanoic acid, 4-[(trimethylsilyl)oxy]-, trimethylsilyl ester	$C_{10}H_{21}Si_2O_3$	4-hydroxybutanoic acid	245.45	7.97 (minor)	80

Table 3.5.2-1: Global results of the GC-MS investigation of the intermediates of valeric acid. "Peak no." refers to the peak numbers on the total ion chromatogram shown in figures 3.5.2-2 to 3.5.2-4. "Compound" refers to the derivatized compounds that have been identified by using the mass spectral library following the GC-MS analysis of the derivatized extract. "Correlates to" refers to the underivatized form of these compounds. "Molecular weight" refers to the molecular weight of the derivatized compounds that have been identified by using the mass spectral library following the GC-MS analysis of the derivatized extract. Shaded compounds are those for which the match was judged to be improbable (see text).

Peak no.	Compound	General formula	Correlates to	Molecular weight	Retention time	% match
10	4-hydroxy-n-valeric acid 2 TMS	$C_{11}H_{25}Si_2O_3$	4-hydroxyvaleric acid	261.49	8.09 (medium)	43
11	2-pentenoic acid, 2-[(trimethylsilyl)oxy]-, trimethylsilyl ester	$C_{11}H_{24}Si_2O_3$	2-hydroxy-2-pentenoic acid	260.48	8.18 (minor)	90
12	3-oxovaleric acid-bis(TMS ester)	$C_{11}H_{24}Si_2O_3$	3-hydroxyvaleric acid	260.48	8.24 (major)	97
13	Butanedioic acid, bis(TMS)ester	$C_{10}H_{22}Si_2O_4$	Butanedioic acid	262.45	8.37 (minor)	93
14	5-hydroxy-n-valeric acid 2TMS	$C_{11}H_{26}SI_2O_3$	5-hydroxyvaleric acid	262.50	8.45 (minor)	83
15	**Propanedioic acid, bis(trimethylsilyl)ester**	$C_9H_{20}Si_2O_4$	**Propanedioic acid**	**248.43**	**8.77 (major)**	**72**
16	2-pentenedioic acid, bis(trimethylsilyl)ester	$C_{11}H_{22}Si_2O_3$	2-pentenedioic acid	258.46	8.85(intermediate)	16
17	Propanedioic acid, methyl-, bis(TMS)ester)	$C_{10}H_{22}Si_2O_4$	2-methylpropanedioic acid	262.45	9.82 (minor)	58
18	Hexanoic acid, TMS ester	$C_9H_{20}SiO_2$	Hexanoic acid	188.34	9.91 (minor)	76

Table 3.5.2-1 (Cont.): Same as above.

of solvent required to recover the irradiated residue contributed to also concentrate any adventitious impurities present in the solvent. Such impurities may interfere with the mass spectroscopic analysis of valeric acid and its intermediates, thus affecting the quality of the match achieved with the mass spectral library. Consequently, the %match given by the library must be used with some reservation and should only be seen as a possible match.

The retention time of these intermediates is a very good reference to use in assessing the validity of the matches performed when using the mass spectral library. Indeed, when GC-FID was used in the previous experiments, much valid empirical information was derived on the behavior of the thimethylsylil derivatives of typical acids relative to one another (see table 3.4.2-1 of section 3.4.2). It was in fact demonstrated that for the linear aliphatic carboxylic acid series, the retention times followed the order acetic < propanoic < butanoic < valeric acid. For oxidized acids vs. non-oxidized acids, the elution order was: linear form < 2-keto form < 2-hydroxy form. As a general trend then, the elution order increased with increase in molecular weight, except for the compound bearing some degree of unsaturation on their carbon backbone. This knowledge can be useful in validating the results found in table 3.5.2-1 above.

The first exclusion that can be made is that of peak no-18, which was identified as hexanoic acid. Even though the %match given by the spectral library was fairly good (76%), it it unlikely that this compound (molecular weight, 188.34 g/mol) has such a long retention time (9.91 minutes) when compared to butanoic acid (6.22 minutes) and valeric acid (6.60 minutes).

The second exclusion is peak no.-7 which was assigned to 2-methoxyethanol. Once again, with no double bond and such a low molecular weight (148.28 g/mol), it appears at too long a retention time (7.83 min).

The third exclusion goes to peak no.-4 that was assigned as 2-hydroxybutanoic acid. Considering the results of table 3.4.2-1, where all hydroxy-compounds eluted after the keto-compounds, the actual match is perceived as an anomaly. This is reinforced by the 93% match that was obtained for peak no.-5, which was identified as being 4-ketovaleric acid, which would be expected to elute before a hydroxy-compound. The same applies to the match with ethanedioic acid which, with a molecular weight of 234.40 g/mol, should have eluted at a longer retention time.

The fourth exclusion goes to peak no.-8 which was identified as being 2-hydroxy-2-pentenoic acid. With a molecular weight of 260.48 g/mol, a double bond and a hydroxyl group on its carbon backbone, it appears to have too short a retention time to be what the spectral library says it is. In fact the same compound was proposed for peak no.-11, which make more sense.

The fifth exclusion goes to peak no.-6, which was identified as being 2-hydroxy-2-methylpropanoic acid. Two reasons lead to this decision: 1) its very low correlation with the spectrum of the library (match = 14%) and 2) its retention time as opposed to its molecular weight (248.47 g/mol).

The sixth and last exclusion goes to peak no.-15 which was identified as being propanedioic acid. This compound should elute before butanedioic acid, which appears to be peak no.-13 (match = 93%). Its retention time appears to be too high for its molecular weight (248.47 g/mol).

All of the other matches that have been obtained, when considering the retention times of these compounds relative to one another, seem highly probable. Table 3.5.2-2 below provides the final results following the above analysis. According to the above results, the vast majority of the intermediates formed from the heterogeneous photocatalytic degradation of valeric acid are aliphatic saturated carboxylic acids with shorter chains than the parent compound, as evidenced from the identification of butanoic acid. This compound was also positively identified by the two previous methods. The presence of 2-methylbutanoic acid and of 2-methylpropanedioic acid indicates that addition of alkyl groups on the main carbon backbone also occurs. The remaining intermediates were (1) saturated and unsaturated hydroxyacids (4-hydroxybutanoic acid, 3-hydroxyvaleric acid, 4-hydroxyvaleric acid, 5-hydroxyvaleric acid, and 2-hydroxy-2-pentenoic acid), (2) saturated ketoacids (4-ketovaleric acid), and (3) saturated and unsaturated diacids (butanedioic acid, 2-pentenedioic acid, and 2-methylpropanedioic acid).

The presence of 2-hydroxy-2-pentenoic acid indicates that hydroxylation is takes place on the alpha-carbon of valeric acid. However, the evidence does not indicates that hydroxylatior. of valeric acid occurred as a primary step or once the double bond was formed. 2-Hydroxyvaleric acid was not identified as an intermediate of valeric acid by the two previous methods used (HPLC-UV and GC-FID). There is, however, no doubt that hydroxylation takes place on carbon atoms other than onto the alpha-carbon of valeric acid, as indicated by the presence of 3-hydroxyvaleric acid, 4-hydroxyvaleric acid, 5-hydroxyvaleric acid. Once hydroxylated, the hydroxyacid

Peak no.	Compound	General formula	Correlates to	Molecular weight	Retention time	% match
1	Butanoic acid, trimethylester	$C_7H_{16}SiO_2$	Butanoic acid	160.29	6.22 (minor)	40
2	Butanoic acid, 2-methyl-, trimethylester	$C_8H_{18}SiO_2$	2-methylbutanoic acid	174.31	6.28 (minor)	72
3	**Pentanoic, trimethylsilylester**	**$C_8H_{18}SiO_2$**	**Valeric acid**	**174.31**	**6.6 (major)**	**80**
5	Pentanoic acid, 4-oxo-, trimethylsilyl ester	$C_8H_{16}SiO_3$	4-ketovaleric acid	188.30	7.45 (major)	93
9	Butanoic acid, 4-[(trimethylsilyl)oxy]-, trimethylsilyl ester	$C_{10}H_{21}Si_2O_3$	4-hydroxybutanoic acid	245.45	7.97 (minor)	80
10	4-hydroxy-n-valeric acid 2 TMS	$C_{11}H_{25}Si_2O_3$	4-hydroxyvaleric acid	261.49	8.09 (medium)	43
11	2-pentenoic acid, 2-[(trimethylsilyl)oxy]-, trimethylsilyl ester	$C_{11}H_{24}Si_2O_3$	2-hydroxy-2-pentenoic acid	260.48	8.18 (minor)	90
12	3-oxovaleric acid-bis(TMS ester)	$C_{11}H_{24}Si_2O_3$	3-hydroxyvaleric acid	260.48	8.24 (major)	97
13	Butanedioic acid, bis(TMS)ester	$C_{10}H_{22}Si_2O_4$	Butanedioic acid	262.45	8.37 (minor)	93
14	5-hydroxy-n-valeric acid 2TMS	$C_{11}H_{26}SI_2O_3$	5-hydroxyvaleric acid	262.50	8.45 (minor)	83
16	2-pentenedioic acid, bis(trimethylsilyl)ester	$C_{11}H_{22}Si_2O_3$	2-pentenedioic acid	258.46	8.85(intermediate)	16
17	Propanedioic acid, methyl-, bis(TMS)ester)	$C_{10}H_{22}Si_2O_4$	2-methylpropanedioic acid	262.45	9.82 (minor)	58

Table 3.5.2-2: Final results of the GC-MS investigation of the intermediates of valeric acid following the exclusion of questionable matches (see above text). See table 3.4.2-1 for other details regarding the interpretation of this table.

is further oxidized to the keto form, as indicated by the presence of 4-ketovaleric acid, which must have formed from 4-hydroxyvaleric acid. The presence of diacids (butanedioic acid, 2-methylpropanedioic acid, and 2-pentenedioic acid) is not really surprising given that we have identified hydroxyacids onto which that hydroxyl group is located on the last carbon atom where further oxidation on can lead to a carboxyl group. Table 3.5.2-3 summarizes the entire results that have been obtained by the three methods that were used and discussed in the last sections:

Compound	Positive ID by HPLC-UV	Positive ID by GC-FID	Identified by GC-MS
Formic	No [1]	No [1]	No [1]
Acetic	**Yes**	No [1]	No [1]
2-hydroxyacetic	No	No	No
Propanoic	**Yes**	**Yes**	No [1]
2-hydroxypropanoic	No	No	No
2-ketopropanoic	No	No	No
2-methylpropanedioc	Not investigated	Not investigated	**Yes**
Butanoic	**Yes**	**Yes**	**Yes**
2-hydroxybutanoic	**Yes**	**Yes**	No
4-hydroxybutanoic	Not investigated	Not investigated	**Yes**
2-ketobutanoic	No	**Yes**	No
2-methylbutanoic	Not investigated	Not investigated	**Yes**
Butanedioic acid	Not investigated	Not investigated	**Yes**
Oxalacetic or 3-ketobutanedioic acid	No	No	No
Acrylic	Yes	No	No
2-ketovaleric	No	No	No
2-hydroxyvaleric	No	No	No

Table 4.5.2-3: Combined HPLC-UV, GC-FID, and GC-MS identification results for the investigation on the intermediates of valeric acid. [1] Eluted in the solvent front.

Compound	Positive ID by HPLC-UV	Positive ID by GC-FID	Identified by GC-MS
3-hydroxyvaleric	Not investigated	Not investigated	**Yes**
4-hydroxyvaleric	Not investigated	Not investigated	**Yes**
4-ketoxyvaleric	Not investigated	Not investigated	**Yes**
5-hydroxyvaleric	Not investigated	Not investigated	**Yes**
2-hydroxy-2-pentenoic	Not investigated	Not investigated	**Yes**
2-pentedioic	Not investigated	Not investigated	**Yes**

Table 4.5.2-3 (Cont.): Same as above.

Only butanoic acid was confirmed by all three methods. It does not mean, however, that all other identifications are to be discarded. Each of the three methods used had their limitation and were apt to detect some compounds that the other two methods could not. A good example is that of propanoic acid that was positively identified by HPLC-UV and by GC-FID but not by GC-MS, because in the latter case, the retention time of the derivatized form of that acid was such that it was ignored by the solvent delay (eluted with the solvent front). Nevertheless, the above evidence indicates that hydroxylation and alkylation of the carbon backbone of these aliphatic saturated carboxylic acid took place, that compounds with less carbon atoms than the parent compound was formed, and that some oxidative process led to some saturated compounds. Taking into consideration the above evidence, we can propose the degradation pathway illustrated in figure 3.5.2-4.

Formation of the primary intermediate **10** (4-hydroxyvaleric acid) probably arises from attack of a hydroxyl radical on the C_4 carbon atom of valeric acid, thus creating a

secondary radical intermediate that further combines with a second hydroxyl radical to form a hydroxyacid, in this case 4-hydroxyvaleric acid (see equations 1 to 2).

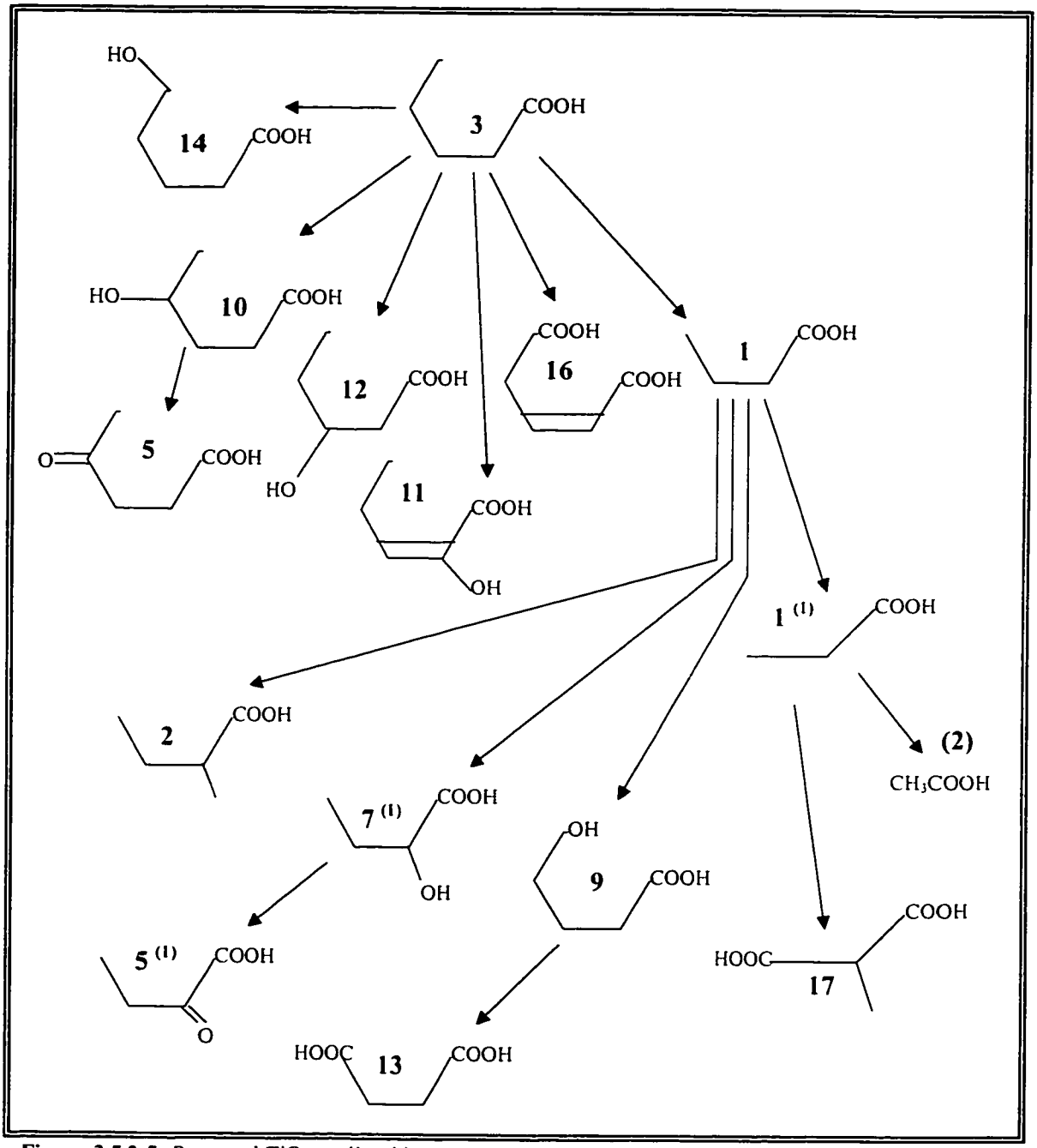

Figure 3.5.2-5: Proposed TiO_2 mediated heterogeneous photocatalytic degradation scheme for valeric acid based on the results obtained from the HPLC-UV co-elution experiments [2], the GC-FID relative retention time experiments [1], and the GC-MS analysis of the degraded solution. [1] Refer to the GC-FID chromatogram of section 3.4.2, figure 3.4.2-4.

$CH_3CH_2CH_2CH_2COOH_{ads} + HO\bullet_{ads} \rightarrow CH_3{}^{\bullet}CHCH_2CH_2COOH_{ads} + H_20$ (1)

$CH_3{}^{\bullet}CHCH_2CH_2COOH_{ads} + HO\bullet_{ads} \rightarrow CH_3CH\mathbf{(OH)}CH_2CH_2COOH_{aq}$ (2)

The same applies to intermediate **12** (3-hydroxyvaleric acid, reactions 3 to 4) and to intermediate **14** (5-hydroxyvaleric acid, reactions 5 to 6):

$CH_3CH_2CH_2CH_2COOH_{ads} + HO\bullet_{ads} \rightarrow CH_3CH_2{}^{\bullet}CHCH_2COOH_{ads} + H_20$ (3)

$CH_3CH_2{}^{\bullet}CH\ CH_2COOH_{ads} + HO\bullet_{ads} \rightarrow CH_3CH_2CH\mathbf{(OH)}CH_2COOH_{aq}$ (4)

$CH_3CH_2CH_2CH_2COOH_{ads} + HO\bullet_{ads} \rightarrow {}^{\bullet}CH_2CH_2CH_2CH_2COOH_{ads} + H_20$ (5)

${}^{\bullet}CH_2CH_2CH_2CH_2COOH_{ads} + HO\bullet_{ads} \rightarrow CH_2\mathbf{(OH)}CH_2CH(OH)CH_2COOH_{aq}$ (6)

It is rather surprising to see that hydroxylation occurred on the C3, C4 and C5 carbon atoms of valeric acid. Valeric acid being adsorbed onto TiO_2 through its carboxylic group, if its chain was oriented perpendicular to the titanium dioxide pigment, the hydroxyl radical would have to migrate in solution to reach these sites. This has been declared as being possible based on the rate of electron trapping, the rate of diffusion of molecules in water, and finally the reaction rate of the hydroxyl radical [74]. Nevertheless, even though HO• can migrate in solution and undergo homogeneous reactions, its total contribution is believed to be minimal [75]. Even if it did migrate, it would not go far from the photogenerated active sites on TiO_2, the degradation process must occur at the photocatalyst surface or within a few atomic distances from the surface [76].

A minimal contribution to a pathway would possibly not permit such intermediates to be detected when analyzed by any given method, unless they are resistant to oxidation to the point where they would accumulate in solution and reach high enough concentrations to be detected. We have, however, demonstrated that the rate

of disappearance of aliphatic hydroxylated carboxylic acid is relatively high with respect to their non-oxidized parent, which makes this possibility fairly improbable. There is thus the possibility that valeric acid adopts a position on TiO_2 whereby it lies flat onto the semiconductor's surface. Such an arrangement would still permit the adsorption of the acid on TiO_2 via the carboxylic group but yet, it would bring the carbon chain in close proximity to the adsorbed hydroxyl radical present onto the semiconductor's surface and would thus expose all of the acid carbon backbone to the oxidant. This hypothesis is reinforced by the presence of intermediates **16** and **11** (2-pentenedioic acid and 2-hydroxy-2-pentenoic acid). It seems very likely that such compounds were formed while being attacked by a number of hydroxyl radicals before desorbing from the catalyst surface as opposed to desorbing after each attack. It is envisaged that intermediate **16** was formed after being simultaneously attacked at carbons C_2, C_3 (thus producing the double bond), and C_5 (thus producing the carboxylic group).

Intermediate **5** (4-ketovaleric acid) is a secondary intermediate that was possibly formed from 4-hydroxyvaleric acid (intermediate **10**). Alcohols are reported to adsorb onto TiO_2 by forming alkoxides [77]. Once hydroxylated on its C_4 carbon, 4-hydroxyvaleric acid could also adsorb on TiO_2 via this hydroxyl group which could be further oxidized to a ketone. The same principle can thus apply to intermediate **5** (2-ketobutanoic acid) which probably followed the oxidation of 2-hydroxybutanoic acid.

Acids having less carbon atoms than the starting compound have been identified. Hence, butanoic acid (**1**), propanoic acid ($\mathbf{1^{(1)}}$) and acetic acid ((**2**)) were all detected. The formation of acids having shorter carbon chains than the starting compound were explained as follows [78]: Reaction of a valeric acid molecule with a photogenerated hole in

the valence band of TiO_2 (eq. 7) followed by decarboxylation of the acid radical intermediate leading to formation of carbon dioxide and an alkyl radical intermediate (eq. 8):

$$CH_3CH_2CH_2CH_2COOH + h^+ \rightarrow CH_3CH_2CH_2CH_2COO\bullet + H^+ \quad (7)$$

$$CH_3CH_2CH_2CH_2COO\bullet \rightarrow CH_3CH_2CH_2CH_2\bullet + CO_2 \quad (8)$$

The alkyl radical intermediate can then by converted into an alcohol following attack of a hydroxyl radical which, following a series of similar oxidation, can ultimately lead to the formation of butanoic acid:

$$H_2O + h^+ \rightarrow HO\bullet + H^+ \quad (9)$$

$$CH_3CH_2CH_2CH_2\bullet + HO\bullet \rightarrow CH_3CH_2CH_2CH_2OH \quad (10)$$

$$CH_3CH_2CH_2CH_2OH + 2h^+ \rightarrow CH_3CH_2CH_2CHO + 2H^+ \quad (11)$$

$$CH_3CH_2CH_2CHO + 2h^+ + H_2O \rightarrow CH_3CH_2CH_2COOH + 2H^+ \quad (12)$$

This scheme may then repeat itself in leading to propanoic acid and to acetic acid. Other schemes have been proposed to explain such reactions following the demonstration that the rate at which hydroxyl radicals oxidize similar compounds to those involved in this study was much less than their combination rate with dissolved oxygen [79]. In this case, the mechanism under which valeric acid could lead to butanoic acid involves, just as shown above, the initial photocatalyzed decarboxylation of valeric acid leading to an alkyl radical intermediate (eqs. 7 to 8). However, instead of having the rest of the process taken care of by further oxidation involving hydroxyl radicals, the alkyl radical intermediate would react with molecular oxygen to form a peroxy radical (eq. 13), to then combine with a superoxide radical to form an unstable tetraoxide (eq. 14) that

decomposes to an aldehyde, water, and molecular oxygen (eqns. 15, Russel-like reaction):

$CH_3CH_2CH_2CH_2\bullet + O_2 \rightarrow CH_3CH_2CH_2CH_2\text{-}O\text{-}O\bullet$ (13)

$CH_3CH_2CH_2CH_2\text{-}O\text{-}O\bullet + \bullet OOH \rightarrow CH_3CH_2CH_2CH_2OOOOH$ (14)

$CH_3CH_2CH_2CH_2OOOOH \rightarrow CH_3CH_2CH_2CHO + H_2O + O_2$ (15)

Under such a scheme, 2-methylvaleric acid, which could form following the addition of a methyl radical on the alpha carbon, would lead to a ketone:

$CH_3CH_2CH_2^{\bullet}CHCH_3 + O_2 \rightarrow CH_3CH_2CH_2CH(\text{-}O\text{-}O\bullet)CH_3$ (16)

$CH_3CH_2CH_2CH(\text{-}O\text{-}O\bullet)CH_3 + \bullet OOH \rightarrow CH_3CH_2CH_2CH(OOOOH)CH_3$ (17)

$CH_3CH_2CH_2CH(OOOOH)CH_3 \rightarrow CH_3CH_2CH_2COCH_3 + H_2O + O_2$ (18)

whereas 2-hydroxyvaleric acid would lead directly to butanoic acid:

$CH_3CH_2CH_2^{\bullet}CHOH + O_2 \rightarrow CH_3CH_2CH_2CH(\text{-}O\text{-}O\bullet)OH$ (19)

$CH_3CH_2CH_2CH(\text{-}O\text{-}O\bullet)OH + \bullet OOH \rightarrow CH_3CH_2CH_2\ CH(OOOOH)OH$ (20)

$CH_3CH_2CH_2\ CH(OOOOH)OH \rightarrow CH_3CH_2CH_2COOH + H_2O + O_2$ (21)

In the former case (eqns. 7 to 12), formation of an acid having one carbon atom less than the starting compound involves the formation of an alcohol and of an aldehyde along the way. None of these compounds were detected by GC-MS. The same applies to the Russel-like mechanism that leads, in the case of valeric acid, to an aldehyde that would be further oxidized to an acid. Alhehydes and ketones would have been left intact by the derivatization procedure employed in this study. Given the high volatility of butanal, if it were present in solution, it would have eluted in the solvent front. Since butanal is the highest molecular weight aldehyde that could have been produced in such a scheme (assuming no major combination reaction schemes), no aldehydes could have

been detected by the procedure that was employed. As far as butanol is concerned (once again, the alcohol that would have had the highest molecular weight of all possible alcohols that could have formed from these reaction schemes, assuming no combination reactions), it would have had a poor recovery from the irradiated valeric acid suspension by using the up-scaled extraction procedure because of its high water solubility. In addition to that, its derivatization would have lead to $CH_3CH_2CH_2CH_2OSi(CH_3)_3$, a derivative of a molecular weight of 146.30 g/mol, thus having no chance to come out of the solvent front. This shows once again that there are numerous compounds that might have been present but yet that were not detected. With the available analytical tools, it was not possible to obtain a full picture of the degradation events.

Alkylated coumpounds such as 2-methylbutanoic acid **(2)** and 2-methylpropanedioic acid **(17)** possibly formed following a recombination process between two alkyl radicals as shown below for 2-methylbutanoic acid:

$$CH_3CH_2CH_2COOH_{ads} + HO\bullet \rightarrow CH_3CH_2\overset{\bullet}{C}HCOOH_{ads} + H_2O \qquad (22)$$

$$CH_3CH_2\overset{\bullet}{C}HCOOH_{ads} + \overset{\bullet}{C}H_{3\,ads} \rightarrow CH_3CH_2CH(CH_3)COOH_{aq} \qquad (23)$$

The methyl radical possibly originated from the decarboxylation of acetic acid in the same manner as equations 7 to 8. Acetic acid was indeed identified as an intermediate product of valeric acid. The formation of double bounds on the carbon chain of these aliphatic carboxylic acids could be explain by equations 24 to 25:

$$CH_3CH_2\,CH_2CH_2COOH_{ads} + 2HO\bullet \rightarrow CH_3CH_2\overset{\bullet}{C}H\overset{\bullet}{C}HCOOH_{ads} + 2H_2O \qquad (24)$$

$$CH_3CH_2\overset{\bullet}{C}H\overset{\bullet}{C}HCOOH_{ads} \rightarrow CH_3CH_2CH{=}CHCOOH_{aq} \qquad (25)$$

3.6 Adsorption equilibrium constant K in the dark and under illumination conditions

3.6.1 Introduction

Numerous events take place inside of and on the surface of the TiO_2 photocatalyst upon illumination. Illumination of TiO_2 particles in solution influences the equilibrium between the adsorbed molecules and the surface of the semiconductor. In the absence of organic species, the oxygen atoms of metal oxides exchange with the oxygen atoms from gaseous O_2 upon illumination [80]. Is has also been demonstrated that the surface of the TiO_2 particles becomes positively charged upon UV irradiation because of the production of hydrogen cations from the splitting of water [81]. Photons can also easily create new active sites on the semiconductor particle as well as causing possible changes in the surface adsorption/desorption characteristics of adsorbates on the photocatalyst surface, which renders difficult the determination of the number of actives sites in a catalyst [82].

If these surface changes were significant, there should be a noticeable difference between the adsorption equilibrium constant when determined in the dark from an adsorption isotherm versus the same constant when determined kinetically and under illumination conditions.

3.6.2 K determined kinetically and from adsorption isotherms

The adsorption equilibrium constant under illumination conditions (the kinetically determined adsorption equilibrium constant) was determined from the plot of $1/r_0$ versus $1/C_0$, obtained from a series of degradation runs at various concentrations under otherwise identical conditions. Given the numerous data collected in this series of experiments, typical results will be shown for formic acid only. Figures 3.6.2-1 to 3.6.2-

7 show the initial rate data obtained for the degradation of formic acid at various concentrations.

Figure 3.6.2-1: umoles Formic acid vs Irradiation time,
$[\ ]_o = 4.90 \times 10^{-4}$M

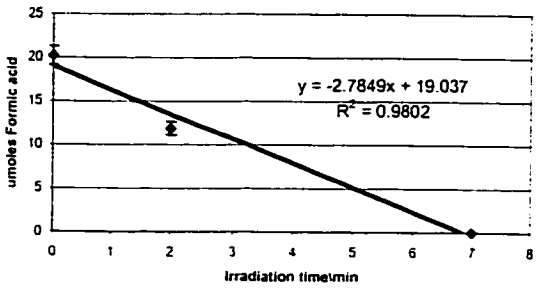

Figure 3.6.2-2: umoles Formic acid vs Irradiation time,
$[\ ]_o = 7.34 \times 10^{-4}$M

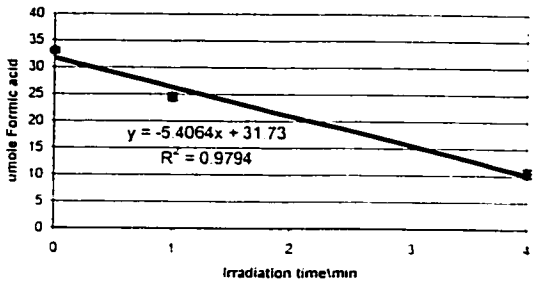

Figure 3.6.2-3: umole Formic acid vs Irradiation time,
$[\ ]_o = 9.79 \times 10^{-4}$M

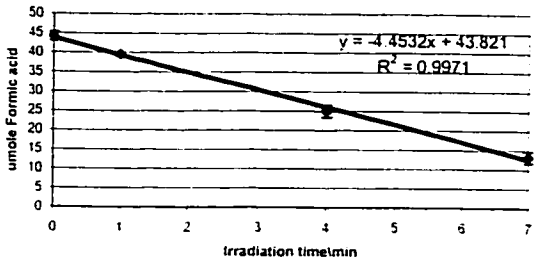

Figure 3.6.2-4: umole Formic acid vs Irradiation time,
$[\ ]_o = 1.47 \times 10^{-3}$M

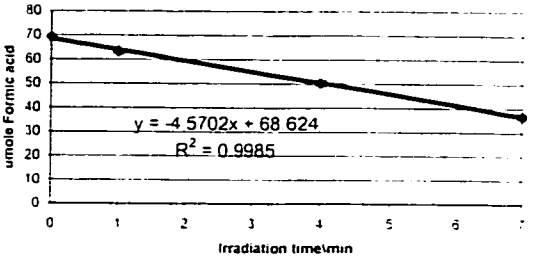

Figure 3.6.2-5: umoles Formic acid vs Irradiation time,
$[\ ]_o = 1.96 \times 10^{-3}$M

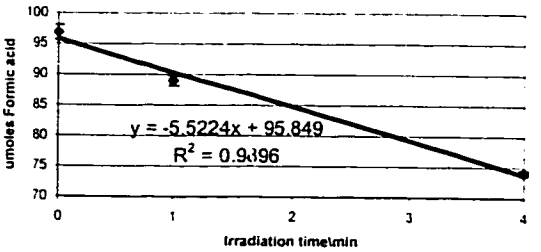

Figure 3.6.2-6: umole Formic acid vs Irradiation time,
$[\ ]_o = 3.92 \times 10^{-3}$M

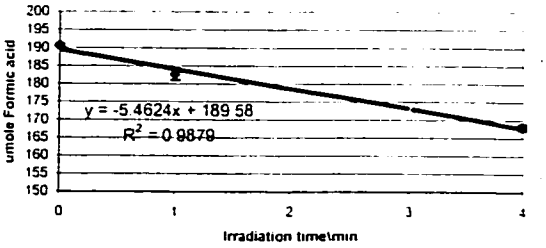

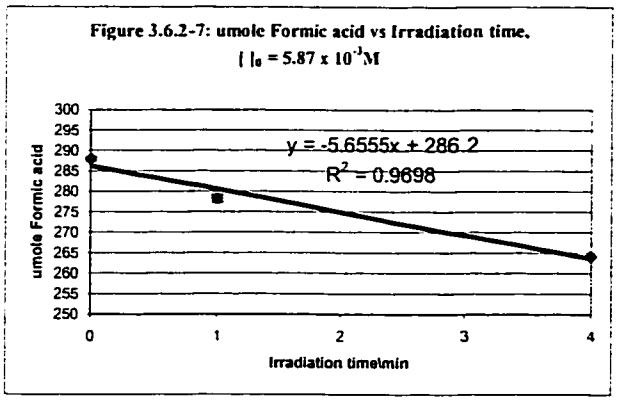

Across the concentration range of 4.90×10^{-4} M to 5.87×10^{-3} M, the temporal decrease of formic acid exhibited zero-order kinetics; relevant correlation factors (square root of R^2 on graphs) are 0.98 or greater. Error bars represent the standard deviation on multiple HPLC runs performed on the samples collected at each time point.

The plot of r_0 versus C_0 and that of $1/r_0$ versus $1/C_0$ derived from the degradation of formic acid in the above concentration range are shown in figures 3.6.2-8 and 3.6.2-9, respectively.

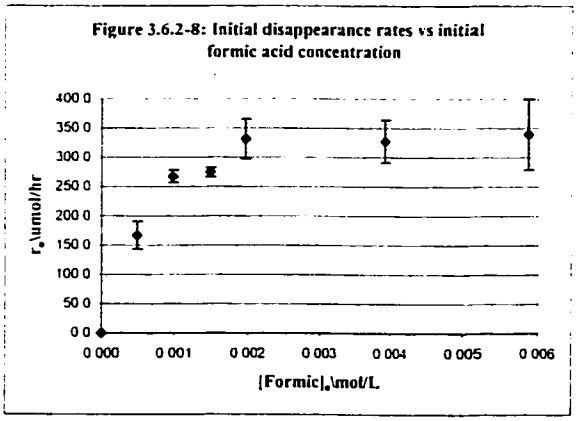

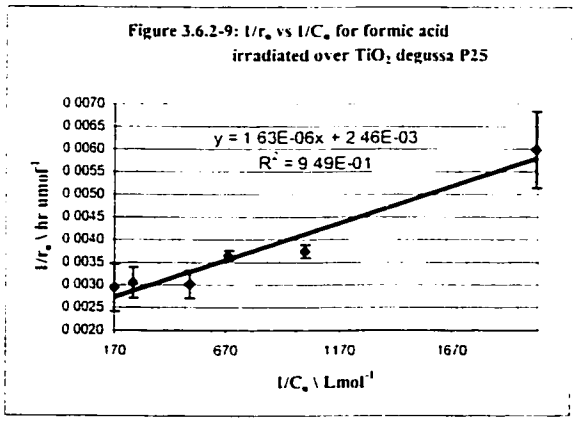

The profile of the curve shown on figure 3.6.2-8 is typical of a Langmuir-Hinshelwood type of adsorption phenomenon on the particle surface where the general trend is a linear increase in the disappearance rate at low concentrations followed by a sub-linear increase reaching a plateau at ca. 1.96×10^{-3} M, and at which the rates are no longer dependent on [formic acid]. This concentration is taken as the point at which the surface of the photocatalyst becomes saturated with formic acid, and a further increase of

the concentration of formic acid no longer impacts on the kinetics. Similar observations (i.e. a saturation at a concentration of approximately 1.96 x 10^{-3} M) were evident for the two other acids included in this study (propanoic acid and 2-methylbutanoic acid). For these acids the plots of r_o vs C_o are shown in figures 3.6.2-10 and 3.6.2-11.

This result is important in the sense that the earlier experiments that were performed on the rates of disappearance of these aliphatic saturated carboxylic acids were

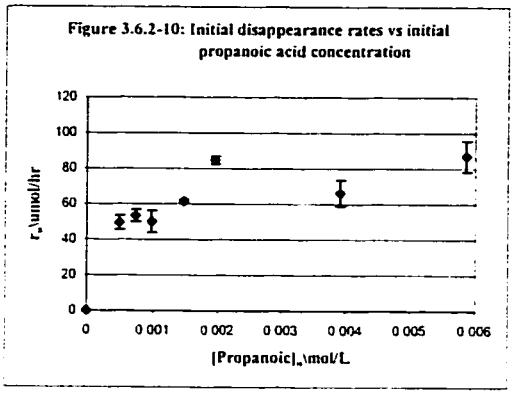

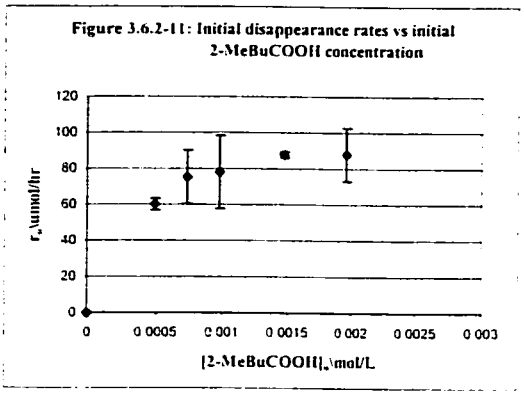

all carried on at a concentration of 2.0 x 10^{-3} M in acid, a concentration at which the surface of the photocatalyst is saturated with the substrate. The trends observed on the rates of disappearance relative to one another are thus valid since they were all compared on the same basis. Therefore, not only were the reactor design, the light intensity, the distance of the reactor from the light source, the reaction medium's temperature, the catalyst load and source, and the volume of solution controlled, but the conditions were such that the catalyst's surface was also saturated with all of the these acids.

The data points of figures 3.6.2-8 and 3.6.2-9 represent the slope of the linear regression curves obtained from figures 3.6.2-1 to 3.6.2-7 (slope of [Formic] vs. irradiation time). Error bars in figures 3.6.2-8 and 3.6.2-9 represent the error on the slope derived from the rate data of formic acid at each concentration. The adsorption equilibrium constant was calculated from the y intercept (reciprocal of the y-intercept

corresponds to the rate constant) and the slope of the straight line obtained from the plot of $1/r_o$ vs. $1/C_o$. The error on the adsorption equilibrium constant was calculated statistically based on the linear regression model using the slope, the y-intercept and their associated errors.

The adsorption equilibrium constant in the dark was determined by the methodology of Cunningham and al [83]; more specifically, from the ratio of the slope and the y intercept of a plot of the ratio of $[formic]_{eq}$ to the number of moles of formic acid adsorbed per gram of TiO_2 versus $[formic]_{eq}$. The concentration of formic acid at equilibrium (its bulk concentration after equilibration in the dark over TiO_2) as well as the number of moles of formic acid adsorbed onto the photocatalyst was determined from HPLC measurements from the differential of the peak areas between a sample exposed to TiO_2 and a second one treated the same way without involving the photocatalyst. Figure 3.6.2-12 shows the adsorption isotherm of formic acid whereas figure 3.6.2-13 shows the plot of the ratio of $[formic]_{eq}$ to the number of moles of formic acid adsorbed per gram of TiO_2 versus $[formic]_{eq}$ from which the adsorption equilibrium constant K in the dark was calculated.

The adsorption isotherm of formic acid (figure 3.6.2-12) again exhibited a pattern typical of the simple Langmuir isotherm. Even though the first data points are scattered, the global trend indicates that a plateau is attained at a concentration around 2.0 x $x10^{-3}$ M. This is consistent with the rate data (r_0 vs C_0) presented above (figure 3.6.2-8). The adsorption equilibrium constants K determined under illumination conditions and in the dark (referred as Ki and Kd respectively) for formic acid, propanoic acid, and 2-methylpropanoic acid are given in figure 3.6-2-14.

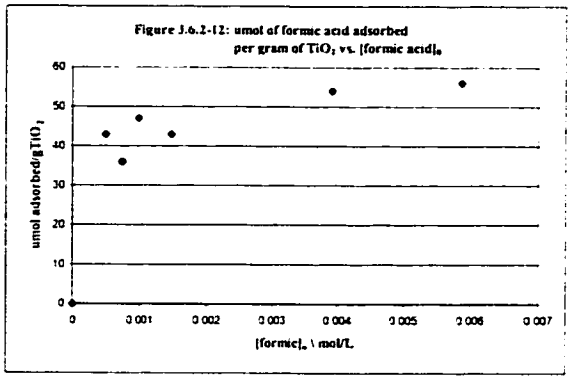

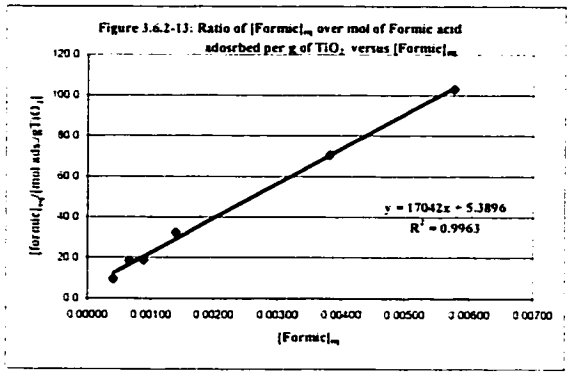

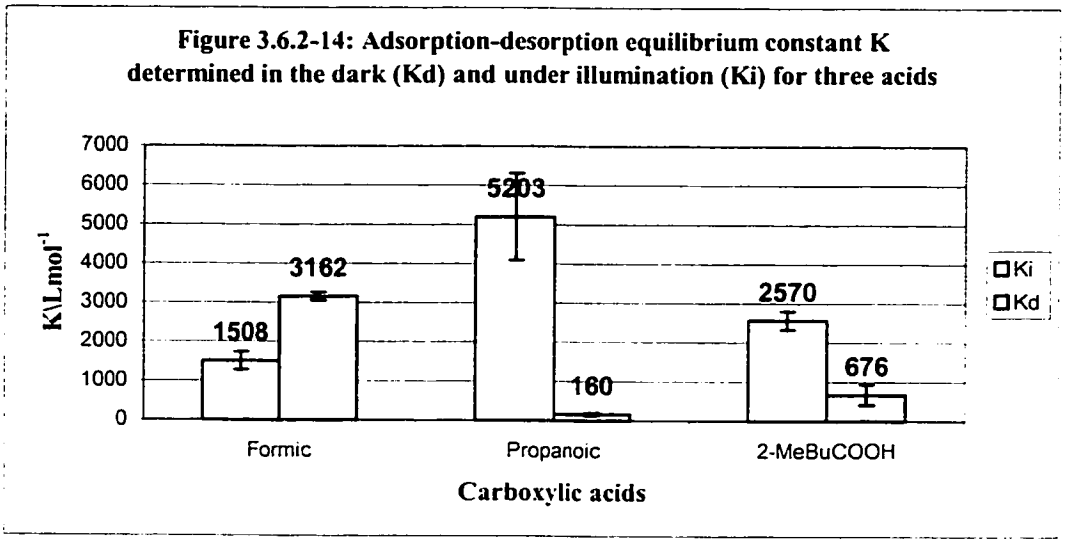

The adsorption equilibrium constants determined under illumination conditions were 1508 ± 224 mol·L^{-1}, 5203 ± 1108 mol·L^{-1}, and 2570 ± 235 mol·L^{-1} for formic acid, propanoic acid, and 2-methylbutanoic acid respectively, values of 3162 ± 96 mol·L^{-1}, 160 ± 34 mol·L^{-1}, and 676 ± 261 mol·L^{-1} (in the same order listed)· were obtained when determined in the dark. The difference between the constants determined in the dark and those determined under illumination conditions are significantly different since there is a total absence of overlap between the error bars of each data set. The analysis if the two

data sets reveals that there is a correlation between the two "types" of equilibrium constant. The correlation factor is negative ($r = -0.8237$), indicating an inverse relationship between the two data sets whereby K_i increases when K_d decreases.

Given that the TiO_2 surface becomes positive due to the splitting of water upon irradiation, it can be expected that such a phenomenon will favor the adsorption of carboxylic acids onto the surface of the photocatalyst because of an increased electrostatic attraction of the deprotonated acid molecules onto the increased positively charged surface. The depletion of the surface of the photocatalyst from substrate molecules following the irradiation of the photocatalyst is another factor that contributes to the disruption of the adsorption equilibrium that takes place in the dark. This is consistent with the results that were obtained for propanoic acid and for 2-methylbutanoic acid for which the kinetically determined adsorption equilibrium constants were higher than those determined under dark conditions. This does not hold for formic acid, however.

3.7 Limiting photonic efficiency of formic acid and proposed quantum yield for a few selected carboxylic acids

3.7.1 Introduction

Among the many aliphatic saturated carboxylic acids that have been studied in this work, formic acid is by far the best acid to chose in selecting a standard test molecule that is to become a reference in generating standard kinetic information on reactor and process efficiencies. Earlier in this work, the results that were obtained for the TiO_2-mediated photocatalyzed degradation of formic acid indicated no formation of intermediate products to a significant level. This was shown by the absence of peaks on the HPLC chromatograms obtained following the analysis of aliquots of the irradiated suspension at various time intervals. Moreover, the rate of disappearance of formic acid, as determined by HPLC, equated the rate of disappearance of total organic carbon from solution, indicating once again that no carbon-containing compounds were accumulating in solution as the degradation proceeded. The rate of disappearance of formic acid cannot thus be impacted by the presence of intermediate products that could compete for the same active site, a phenomenon that would forcibly lead to some inaccuracy on the experimentally determined quantum yield of this proposed reference compound. The consequence would be that the quantum yield of any test molecule derived from that of such a reference compound would also be inexact.

For all of the above reasons, formic acid was selected as the reference compound. Its quantum yield was determined from its limiting photonic efficiency. This latter value was then used in conjunction with the photonic efficiency of acetic acid, propanoic acid, butanoic acid, valeric acid, and 2-methylbutanoic acid relative to that of formic acid. We

are thus proposing quantum yields for these six acids by (1) determination of the quantum yield of formic acid from its limiting photonic efficiency and (2) determination of the quantum yield of acetic acid, propanoic acid, butanoic acid, valeric acid, and 2-methylbutanoic acid form their relative photonic efficiency (their photonic efficiency relative to that of formic acid) and the quantum yield or the limiting photonic efficiency of formic acid.

3.7.2 Limiting photonic efficiency and Quantum yields

The plot of r_o vs. $[\text{formic acid}]_o$ was derived in earlier experiments (refer to section 3.6). It was shown that the rate of disappearance of formic acid reached a plateau at a concentration of approximately 1.96×10^{-3} M. Just to be on the safe side, formic acid was used at twice that concentration when the plot of r_0 vs. TiO_2 loading was derived. Figures 3.7.2-1 to 3.7.2-4 show the rate of disappearance of formic acid at TiO_2 loadings of 0.3000g, 0.6000g, 0.9000g, and 1.2000g per 50 ml of solution while table 3.7.2-1 shows the entire series of results:

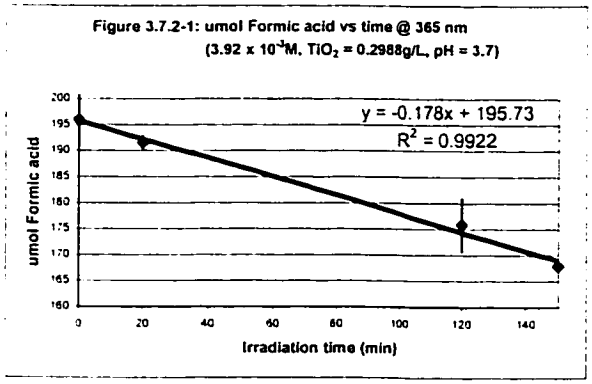

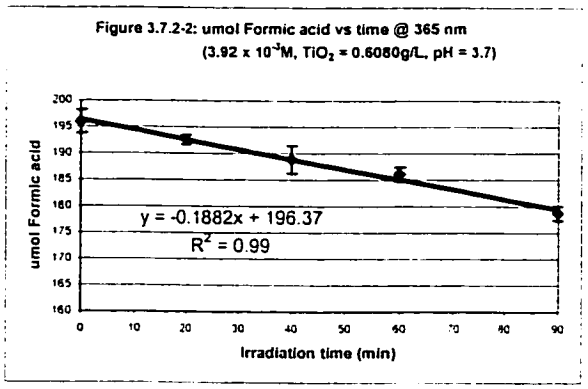

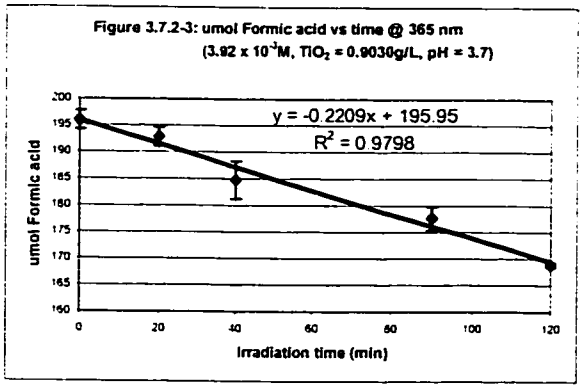

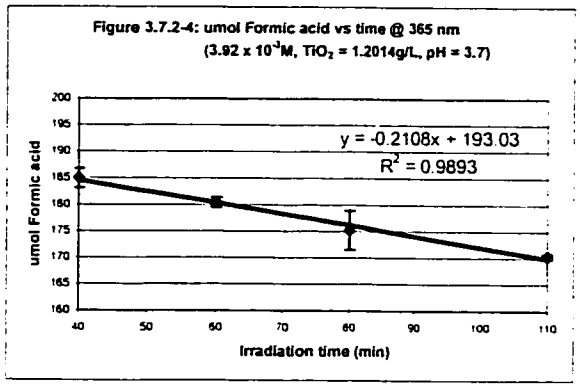

TiO_2 load (g/L)	Correlation factor r	r_0 (umol/hr)	Std (umol/hr)
0.2988	0.9961	10.7	0.65
0.6080	0.9950	11.3	0.58
0.9030	0.9898	13.3	1.13
1.2014	0.9946	12.6	0.97
1.5110	0.8800	14.0	3.84
1.8068	0.9954	14.4	0.80
2.1000	0.9973	14.3	0.52

Table 3.7.2-1: rate data obtained from the degradation of formic acid (3.96×10^{-3}M) at TiO2 loads ranging from 0.2988 g/L to 2.100 g/L.

The y error bars on the data points of the above graphs were calculated from the replicate analyses performed on each sample collected at each time interval. The time over which the samples were collected was long. For example, at a catalyst load of 0.2988 g/L, samples were collected from the reactor over 150 minutes (see figure 3.7.2-1). This does not mean that initial rates of disappearance were not dealt with. Over that time period, 13% of the initial formic acid concentration of 3.96×10^{-3} M was degraded, leaving behind a residual concentration of 3.44×10^{-3} M, a concentration still 72% greater than the concentration at which the rates of disappearance of formic acid would fall off

the plateau (r_0 vs. C_0). The main reason why the rates of disappearance of formic acid were so low is due to the fact that these experiments were carried on at a single wavelength (365 nm), thus excluding a significant amount of photons from the degradation process. The same applies to each of the runs that were performed at different catalyst load. The data of table 3.7.2-1 are plotted in figure 3.7.2-5 (r_0 vs. TiO_2 loading):

Figure 3.7.2-5: Initial disappearance rates of Formic acid vs TiO_2 load (g/L)

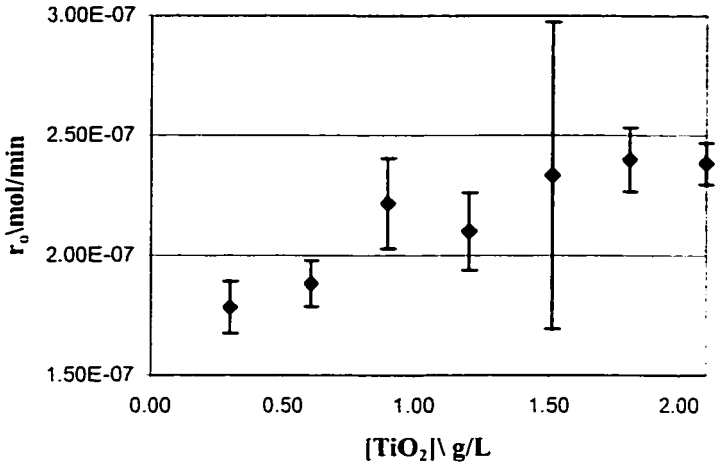

The rates of disappearance of formic acid are increasing linearly with an increase in catalyst load to then deviate from linearity and reach a plateau at high catalyst load. In this case, the plateau was reach at a catalyst load of approximately 1.8 g/L. This departure from linearity at high catalyst lead is attributed to the increasing opacity of the solution as well as an increasing level of light scattering and reflection by the TiO_2 pigments, causing a drop in average light intensity in the photoreactor. The monochromatic photon flow from the source was determined to convert the above rates

into photonic efficiencies. The photon flow was determined with a chemical Actinometer (Aberchrome 540). The method involved determining the rate of change in absorbance at a given wavelength as a function of time and convert the slope thus obtained into photon flux. Three runs were performed to obtain a robust photon flow value. Figure 3.7.2-6 illustrates the result obtained for one of these runs. A very good linearity was obtained in all three cases. A mean value of $2.01 \pm 0.26 \times 10^{-6}$ Einstein/min was obtained. The initial rates of disappearance of formic acid illustrated in graph 3.7.2-5 were converted into photonic efficiencies and the reciprocal of these values was plotted against the reciprocal of the TiO_2 loadings (figure 3.7.2-7):

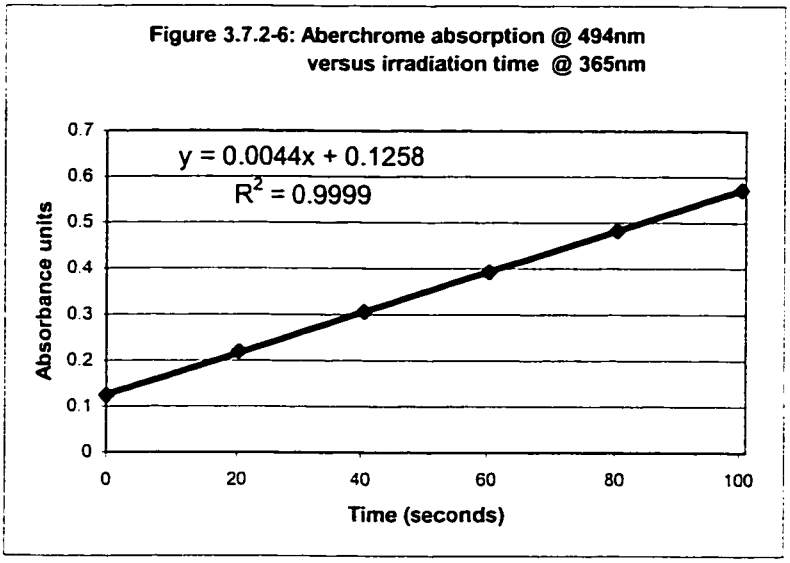

Figure 3.7.2-6: Aberchrome absorption @ 494nm versus irradiation time @ 365nm

The reciprocal of the y-intercept of figure 3.7.2.7 yielded the limiting photonic efficiency of formic acid (i.e., its overall quantum yield). We are thus proposing a value

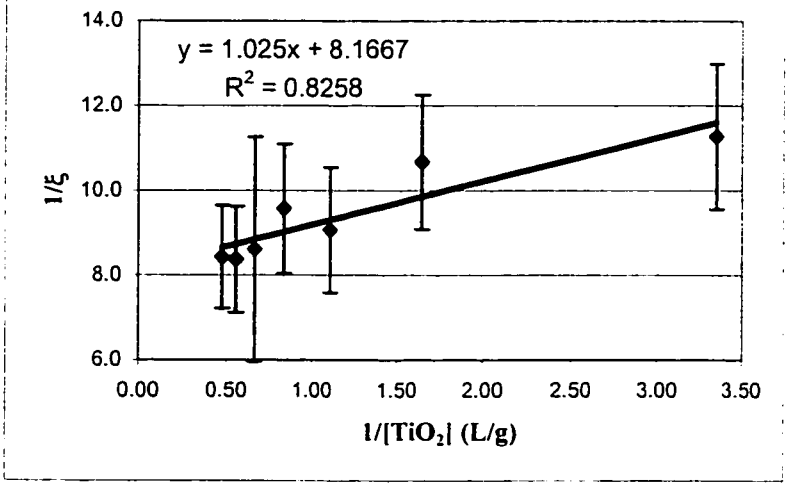

Figure 3.7.2-7: Reciprocal of formic acid photonic efficiency vs the reciprocal of TiO_2 load (L/g)

of $\Phi_{formic} = 0.12 \pm 0.02$ for formic acid, a reference standard representing aliphatic organic compounds. Acetic acid, propanoic acid, butanoic acid, valeric acid, and 2-methylbutanoic acid were degraded under the exact same conditions as formic acid. The quantum yield of our model compound formic acid, and the relative photonic efficiencies of the former acids versus our model compound, allows us to propose the following quantum yields for the previous five acids (table 4.7.2-2).

Acid	ξ_r	Φ
Formic	1.000	0.120 ± 0.020
Acetic	0.085 ± 0.01	0.010 ± 0.002
Propanoic	0.20 ± 0.03	0.024 ± 0.006
Butanoic	0.28 ± 0.06	0.034 ± 0.009
Valeric	0.56 ± 0.07	0.067 ± 0.015
2-methylbutanoic	0.31 ± 0.05	0.037 ± 0.008

Table 3.7.2-2: Relative photonic efficiencies and quantum yields for selected acids versus formic acid. $\xi_{lim,\ formic} = \Phi_{formic} = 0.12 \pm 0.02$

It is interesting to note that the acid with the lowest quantum yield is acetic acid. In previous experiments, acetic acid had the lowest degradation rate of the C1 to C5 liners series. The quantum yield is also increasing when going from acetic acid to valeric acid. As the chain length increases, the acid bears an increasing amount of secondary C-H bonds for which the dissociation energy is lower than of primary C-H bonds. There is also a good correlation between the above quantum yields and the kinetically determined rate constant of the above acids, as indicated in figure 3.7.2-8.

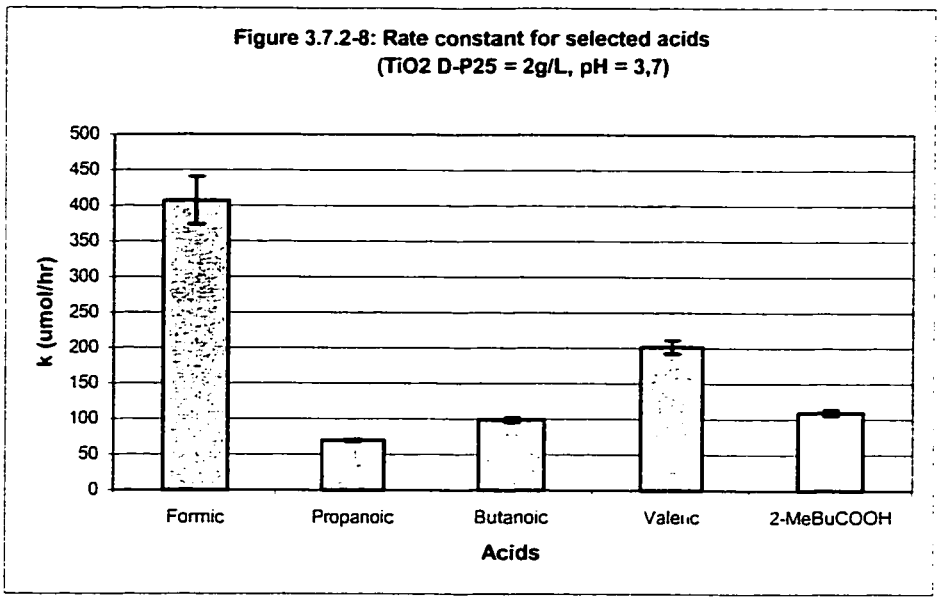

The above reported relative photonic efficiencies must be carefully examined when assessing process efficiencies as there is a pitfall: these values are derived from the rate of a test molecule against that of a reference compound. Low relative photonic efficiencies do not mean that the process is inefficient but rather that under otherwise identical experimental conditions, the rate of degradation of the test compound was less than that of the reference compound. For example, while the rate of degradation of formic acid under the applied conditions was 328 umol/hr, that of valeric acid was 185 umol/hr, hence a relative photonic efficiency of 0.56. On the other hand, if the relative photonic efficiency of valeric acid had been determined against acetic acid (rate of degradation, 28 umol/hr), its relative photonic efficiency would have been 6.6, which could be interpreted has highly efficient. It is thus important, when reporting such values, to indicate against what compounds they are measured.

Chapter 4

General Conclusions

The linear C1 to C5 saturated aliphatic carboxylic acids, their branched analogues, and their 2-hydroxy and 2-keto derivatives included in this study were poor adsorbers. Their extent of dark adsorption on TiO_2 Degussa P25 ranged from 1.4% ± 0.2% (2-ketovaleric acid) 5.5% ± 0.2% (2-hydroxy-2-methylbutanoic acid). The observed trends between the extent of dark adsorption and pH could be rationalized by an electrostatic model where adsorption is proportional to the amount of deprotonated aliphatic carboxylic acid molecules present in solution under conditions where the surface of TiO_2 is positively charged i.e., at pH below its point of zero charge. When irradiated with white light over TiO_2 Degussa P25, these acids were completely degraded and mineralized, as evidenced from HPLC-UV and TOC analysis. The trends observed in the rate of degradations were explained on the basis of (1) the extent of dark adsorption, (2) the pH of the suspensions that impacts the former factor and the the oxidative power of the photocatalyst, (3) C-H bond strengths, and (4) the stability of the radical intermediate products that can possibly form following the abstraction of a hydrogen atom for the carbon skeleton of these acids or following their photo-assisted decarboxylation. The trends observed between the rates of degradation and between the rates of mineralization were different. This was attributed to the formation of carbon-containing intermediates that impact the overall observed rates of mineralization, as evidenced by the presence of additional peaks in the chromatograms obtained from HPLC analysis.

The use of three different analytical methods, namely (1) HPLC-UV, (2) GC-FID and (3) GC-MS, lead to the identification of 15 degradation products from the degradation of valeric acid. These compounds are (1) aliphatic saturated and unsaturated carboxylic acids and dicacids with the same or shorter chain length than the parent compound, (2) methylated branched saturated aliphatic acids and diacids of shorter chain length than the parent compound, (3) saturated and unsaturated hydroxyacids of the same or shorter chain length than the parent compound, and (4) saturated ketoacids of the same or shorter chain length than the parent compound (4-ketovaleric acid, 2-ketobutanoic acid). No evidence was established that the primary and preferred step in the degradation of valeric acid involves hydroxylation of the alpha carbon atom, followed by the formation of 2-keto acid upon further oxidation. However, evidences were established whereby the hydroxylation of the carbon backbone of valeric acid takes place and that these reactions are involved in the primary steps leading to the degradation of this acid. The fact that the 4-hydroxyvaleric acid/4-ketoxyvaleric acid couple and the 2-hydrobutanoic acid/2-ketobutanoic acid couple were identified demonstrates that once hydroxylated, the hydroxyl group is further oxidized to the keto derivative.

The adsorption equilibrium constants determined under illumination conditions for formic acid, propanoic acid, and 2-methylbutanoic acid were statistically different. This difference was attributed to a disruption of the adsorption equilibrium that takes place in the dark between the adsorbate molecules and the photocatalyst's surface. This disruption could be attributed to changes that occur at the surface in the presence of photons.

By using simple instrumentation and determining the photon flow from the lamp source by chemical actinometry using Aberchrome 540, a value of 0.12 ± 0.02 was obtained for the limiting photonic efficiency of Formic acid. This is indeed equivalent to its overall quantum yield. Photonic efficiencies relative to formic acid of 0.08 ± 0.01, 0.20 ± 0.03, 0.28 ± 0.06, 0.56 ± 0.07, and 0.31 ± 0.05 were obtained for acetic acid, propanoic acid, butanoic acid, valeric acid, and 2-methylbutanoic acid, respectively, which, from the limiting photonic efficiency of formic acid lead to overall quantum yields of 0.01 ± 0.002, 0.02 ± 0.006, 0.03 ± 0.009, 0.07 ± 0.015, and 0.04 ± 0.008 for acetic acid, propanoic acid, butanoic acid, valeric acid, and 2-methylbutanoic acid, respectively.

References

1) N. Serpone and R. F. Khairutdinov, *Application of nanoparticles in the photocatalytic degradation of water pollutants*, Laboratory of pure and applied studies in catalysis, environment and materials, department of chemistry and biochemistry, Concordia University, 1455 de Maisonneuve Blvd. West, Montreal (Quebec), Canada H3G 1M8;

2) Craig S. Turchi and David F. Ollis, Journal of Catalysis 122, 178-192 (1990);

3) Bernhard Kraeutler, Allen J. Bard, Journal of the American Chemical Society / 100:7 / March 29, 1978, Communications to the editor, pp. 2239 – 2240;

4) Bernhard Kraeutler, Allen J. Bard, Nouveau Journal de Chimie, vol. 3, N° 1-1979, p. 31;

5) D. Bahnemann, J. Cunningham, M. a. Fox, E. Pelizzetti, P. Pichat, and N. Serpone, *Photocatalytic treatment of waters, Aquatic and surface photochemistry*, Chapter 21, pp. 261-315, Edited by George R. Helz, Richard G. Zepp, Donald G. Crosby, Lewis Publishers, 1994;

6) Nick Serpone and Angela Salinaro, Pure & Appl. Chem., Vol. 71, No. 3, pp. 000-000, 1999, Paper 159;

7) H. Gerischer, J. Phys. Chem. **1984**, 88, 6096 – 6097;

8) M. R. Prairie, B. M. Stange, and L. R. Evans, Photocatytic Purification and Treatment of Water and Air, pp. 353-363, D. F. Ollis and H. Al-Ekabi (Editors), © 1993 Elsevier Science Publisher, B. V., All rights reserved;

9) Pierre Pichat, Chantal Guillard, Laurence Amalric, An-Christel Renard, Olivier Plaidy, Solar energy materials and solar cells 1242 (1995) xxx C;

10) C. Minero, V. Maurino, E. Pelizzetti, Marine Chemistry 58 (1997) 361-372;

11) V. Brezova, A. Stasko, M. Ceppan, M. Mikula, J. Blecha, M. Vesely, A. Blazkova and L. Lapeik, Photocatytic Purification and Treatment of Water and Air, pp. 659-664, D. F. Ollis and H. Al-Ekabi (Editors), © 1993 Elsevier Science Publisher, B. V., All rights reserved;

12) Marye Anne Fox, Photocatytic Purification and Treatment of Water and Air, pp. 163-166, D. F. Ollis and H. Al-Ekabi (Editors), © 1993 Elsevier Science Publisher, B. V., All rights reserved;

13) D. Lawless, N. Serpone, and D. Meisel, The Journal of Physical Chemistry, Vol. 95, No. 13, 1991;

14) Calvin D. Jaeger and Allen J. Bard, The Journal of Physical Chemistry, Vol. 83, No. 24, 1979;

15) Andrew Mills, Stephen Le Hunte, Journal of Photochemistry and Photobiology A: Chemistry 108 (1997) 1-35;

16) Marye Anne Fox, r. Barton Draper, Maria Dulay, and Kevin O'Shea, E. Pelizzetti and M. Schiavello (eds.), Photochemical conversion and storage of solar energy, 323-335, Copyright 1991 Kluwer Academic publishers. Printed in the Netherlands;

17) Kevin O'Shea and Anthony Conde, Photocatytic Purification and Treatment of Water and Air, pp. 707-712, D. F. Ollis and H. Al-Ekabi (Editors), © 1993 Elsevier Science Publisher, B. V., All rights reserved;

18) Nick Serpone, Ezio Pelizzetti and Hisao Hidaka, Photocatytic Purification and Treatment of Water and Air, pp. 225-250, D. F. Ollis and H. Al-Ekabi (Editors), © 1993 Elsevier Science Publisher, B. V., All rights reserved;

19) P.W. Atkins, *Physical Chemistry*, Fourth edition, copyright © 1978, 1982, 1986, 1990 by P.W. Atkins;

20) Andrew Mills, Stephen Le Hunte, Journal of Photochemistry and Photobiology A: Chemistry 108 (1997) 1-35;

21) Nick Serpone, IUPAC Commision (Position paper), June 25, 1995;

22) N. Serpone, G. Sauvé, R. Koch, H. Tahiri, P. Pichat, P. Piccinini, E. Pelizzatti, H. Hidaka, J. Photochem. Photobiol. A: Chem. 94 (1996) 191;

23) N. Serpone, R. Terzian, D. Lawless, P. Kennepohl, G. Sauvé, J. Photochem. Photobiol. A: Chem. 73 (1993) 11;

24) Nick Serpone and Angela Salinaro, Pure & Appl. Chem., Vol. 71, No. 3, pp. 000-000, 1999, Paper 159;

25) J. W. Verhoeven, Pure Appl. Chem. 68, 2223 (1996);

26) (a) J. G. Calvert, J. N. Pitts Jr., Photochemistry, p. 780, Wiley, New York (1966), (b) S. L. Murov, et al., Handbook of Photochemistry, 2nd edn., Marcel Dekker, New York (1993);

27) A. M. Braun, M. T. Maurette, E. Oliveros, Photochemical technology, chap. 2, Wiley, New York (1991);

28) Nick Serpone, Newsletter No. 58, November 1996;

29) Health Canada, *Guidelines for Canadian Drinking Water Quality*, Sixth Edition, © Minister of Supply and Services Canada 1996;

30) David F. Ollis, Chen-Yung Hsiao, Lely Budiman, and Chung-Li Lee, Journal of Catalysis **88**, 89 – 96 (1984);

31) Ezio Pelizzatti, Claudio Minero, Hisao Hidaka, and Nick Serpone, Photocatytic Purification and Treatment of Water and Air, pp. 261-273, D. F. Ollis and H. Al-Ekabi (Editors), © 1993 Elsevier Science Publisher, B. V., All rights reserved;

32) Yun Mao, Christian Schöneich, and Klaus-Deiter Asmus, J. Phys. Chem. 1991, 95, 10080-10089;

33) Jörg Schwitzgebel, J. G. Ekerdt, H. Gerisher, and Adam Heller, J. Phys. Chem. 1995, 99, 5633-5638;

34) Andrew Mills, Stephen Le Hunte, An overview of semiconductor photocatalysis, Journal of Photochemistry and Photobiology A: Chemistry 108 (1997) 1-35;

35) Joseph Cunningham and Petr Sedlak, Photocatalytic purification and treatment of water and air, D. F. Ollis and H. Al-Ekabi (Editors), pp. 67-81, Copyright 1993 Elsevier Science Publishers B. V., All right reserved;

36) N. Serpone and R. F. Khairutdinov, Laboratory of pure and applied studies in catalysis, environment and materials, department of chemistry and biochemistry, Concordia University, 1455 de Maisonneuve Blvd. West, Montreal (Quebec), Canada H3G 1M8;

37) D. Bahnemann, J. Cunningham, M. a. Fox, E. Pelizzetti, P. Pichat, and N. Serpone, *Photocatalytic treatment of waters, Aquatic and surface photochemistry*, Chapter 21, pp. 261-315, Edited by George R. Helz, Richard G. Zepp, Donald G. Crosby, Lewis Publishers, 1994;

38) Pierre Pichat, Chantal Guillard, Laurence Amalric, An-Christel Renard, Olivier Plaidy, Solar energy materials and solar cells 1242 (1995) xxx C;

39) C. Minero, V. Maurino, E. Pelizzetti, Marine Chemistry 58 (1997) 361-372;

40) H. L. Chum, M. Ratcliff, F. L. Posey, J. A. Turner, and A. J. Nozik, J. Phys. Chem. 1983, 87, 3089 – 3093;

41) Tadayoshi Sakata, Tomoji Kaeai, and Kazuhito Hashimoto, J. Phys. Chem. 1984, 88, 2344 – 2350;

42) Ralph W. Matthews, Purification and Treatment of Water and Air, pp. 121-138, D. F. Ollis and H. Al-Ekabi (Editors), © 1993 Elsevier Science Publisher, B. V., All rights reserved;

43) David F. Ollis, Chen-Yung Hsiao, Lely Budiman, and Chung-Li Lee, Journal of Catalysis **88**, 89 – 96 (1984);

44) Hussain Al-Ekabi and Nick Serpone, J. Phys. Chem., 92, 5726 – 5731 (1988);

45) Ralph W. Matthews, Journal of Catalysis 111, 264-272 (1988);

46) Ghassan Al-Sayyed, Jean-Christophe D'Oliveira and Pierre Pichat, URA au CNRS "Photocatalyse, Catalyse et Environnement", Ecole Centrale de lyon, BP 163, 69131 Ecully Cédex, France;

47) Marye Anne Fox, r. Barton Draper, Maria Dulay, and Kevin O'Shea, E. Pelizzetti and M. Schiavello (eds.), Photochemical conversion and storage of solar energy, 323-335, Copyright 1991 Kluwer Academic publishers. Printed in the Netherlands;

48) David F. Ollis, E. Pelizzetti and M. Schiavello (eds.), Photochemical conversion and storage of solar energy, 593-623, Copyright 1991 Kluwer Academic publishers. Printed in the Netherlands;

49) P. Pichat, C. Guillard, C. Maillard, L. Amalric and J.-C. D'oliveira, Photocatytic Purification and Treatment of Water and Air, pp. 207-223, D. F. Ollis and H. Al-Ekabi (Editors), © 1993 Elsevier Science Publisher, B. V., All rights reserved;

50) Jean-Christophe D'oliveira, Claudio Minero, Ezio Pelizzetti and Pierre Pichat, J. Photochem. Photobiol. A: Chem., 72 (1993) 261-267;

51) N. Nageswara Rao, Sangeeta Dube, Journal of Molecular Catalysis A: Chemical 104 (1996) L197-L199;

52) Andrew Mills, Stephen Le Hunte, An overview of semiconductor photocatalysis, Journal of Photochemistry and Photobiology A: Chemistry 108 (1997) 1-35;

53) C. Minero, V. Maurino, E. Pelizzetti, Marine Chemistry 58 (1997) 361-372;

54) Yun Mao, Christian Schöneich, and Klaus-Deiter Asmus, J. Phys. Chem. 1991, 95, 10080-10089;

55) Y. Mao, C. Schöneich and K.-D. Asmus, Photocatalytic purification and treatment of water and air, D. F. Ollis and H. Al-Ekabi (Editors), pp. 49-65, Copyright 1993 Elsevier Science Publishers B. V., All right reserved;

56) Kevin O'Shea and Anthony Conde, Photocatytic Purification and Treatment of Water and Air, pp. 707-712, D. F. Ollis and H. Al-Ekabi (Editors), © 1993 Elsevier Science Publisher, B. V., All rights reserved;

57) Tadayoshi Sakata, Tomoji Kaeai, and Kazuhito Hashimoto, J. Phys. Chem. 1984, 88, 2344 – 2350;

58) N. Serpone, D. Lawless, R. Terzian, C. Minero, and E. Pelizzetti, E. Pelizzetti and M. Schiavello (eds.), Photochemical conversion and storage of solar energy, 451-475, Copyright 1991 Kluwer Academic publishers. Printed in the Netherlands;

59) Y. Mao, C. Schöneich and K.-D. Asmus, Photocatalytic purification and treatment of water and air, D. F. Ollis and H. Al-Ekabi (Editors), pp. 49-65, Copyright 1993 Elsevier Science Publishers B. V., All right reserved;

60) M. R. Prairie, B. M. Stange, and L. R. Evans, Photocatytic Purification and Treatment of Water and Air, pp. 353-363, D. F. Ollis and H. Al-Ekabi (Editors), © 1993 Elsevier Science Publisher, B. V., All rights reserved;

61) Kevin O'Shea and Anthony Conde, Photocatytic Purification and Treatment of Water and Air, pp. 707-712, D. F. Ollis and H. Al-Ekabi (Editors), © 1993 Elsevier Science Publisher, B. V., All rights reserved;

62) Ralph W. Matthews, Photocatytic Purification and Treatment of Water and Air, pp. 121-138, D. F. Ollis and H. Al-Ekabi (Editors), © 1993 Elsevier Science Publisher, B. V., All rights reserved;

63) Nick Serpone, Halima Tahiri, Raymond Le Van Mao, J. Photochem. Photobiol., June 20, 1995;

64) L. Tinucci, E. Borgarello, C. Minero and Pelizzetti, Photocatytic Purification and Treatment of Water and Air, pp. 585-594, D. F. Ollis and H. Al-Ekabi (Editors), © 1993 Elsevier Science Publisher, B. V., All rights reserved;

65) Ralph W. Matthews, Journal of Catalysis 111, 264-272 (1988);

66) Nick Serpone, Halima Tahiri, Raymond Le Van Mao, J. Photochem. Photobiol., June 20, 1995;

67) L. Tinucci, E. Borgarello, C. Minero and Pelizzetti, Photocatytic Purification and Treatment of Water and Air, pp. 585-594, D. F. Ollis and H. Al-Ekabi (Editors), © 1993 Elsevier Science Publisher, B. V., All rights reserved;

68) N. Serpone, D. Lawless, R. Terzian, C. Minero, and E. Pelizzetti, E. Pelizzetti and M. Schiavello (eds.), Photochemical conversion and storage of solar energy, 451-475, Copyright 1991 Kluwer Academic publishers. Printed in the Netherlands;

69) N. Serpone and R. F. Khairutdinov, Laboratory of pure and applied studies in catalysis, environment and materials, department of chemistry and biochemistry, Concordia University, 1455 de Maisonneuve Blvd. West, Montreal (Quebec), Canada H3G 1M8;

70) N. Serpone, D. Lawless, R. Terzian, C. Minero, and E. Pelizzetti, E. Pelizzetti and M. Schiavello (eds.), Photochemical conversion and storage of solar energy, 451-475, Copyright 1991 Kluwer Academic publishers. Printed in the Netherlands;

71) C. Minero, V. Maurino, E. Pelizzetti, Marine Chemistry 58 (1997) 361-372;

72) D. Bahnemann, J. Cunningham, M. a. Fox, E. Pelizzetti, P. Pichat, and N. Serpone, *Photocatalytic treatment of waters, Aquatic and surface photochemistry*, Chapter 21, pp. 261-315, Edited by George R. Helz, Richard G. Zepp, Donald G. Crosby, Lewis Publishers, 1994;

73) Tadayoshi Sakata, Tomoji Kaeai, and Kazuhito Hashimoto, J. Phys. Chem. 1984, 88, 2344 – 2350;

74) Craig S. Turchi and David F. Ollis, Journal of Catalysis 122, 178-192 (1990);

75) Nick Serpone, Ezio Pelizzetti and Hisao Hidaka, Photocatytic Purification and Treatment of Water and Air, pp. 225-250, D. F. Ollis and H. Al-Ekabi (Editors), © 1993 Elsevier Science Publisher, B. V., All rights reserved;

76) D. Bahnemann, J. Cunningham, M. a. Fox, E. Pelizzetti, P. Pichat, and N. Serpone, *Photocatalytic treatment of waters, Aquatic and surface photochemistry*, Chapter 21, pp. 261-315, Edited by George R. Helz, Richard G. Zepp, Donald G. Crosby, Lewis Publishers, 1994;

77) Sadamu Yamagata, Ryo Baba, and akira Fujishima, Bull. Chem. Soc. Jpn., 62, 1004 – 1010 (1989);

78) Tadayoshi Sakata, Tomoji Kaeai, and Kazuhito Hashimoto, J. Phys. Chem. 1984, 88, 2344 – 2350;

79) Jörg Schwitzgebel, J. G. Ekerdt, H. Gerisher, and Adam Heller, J. Phys. Chem. 1995, 99, 5633-5638;

80) P. Pichat, E. Pelizzetti and M. Schiavello (eds.), Photochemical conversion and storage of solar energy, 277-293, Copyright 1991 Kluwer Academic publishers. Printed in the Netherlands;

81) Kayo Nohara, Hisao Hidaka, Ezio Pelizzetti, and Nick Serpone, J. Photochem. Photobiol. A:Chem, November 3, 1995;

82) Nick Serpone, IUPAC Commision (Position paper), June 25, 1995;

83) Joseph Cunningham and Petr Sedlak, Photocatalytic purification and treatment of water and air, D. F. Ollis and H. Al-Ekabi (Editors), pp. 67-81, Copyright 1993 Elsevier Science Publishers B. V., All right reserved;